

The Surface Passivation and Potential Sensing Applications of Silicon Nanocrystals

by

Christina Marie Gonzalez

A thesis submitted in partial fulfillment of the requirements for the degree of

Doctor of Philosophy

Department of Chemistry  
University of Alberta

© Christina Marie Gonzalez, 2016

## Abstract

Silicon nanocrystals (SiNCs) have been explored as active materials in a variety of prototype applications including photovoltaics, electronics, photonics, and sensors based on their optical and electronic properties. Using SiNCs are appealing because their source material (*i.e.*, silicon) is abundant, they exhibit limited toxicity, and their optical as well as electronic properties are tunable. To further the advancement of SiNC-based applications, there is a need to develop surface functionalization methods that provide stability and render the SiNCs solution-processable. This must be achieved while maintaining, and even tailoring SiNC optical response. This thesis consists of two overarching themes: the surface passivation of SiNCs (Chapters 2-3) and the development of SiNC-based sensors (Chapters 4-5).

Chapter 2 investigates the hydrosilylation of SiNCs with a variety of alkenes and alkynes using two common radical initiators (*i.e.*, azobisisobutyronitrile and benzoyl peroxide). Chapter 3 examines the use of a compact fluorescent light source for the generation of thiyl radicals from two disulfide containing ligands (*i.e.*, lipoic acid and dibutyl disulfide) to promote radical initiation of the SiNC surface to generate Si-S surface bonds.

Chapter 4 describes the development of a luminescent paper-based sensor using dodecyl functionalized SiNCs for its optical response towards nitro-group containing high energy compounds (*i.e.*, trinitrotoluene (TNT), cyclotrimethylenetrinitramine (RDX) and pentaerythritol tetranitrate (PETN)). Ester functionalized SiNCs were embedded into polydimethylsiloxane (PDMS) based-substrates for the optical detection of biogenic amine vapors released during food spoilage in Chapter 5.

Finally, in Chapter 6, a summary of the findings of SiNC surface passivation and sensors is presented, followed by possible future research directions in these areas.

## Preface

A portion of Chapter 1 has been published as the review article, C. M. Gonzalez and J. G. C. Veinot, *J. Mater. Chem. C*, **2016**, *4*, 4836-4846. I was responsible for the comprehensive review of the literature and the manuscript composition. J. G. C. Veinot was the supervisory author and was involved with the concept formation and manuscript composition.

Chapter 2 of this thesis has been published as Z. Yang, C. M. Gonzalez, T. K. Purkait, M. Iqbal, A. Meldrum, J. G. C. Veinot, *Langmuir*, **2015**, *31*, 10540-10548. Z. Yang and C. M. Gonzalez have made equal contribution to this work which included data collection and analysis and manuscript composition. T. K. Purkait aided in high resolution transmission electron microscopy data acquisition and performed proton nuclear magnetic resonance and thermogravimetric analysis measurements and analysis. M. Iqbal aided with data acquisition and monitoring of experiments. A. Meldrum assisted with photoluminescence lifetime measurements and data analysis. J. G. C. Veinot was the supervisory author and was involved with the concept formation and manuscript composition.

Chapter 3 is an original work. Md. H. Mobarok was involved with concept formation, data collection and analysis of proton nuclear magnetic resonance data presented and also assisted with X-ray photoelectron spectroscopy data acquisition and analysis. T. K. Purkait assisted with electron microscopy analysis.

A portion of Chapter 4 of this thesis has been published as C. M. Gonzalez, M. Iqbal, M. Dasog, D. G. Piercey, R. Lockwood, T. M. Klapötke, J. G. C. Veinot, *Nanoscale*, **2014**, *6*, 2608-2612 and

was part of an international collaboration with D. G. Piercey and T. M. Klapötke at Ludwig-Maximilian University. I was responsible for concept formation, data acquisition and analysis as well as manuscript composition. M. Iqabl assisted in data acquisition of solid nitroaromatic sensor testing and image collection. M. Dasog was involved with concept formation of the project as well as collection of solution based sensor studies involving high energy materials (*i.e.*, trinitrotoluene, cyclotrimethylenetrinitramine, pentaerythritol tetranitrate). D. G. Piercey synthesized the high energy materials (*i.e.*, trinitrotoluene, cyclotrimethylenetrinitramine, pentaerythritol tetranitrate) used. R. Lockwood contributed to the data acquisition and analysis of photoluminescent lifetimes. Professor T. M. Klapötke is the lead investigator at Ludwig-Maximilian University where the studies involving the synthesis and data collection using high energy materials (*i.e.*, trinitrotoluene, cyclotrimethylenetrinitramine, pentaerythritol tetranitrate) was performed. J. G. C. Veinot was the supervisory author and was involved with the concept formation, experiments involving high energy materials (*i.e.*, trinitrotoluene, cyclotrimethylenetrinitramine, pentaerythritol tetranitrate) and interferences, and manuscript composition. Unpublished results concerning thin layer chromatography were conducted in collaboration with T. K. Purkait, R. Erickson and K. Gottschling.

Chapter 5 is an original work where I was responsible for concept formation and data acquisition and analysis. Initial solution titrations with allylamine and development of silicon nanocrystals (SiNCs) embedded in polydimethylsiloxane (PDMS) were done with assistance by S. Nerdoly. L. Haddick assisted with the development of porous PDMS embedded SiNCs, data collection and analysis of solution based studies involving biogenic amines, vapor studies involving putrescine, and food spoilage experiments. A. Nguyen assisted with data collection of the prepared sensors

with argon, putrescence, water and ethanol vapors. Professor A. Meldrum developed the custom gas chamber for vapor studies and assisted with the data analysis of the interaction of the sensors with putrescence vapor. R. Sinelnikov also assisted with the data analysis of the interaction of the sensors with putrescence vapor. J. G. C. Veinot was involved with concept formation.

This thesis is in memory of my father,

David Gonzalez.

## Acknowledgements

There have been many people throughout my graduate studies, that I would like to thank. I would not have been able to complete this program without their guidance, help, and support.

First, I would like to thank my supervisor and mentor Dr. Jonathan Veinot for his support throughout my doctoral journey. He has always given me the freedom to play around in the lab and explore research projects. He also encouraged me to collaborate with fellow group members as well as other research groups outside of the Chemistry department. Most importantly, he has always reminded me that it is ok take care of my personal well-being and health over science when the time arises.

I would also like to thank my committee members Drs. Jillian Buriak, Mark McDermott, and Mike Serpe for their valuable input and time. Furthermore, I would like to thank Dr. Andrea Goforth for serving as an external committee member.

I was fortunate enough to work with amazing people throughout my entire time in the Veinot research group. Drs. Muhammad Iqbal, Mita Dasog, Tapas Purkait, Zhenyu Yang, and Md Hosnay Mobarok really inspired me to push myself to my limits as well as take me under their wing of their various expertise. I am truly grateful for all I have learned from each and every one of you. I also had the opportunity to work with both undergraduates and international students. Thanks to Shawna Neddoly, Reid Erickson, Kerstin Gottschling, and Lisa Haddick for your great work, time, effort, and contributions to this thesis! Dr. Melanie Hoffman, you have been a great fellow student mentor, colleague and friend throughout the years! Also, a special thanks goes to Lida Hadidi who has been through every single step of this program with me. Regina Sinelnikov, thank you for your constant support, being my gym buddy, and your never-ending supply of chocolate. Kelsey Deustch and Alyx Aarbo, thanks for always “meowing” with me and your

friendship. I also would like to thank Drs. Rhett Clark and John Washington for all the fun times and the formation of the “Nano Tigers” running group.

I would like to also thank Dr. Al Meldrum for his support and guidance in the physics aspects of my research. He allowed me to learn how to work with lasers independently and always had an open door for me to go and ask questions. The entire Meldrum group has been such a pleasure to work with and were more than happy to help. Dr. Ross Lockwood, thank you for your help with the lifetime measurements as well as showing me the ways of the gas chamber set up. Also, An Nguyen needs to be thanked for all her help with the putrescine vapor sensing experiments and for being a great friend outside of the lab. Your optimism is inspiring!

The work in this thesis would not have been possible without the help of the amazing technical and department support staff here at the UofA. Wayne Moffat (Analytical Services), Shihong Xu (XPS), Jing Zheng (Mass Spec), and Kai Cui (TEM), thank you all for your time and valuable input. Furthermore, Anita Weiler, Bonnie Gover, Ryan Lewis, and Bernie Hippel, thanks for all your help outside of the lab. The department would not function the same without you all.

Finally, I would like to thank my family and friends. To my mother, you have been the greatest support a daughter could ever ask for. Also, thanks to my sister Jessica, brother-in-law Aaron, and cousin Jenny for your love and support. To my best friends from home, Suzy, Sandy, Rosanna, and Joei, you girls have stuck by me for so many years and have not forgotten about me. Even though our lives are so busy, we always make the time for one another and I am truly grateful. To the great friends I have made here, Akemi Darlington, Dr. Sonja Francis, Dr. Paul Lummis, Melanie Lui, and Anthony Nguyen, thanks for all the support, laughs, and giving me a life outside of the lab!

# Table of Contents

<b>Chapter 1 Introduction.....</b>	<b>1</b>
1.1 Nanotechnology and quantum dots .....	2
1.2 Silicon Nanocrystals.....	6
1.3 Synthesis of SiNCs.....	9
1.3.1 Top-down Methods.....	9
1.3.2 Bottom-up/Solution-based.....	10
1.3.3. Gas-Phase Methods .....	12
1.3.4 Solid-state/silicon rich oxides.....	13
1.4 Surface Passivation of SiNCs.....	16
1.4.1. Silicon Hydride Surfaces .....	17
1.4.1.1 Hydrosilylation .....	17
1.4.1.2 Chalcogenides .....	20
1.4.1.3. Other surface modification protocols.....	22
1.4.2. Halogens and Oxide reactivity .....	24
1.4.3 Surface Passivation Effects on the Optical Properties of SiNCs.....	26
1.5 SiNC-based sensing platforms. ....	27
1.5.1 Representative Quantum Dot Based Sensing Mechanisms .....	28
1.5.1.1 Electron transfer.....	29
1.5.1.2 Fluorescence Resonance Energy Transfer (FRET).....	30

1.5.1.3. Photocurrent Generation and Other Sensing Strategies .....	33
1.5.2 Examples of SiNC Sensors.....	35
1.5.2.1 High Energy Materials.....	35
1.5.2.2 Metal Cations.....	38
1.5.2.3 Biologically Relevant Molecules.....	40
1.5.2.4 Antibiotics.....	44
1.5.2.5 Pesticides.....	45
1.5.2.6 Environmental and Biological pH .....	47
1.6 Thesis outline .....	50
<b>Chapter 2 Radical Initiated Hydrosilylation on Silicon Nanocrystal Surfaces: An evaluation of functional group tolerance and mechanistic study .....</b>	<b>51</b>
2.1 Introduction .....	52
2.2 Experimental .....	54
2.2.1 Reagents and Materials.....	54
2.2.2 Material Characterization and Instrumentation .....	54
2.2.3 Preparation of oxide-embedded SiNCs ( $d_{avg} = \sim 3, 5, \text{ and } 8 \text{ nm}$ ).....	56
2.2.4 Preparation of hydride-terminated SiNCs .....	56
2.2.5 Radical initiated hydrosilylation of alkenes/alkynes by H-SiNCs .....	57
2.2.6 Thermal functionalization of H-SiNCs.....	58
2.2.7 Reaction of TEMPO with SiNCs.....	58

2.2.8 Reaction of dodecene with radical initiators .....	58
2.2.9 Reaction of TEMPO and SiNCs in absence of radical initiators.....	59
2.2.10 Evaluation of the influence of reaction time .....	59
2.2.11 Estimation of surface coverage.....	60
2.3 Results and Discussion.....	60
2.4 Conclusions .....	88
<b>Chapter 3 The Formation of Si-S bonds on the Silicon Nanocrystal Surface via a</b>	
<b>Commerical Fluorescent Light Source .....</b>	<b>90</b>
3.1 Introduction .....	91
3.2 Experimental .....	93
3.2.1 Reagents and Materials.....	93
3.2.2 Material Characterization and Instrumentation. ....	93
3.2.3 Preparation of oxide-embedded SiNCs ( $d_{\text{avg}} = 3, 5, \text{ and } 8 \text{ nm}$ ).....	95
3.2.3 Preparation of hydride-terminated SiNCs. ....	95
3.2.4 Commercial fluorescent light induced functionalized of H-SiNCs.....	96
3.2.5 Reaction of H-SiNCs with lipoic acid in the absence of heat and light .....	98
3.2.6 Thermal reaction of H-SiNCs with lipoic acid.....	98
3.2.7 Reaction of H-SiNCs with lipoic acid in the presence of trace water .....	98
3.3 Results and discussion.....	99
3.3.1 Investigation the origin of the reactivity.....	116

3.3.2 Proposed Reaction Mechanism .....	117
3.4 Conclusion.....	118
<b>Chapter 4 Detection of High-Energy Compounds Using Photoluminescent Silicon</b>	
<b>Nanocrystal Paper Based Sensors .....</b>	<b>120</b>
4.1 Introduction.....	121
4.2 Experimental .....	123
4.2.1 Chemicals/Reagents and Materials.....	123
4.2.2 Preparation of hydride-terminated Si nanocrystals. ....	124
4.2.3 Synthesis of dodecyl functionalized silicon nanocrystals .....	125
4.2.4 Synthesis of carboxylic acid functionalized silicon nanocrystals .....	125
4.2.5 Coupling of carboxylic acid functionalized silicon nanocrystals to TLC plates .....	126
4.2.6 Material Characterization and Instrumentation .....	126
4.2.7 Solution phase PL quenching studies .....	127
4.2.8 Solution phase PL lifetime studies .....	127
4.2.9 SiNCs paper sensor for visual detection of nitroaromatic compounds .....	128
4.2.10 TLC separation of nitroaromatic compounds.....	129
4.3 Results and Discussion.....	130
4.3.1 Characterization of dodecyl functionalized SiNCs .....	130
4.3.2 Fluorescence quenching by nitroaromatic compounds .....	131
4.3.4 Visual Detection using paper supported SiNCs .....	137

4.3.5 Separation of nitroaromatics via SiNCs coupled to TLC plates by esterification.....	142
4.4 Conclusions .....	147
<b>Chapter 5 Silicon Nanocrystals for the Development of Biogenic Amine Sensing</b>	
<b>Platforms.....</b>	<b>149</b>
5.1 Introduction.....	150
5.2 Experimental and Methods.....	152
5.2.1 Materials.....	152
5.2.2 Material Characterization and Instrumentation.....	153
5.2.3 Preparation of oxide-embedded SiNCs.....	154
5.2.4 Preparation of hydride-terminated SiNCs.....	154
5.2.5 Preparation of alkyl oligomer SiNCs.....	155
5.2.6 Preparation of alkyl and ester monolayer SiNCs.....	155
5.2.7 Purification and preparation of SiNC stock solutions.....	156
5.2.8 PDMS film containing ester monolayer functionalized SiNCs.....	156
5.2.9 PDMS sponge containing ester monolayer functionalized SiNCs.....	157
5.2.10 Solution Phase PL Studies of Titrations of SiNCs with Amines.....	157
5.2.11 Vapor Phase Studies Experimental Setup.....	158
5.2.12 PDMS film or sponge containing SiNCs luminescence studies with Ar vapor.....	159
5.2.13 PDMS film or sponge containing SiNCs luminescence bleaching and recovery studies.....	159

5.2.14 PDMS film or sponge containing SiNCs luminescence studies with putrescine vapor.	159
5.2.15 PDMS film or sponge containing SiNCs luminescence studies with water or ethanol vapor.	160
5.2.16 PDMS film or sponge containing SiNCs luminescence studies after exposure with raw food.	160
5.2.17 Visual Monitoring SiNC to Raw Meat.	161
5.3 Results and Discussion.	161
5.4 Conclusions	182
<b>Chapter 6 Conclusions and Future Directions</b>	<b>184</b>
6.1 Conclusions	185
6.2 Future Directions	188
6.2.1 Exploration of solubility with lipoic acid based ligands	188
6.2.2 Functionalization of SiNCs using thioketones	190
6.2.3 Development of a ratiometric sensor	191
6.2.4 Exploration of SiNCs embedded within porous structures for sensing	192
6.2.4.1 Development of SiNCs coated with MIPs	193
6.2.4.2 Development of SiNC vapor sensors through the use of aerogel hybrids	194
<b>Appendix</b>	<b>193</b>
<b>References</b>	<b>196</b>

## List of Tables

<b>Table 1-1:</b> Overview of the SiNC-based sensor systems discussed in this review.....	49
<b>Table 2-1:</b> Determination of surface coverage using <sup>1</sup> H NMR.....	69
<b>Table 2-2:</b> Surface coverage metrics determined using TGA.....	69
<b>Table 2-3:</b> Wavelengths of PL maxima of 3 nm SiNCs functionalized with various ligands using AIBN and BP as reaction initiators (unit: nm).....	82
<b>Table 2-4:</b> Results of PL lifetime decay ( $\tau$ ) of 3 nm SiNCs functionalized with various ligands using AIBN and BP as reaction initiators (unit: $\mu$ s). ....	82
<b>Table 4-1:</b> Concentrations of nitroaromatics ( <i>i.e.</i> , NB, MNT and DNT) used for PL and lifetime measurements.....	128
<b>Table 5-1:</b> The determination of $K_{sv}$ ( $\text{ppm}^{-1}$ ) and the limit of detection (ppm) based on the Stern-Volmer analysis of photoluminescence quenching in ester monolayer functionalized SiNCs after exposure to biogenic amines. Also shown is the reported oral toxicity levels <sup>378</sup> for comparison to limit of detection. ....	168
<b>Table 5-2:</b> Luminescence lifetimes of SiNCs after exposure to biogenic amines ( <i>i.e.</i> , putrescine, spermidine, cadaverine) in the concentration range of 0.5 - 5 ppm.....	169

## List of Figures

- Figure 1-1:** A plot displaying the number of published papers and citations of semiconductor QDs in the 25 years between 1991-2016. Note: The data was collected during the first week of Jan 2016, with data from 2015 being partial. Reproduced with permission from *J. Phys. Chem. Lett.* **2016**, 7, 584-585 (reference 16). Copyright 2016 American Chemical Society ..... 3
- Figure 1-2:** Image relating the changes in band structure and band gap as a function of size in quantum dots. (Image taken from [www.sigmaaldrich.com](http://www.sigmaaldrich.com))..... 5
- Figure 1-3:** Comparison of a) direct bandgap and b) indirect band gap materials. (Image reproduced and modified from reference 51.) ..... 7
- Figure 1-4:** Illustration of high energy reactive ball milling to simultaneously produce and functionalize SiNCs. Image reproduced with permission from *Adv. Mater.* **2007**, 19, 3984-3988 (reference 76). Copyright 2007 Wiley-VCH. .... 10
- Figure 1-5:** Images of SiNCs of different sizes under UV-light (365 nm) prepared via plasma pyrolysis of silane gas. Reproduced with permission from *Nanotechnology*, **2008**, 19, 245603 (reference 105). Copyright 2008 IOP Science. .... 13
- Figure 1-6:** Photoluminescence spectra of hydride terminated SiNCs using various etching times. Reproduced with permission from *Chem. Mater.*, **2006**, 18, 6139-6146 (reference 112). .... 15
- Figure 1-7:** Transmission Electron Microscope images of SiNC cubes. Adapted with permission from *J. Amer. Chem. Soc.*, **2012**, 134, 13958-13961 (reference 113)..... 16
- Figure 1-8:** Proposed hydrosilylation mechanisms on the SiNC surface involving a) free radical or b) exciton mediated in comparison to c) exciton-mediated hydrosilylation of bulk

silicon surfaces. Reproduced with permission from *J. Am. Chem. Soc.*, **2011**, *133*, 9564-9571 (reference 144). Copyright 2011 American Chemical Society. .... 20

**Figure 1-9:** Representation of different QD-based sensing designs: (a) electron transfer, ET, (b) FRET, or (c) photocurrent generation as readout signals. The green, blue, red, and grey structures on the QD represent difference surface groups. Reproduced and modified with permission from *ACS Appl. Mater. Interfaces*, **2013**, *5*, 2815–2834 (reference 32). Copyright 2013 American Chemical Society. .... 29

**Figure 1-10:** Pictorial representation of (a) electron transfer from a QD to an electron acceptor (A), and (b) electron transfer from an electron donor (D) to a QD. Reproduced with permission from *Chem. Soc. Rev.*, **2015**, *44*, 4275-4289 (reference 214). Copyright 2015 Royal Society of Chemistry. .... 30

**Figure 1-11:** Pictorial representation of fluorescence resonance energy transfer (FRET) (a) from a photoexcited QD to a molecular energy acceptor (A), and (b) from a photoexcited molecular energy donor (D) to a QD. Reproduced with permission from *Chem. Soc. Rev.*, **2015**, *44*, 4275-4289 (reference 214). Copyright 2015 Royal Society of Chemistry. .... 31

**Figure 1-12:** Representation of the four different sensing strategies using FRET. Reproduced with permission from *J. Mater. Chem. C*, **2014**, *2*, 595-613 (reference 208). Copyright 2014 Royal Society of Chemistry. .... 33

**Figure 1-13:** Representation of a QD-based photoelectrochemical sensor where QDs are immobilized by a linker to an electrode, which is placed in a solution. Upon illumination a photocurrent is generated and monitored after addition of a target

analyte. Reproduced with permission from *ACS Appl. Mater. Interfaces*, **2013**, *5*, 2800–2814 (reference 215). Copyright 2013 American Chemical Society. .... 34

**Figure 1-14:** A luminescent SiNC paper-based sensor that quenches in the presence of high energy molecules of TNT, PETN, and RDX. Reproduced with permission from *Nanoscale*, **2014**, *6*, 2608-2612 (reference 226). Copyright 2014 Royal Society of Chemistry. 37

**Figure 1-15:** The proposed FRET mechanism between TNT-amine complexes and SiNCs. Reproduced with permission from *Anal. Methods*, **2015**, *7*, 1732-1737 (reference 227). Copyright 2015 Royal Society of Chemistry. .... 37

**Figure 1-16:** a) SiNCs with different surface groups i) alkyl oligomer, ii) alkyl monomer, and iii) alkyl amine. b) Change in the luminescence of alkyl monomer dodecyl functionalized SiNCs in filter paper after exposure to varying concentrations of nitrobenzene (NB) vapor. Reproduced and modified with permission from *Nanotechnology*, **2016**, *27*, 105501 (reference 228). Copyright 2016 IOP Publishing. .... 38

**Figure 1-17:** The effect of SiNC luminescence by varying concentration of  $Hg^{2+}$ . Reproduced and modified with permission from *Nanoscale*, **2014**, *6*, 4096-4101 (reference 232). Copyright 2014 Royal Society of Chemistry. .... 39

**Figure 1-18:** Illustration of a SiNC-based glucose sensor. Reproduced and modified with permission from *Chem. Commun.*, **2013**, *49*, 612-614 (reference 239). Copyright 2013 Royal Society of Chemistry. .... 41

**Figure 1-19:** The proposed fluorescence quenching mechanism of SiNC by dopamine. Reproduced with permission from *Anal. Chem.*, **2015**, *87*, 3360–3365 (reference 244). Copyright 2015 American Chemical Society. .... 42

**Figure 1-20:** The integrated fluorescence intensity as a function time for a SiNC fiber sensor in O<sub>2</sub>, air, and air saturated with water, ethanol, or a 50% mixture of both. Reproduced with permission from *Sens. Actuators, B*, **2013**, *181*, 523-528 (reference 251). Copyright 2013 Elsevier. .... 43

**Figure 1-21:** The proposed mechanism of SiNC fluorescence quenching by TCs. Photo: SiNCs excited by UV light at 365 nm before (left) and after (right) 10 mM of TC. Reproduced and modified with permission from *RSC Adv.*, **2015**, *5*, 27458-27463 (reference 219). Copyright 2013 Royal Society of Chemistry. .... 45

**Figure 1-22:** Mechanism of a SiNC based pesticide sensor. Reproduced and modified with permission from *Anal. Chem.*, **2013**, *85*, 11464–11470 (reference 259). Copyright 2013 American Chemical Society..... 47

**Figure 2-1:** Photographs of suspensions/solutions of 3 nm hydride-terminated SiNCs/dodecene mixture under visible light and UV light irradiation. (a, b) AIBN and (c, d) BP are used as radical initiators. Samples were extracted from dispersions at predesigned reaction time (from left to right in each image: 1, 2, 3, 5, and 19 h). .... 63

**Figure 2-2:** FT-IR spectra of 3 nm SiNCs obtained from BP initiated reactions with indicated surface functionalities: a) hydride, b) dodecene, c) octyne, d) methyl-10-undecenoate, e) pentenoic acid, f) styrene, and g) phenylacetylene. .... 64

**Figure 2-3:** FT-IR spectra of 3 nm SiNCs obtained from AIBN initiated reactions with indicated surface functionalities: a) hydride, b) dodecene, c) octyne, d) methyl-10-undecenoate, e) pentenoic acid, f) styrene, and g) phenylacetylene. .... 65

**Figure 2-4:** <sup>1</sup>H NMR spectra in CDCl<sub>3</sub> containing 0.01% (v/v) TMS of dodecyl-SiNCs obtained from indicated functionalization method showing integration of dodecyl methyl

protons (3H) to TMS protons (12 H). Dodecyl methyl protons and chain methylene protons denoted by a and b respectively. Solvent impurities denoted by an asterisk (\*).

..... 67

**Figure 2-5:**  $^1\text{H}$  NMR spectra in  $\text{CDCl}_3$  containing 0.01% (v/v) TMS of a) methyl-10-undecenoate and b) pentanoic acid functionalized SiNCs obtained from BP initiated functionalization. Solvent impurities denoted by an asterisk (\*). ..... 68

**Figure 2-6:** EI-MS taken after reaction of dodecene and AIBN. No dodecene oligomeric species were detected. .... 71

**Figure 2-7:** EI-MS taken after reaction of dodecene and BP. No dodecene oligomeric species were detected. .... 72

**Figure 2-8:** NALDI-MS spectra of 3 nm dodecyl-passivated SiNCs functionalized at different predesigned reaction time using AIBN as reaction initiator: (a) background, (b) 1, (c) 2, (d) 3, (e) 5, and (f) 12 h in the range of 200-1500 m/z. .... 73

**Figure 2-9:** NALDI-MS spectra of 3 nm dodecyl-passivated SiNCs functionalized at different predesigned reaction time using AIBN as reaction initiator as: (a) background, (b) 1, (c) 2, (d) 3, (e) 5, and (f) 12 h in the range of 475-825 m/z. Note: These spectra are a “zoom-in” of those shown in Figure 2-8. .... 74

**Figure 2-10:** NALDI-MS spectra of 3 nm dodecyl-passivated SiNCs functionalized at different predesigned reaction time using BP as reaction initiator: (a) background, (b) 1, (c) 2, (d) 3, (e) 5, and (f) 12 h. Insets are the spectra in the range of 200-1500 m/z. .... 75

**Figure 2-11:** NALDI-MS spectra of 3 nm dodecyl-passivated SiNCs functionalized at different predesigned reaction time using BP as reaction initiator: (a) background, (b) 1, (c) 2,

(d) 3, (e) 5, and (f) 12 h. Insets are the spectra in the range of 475-825 m/z. Note: These spectra are a “zoom-in” of those shown in Figure 2-10. .... 76

**Figure 2-12:** NALDI-MS spectra of 3 nm styrene-passivated SiNCs functionalized using (a) AIBN or (b) BP as reaction initiator. Asterisks indicate background signals. Insets are the spectra in the range of 400-800 m/z. .... 77

**Figure 2-13:** High-resolution XPS spectra of silicon (2p) signals for SiNCs passivated with different ligands using BP as reaction initiator. Si (0), Si (I), Si (II), Si (III), and Si (IV) are denoted as (0), (I), (II), (III), and (IV), respectively. Black curves and circles correspond to the original data and fit spectra, respectively. Fitting results are shown for the Si 2p<sub>3/2</sub> components. The Si 2p<sub>1/2</sub> signals have been omitted for clarity. .... 79

**Figure 2-14:** High-resolution XPS spectra of silicon (2p) signals for SiNCs passivated with different ligands using AIBN as reaction initiator. Si (0), Si (I), Si (II), Si (III), and Si (IV) are denoted as (0), (I), (II), (III), and (IV), respectively. Black curves and circles are correspondent to original and fit spectra, respectively. Fitting results are shown for the Si 2p<sub>3/2</sub> components. The Si 2p<sub>1/2</sub> signals have been omitted for clarity. .... 80

**Figure 2-15:** Representative schematic highlighting the complexity of SiNC surfaces after functionalization with an alkene or alkyne (denoted as R) via radical initiated hydrosilylation with AIBN or BP. .... 81

**Figure 2-16:** FT-IR spectra of a) 8 nm and b) 5 nm dodecyl-SiNCs functionalized using BP and c) 8 nm and d) 5 nm dodecyl-SiNCs functionalized using AIBN. .... 83

**Figure 2-17:** Bright-field TEM and HRTEM images of dodecyl-passivated SiNCs of various sizes: ((a, d) 3 nm, (b, e) 5 nm and (c, f) 8 nm) functionalized using AIBN or BP as reaction initiator. .... 84

**Figure 2-18:** Size distribution of dodecyl-passivated SiNCs of various sizes: ((a, d) ~3 nm, (b, e) ~5 nm and (c, f) ~8 nm) functionalized using AIBN or BP initiator. Note: Particle size histograms were assembled by counting 200 SiNCs through the longest diameter present with Image J software. .... 85

**Figure 2-19:** Size-dependent PL spectra of dodecyl-functionalized SiNCs in toluene using (a) AIBN or (b) BP as initiator. (Excitation wavelength used,  $\lambda = 476$  nm.) ..... 86

**Figure 2-20:** FT-IR spectra of a) hydride-terminated SiNCs, b) TEMPO and c) TEMPO-capped SiNCs using AIBN, and d) TEMPO-capped SiNCs using BP. .... 87

**Figure 3-1:** Emission spectrum of compact fluorescent light source..... 97

**Figure 3-2:** A) FT-IR spectra of neat lipoic acid, H-SiNCs and LA-SiNCs (3 nm, 6 nm, and 8 nm). B) FT-IR spectra of neat dibutyl disulfide, H-SiNCs and DBDS SiNCs (3 nm and 6 nm). .... 102

**Figure 3-3:** High-resolution XPS spectra of silicon ( $2p_{3/2}$ ) and sulfur (2p) signals for 3, 6, and 8 nm LA-SiNCs. Fitting results for Si 2p are shown for the Si  $2p_{3/2}$  components while Si  $2p_{1/2}$  signals have been omitted for clarity. Si (0), Si (I), Si (II), Si (III), and Si (IV) are denoted as (0), (I), (II), (III), and (IV), respectively. For S 2p spectra, ‘bound’ refers to Si-S and ‘unbound’ indicates free sulfur. For all spectra, black curves and circles correspond to the original data and fit spectra, respectively. .... 105

**Figure 3-4:** High-resolution XPS spectra of silicon ( $2p_{3/2}$ ) and sulfur (2p) signals for 3 and 6 nm DBDS-SiNCs. Fitting results are shown for the Si  $2p_{3/2}$  components. Si  $2p_{1/2}$  signals

have been omitted for clarity. Si (0), Si (I), Si (II), Si (III), and Si (IV) are denoted as (0), (I), (II), (III), and (IV), respectively. For S 2p spectra, ‘bound’ refers to Si-S and ‘unbound’ indicates free sulfur. For all spectra, black curves and circles correspond to the original data and fit spectra, respectively..... 106

**Figure 3-5:** NALDI-MS spectra of A) 3 nm, B) 6 nm, C) 8 nm LA-SiNCs D) NALDI-MS spectrum of lipoic acid after exposure to fluorescent light. .... 108

**Figure 3-6:** TGA curves of LA-SiNCs with d = (A) 3 nm, (B) 6 nm, and (C) 8 nm..... 109

**Figure 3-7:** TGA curve of DBDS-SiNC with d = 3 nm..... 110

**Figure 3-8:** <sup>1</sup>H NMR spectra of A) 8 nm, B) 6 nm, and C) 3 nm LA-SiNCs. D) <sup>1</sup>H NMR spectra of neat lipoic acid. \* Denotes free lipoic acid and/or trace impurities..... 111

**Figure 3-9:** Representative schematic of the surface of SiNCs after reactions with A) lipoic acid or B) dibutyl disulfide. .... 112

**Figure 3-10:** TEM images LA-SiNCs with diameter: (a) 3 nm, (b) 5 nm, (c) 8 nm. TEM images of DBDS-SiNCs with diameter: (d) 3 nm, (e) 5 nm. (f) HRTEM image of LA-SiNCs with diameter 8 nm. .... 113

**Figure 3-11:** A) Photoluminescence spectra of LA-SiNCs (d = 3, 6, or 8 nm) functionalized with lipoic acid upon excitation at 350 nm. B) Photographs of LA-SiNCs (d = 3, 6, 8 nm) upon exposure to 365 nm light. C) Photoluminescence spectra of DBDS-SiNCs (d = 3 or 6 nm) upon excitation at 350 nm. D) Photographs of DBDS-SiNCs (d = 3, 6 nm) upon excitation at 365 nm. .... 115

**Figure 3-12:** Vials containing reaction mixtures A) immediately after B) and two weeks after the reactions of i) H-SiNCs (d = 3 nm) and lipoic acid heated to 45 °C and ii) H-SiNCs (d = 3 nm) and lipoic acid in subdued light and heat. .... 117

**Figure 4-1:** Characterization of dodecyl functionalized SiNCs. (A) FTIR spectrum of SiNCs. (B) Fluorescence spectrum of SiNCs with an inset of the nanocrystals displaying the red-orange luminescence atop UV benchtop. (C) TEM image of resulting nanocrystals and (D) the particle size distribution analysis of the SiNCs. Note: Particle size histograms were assembled by counting 200 SiNCs through the longest diameter present with Image J software..... 131

**Figure 4-2:** Fluorescence quenching spectra of SiNCs by increasing concentrations of (A) NB, (B) MNT, (C) DNT in solution with an inset showing the quenching effect with 0 and 25 mM DNT atop bench-top UV-lamp. (D) The Stern-Volmer plot for the quenching efficiencies of NB, MNT and DNT at different concentrations. .... 133

**Figure 4-3:** The PL lifetimes of SiNCs with varying concentrations of (A) NB, (B) MNT, and (C) DNT in solution. (D) The Stern-Volmer plot for the PL lifetime decays of SiNCs of NB, MNT, and DNT at different concentrations. .... 136

**Figure 4-4:** Solution spot tests of A) nitroaromatics NB, MNT, and DNT (left to right: 2  $\mu$ L aliquots of 0.25, 5 and 25 mM, in toluene) or B) toluene (2  $\mu$ L)..... 138

**Figure 4-5:** Images of SiNC coated filter paper under a handheld UV-lamp without the presence of nitrocompounds and in the presence of solutions of TNT, PETN, and RDX as indicated. .... 139

**Figure 4-6:** Solid DNT residue testing onto SiNC filter paper by (A) cotton swab tips having different amounts of DNT, the DNT residue left after visibly brushing off 0.5 mg DNT from a (B) plastic tray and a (C) cotton fabric, respectively..... 140

**Figure 4-7:** Solid DNT residue testing on glove. The gloved finger was “finger-printed” successively onto the luminescent filter paper up to four times. .... 140

<b>Figure 4-8:</b> Images of (A) a spotted filter paper with SiNCs, (B) a gloved finger with trace amounts of solid TNT, (C) application of solid TNT to the coated filter paper, and (D) observed quenching of luminescent filter paper after contact with the solid TNT residue....	141
<b>Figure 4-9:</b> Images of SiNC impregnated filter paper under a handheld UV-lamp (A) without the presence of nitrobenzene vapor, (B) after quenching with nitrobenzene vapor, and (C) the quenched filter paper after 2 min in N <sub>2</sub> airstream. ....	142
<b>Figure 4-10:</b> Characterization of pentanoic acid functionalized SiNCs. (A) FTIR spectrum of SiNCs. (B) Fluorescence spectrum of SiNCs. (C) TEM image of resulting nanocrystals.....	144
<b>Figure 4-11:</b> Reaction setup for esterification of pentanoic acid functionalized SiNCs to non-fluorescent TLC plates. ....	146
<b>Figure 4-12:</b> UV illumination images of (A) non-fluorescent TLC plate before modification with SiNCs, (B) luminescent TLC plate after surface modification with SiNCs, (C) multilane image of developed TLC plate lanes (1) MNT and (2) DNT using a mixture of 1:1 of CH <sub>2</sub> Cl <sub>2</sub> : hexanes (D) separation of a mixture of MNT and DNT using a mixture of 1:1 of CH <sub>2</sub> Cl <sub>2</sub> : hexanes. ....	147
<b>Figure 5-1:</b> Various types of biogenic amines. ....	151
<b>Figure 5-2:</b> FT-IR (A) and photoluminescence (B) spectra for i) alkyl oligomer, ii) alkyl monolayer and iii) ester monolayer functionalized SiNCs. ....	162
<b>Figure 5-3:</b> TEM and particle size distribution for alkyl oligomer (A-B), alkyl monolayer (C-D), and ester monolayer (E-F) functionalized SiNCs. Note: Particle size histograms were assembled by counting 200 SiNCs through the longest diameter present with Image J software. ....	163

**Figure 5-4:** Photoluminescence quenching spectra of SiNCs functionalized with A) alkyl oligomer, B) alkyl monomer, or C) ester monolayer by increasing concentrations of allylamine in solution in the range of 0 and 0.5 M. .... 165

**Figure 5-5:** Photoluminescence quenching spectra of SiNCs with increasing concentrations of (A) putrescine, (B) spermidine, and (C) putrescine (D) A Stern-Volmer plot for the quenching efficiencies of putrescine, spermidine and cadaverine. .... 166

**Figure 5-6:** The Stern-Volmer plot for the quenching efficiencies of putrescine, spermidine and cadaverine at different concentrations. .... 170

**Figure 5-7:** Photoluminescence spectra of PDMS A) film and B) sponge containing SiNCs. Insets are images of materials upon exposure to a benchtop UV lamp. SEM images of PDMS C) film containing SiNCs and D) sponge containing SiNCs. .... 172

**Figure 5-8:** Custom vapor sensing experimental setup. The bubbler filled with analyte of interest is connected to a carrier gas (argon), that is then passed through the gas chamber holding the PDMS film sponge containing SiNCs sensor. The sensor is excited by the LED ( $\lambda = 405 \text{ nm}$ ) and the luminescence is first passed through a longpass filter ( $\lambda = 550 \text{ nm}$ ) before collection by the optical fiber. .... 174

**Figure 5-9:** PDMS A) film B) sponge containing SiNCs luminescence intensity after exposure to LED excitation source (405 nm) under argon gas (4 L/min). PDMS C) film D) sponge containing SiNCs luminescence intensity over time after exposure to LED excitation source in 10 min intervals under argon gas (4 L/min). .... 175

**Figure 5-10:** PDMS film (A) and PDMS sponge (B) containing SiNCs luminescence intensity over time after exposure to putrescine vapor (4 L/min). The line of best fit of PDMS film (A) and PDMS sponge (B) is shown as the black line. .... 177

**Figure 5-11:** PDMS film (A) and PDMS sponge (B) containing SiNCs luminescence intensity over time after exposure to water vapor (4 L/min). PDMS film (C) and PDMS sponge (D) containing SiNCs luminescence intensity over time after exposure to 100 % ethanol vapor (4 L/min). The dashed red line indicates the time at which water or ethanol vapor was introduced into the system. .... 178

**Figure 5-12:** PDMS film (A) and PDMS sponge (B) containing SiNCs maximum luminescence intensity over period of 4 days at room temperature after raw food exposure. PDMS film (C) and PDMS sponge (D) containing SiNCs maximum luminescence intensity over period of 4 days at 4 °C after raw food exposure. .... 180

**Figure 5-13:** Digital images of PDMS film and PDMS sponge containing SiNCs substrates exposed to raw pork, salmon, chicken, beef or pickerel for 0 - 24 h at room temperature. (Note: Ambient light passed through 550 nm filter, UV light,  $\lambda=365$  nm) ..... 182

**Figure 6-1:** Images of a SiNC-silica aerogel hybrid material a) before, b) partial and c) complete exposure to nitrobenzene. Image reproduced with permission from *Chem. Mater.*, **2016**, *28*, 3877-3886 (reference 403). Copyright 2016 American Chemical Society. .... 195

## List of Schemes

- Scheme 1-1:** Solution-based reduction methods to produce SiNCs. Adapted with permission from *Chem. Soc. Rev.*, **2014**, *43*, 2680-2700 (reference 63). Copyright 2014 Royal Society of Chemistry..... 11
- Scheme 1-2:** Schematic of the use of Zintl salts/metal silicides for the production of SiNCs. Reproduced and adapted with permission from *Inorg. Chem.*, **2015**, *54*, 396-401 (reference 92), *Chem. Comm.*, **2006**, 4160-4168 (reference 62), and *Angew. Chem. Int. Ed.*, **2016**, *55*, 2322-2339 (reference 93). Copyrights 2015 American Chemical Society, 2006 Royal Society of Chemistry, and 2016 Wiley-VCH..... 12
- Scheme 1-3:** Reaction scheme of common gas phase methods for the production of SiNCs. Note photoluminescence color can be tuned across the visible spectrum. Reproduced and adapted with permissions from *Angew. Chem. Int. Ed.*, **2016**, *55*, 2322-2339 (reference 93). Copyright 2016 Wiley-VCH..... 13
- Scheme 1-4:** The synthesis of SiNCs ( $d = 3$  nm) embedded in silica from the thermal decomposition of HSQ. Note: The form of HSQ used for SiNC synthesis is  $(\text{HSiO}_{1.5})_n$ . ..... 15
- Scheme 1-5:** Reaction scheme of possible hydrosilylation methods used for SiNCs..... 19
- Scheme 1-6:** Schematics of a) porous silicon and dichalcogenides and c) H-SiNCs and dodecanthiol. Adapted and reproduced with permission from *ACS Appl. Mater. Interfaces*, **2016**, *8*, 11091-11099 (reference 174) and *Langmuir*, **2015**, *31*, 6886-6893 (reference 125). Copyright 2015 and 2016 American Chemical Society. .... 21

<b>Scheme 1-7:</b> Recent reactivity shown on hydride-SiNCs. Reproduced and adapted with permissions from <i>Angew. Chem. Int. Ed.</i> , <b>2016</b> , 55, 2322-2339 (reference 93). Copyright 2016 Wiley-VCH.....	24
<b>Scheme 1-8:</b> Various surface modifications on chlorinated SiNC surfaces. Reproduced and adapted from <i>Chem. Comm.</i> , <b>2006</b> , 4160-4168 (reference 62). Copyright 2006 Royal Society of Chemistry.....	25
<b>Scheme 2-1:</b> Synthesis and radical initiated functionalization of 3 nm SiNCs. Additional annealing at 1200 °C (d = 5 nm) and 1300 °C (d = 8 nm) prior to HF etching is required to achieve larger particles. Note: The HSQ used for SiNC synthesis is in its polymeric form (HSiO <sub>1.5</sub> ) <sub>n</sub> , as mentioned in Section 1.3.4.....	62
<b>Scheme 2-2:</b> Mechanism of SiNC surface hydrosilylation driven by pyrolysis of radical initiators as proposed previously by Linford and Chidsey. <sup>136,181</sup> .....	88
<b>Scheme 3-1:</b> Fluorescent light induced functionalization of H-SiNCs with A) lipoic acid or B) dibutyl disulfide. ....	100
<b>Scheme 3-2:</b> Proposed reaction mechanisms for H-SiNCs reacted with a) lipoic acid or b) dibutyl disulfide via fluorescent light.....	118
<b>Scheme 4-1:</b> Proposed electron transfer quenching mechanism of SiNCs by nitroaromatic compounds, where CB and VB represent the conduction band and the valence band, respectively. ....	135
<b>Scheme 4-2:</b> Schematic representation of the preparation and use of SiNC based sensor paper. (1) A piece of filter paper is dip coated in a solution of concentrated SiNCs, (2) the resulting paper is fluorescent under UV light ( $\lambda = 365$ nm), (3) nitroaromatic solution	

is spotted onto the sensing paper, and (4) quenching of the spot is observed under UV light ( $\lambda = 365$ nm). .....	137
<b>Scheme 4-3:</b> Steglich esterification of pentenoic acid functionalized SiNCs with non-fluorescent TLC plates.....	146
<b>Scheme 5-1:</b> Proposed electron transfer quenching mechanism of SiNCs by biogenic amine compounds, where $e^-$ , $h^+$ , CB and VB represent an electron, hole, conduction band and the valance band, respectively. ....	167
<b>Scheme 5-2:</b> Preparation of A) PDMS films containing SiNCs and B) PDMS sponges containing SiNCs. ....	171
<b>Scheme 6-1:</b> A) The modification of lipoic acid with dodecanol or polyethylene glycol by Steglich Esterification using <i>N,N'</i> -dicyclocarbodiimide (DCC) and 4-(dimethylamino)pyridine (DMAP). <sup>359</sup> B) The functionalization of SiNCs with modified lipoic acid molecules by a fluorescent light source. ....	189
<b>Scheme 6-2:</b> Reaction of SiNCs with various thioketones at room temperature (RT). ....	190
<b>Scheme 6-3:</b> Proposed reaction scheme to generate a SiNC ratiometric sensor. A) Reaction of blue-emitting $NH_2$ terminated SiNCs <sup>83</sup> reacted with tetraethyl orthosilicate (TEOS) to generate silica coated SiNCs (SiNC@SiO <sub>2</sub> ). <sup>394</sup> B) Coupling of SiNC@SiO <sub>2</sub> with acid terminated SiNCs to achieve sensor material. <sup>148,359</sup> C) Use of prepared sensor in the presence of an analyte. ....	192
<b>Scheme 6-4:</b> Schematic for the preparation of SiNC@MIP and the sensing mechanism.....	194

## List of Symbols, Nomenclature, and Abbreviations

°C:	Degrees Celsius
<sup>1</sup> H NMR:	Proton nuclear magnetic resonance spectroscopy
a.u.:	Arbitrary units
Å:	Angstrom
ACh:	Acetylcholine
AChE:	Acetylcholinesterase
AIBN:	2,2'-azobis(2-methylpropionitrile)
BDE:	Bond dissociation energy
BP:	Benzoyl peroxide
BR:	Britton-Robinson
CB:	Conduction band
ChOx:	Choline oxidase
CMOS:	Complementary metal-oxide-semiconductor
CTAB:	Cetyltrimethylammonium bromide
CTC:	Chlorotetracycline
d(avg):	Diameter (average)
DBDS:	Dibutyl disulfide
DBDS-SiNCs:	Ddibutyl disulfide functionalized silicon nanocrystals
DCC:	<i>N,N'</i> -dicyclocarbodiimide
DLS:	Dynamic light scattering
DMAP:	(Dimethylamino)pyridine
DNT:	Dinitrotoluene

DOS:	Density of states
$e^-$ :	Electron
Eg:	Band gap
EI-MS:	Electron spray ionization-mass spectrometry
EMA:	Effective Mass Approximation
ET:	Electron transfer
FRET:	Fluorescence resonance energy transfer
FT-IR:	Fourier transform-infrared spectroscopy
GOx:	Glucose oxidase
h:	Hour(s)
$\hbar$ :	Planck's constant
$h^+$ :	Hole
HERBM:	High energy reactive ball milling
HF:	Hydrofluoric acid
HOMO:	Highest occupied molecular orbital
HRTEM:	High resolution transmission electron microscopy
H-SiNCs:	Hydride-terminated silicon nanocrystals
HSQ:	Hydrogen silsesquioxane
IUPAC:	International Union of Pure and Applied Chemists
K:	Kelvin
$K_{sv}$ :	Stern Volmer constant
LA:	Lipoic acid
LA-SiNCs:	Lipoic acid functionalized silicon nanocrystals

LED:	Light emitting diode
LOD:	Limit of detection
LUMO:	Lowest unoccupied molecular orbital
min:	Minute(s)
MIP(s):	Molecularly imprinted polymer(s)
MNT:	Mononitrotoluene
NALDI-MS:	Nanostructured-assisted laser desorption/ionization mass spectrometry
NB:	Nitrobenzene
NC(s):	Nanocrystal(s)
nm:	Nanometer
OTC:	Oxytetracycline
PAMAM-OH:	Hydroxyl poly(amidoamine)
PBS:	Phosphate buffered saline
PDMS:	Polydimethylsiloxane
PEG:	Polyethylene glycol
PETN:	Pentaerythritol tetranitrate
PL:	Photoluminescence
ppm:	Parts per million
PTFE:	Polytetrafluoroethylene
PVC:	Poly-vinyl chloride
QD:	Quantum dot
QD@MIP:	Quantum dot encapsulated in a molecular imprinted polymer shell
RDX:	Cyclotrimethylenetrinitramine

R <sub>f</sub> :	Retention factor
rpm:	Rotations per minute
RT:	Room temperature
SEM:	Scanning electron microscopy
SiNC(s):	Silicon nanocrystal(s)
SiNC@SiO <sub>2</sub> :	Silicon nanocrystal encapsulated in a silicon shell
SiNC-TLC:	Silicon nanocrystal coupled TLC plate
SRO:	Silicon rich oxide
TC:	Tetracycline
TEM:	Transmission electron microscopy
TEMPO:	2,2,6,6-tetramethyl-1-piperidinyloxy
TEOS:	Tetraethyl orthosilicate
TGA:	Thermogravimetric analysis
THF:	Tetrahydrofuran
TLC:	Thin layer chromatography
TMB:	3,3',5,5'-tetramethylbenzide
TMS:	Tetramethylsilane
TNP:	Trinitrophenol
TNT:	Trinitrotoluene
TOAB:	Tetraoctyl ammonium bromide
UV:	Ultraviolet
VB:	Valence band
W:	Watt

XPS: X-ray photoelectron spectroscopy

$\tau$ : Lifetime

# Chapter 1

## Introduction.<sup>1</sup>

---

<sup>1</sup> A portion of this chapter has been published:

Gonzalez, C. M. and Veinot, J. G. C. *Journal of Materials Chemistry C* **2016**, *31*, 10540-10548.

## 1.1 Nanotechnology and quantum dots

“I would like to describe a field, in which little has been done, but in which an enormous amount can be done in principle...What I want to talk about is the problem of manipulating and controlling things on a small scale.”<sup>1</sup> These words were spoken by Richard Feynman in his speech, “There’s Plenty of Room at the Bottom,” delivered at the 1959 American Physical Society Annual Meeting, in which he envisioned and encouraged the audience to consider the advantages of studying the properties of nanoscale materials; and thus the modern age of nanotechnology began. The term “nanotechnology” was first used by Norio Taniguchi in 1974 at the International Conference on Precision Engineering.<sup>2</sup> A more current definition suggested by the National Aeronautics and Space Administration (NASA) is, “the creation of functional materials, devices, and systems through the control of matter on the nanometer length scale (1-100 nm), and exploitation of novel phenomena and properties.”<sup>2</sup> Types of nanostructures (*i.e.*, structures that have at least one dimension between 1 and 100 nm) that have been developed and investigated include two- (*e.g.*, nanosheets), one- (*e.g.*, nanowires), and zero- (*e.g.*, nanoparticles) dimensional structures.<sup>3</sup>

Why are these nanostructures of such interest to researchers? While bulk materials have been studied by scientists for years, nanostructured materials have not.<sup>4</sup> Once a material is the size of 1-100 nm, size and shape dependent properties became apparent and are different than those observed for molecular or bulk systems.<sup>4</sup> Also of significant importance, is the change in the surface/volume ratio, resulting in many atoms being located on the surface of the materials as opposed to the interior. Some of the observed changes in materials related to nanoscale size include thermal,<sup>5,6</sup> electrical,<sup>7,8</sup> optical,<sup>4,9</sup> and magnetic<sup>10,11</sup> properties.

One important class of nanomaterials is semiconductor quantum dots (QDs). These materials are classified as zero-dimensional (confined in all three spatial dimensions) semiconductor materials with the size of the order of or smaller than the Bohr exciton (electron-hole pair) radius.<sup>12</sup> Since their discovery in the 1980s by Brus and coworkers,<sup>13,14</sup> QDs have been one of the major advances in materials science over the past three decades.<sup>15</sup> A recent editorial by Kamat highlighted this impact based on the number of published papers and their citations over the 25-year period of 1991 and 2016 (Figure 1-1).<sup>16</sup> Within the last 5 years, an average of 1800-2000 papers concerning semiconductor QDs are published annually (Figure 1-1).<sup>16</sup> These materials can be classified into different groups, for example, group II-VI (*e.g.*, CdS, CdSe, CdTe, ZnS, ZnSe, *etc.*),<sup>17-19</sup> group III-V (*e.g.*, GaAs, InP, InAs, *etc.*),<sup>20-23</sup> group IV (*e.g.*, Si, Ge, *etc.*),<sup>24,25</sup> and group IV-VI (*e.g.*, SnS, PbS, PbSe, *etc.*)<sup>26-28</sup> have all been studied. The interest in these materials has largely arisen due to their size and shape-tailorable luminescence that is stable against photobleaching.<sup>15</sup>

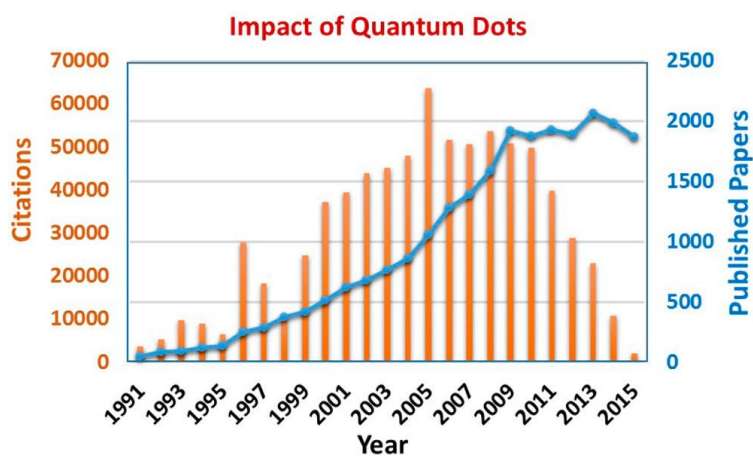


**Figure 1-1:** A plot displaying the number of published papers and citations of semiconductor QDs in the 25 years between 1991-2016. Note: The data was collected during the first week of Jan 2016, with data from 2015 being partial. Reproduced with permission from *J. Phys. Chem. Lett.* **2016**, 7, 584-585 (reference 16). Copyright 2016 American Chemical Society

What causes this highly desirable size and shape-tailorable QD luminescence? To answer this question, it is first necessary to briefly discuss the structure of extended solids. In these structures, a large number of discrete energy levels combine to create a continuous band.<sup>29</sup> Semiconductors contain bands known as the valence band (VB) and conduction band (CB) and are separated by forbidden levels known as the band gap ( $E_g$ ) shown in Figure 1-2.<sup>30</sup> The luminescence observed in QDs occurs when an electron is excited from the VB to the CB, creating an electron-hole pair (exciton). The relaxation of the CB electron to fill the hole of the VB (recombination), is usually accompanied by light emission or heat.<sup>2</sup> The tailorability of the luminescence arising from the size and shape of the QDs results from quantum confinement. The density of states (DOS) of the VB and CB are not uniform, and are densest at the centers (where they are centered about atomic energy levels) of the bands, and are sparse at the edges.<sup>9,30</sup> Therefore, as the size of the QD decreases, the number of orbitals decreases, resulting in the continuous band edges to become discrete, and the  $E_g$  to widen and shift to a higher energy (Figure 1-2).<sup>31</sup> This results in the  $E_g$  varying with QD dimensions. This is a quantum effect because it is governed by the nature of standing waves of the confined system rather than by a fraction of atoms at the surface.<sup>30</sup> This change in the  $E_g$  with size/dimension, causes the change in luminescence emission maxima as depicted in Figure 1-2.

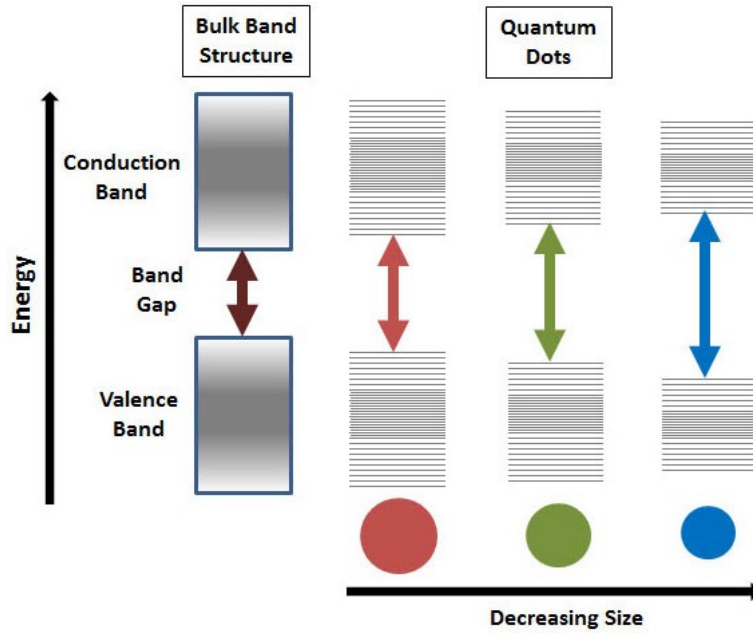


**Figure 1-2:** Image relating the changes in band structure and band gap as a function of size in quantum dots. (Image taken from [www.sigmaaldrich.com](http://www.sigmaaldrich.com))

One model to describe the relation between nanoparticle size and the band gap is the effective mass approximation (EMA; Equation 1-1):

$$E(R) = E_g + \frac{\hbar^2 \pi^2}{2R^2} \left( \frac{1}{m_e^*} + \frac{1}{m_h^*} \right) - \frac{1.786e^2}{\epsilon_r R} + 0.284 E_R \quad \text{Equation 1-1}$$

where  $R$  is the diameter of the nanocrystal,  $E_g$  is the band gap of the bulk material,  $\hbar$  is Planck's constant,  $m_e^*$  and  $m_h^*$  represent the effective mass of the electron and hole, respectively,  $e$  is the charge of the electron,  $\epsilon_r$  is the relative permittivity, and  $E_R$  is the Rydberg energy for the bulk semiconductor and is material dependent.<sup>2</sup> Based on this relationship, it can be seen that the absorption energy of the QDs will shift to a higher frequency with decreasing diameter of the QDs,

and is dependent of  $1/R^2$ . This can be seen from the reflected colors of QDs with varying diameters, shifting from blue to red with increasing size (Figure 1-2).

In contrast to organic fluorophores, QDs exhibit large Stokes shifts and high luminescence quantum yields.<sup>32,33</sup> Also adding to their appeal, is their tunable functionalization/capping of the QD surface allows for integration into many platforms.<sup>32</sup> These properties have led to potential QD applications in light-emitting diodes,<sup>34</sup> bioimaging,<sup>35</sup> and sensors.<sup>15</sup> Unfortunately, group II-VI and group III-V QDs have inherent toxicity,<sup>36-38</sup> and therefore the exploration and exploitation of alternative non-toxic materials, such as silicon nanocrystals, is of the utmost importance.

## 1.2 Silicon Nanocrystals

Silicon nanocrystals (SiNCs) have intrigued researchers partly due to their advantages compared to other existing QDs such as their source material (*i.e.*, silicon) is abundant, they exhibit limited toxicity, they are well-suited for integration with existing technology, and they display photoluminescence that is not observed in bulk silicon.<sup>39-42</sup> While porous silicon was discovered in the 1956,<sup>43</sup> it was not until 1990 when Canham demonstrated the material was luminescent.<sup>44</sup> Porous silicon is produced during anodic galvanostatic, chemical or photochemical etching of monocrystalline silicon in the presence of hydrofluoric acid (HF).<sup>45</sup> Pore sizes in the range of a few nanometers to a few micrometers can be obtained during the etching process by changing the concentration of HF in the electrolyte, the current density, surfactant type, and the density of silicon dopants and the illumination process, while the etching time determines the pore length.<sup>46-48</sup> It may seem odd that the observation of luminescence from porous silicon took over 30 years to discover, however, bulk silicon is deemed to have a forbidden optical band gap transition, making luminescence unlikely. This is because bulk silicon, an intrinsic semiconductor, has an indirect

band gap of 1.12 eV at 300 K.<sup>2,49</sup> A comparison between direct and indirect band gap materials can be seen in Figure 1-3. A direct band gap material (Figure 1-3a) has the maximum of the VB and the minimum of the CB located in the same coordinate in  $k$ -space, allowing for the electron-hole recombination to occur without any change in momentum. However, for indirect band gap materials like silicon, the VB maximum and the CB minimum are not in the same coordinate in  $k$ -space (Figure 1-3b), so in order for promotion or relaxation to occur between the band gap, the electron needs to have a shift in momentum that is disallowed by symmetry and the Law of Conservation of Momentum (*i.e.*, energy would not be conserved).<sup>2,50</sup> Therefore, an indirect recombination mechanism occurs in where an interstitial defect or lattice vibrations (phonon) captures the electron to facilitate the recombination and is accompanied by the release of a phonon, rather than light emission.<sup>2,51</sup>

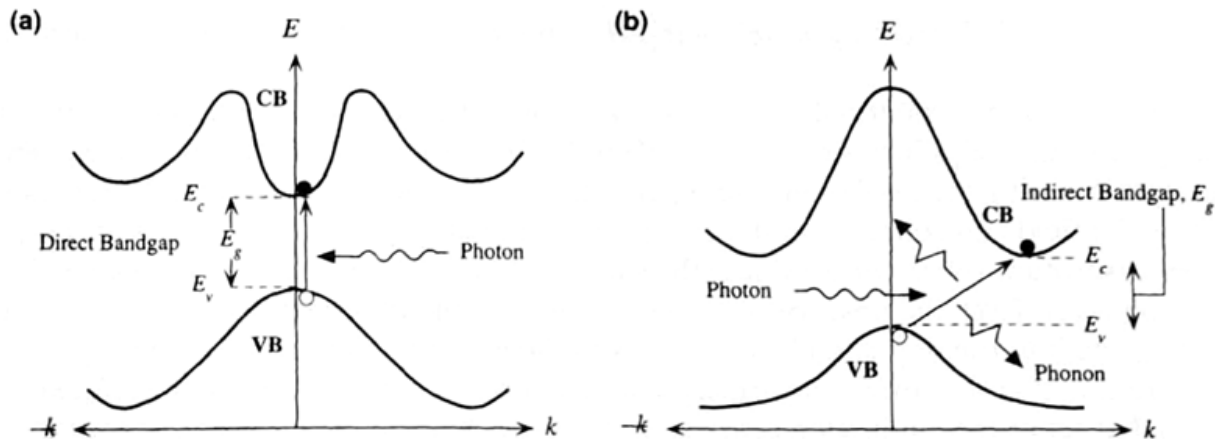


**Figure 1-3:** Comparison of a) direct bandgap and b) indirect band gap materials. (Image reproduced and modified from reference 51.)

Canham proposed, that fabricating silicon structures small enough (*i.e.*, less than the Si Bohr exciton radius, 4.5 nm) to exploit quantum confinement effects on the band structures, could

overcome the low probability of intrinsic radiative recombination.<sup>44</sup> As the size of silicon decreases to the order of or smaller than the Bohr exciton radius, the electron and hole (exciton) are confined, causing a relaxation of the momentum conservation. This is based on the Heisenberg uncertainty principle,  $\Delta q \sim 1/R$ , where  $\Delta q$  is the wavevector uncertainty and  $R$  is the radius of the SiNC.<sup>52,53</sup> As the SiNC becomes smaller, the  $\Delta q$  becomes comparable to the change in momentum ( $\Delta k$ ) and therefore leads to an enhancement of the probability of recombination occurring.<sup>52</sup>

The tuning of the emission of SiNCs by changing the size of the particle has been reported and appears to follow the quantum confinement effect.<sup>54,55</sup> In a 2013 study conducted on single freestanding SiNCs, scanning tunneling spectroscopy measurements on dodecyl functionalized SiNCs indicated an increase in the band gap ( $E_g$ ) with decreasing SiNC size.<sup>55</sup> However, quantum confinement being the sole cause of SiNC luminescence is the subject of ongoing debate. Also shown to effect the luminescent properties, are different surface passivation groups which could lead to size-independent luminescence across the visible spectra.<sup>55,56</sup> The effect of surface states is described in further detail in Section 1.4.3.

Since the observation of luminescent porous silicon, the development of luminescent silicon nanostructures<sup>50</sup> such as silicon nanosheets,<sup>57,58</sup> nanowires,<sup>59-61</sup> and nanocrystals<sup>62,63</sup> have been reported. SiNCs have been implemented in many areas of application including catalysis,<sup>64</sup> photonics,<sup>65</sup> electronics,<sup>66</sup> photovoltaics,<sup>67,68</sup> water remediation,<sup>69</sup> bioimaging,<sup>70,71</sup> and sensors.<sup>72</sup> A detailed discussion of SiNCs for the use of sensing platforms is presented in Section 1.5. The remainder of this thesis will focus on SiNCs.

## 1.3 Synthesis of SiNCs

There have been a variety of reported synthetic methods developed for the synthesis of SiNCs. In this section, key examples are summarized into four categories: top-down (mechanical), solution-phase (bottom-up), gas-phase, and solid-state.

### 1.3.1 Top-down Methods

The use of silicon wafers is a straight-forward method to generate SiNCs. One example of a top-down methodology involves the ultrasonication of porous silicon to yield photoluminescent particles.<sup>73-75</sup> It was shown that the size and shape of the resulting SiNCs is dependent on both the etching process and sonication time. Alternatively, mechanochemical ball milling of bulk silicon can also yield SiNCs.<sup>76,77</sup> By using high energy reactive ball milling (HERBM), SiNCs can simultaneously be produced and functionalized with a variety of ligands (*i.e.*, n-alkynes, alkenes, aldehydes, carboxylic acids and alcohols) and all displayed blue luminescence (Figure 1-4).<sup>76,77</sup> Recent work on using ball milling incorporate the use of an inert salt buffer (*i.e.*, LiCl) to limit the formation of amorphous SiNCs produced.<sup>78</sup>

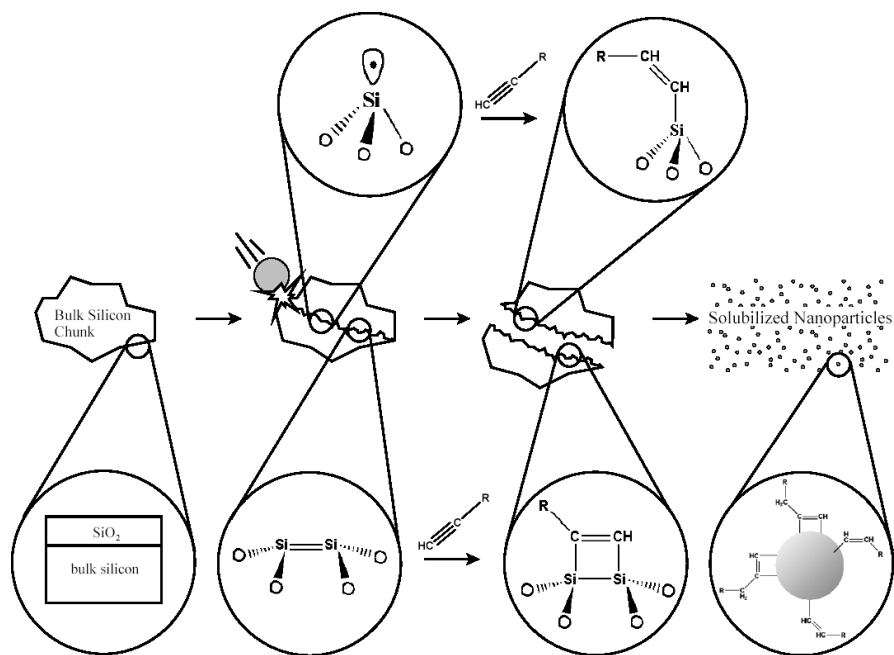
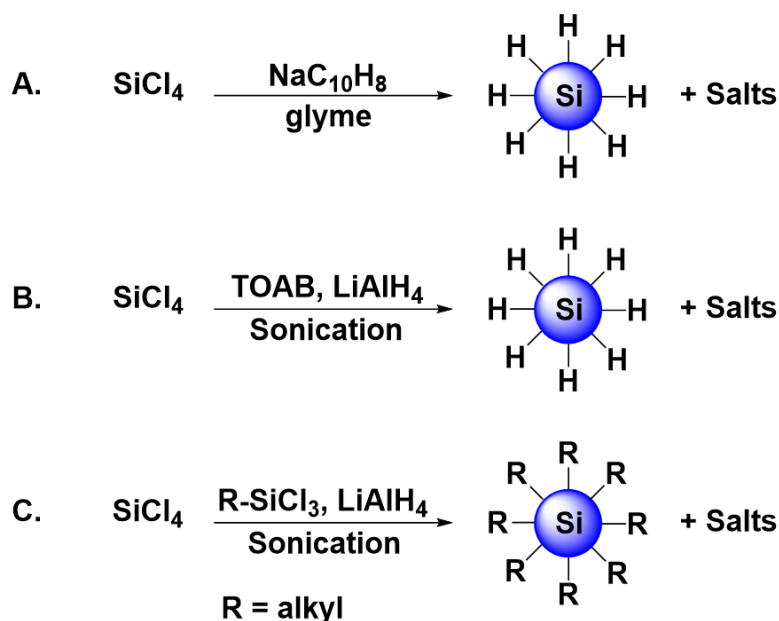


**Figure 1-4:** Illustration of high energy reactive ball milling to simultaneously produce and functionalize SiNCs. Image reproduced with permission from *Adv. Mater.* **2007**, *19*, 3984-3988 (reference 76). Copyright 2007 Wiley-VCH.

### 1.3.2 Bottom-up/Solution-based

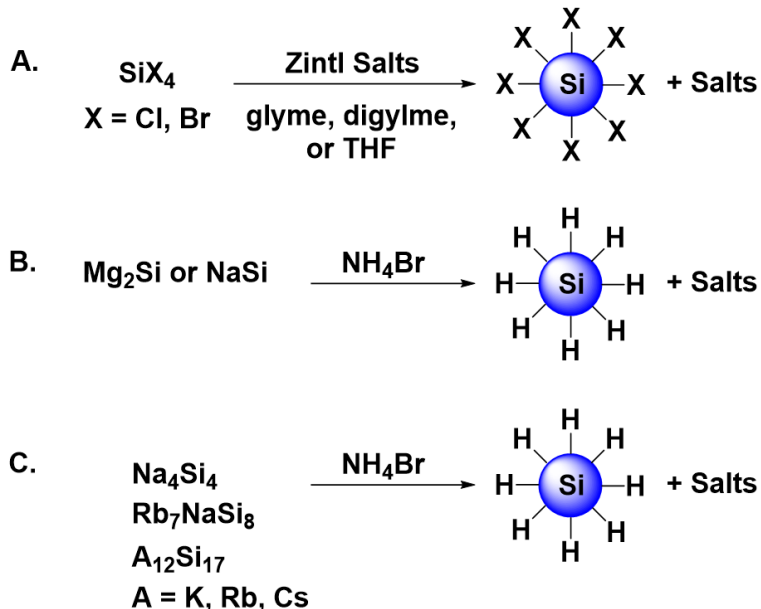
The most commonly employed method for preparing SiNCs involves solution-phase synthesis. The field was widely developed after Heath's initial report involving the reaction of  $\text{SiCl}_4$  and octyltrichlorosilane at high temperature ( $385\text{ }^\circ\text{C}$ ) and pressure ( $> 100\text{ atm}$ ) for a period of 3-7 days to produce a low yield of polydispersed ( $d = 2\text{-}9\text{ nm}$ ) SiNCs.<sup>79</sup> Other reduction methods use  $\text{SiCl}_4$  as the silicon source along with sodium metal with tetraethyl orthosilicate (TEOS)<sup>80</sup> or sodium naphthalenide ( $\text{NaC}_{10}\text{H}_8$ ) in glyme (dimethoxyethane),<sup>81</sup> however, these methods resulted in polydisperse particles that exhibited only blue luminescence (Scheme 1-1). Further investigation involved  $\text{SiCl}_4$  as a silicon source and  $\text{LiAlH}_4$  as a reducing agent; a surfactant (*e.g.*, tetraoctyl ammonium bromide, TOAB) was employed to arrest particle growth.

This procedure generated hydride-terminated SiNCs (H-SiNCs).<sup>82-84</sup> Variations of this method also saw alkyl silanes used as capping agents.<sup>85</sup> These arrested growth methods provided SiNCs of relatively narrow size distributions that showed blue photoluminescence. An unfortunate drawback of these reaction conditions using LiAlH<sub>4</sub> is the formation of pyrophoric silane.<sup>86</sup>



**Scheme 1-1:** Solution-based reduction methods to produce SiNCs. Adapted with permission from *Chem. Soc. Rev.*, **2014**, *43*, 2680-2700 (reference 63). Copyright 2014 Royal Society of Chemistry.

Another class of solution-based methods exploit the reaction of Zintl salts with silicon halides, ammonium bromide or bromine. Zintl salts (NaSi,<sup>87</sup> KSi,<sup>88</sup> and Mg<sub>2</sub>Si<sup>89</sup>) reduce SiCl<sub>4</sub> in solutions of glyme, diglyme or THF (Scheme 1-2). Also, the reaction of magnesium silicide (MgSi<sub>2</sub>) with Br<sub>2</sub> under reflux also produced SiNCs.<sup>90,91</sup> A recent study also showed the Zintl phases, Na<sub>4</sub>Si<sub>4</sub>, Rb<sub>7</sub>NaSi<sub>8</sub> and A<sub>12</sub>Si<sub>17</sub> (A = K, Rb, Cs), could also be used as precursors for the synthesis of SiNCs.<sup>92</sup> Again, all SiNCs produced via Zintl salts/phases and magnesium silicide displayed blue luminescence.<sup>93</sup>



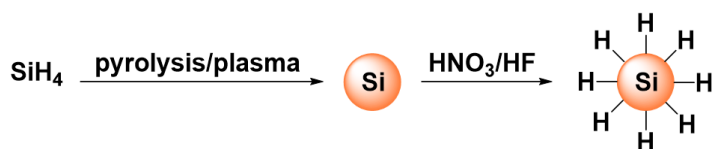
**Scheme 1-2:** Schematic of the use of Zintl salts/metal silicides for the production of SiNCs. Reproduced and adapted with permission from *Inorg. Chem.*, **2015**, *54*, 396-401(reference 92), *Chem. Comm.*, **2006**, 4160-4168 (reference 62), and *Angew. Chem. Int. Ed.*, **2016**, *55*, 2322-2339 (reference 93). Copyrights 2015 American Chemical Society, 2006 Royal Society of Chemistry, and 2016 Wiley-VCH.

### 1.3.3 Gas-Phase Methods

Multiple gas-phase methods have been reported that afford SiNCs; they typically involve the pyrolysis of silane ( $\text{SiH}_4$ ) gas (Scheme 1-3). Murthy *et al.* first reported gas-phase synthesis of SiNCs in 1976, by the thermal decomposition of silane in hydrogen at high temperature (1000 - 1100 °C) to obtain octahedral SiNCs (30 - 80 nm).<sup>94</sup> It was later shown by Cannon *et al.* that exposure to a  $\text{CO}_2$  laser could induce silane pyrolysis and generate gram quantities of agglomerated silicon particles.<sup>95,96</sup> However, these early reports of SiNCs generation via pyrolysis

did not display luminescence unless they were subsequently etched with HF.<sup>97-99</sup> Swihart and coworkers further showed this laser pyrolysis method could lead to SiNC production rates at ~20-200 mg/h, tunable luminescence across the visible spectrum, and high photoluminescent quantum yields (as high as 39%).<sup>100-102</sup>

An alternative method to laser pyrolysis uses non-thermal plasma, or “hot electrons” within the plasma to induce the decomposition of silane.<sup>103</sup> Plasma-based pyrolysis systems for the generation of SiNCs can also result in size-based luminescence across the visible spectrum as seen in Figure 1-5.<sup>104</sup>



**Scheme 1-3:** Reaction scheme of common gas phase methods for the production of SiNCs. Note photoluminescence color can be tuned across the visible spectrum. Reproduced and adapted with permissions from *Angew. Chem. Int. Ed.*, **2016**, *55*, 2322-2339 (reference 93). Copyright 2016 Wiley-VCH.

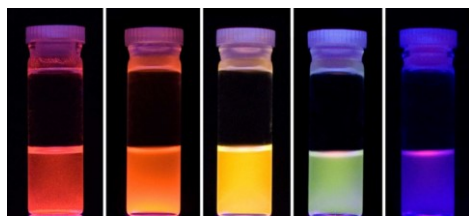


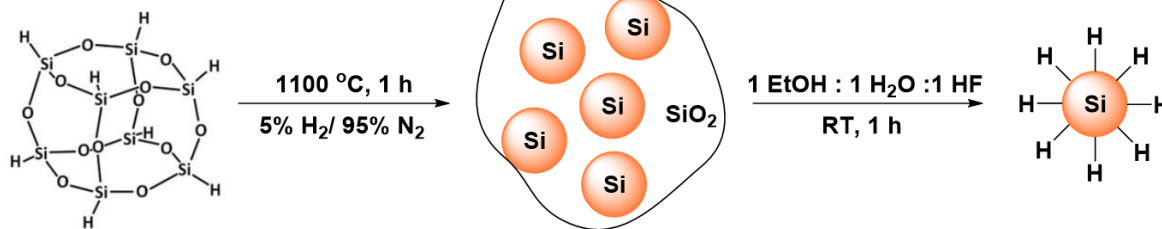
**Figure 1-5:** Images of SiNCs of different sizes under UV-light (365 nm) prepared via plasma pyrolysis of silane gas. Reproduced with permission from *Nanotechnology*, **2008**, *19*, 245603 (reference 105). Copyright 2008 IOP Science.

### 1.3.4 Solid-state

The solid-state synthesis approach to the generation of SiNCs typically requires silicon rich oxides (SRO) (*i.e.*, non-stoichiometric oxides  $\text{SiO}_x$  ( $0 \leq x \leq 2$ )) and sol-gel polymers ( $(\text{HSiO}_{1.5})_n$ ), as precursors. These precursors are thermally processed to produce SiNCs in silicon oxide. Subsequent HF etching of the crude product provides H- SiNCs.<sup>24</sup> Common methods for preparing the  $\text{SiO}_x$  precursor include, ion implantation,<sup>105,106</sup> chemical vapor deposition,<sup>107,108</sup> co-sputtering,<sup>109</sup> and molecular beam epitaxy.<sup>24</sup> One of the first examples of the production of SiNCs from  $\text{SiO}_x$  was performed by Liu *et al.*,<sup>110,111</sup> where they thermally annealed commercial, amorphous  $\text{SiO}_x$ , to obtain SiNCs with diameters in the range from 2 - 16 nm.

The use of a commercially available SRO, hydrogen silsesquioxane ( $\text{H}_8\text{Si}_8\text{O}_{12}$ , HSQ), as a precursor for the size and shape controlled synthesis of SiNCs has been established by the Veinot group.<sup>112</sup> Thermal processing of polymeric HSQ ( $(\text{HSiO}_{1.5})_n$ ) at 1100 °C under a slightly reducing atmosphere (95 %  $\text{N}_2$ / 5%  $\text{H}_2$ ) produced SiNCs ( $d = 3$  nm) embedded in a silica ( $\text{SiO}_2$ ) matrix (Scheme 1-4).<sup>112</sup> The SiNCs were liberated from the  $\text{SiO}_2$  matrix through HF etching, to produce spherical H-SiNCs that displayed size-dependent photoluminescence (Figure 1-6). It is postulated that the mechanism of HSQ decomposition first involves the loss of  $\text{SiH}_4$  in the temperature range of 250 - 350 °C, followed by the disproportionation of the silicon rich oxide to form  $\text{Si}(0)$  and  $\text{SiO}_2$  at 350 - 450 °C.<sup>112</sup>

### Hydrogen Silsesquioxane



**Scheme 1-4:** The synthesis of SiNCs ( $d = 3$  nm) embedded in silica from the thermal decomposition of HSQ. Note: The form of HSQ used for SiNC synthesis is  $(\text{HSiO}_{1.5})_n$ .

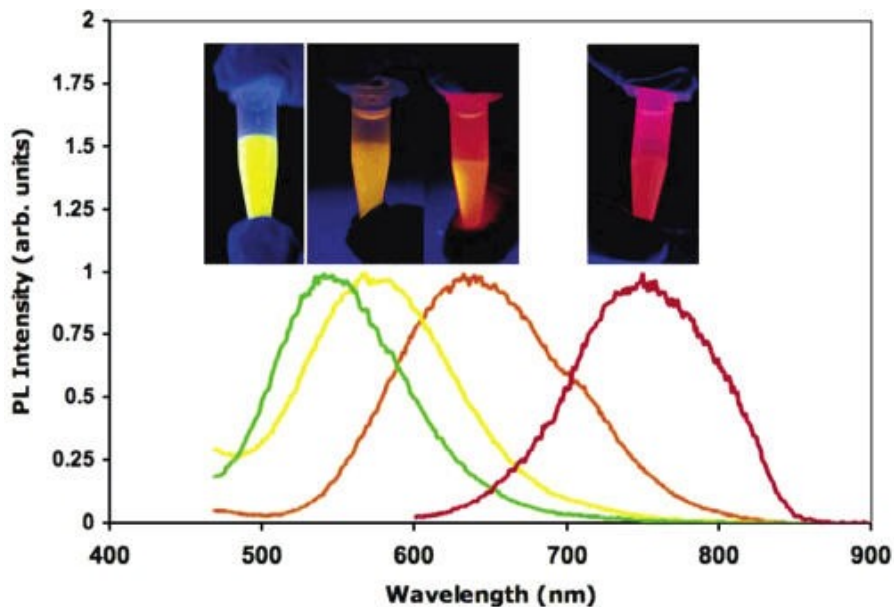


**Figure 1-6:** Photoluminescence spectra of hydride terminated SiNCs using various etching times. Reproduced with permission from *Chem. Mater.*, **2006**, *18*, 6139-6146 (reference 112).

Further investigation of the effect of increasing the annealing temperature to 1200 and 1300 °C yielded spherical SiNCs with sizes of 6 and 9 nm, respectively.<sup>54</sup> More recently, it was observed that longer processing times could lead to a variety of non-spherical shapes of SiNCs

including cubes<sup>113</sup> and hexagonal and truncated trigonal prisms (Figure 1-7).<sup>114</sup> It is believed that at higher temperatures, the integrity of the SiO<sub>2</sub> matrix is compromised as a result of softening and more rapid diffusion of Si atoms promotes particle growth and shape evolution.<sup>114</sup>

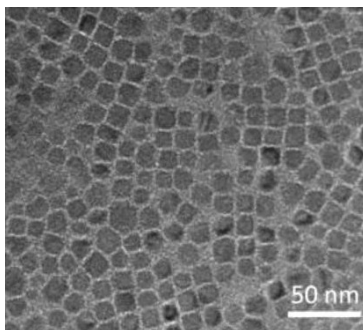


**Figure 1-7:** Transmission Electron Microscope images of SiNC cubes. Adapted with permission from *J. Amer. Chem. Soc.*, **2012**, *134*, 13958-13961 (reference 113).

## 1.4 Surface Passivation of SiNCs

The SiNC synthetic procedures described in Section 1.3 often yield SiNCs with hydride or halogen surfaces. Unfortunately, these surfaces are not stable in the presence of oxygen, and can result in the optical properties being compromised.<sup>115,116</sup> While other QD luminescence properties are typically stabilized by the addition of a lattice-matching, wide-band-gap shell to coat the core QD (*i.e.*, core-shell structures),<sup>117-119</sup> these methods are not readily available for SiNCs. Another drawback of the as prepared surfaces, is the lack of dispersibility in common solvents which could hinder their use in applications. Ligand exchange is the most highly used approach for the surface modification in QD systems.<sup>120-124</sup> However, examples of ligand exchange on SiNCs are limited

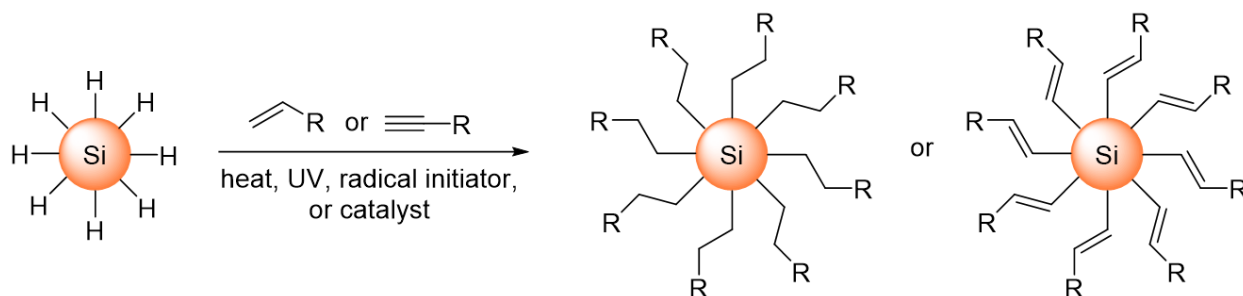
and are in the early stages of development.<sup>125,126</sup> It has also been predicted that the increase of the surface area to volume ratio of NCs could lead to the surface chemistry having an effect on the optical band gap of the material.<sup>127,128</sup> Furthermore, various surface linkages could result in changes in photoluminescence which are size-independent, and do not necessarily follow the quantum confinement model described above.<sup>56,129,130</sup> Therefore, there is a need to explore various synthetic approaches to tailor the surface chemistry of SiNCs. The most common approaches involve the functionalization of SiNCs directly with organic ligands and result in robust covalent linkages.<sup>63,93</sup> Many relevant reviews have been written discussing silicon surface modification.<sup>62,63,93,131,132</sup> It can be seen that many approaches to functionalize SiNCs have been drawn from molecular analogues,<sup>133</sup> as well as bulk and porous silicon,<sup>131</sup> however, it is important to note that this does not mean all methods are transferable to SiNCs.<sup>134,135</sup> This section briefly describes common surface passivation methods and the resulting effects on the luminescence of SiNCs.

## **1.4.1 Silicon Hydride Surfaces**

### **1.4.1.1 Hydrosilylation**

The most widely implemented approach to surface passivation on H-SiNCs is hydrosilylation. Hydrosilylation is the addition of an unsaturated bond (*i.e.*, double or triple bonds) into the silicon-hydride (Si-H) group. Hydrosilylation was first shown on bulk hydride terminated silicon surfaces, Si (111) and Si (100), by Lindford and Chidsey from the pyrolysis of diacyl peroxides.<sup>136</sup> Since then, several researchers explored hydrosilylation on bulk, porous and SiNC surfaces. Numerous hydrosilylation methods (Scheme 1-5) have been shown for silicon surfaces including thermal,<sup>137,138</sup> photochemical/light,<sup>101,139-145</sup> radical initiators,<sup>146-150</sup> catalytic

treatments,<sup>84,151-154</sup> and plasmons.<sup>155,156</sup> Thermal hydrosilylation on silicon surfaces is well-known,<sup>131,157</sup> and in the case of SiNCs, is particle size-independent; however, this method requires high temperatures (greater than 140 °C).<sup>62</sup> Also, this method can generate surface bonded oligomers that may hinder some applications such as sensing (discussed in Section 1.5.1.1).<sup>158</sup> UV irradiation<sup>140,141,159,160</sup> and white light<sup>143,161</sup> are also capable to cause hydrosilylation on bulk and porous silicon. Again, photochemical processes involving the use of UV light has also been shown to achieve hydrosilylation on SiNCs allowing for the use of lower boiling point ligands. Unfortunately, this method is size-dependent and takes longer for larger sized SiNCs.<sup>142,144</sup> Thermally activated radical initiators, such as diacyl peroxides discussed above,<sup>136</sup> have also been used for SiNCs functionalization and were shown to lead to the formation of monolayer surfaces, are size-independent, and can proceed at lower temperatures than thermal hydrosilylation (65 - 100 °C) depending on the initiator used.<sup>146,148,149</sup> Drawing on the work of Buriak on hydride terminated porous silicon,<sup>150</sup> diazonium salts have also been shown to induce hydrosilylation on SiNCs, and these reactions proceed at room temperature.<sup>147</sup> Chloroplatonic acid ( $\text{H}_2\text{PtCl}_6$ )<sup>84,154</sup> and the Lewis Acid,  $\text{BH}_3 \cdot \text{THF}$ ,<sup>152</sup> were employed as catalysts to induce hydrosilylation on H-SiNC surfaces. Unfortunately, removing residual chloroplatonic acid from SiNC surfaces is difficult and the procedure can compromise the material properties (*e.g.*, quench or alter the photoluminescence).<sup>152</sup> Again, the use of platinum complexes<sup>162,163</sup> and Lewis Acids (*e.g.*,  $\text{EtAlCl}_2$ )<sup>151</sup> have been shown to achieve hydrosilylation on bulk and porous silicon surfaces.



**Scheme 1-5:** Reaction scheme of possible hydrosilylation methods used for SiNCs.

The mechanism of hydrosilylation on silicon surfaces is still under investigation and was recently reviewed.<sup>132</sup> Depending on the method of initiation employed, a variety of possible mechanisms have been proposed and include: Si-H homolytic cleavage,<sup>141,159,164,165</sup> exciton mediation,<sup>143</sup> photoemission,<sup>166</sup> and radical assisted hydrosilylation.<sup>167</sup> In reactions involving plasmons or excitons, a positive silicon surface charge is induced that allows for the direct addition of the alkene/alkyne, and no radical is formed (Figure 1-8b).<sup>132,145</sup> Homolytic cleavage of the Si-H bond to produce a surface silyl radical ( $\text{Si}\cdot$ ) and a hydrogen radical ( $\text{H}\cdot$ ), allowing for the free radical reaction of the  $\text{Si}\cdot$  and an alkene/alkyne to occur is one of the most generally accepted hydrosilylation mechanisms occurring on the SiNC surface (Figure 1-8a).<sup>132,168</sup> Recently, the Neale group investigated the effects of thermal- and radical-initiated hydrosilylation on non-thermal plasma synthesized SiNCs.<sup>149</sup> They proposed a new reaction mechanism in which cleavage of the Si-SiH<sub>3</sub> bond occurs via the abstraction of SiH<sub>3</sub>, leaving a  $\text{Si}\cdot$  on the SiNC surface that can then react with an alkene/alkyne.

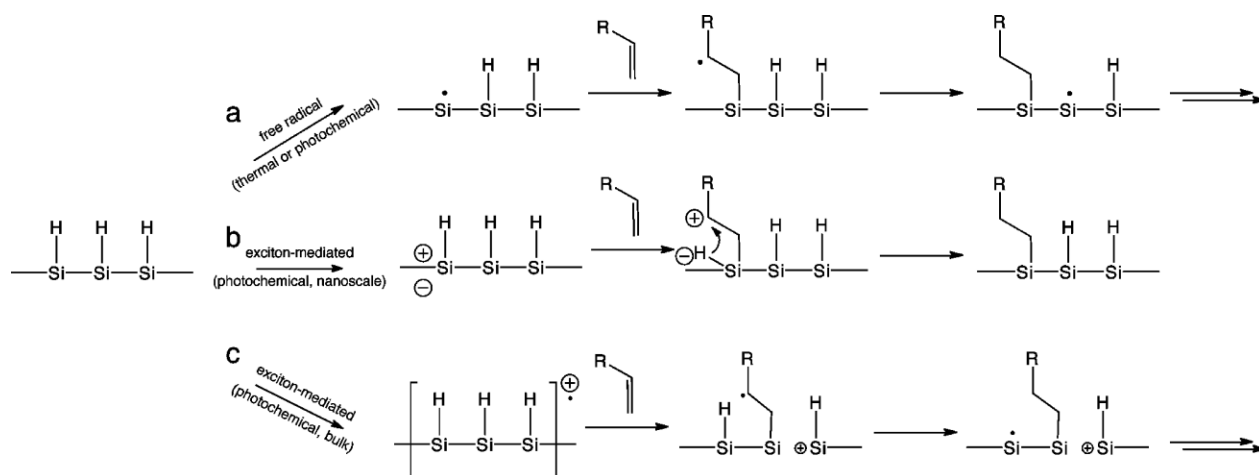
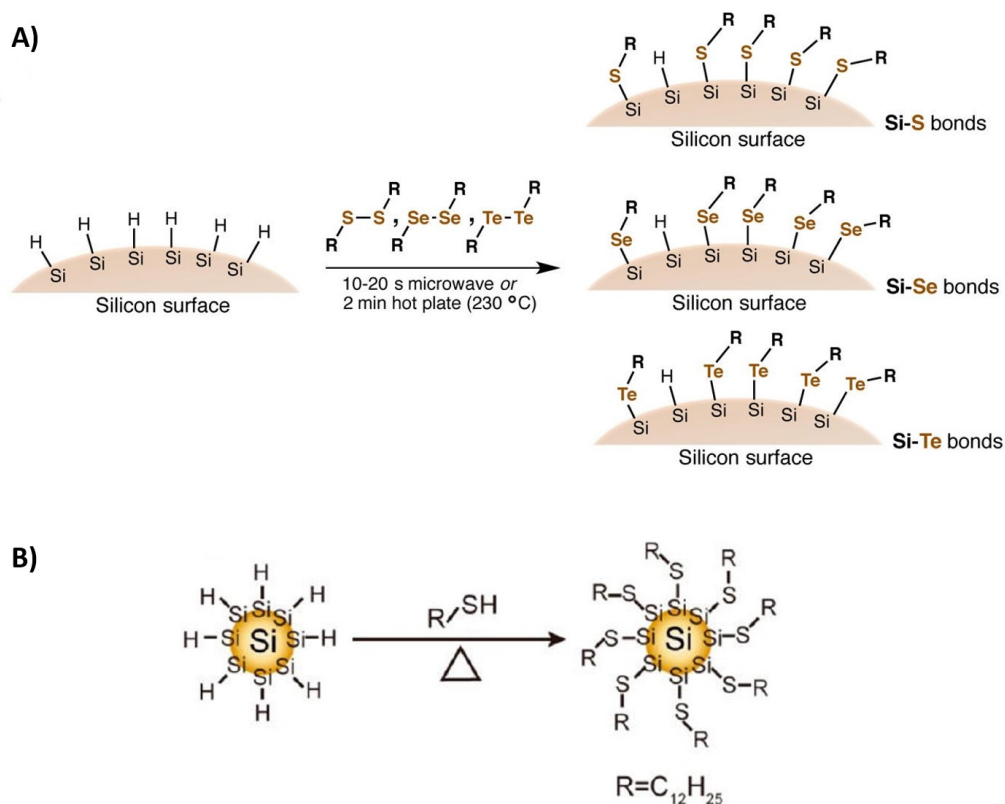


**Figure 1-8:** Proposed hydrosilylation mechanisms on the SiNC surface involving a) free radical or b) exciton mediated in comparison to c) exciton-mediated hydrosilylation of bulk silicon surfaces. Reproduced with permission from *J. Am. Chem. Soc.*, **2011**, *133*, 9564-9571 (reference 144). Copyright 2011 American Chemical Society.

### 1.4.1.2 Chalcogenides

There has also been a recent increase in the functionalization of silicon surfaces with chalcogenides (*i.e.*, S, Se or Te). While initial studies of bulk silicon surfaces were performed in Ultra High Vacuum (UHV) to achieve some of the surfaces,<sup>169-171</sup> other methods such as thermal,<sup>172-176</sup> photochemical (UV<sup>177,178</sup> and white light<sup>179</sup>) and radical initiated<sup>180</sup> performed outside UHV have emerged since the early 2000's. Recently, Buriak et al. studied radical initiated methods (*i.e.*, diazonium salts<sup>180</sup> and thermal<sup>174</sup>) in efforts to achieve the formation of Si-S, Si-Se, and Si-Te bonds onto the porous silicon surface. While the diazonium salt method resulted in Si-S and Si-Se formation, it did not yield Si-Te bonds (due to low solubility).<sup>180</sup> Buriak's follow up study involved a rapid thermal treatment of H-terminated porous silicon with dialkyl or diaryl dichalcogenides to successfully generate Si-S, Si-Se and Si-Te surface functionalization (Scheme

1-6a).<sup>174</sup> Freestanding H-SiNCs were reacted with dodecanethiol via a thermally promoted thiolation reaction by the Korgel group.<sup>125</sup> The reaction was deemed to be size-independent and resulted in similar luminescence observations of alkyl passivated surfaces, however, the surface was inclined to hydrolysis in the presence of moisture (Scheme 1-6b). Nevertheless, an advantage of this lability was the performance of ligand exchange of the Si-S surfaces with alkenes by thermally promoted hydrosilylation.



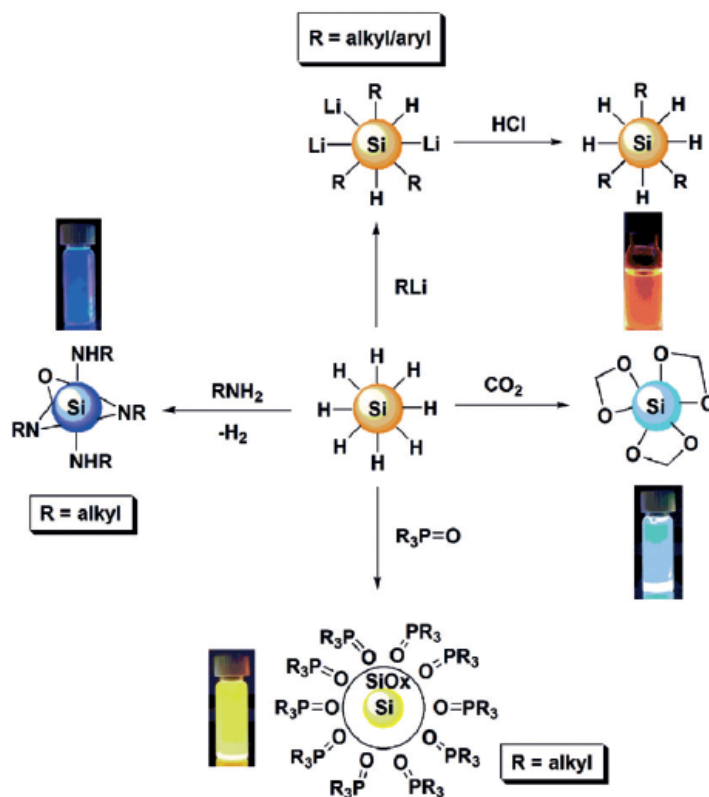
**Scheme 1-6:** Schematics of a) porous silicon and dichalcogenides and c) H-SiNCs and dodecanthiol. Adapted and reproduced with permission from *ACS Appl. Mater. Interfaces*, **2016**, *8*, 11091-11099 (reference 174) and *Langmuir*, **2015**, *31*, 6886-6893 (reference 125). Copyright 2015 and 2016 American Chemical Society.

While the exact mechanisms of the above reactions are unknown, it has been postulated the key step is the formation of a surface silyl radical,<sup>174</sup> that can occur through thermal<sup>181,182</sup> or photochemical<sup>178</sup> driven homolytic Si-H bond cleavage, Si-Si bond cleavage of Si-SiH<sub>3</sub> species,<sup>149</sup> or the removal of the surface hydride by chalcogenyl radicals.<sup>149,183,184</sup> The presence of the silyl radical can then further react directly with a thiyl radical or disulfide species (RS-SR) by S<sub>H</sub>2 addition.<sup>174</sup> Due to the possible induced electronic effects and lability of Si-S surfaces, alternative methods of SiNC functionalization should be conducted. Detailed investigations into a method using a commercial fluorescent light source as a mild alternative to passivate SiNC surfaces with Si-S are discussed in Chapter 3.

#### **1.4.1.3. Other surface modification protocols.**

While hydrosilylation is the most common surface modification approach for H-SiNCs, other surface reactions have been reported (Scheme 1-7). Similar to porous silicon reactivity,<sup>185</sup> Höhle performed a two-step reaction at room temperature with alkyl- and aryl-organolithium reagents with H-SiNCs to yield SiNCs with a mixed surface.<sup>186</sup> It was shown that all SiNCs obtained from this method displayed red-orange luminescence except for those functionalized with phenylacetylene, which were dramatically red-shifted.<sup>186,187</sup> In another study by Höhle, diazonium salts were used to functionalize H-SiNCs with aryl groups by direct reductive grafting of diazonium salts,<sup>147</sup> again, similar to bulk or porous silicon surfaces.<sup>134,150</sup> However, the surface coverage of SiNCs was incomplete and was susceptible towards oxidation. Organosilane surface modification was also shown to occur from H-SiNCs via the use of Wilkinson's catalyst (RhCl(PPh<sub>3</sub>)<sub>3</sub>, Ph = phenyl).<sup>188</sup> Again, this study is a variation of studies conducted on molecular analogues,<sup>189</sup> bulk, and porous silicon surfaces where dehydrogenative coupling was achieved by Wilkinson's catalyst,<sup>190</sup> zirconocene and titanocene catalysts.<sup>191</sup> Unfortunately, the luminescence

of the SiNCs was quenched post reaction, possibly arising from trace Rh. A similar observation on porous silicon was also detected when using Wilkinson's catalyst.<sup>190</sup> Furthermore, H-SiNCs have also been shown to react with alkylamines<sup>129,192</sup> and phosphine oxides<sup>56,192</sup> to form Si-N linkages (blue-emitting luminescence) or oxide coated (yellow-emitting luminescence) SiNCs, respectively.<sup>192</sup> Interestingly, the reaction between H-SiNCs and CO<sub>2</sub> under high pressure caused the formation of acetal surfaces on the SiNC and displayed blue-green luminescence.<sup>56</sup> It has been reported that PCl<sub>5</sub> in the presence of a thermal radical initiator can be used to achieve chlorination of hydride-terminated bulk silicon surfaces.<sup>193,194</sup> H-SiNCs can also react with PCl<sub>5</sub>, Br<sub>2</sub>, and I<sub>2</sub> to generate Si-Cl, Si-Br, and Si-I halide SiNC surfaces at room temperature, respectively, in absence of a radical initiator.<sup>130</sup> These different surfaces are shown to have no luminescence after halogenation.

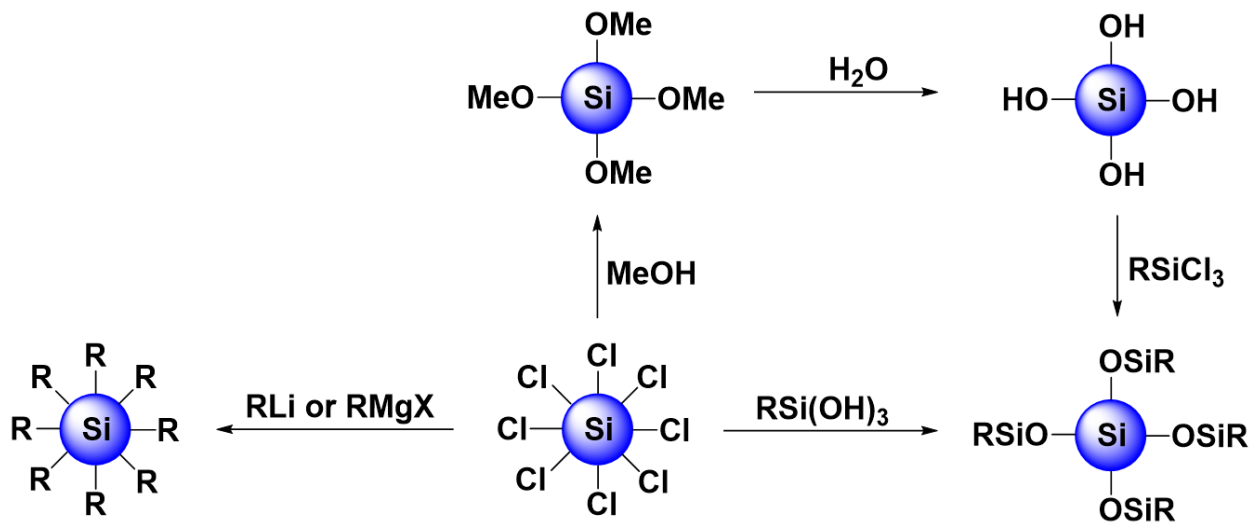


**Scheme 1-7:** Recent reactivity shown on hydride-SiNCs. Reproduced and adapted with permissions from *Angew. Chem. Int. Ed.*, **2016**, 55, 2322-2339 (reference 93). Copyright 2016 Wiley-VCH.

## 1.4.2 Halogens and Oxide reactivity

As described above, Si-X (X = Br, Cl, or I) SiNC surfaces can be generated either *in situ* or from the modification of Si-H surfaces as described above. These active surfaces can then be subsequently modified. The Si-Cl surfaces can be altered using  $\text{LiAlH}_4$  to achieve Si-H surfaces and provide access to the Si-H chemistry described in Section 1.4.1.<sup>90</sup> It was shown that Si-Cl surfaces can also be modified through the use of Grignard reagent or alkyl lithium to achieve alkyl terminated surfaces and blue-emitting photoluminescence (Scheme 1-8).<sup>87,89,91</sup> Grignard reagents could also be used for the addition of alkyl groups onto Si-Br and Si-I SiNC surfaces, and resulted

in red- and yellow-emitting SiNCs, respectively.<sup>130</sup> Again, similar reactivity has been previously reported for bulk silicon surfaces.<sup>193,194</sup> Furthermore, Zhai et al. demonstrated the use of Si-Cl SiNC surfaces for the attachment of sugars and amino acids through an initial thermal reaction to create water soluble SiNCs.<sup>195</sup> Further modification of Si-Cl SiNCs was observed by Kauzlarich et al. when methanol and water exposure generated methoxy SiNC surfaces.<sup>127</sup> A subsequent reaction with an alkyl trichlorosilane, generated a cross-linked siloxane surface (Scheme 1-8). Further controlled oxidation of SiNCs have also been reported.<sup>100,111,196,197</sup> For example, Si-Br surfaces were also shown to be reactive with alcohols to create methoxy SiNCs.<sup>197</sup>



**Scheme 1-8:** Various surface modifications on chlorinated SiNC surfaces. Reproduced and adapted from *Chem. Comm.*, **2006**, 4160-4168 (reference 62). Copyright 2006 Royal Society of Chemistry.

### 1.4.3 Surface Passivation Effects on the Optical Properties of SiNCs

One of the advantageous/attractive properties of SiNCs is luminescence. As discussed above, the photoluminescence of SiNCs has been tuned across the visible spectrum by exploiting surface passivation.<sup>56,198</sup> Not surprisingly, surface oxides and their influence on SiNC luminescence is one of the most studied families of surface terminations.<sup>199-203</sup> Wolkin et al. exposed SiNCs to oxygen and observed a red-shift of the luminescence; they proposed this observation resulted from changes in SiNC size and the influence of a Si=O defect state.<sup>199</sup> For smaller sized particles ( $d < 3$  nm), it was believed that the electrons were trapped within a Si=O defect state, while for larger particles ( $d > 3$  nm), the luminescence is based on the band gap. However, a molecular analogue of Si=O species analogous to a ketone has never been demonstrated without substantial steric protection, and brings into question the existence of this surface species. Further studies conducted by Kanemitsu et al. compared oxidized SiNCs to Si@SiO<sub>2</sub> core-shell structures.<sup>200</sup> They proposed the observed luminescence was occurring due to a radiative recombination process that localized excitons at the interfacial layer between the Si core and SiO<sub>2</sub> surface layer.

As mentioned above (Section 1.3), many solution-based methods to synthesize SiNCs result in SiNCs that display blue photoluminescence. A detailed study conducted by Dasog et al. compared the optical response of SiNCs prepared via high temperature methods and those prepared via the most commonly employed solution-based methods.<sup>129</sup> This study definitively demonstrated that SiNCs that exhibited size-dependent photoluminescence would exhibit size-independent luminescence if nitrogen and oxygen surface species were formed on its surface. Dasog et al. went on to tailor the optical response of SiNCs by modifying surfaces with alkyl, amine, phosphine, and acetal functional groups.<sup>56</sup> Similarly, it was found that SiNCs generated

from reactions originally using halogenated (Si-Cl, Si-Br, or Si-I) SiNC surfaces, also displayed size-independent luminescence, and again this behavior has been attributed to surface-defect states from the initial SiNC halide surface species.<sup>130</sup> It has also been shown by the Goforth group, that exposure of red luminescent ( $\lambda = \sim 580$  nm), alkyl SiNCs to alcohols resulted in the photoluminescence to be converted to blue ( $\lambda = \sim 450$  nm).<sup>204</sup> It was proposed the conversion from red to blue luminescence occurs from dangling bond defect passivation by small alcohol molecules.

More recently, the effects of the electronic structure of surface groups on the optical properties of SiNCs have been explored.<sup>187,198</sup> Wang and coworkers tuned the emission of SiNCs by varying the degree of conjugation in a series of carbazoles.<sup>198</sup> The authors propose that differences in conjugation created unique surface states that altered the band structure of the SiNCs. As previously mentioned in Section 1.4.1.3, the observed luminescence of phenylacetylene functionalized SiNCs via the use of organolithium reagents differed from those of their hexyl- and phenyl-functionalized counterparts.<sup>186</sup> Angi and coworkers further investigated this observation, and determined through scanning tunneling microscopy that an in-gap state near the conduction band edge was only observed for phenylacetylene functionalized SiNCs.<sup>187</sup> It has been proposed that this in-gap state is the cause of the luminescence shift via relaxation across that state.

## **1.5 SiNC-based sensing platforms.**

While there have been many studies using QDs as sensors, the majority used cadmium (Cd)-based materials. Cd-based materials were considered the benchmark for all other types of QDs due to their tunable fluorescence and high quantum yields (70 - 80%).<sup>205</sup> Other advantages of using Cd QDs are they have established synthetic and surface modification protocols and are

commercially available.<sup>206</sup> These QD sensors have been used to detect heavy metal ions, small molecules, explosives, pH, oxygen and others.<sup>207-210</sup> However, using Cd-based QDs is undesirable due to the possible release of toxic Cd<sup>2+</sup> ions.<sup>211</sup> This toxicity is the reason heavy metals such as Cd are regulated in the European Union (European Union Directive 2011/65/EU) and other jurisdictions.<sup>210</sup> These regulations could limit the application of Cd-based systems, hence there is a need to develop and implement alternative sensing systems.

One alternative to toxic metal-based QDs, is SiNCs. The observed photoluminescence, tunable structure, and surface group modification of porous silicon led researchers to investigate porous silicon for its sensing abilities.<sup>45,48,212</sup> It may be possible for researchers to extend the field of porous silicon sensors to the development of luminescent SiNCs sensors. With the recent developments in SiNC synthesis and surface modification as mentioned above, these materials are becoming more widely used in sensing applications. This section outlines general sensing mechanisms and approaches that employ QDs, and then extends discussion to specific examples of SiNC-based sensors.

### **1.5.1 Representative Quantum Dot Based Sensing Mechanisms**

The use of QDs as sensors is mainly based on their optical properties. As mentioned in Section 1.1, the photoexcitation of QDs induces the transfer of valence band electrons to the conduction band and results in an electron-hole pair (exciton). The recombination of the electron-hole pair generates luminescence that can then be used for sensing applications based on different mechanisms. There are three main methods (Figure 1-9) in which QDs are used for sensing applications: (1) electron transfer (ET), (2) fluorescence resonance energy transfer (FRET), and (3) photocurrent generation.<sup>32</sup> The following sections will summarize these main concepts; a more detailed discussion is beyond the scope of this thesis and can be found elsewhere.<sup>15,32,213</sup>

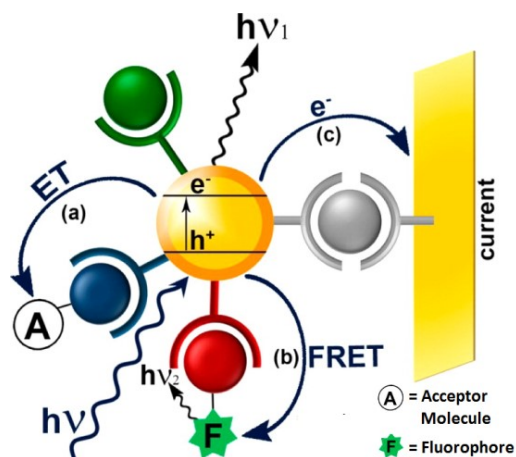


**Figure 1-9:** Representation of different QD-based sensing designs: (a) electron transfer, ET, (b) FRET, or (c) photocurrent generation as readout signals. The green, blue, red, and grey structures on the QD represent different surface groups. Reproduced and modified with permission from *ACS Appl. Mater. Interfaces*, **2013**, 5, 2815–2834 (reference 32). Copyright 2013 American Chemical Society.

### 1.5.1.1 Electron transfer

Electron transfer (Figure 1-9a) is a phenomenon that is frequently employed in QD sensors. This process involves a disruption in the recombination of the electron-hole pair resulting in a quenching of the QD photoluminescence. In order for electron transfer to occur, the energy levels of the QD (*i.e.*, conduction band edge, valence band edge) must be aligned appropriately. One route sees an electron acceptor molecule with a lowest unoccupied molecular orbital (LUMO) level at a lower energy than that of the conduction band edge of the QD donor (Figure 1-10a).<sup>15,214</sup> This condition allows for the transfer of the conduction band electron of the QD to the molecular acceptor, preventing the recombination of the electron-hole pair, and quenching of the QD luminescence. Alternatively, the molecule can act as the electron donor and the QD as the electron acceptor. The highest occupied molecular orbital (HOMO) level of the electron donor is at a higher

energy than the valence band edge of the QD allowing electron transfer from the molecule to the valence band holes of the QD and quenching of the luminescence (Figure 1-10b).<sup>15,214</sup> It is important to note that the electron transfer processes rely heavily on the redox properties of the QDs and can be influenced by the presence of surface traps and surface charges.<sup>215</sup> The term static quenching is often used to describe electron transfer and occurs during the lifetime of the excited state. No changes in the absorption spectra should occur during static quenching.<sup>213</sup>

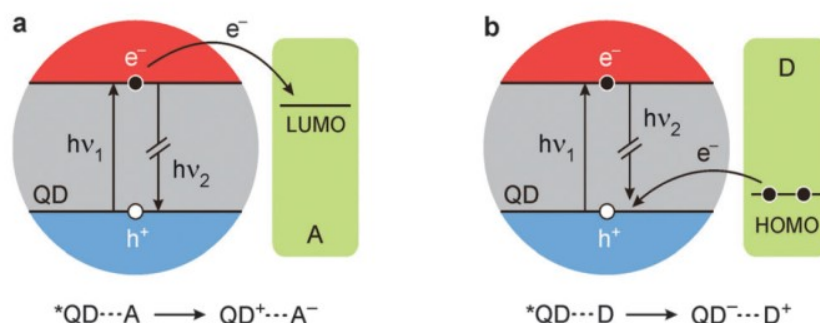


**Figure 1-10:** Pictorial representation of (a) electron transfer from a QD to an electron acceptor (A), and (b) electron transfer from an electron donor (D) to a QD. Reproduced with permission from *Chem. Soc. Rev.*, **2015**, *44*, 4275-4289 (reference 214). Copyright 2015 Royal Society of Chemistry.

### 1.5.1.2 Fluorescence Resonance Energy Transfer (FRET)

Fluorescence resonance energy transfer (FRET) is a non-radiative energy transfer involving dipole-dipole interactions between an excited state donor to a ground state acceptor that operates at larger distances than electron transfer (Figure 1-11).<sup>32,213</sup> The efficiency at which FRET occurs depends on the spectral overlap between the donor emission and the acceptor absorption, photoluminescent quantum yield of the donor, the orientation of the dipoles between

donor and acceptor, and the spatial separation of the donor-acceptor pair.<sup>208</sup> Distance is particularly important in this phenomenon, as FRET only occurs when the donor and acceptor are within 2-8 nm of each other.<sup>32</sup> QDs are good candidates for FRET-based sensing due to their photostability, narrow and adjustable emission, and wide range of excitation wavelengths.<sup>33,209</sup>

This process is a form of dynamic quenching, does not involve the lifetime of the excited state, and forms a non-fluorescent, ground-state complex between the luminescent material and quencher.<sup>213</sup> When this complex absorbs light, it immediately returns to the ground state without the emission of a photon, and can be observed by measuring the absorption spectra. Since the resulting complexes of dynamic quenching are non-fluorescent, the only observed fluorescence that may still remain in the system is from uncomplexed, fluorescent materials.<sup>213</sup>

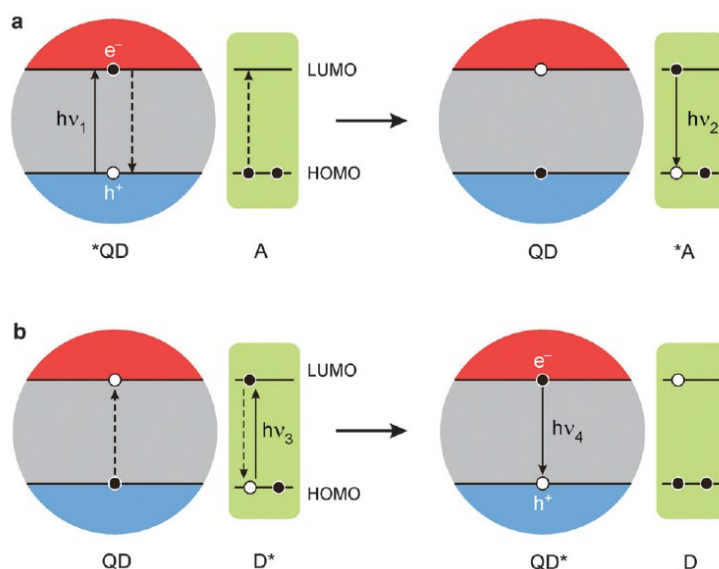


**Figure 1-11:** Pictorial representation of fluorescence resonance energy transfer (FRET) (a) from a photoexcited QD to a molecular energy acceptor (A), and (b) from a photoexcited molecular energy donor (D) to a QD. Reproduced with permission from *Chem. Soc. Rev.*, **2015**, *44*, 4275-4289 (reference 214). Copyright 2015 Royal Society of Chemistry.

There are common methods used to create QD-based FRET sensors (Figure 1-12). In most cases, the QD-molecule hybrids are designed such that the energy is transferred from the QD to the molecule.<sup>214</sup> However, alternative scenarios exist. The most common examples are shown in Figure 1-12. Figure 1-12a highlights a case in which the QD donor and the molecular acceptor are both initially emitting, however, upon exposure to a target analyte, FRET between the QD donor and the molecular acceptor no longer occurs, and no emission is observed from either the QD or the molecular acceptor. Another scenario sees an analyte facilitate binding between a QD and an acceptor leading to FRET from the QD to the molecular acceptor and the quenching of QD luminescence (Figure 1-12b). In contrast, it is also possible to have an analyte bind to the acceptor molecule and facilitate FRET which leads to the quenching of the QD and the emission turn-on of the acceptor molecule (Figure 1-12c). Finally, in another sensing approach the analyte induces spatial separation between the QD donor and the molecular acceptor, preventing FRET from occurring and resulting in the appearance of QD luminescence (Figure 1-12d).

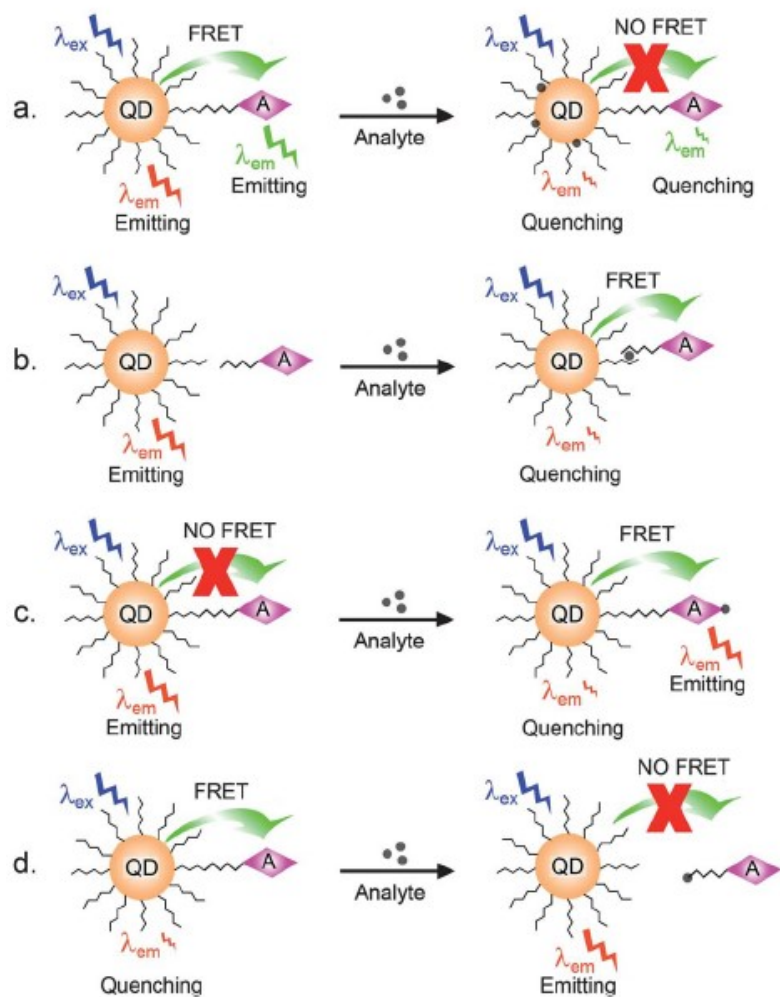


**Figure 1-12:** Representation of the four different sensing strategies using FRET. Reproduced with permission from *J. Mater. Chem. C*, **2014**, 2, 595-613 (reference 208). Copyright 2014 Royal Society of Chemistry.

### 1.5.1.3. Photocurrent Generation and Other Sensing Strategies

Not all QD sensors are based directly on luminescence measurements. The application of QDs in photochemical sensors is also known, and involves the immobilization of QDs on an electrode surface via a molecular linkage (Figure 1-13). Upon illumination, photoexcited conduction-band electrons are injected from the QD to the electrode, generating photocurrents that

may be monitored.<sup>32,215</sup> These photocurrents are sensitive to the chemical environment surrounding the QDs and can respond to different target analytes of varying concentrations. A detailed description of this QD sensing strategy has been reviewed elsewhere.<sup>215</sup>

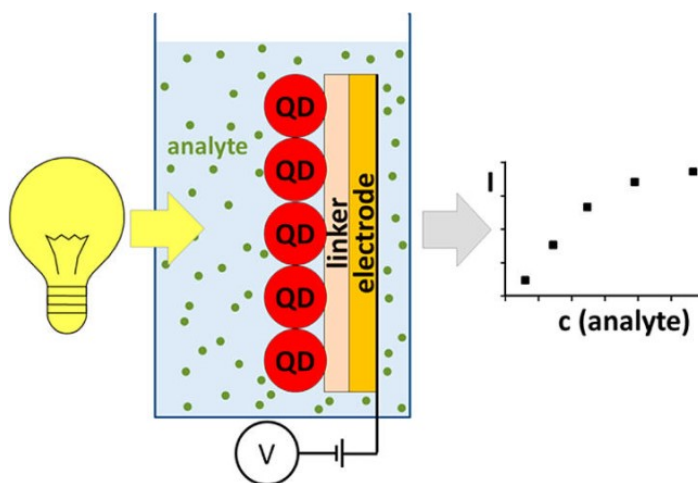


**Figure 1-13:** Representation of a QD-based photoelectrochemical sensor where QDs are immobilized by a linker to an electrode, which is placed in a solution. Upon illumination a photocurrent is generated and monitored after addition of a target analyte. Reproduced with permission from *ACS Appl. Mater. Interfaces*, **2013**, 5, 2800–2814 (reference 215). Copyright 2013 American Chemical Society.

Another QD-based method for sensing includes ratiometric sensors.<sup>216</sup> The ratiometric sensor approach involves measuring changes in the ratios of fluorescence intensities at two different wavelengths, before and after the addition of an analyte.<sup>217</sup> This provides higher sensitivity, selectivity and accuracy.<sup>208,218</sup> Measuring the changes in two emission intensities provides a correction for environmental interference and other non-target factors.<sup>217,219</sup>

Finally, QDs are being used to develop multiplexed detection systems. These sensors can detect multiple analytes in a single assay (parallel detection of different analytes).<sup>33,220</sup> A multiplex

system is desirable for many applications including point of care diagnostics and high-throughput drug screening.<sup>220</sup> These systems can be realized using QDs as they exhibit a wide excitation spectrum in the UV range, allowing QDs with separate emissions to be excited simultaneously.<sup>33</sup> This is advantageous over organic dyes that require the excitation light source to be tuned into their respective narrow absorption bands.<sup>33,221</sup> Multiplex sensors using QDs have already been developed for enzyme and heavy metal detection.<sup>220,221</sup>

These aforementioned processes used for QD sensor development have been widely explored for Cd-based systems. These concepts are now being successfully applied to SiNCs. The following sections will highlight examples of luminescent sensors developed with SiNCs and is subdivided according to target analytes.

## **1.5.2 Examples of SiNC Sensors**

### **1.5.2.1 High Energy Materials**

The development of rapid, cost-effective, on-site sensing platforms for detecting explosives is of great interest because of security, toxicity, and environmental concerns.<sup>222,223</sup> The luminescence of silicon-based nanosystems including porous silicon and agglomerated partially oxidized SiNCs is known to be quenched by nitroaromatic compounds.<sup>224,225</sup> The Sailor group demonstrated the luminescence of porous silicon quenched after the introduction of nitrobenzene (NB), dinitrotoluene (DNT), trinitrotoluene (TNT) vapors in a flowing air stream.<sup>224</sup> The quenching mechanism involved electron transfer from the nanocrystallites in the porous silicon matrix to the nitroaromatic compounds (similarly to what was discussed above in Figure 1-10a). This quenching was reversible only after short exposure times. However, longer exposure times (*i.e.*, times exceeding 5 min) of the porous silicon to the nitroaromatics, led to irreversible

oxidation of the silicon-based donor. The limits of detection for DNT and TNT using this method were 2 ppb and 1 ppb, respectively. Similarly, Germanenko and coworkers illustrated that the luminescence of partially oxidized SiNCs was quenched by nitroaromatics (*e.g.*, 3,5-dinitrobenzotrile, 1,4-dinitrobenzene, 2,4-dinitrotoluene, *etc.*) whose reduction potentials lie below the conduction band edge of SiNCs.<sup>225</sup> These studies provided the groundwork for nanosilicon materials as a practical sensing platform for nitroaromatic based explosives.

Building on these early studies, we employed red luminescent, dodecyl functionalized SiNCs in a paper-based sensor to detect nitroaromatics, nitroamines (*e.g.*, cyclotrimethylenetrinitramine, RDX), and nitrate esters (*e.g.*, pentaerythritol tetranitrate, PETN).<sup>226</sup> The details of this study are discussed in Chapter 4. This paper-based sensor afforded straight forward qualitative detection (Figure 1-14) and a DNT detection limit as low as 18.2 ng. Consistent with the earlier work of Sailor and Germanenko, an electron transfer mechanism is responsible for the luminescence quenching.

Subsequently, Ban and coworkers investigated blue luminescent SiNCs functionalized with 3-aminopropylterminated surface groups using SiNCs for the detection of TNT in aqueous solutions.<sup>227</sup> The detection limit for TNT in aqueous solutions using this system was determined to be 1 nM and the observed quenching was proposed to occur via FRET that is facilitated by surface amine groups (Figure 1-15). The authors also evaluated this sensing platform for other nitroaromatics (*i.e.*, NB and DNT) as well as potential metal ion interferents (*i.e.*,  $\text{Cu}^{2+}$ ,  $\text{Ca}^{2+}$ ,  $\text{Zn}^{2+}$ ,  $\text{Pb}^{2+}$ ,  $\text{Cd}^{2+}$ ,  $\text{Ag}^+$ ,  $\text{Al}^{3+}$ ,  $\text{Fe}^{3+}$ , and  $\text{Fe}^{2+}$ ). It was determined that the influence of metal ion interference was negligible.

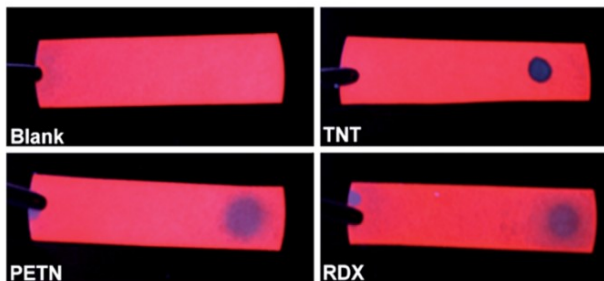


**Figure 1-14:** A luminescent SiNC paper-based sensor that quenches in the presence of high energy molecules of TNT, PETN, and RDX. Reproduced with permission from *Nanoscale*, **2014**, *6*, 2608-2612 (reference 226). Copyright 2014 Royal Society of Chemistry.

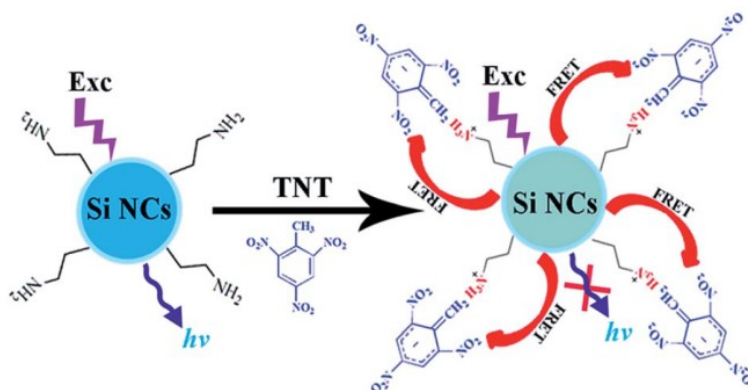


**Figure 1-15:** The proposed FRET mechanism between TNT-amine complexes and SiNCs. Reproduced with permission from *Anal. Methods*, **2015**, *7*, 1732-1737 (reference 227). Copyright 2015 Royal Society of Chemistry.

Further investigations using SiNCs as nitroaromatic sensors have been performed by Nguyen and coworkers.<sup>228</sup> In their study, three different surface groups (Figure 1-16a) were evaluated: alkyl oligomer (red-emitting), alkyl monomer (red-emitting), and alkyl amine (blue-emitting). From these investigations, it was determined that the alkyl monomer surface was more responsive towards vapor-phased nitroaromatics than the oligomers (see Figure 1-16b). The

authors proposed that an electron transfer quenching mechanism is responsible. Surprisingly, the blue-emitting, amine terminated SiNCs were not as sensitive to nitroaromatic exposure as the red-emitting alkyl particles or the previously reported blue-emitting SiNCs systems.<sup>227</sup> These observations may be the result of the amine groups being bonded to the surface of the SiNCs instead of being at the terminus of the capping layer. This different bonding orientation would not facilitate the formation of the Meisenheimer complexes necessary to promote FRET.

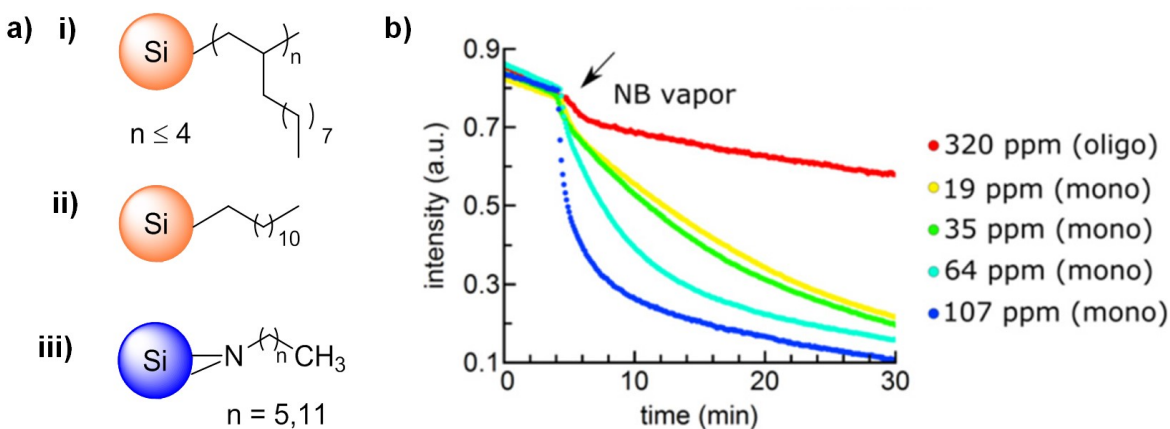


**Figure 1-16:** a) SiNCs with different surface groups i) alkyl oligomer, ii) alkyl monomer, and iii) alkyl amine. b) Change in the luminescence of alkyl monomer dodecyl functionalized SiNCs in filter paper after exposure to varying concentrations of nitrobenzene (NB) vapor. Reproduced and modified with permission from *Nanotechnology*, **2016**, 27, 105501 (reference 228). Copyright 2016 IOP Publishing.

### 1.5.2.2 Metal Cations

Metal cations are a significant health concern. This is highlighted by the recent drinking water conditions in the United States.<sup>229</sup> Therefore, it is important to develop methods with high selectivity and low detection limits that are suitable for trace metal detection. The use of QDs as

optical sensors for metal ions has been comprehensively reviewed elsewhere.<sup>208,209</sup> However, an outstanding question remains: is it appropriate to use toxic metal based sensors (*e.g.*, CdSe QDs) to detect toxic metals? Porous silicon has previously been used to develop electrochemical and transducer sensors suggesting nanocrystalline based systems could provide a useful alternative sensing platform.<sup>230,231</sup>

Blue-emitting, amine terminated SiNCs have been used to detect mercuric ions.<sup>232</sup> After the introduction of  $\text{Hg}^{2+}$  to a solution of SiNCs, the luminescence decreased with the increase of  $\text{Hg}^{2+}$  concentration (Figure 1-17) with a detection limit of 50 nM. The fluorescence was shown to be recovered by the addition of chelating agents. The quenching mechanism was determined to be a combination of both static and dynamic quenching. Blue-emitting SiNCs have also been reported to show sensitivities toward the presence of  $\text{Cu}^{2+}$  and  $\text{Cr}^{4+}$  ions.<sup>233-235</sup>

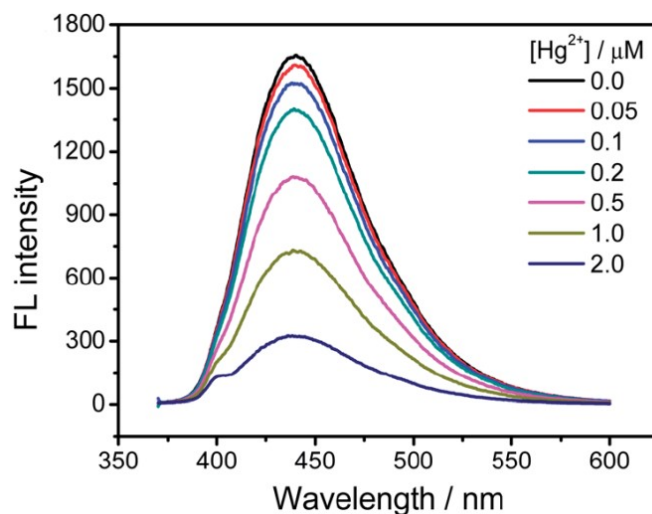


**Figure 1-17:** The effect of SiNC luminescence by varying concentration of  $\text{Hg}^{2+}$ . Reproduced and modified with permission from *Nanoscale*, **2014**, 6, 4096-4101 (reference 232). Copyright 2014 Royal Society of Chemistry.

### 1.5.2.3 Biologically Relevant Molecules

According to the World Health Organization, more than 150 million people worldwide are affected by diabetes making glucose sensing essential.<sup>236</sup> There is a need for simple, reliable, and cost-effective methods for glucose detection. Porous silicon has been employed in a variety of biosensors including those detecting glucose.<sup>45,212,237,238</sup> On the other hand, SiNCs have been less extensively studied for this application. Yi and coworkers developed an indirect glucose sensor by combining blue luminescent, hydride terminated SiNCs with glucose oxidase (GOx) and phosphate buffered saline (PBS) buffer.<sup>239</sup> The luminescence of this solution was stable in air for 6 h under ambient conditions. Adding glucose to the SiNC solution caused the GOx catalyzed oxidation of glucose to produce both gluconic acid ( $C_6H_{12}O_7$ ) and  $H_2O_2$ . Once the  $H_2O_2$  contacts the SiNC surface, an electron transfer from the SiNC conduction band to the active oxygen species of the  $H_2O_2$  occurs (Figure 1-18). This electron transfer results in the quenching of the SiNCs and the production of  $H_2O$  and  $O_2$ . The resulting  $O_2$  can then participate in the catalyzed reaction of GOx, generating a cyclic electron-transfer mechanism upon glucose oxidation.<sup>239,240</sup> The limit of detection for glucose under optimal conditions (pH = 7.4, temperature = 40° C) was 0.68  $\mu$ M. To test the selectivity of the sensor, various metal ions, amino acids, and several glucose analogues were investigated. The possible interferents, when present at concentrations of 20 times higher than glucose, showed minimal effect on the sensor.

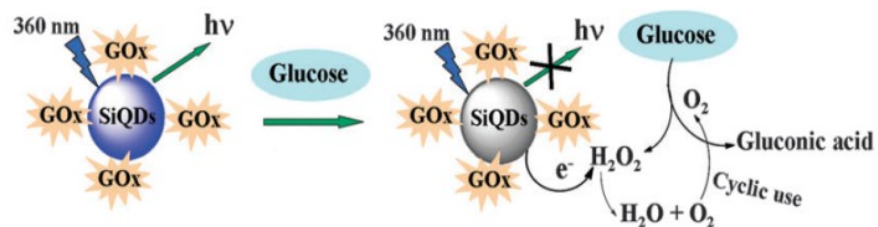


**Figure 1-18:** Illustration of a SiNC-based glucose sensor. Reproduced and modified with permission from *Chem. Commun.*, **2013**, 49, 612-614 (reference 239). Copyright 2013 Royal Society of Chemistry.

Yao's research group also developed another glucose sensor that was based on colorimetric analysis that exploits the intrinsic peroxidase-like activity of SiNCs.<sup>241</sup> The same blue luminescent, hydride terminated SiNCs were employed, and were placed in a solution containing GOx, 3,3',5,5'-tetramethylbenzidine (TMB) and glucose. With H<sub>2</sub>O<sub>2</sub> as a product of the catalytic oxidation of glucose by GOx, the SiNCs were oxidized and the H<sub>2</sub>O<sub>2</sub> decomposed into active oxygen species. This resulted in the SiNCs to become electrophilic and caused the oxidation of the TMB; similarly, to how H<sub>2</sub>O<sub>2</sub> can oxidise the TMB in the presence of peroxidase. The optimum temperature, time and pH were 35 °C, 30 min and 7, respectively with a limit of detection of 0.05 μM/L.

Dopamine is an important neurotransmitter that plays a role in many brain functions.<sup>242</sup> Detecting and quantifying it is vital, as excessive secretion of dopamine could lead to metabolism failure while lack of dopamine can lead to Parkinson's disease.<sup>243,244</sup> Fluorescent QDs have been used to detect dopamine, however, the limit of detection was not sensitive enough to allow for practical applications.<sup>245,246</sup> Zhang and co-workers employed blue luminescent, amine terminated SiNCs for the selective detection of dopamine (Figure 1-19).<sup>244</sup> The as synthesized SiNCs were introduced into a PBS buffer solution, followed by the addition of dopamine solutions, and stirred

for 3 h prior to evaluation of the luminescence response. A linear relationship between the concentration of dopamine and the quenching of SiNC luminescence was observed. The limit of detection for dopamine was determined to be 0.3 nM and the influence of possible interferents (*i.e.*, amino acids, peptides, proteins, metal ions, *etc.*), was minimal. The authors propose FRET as the primary quenching mechanism based on the overlap of the emission spectrum of the SiNCs and the absorption spectrum of the dopamine. This allows for an energy transfer from the excited state SiNCs to the oxidized dopamine molecules. The authors also note the possibility of an electron transfer between the SiNCs (donor) and dopamine (acceptor) that could also be contributing to luminescence quenching.

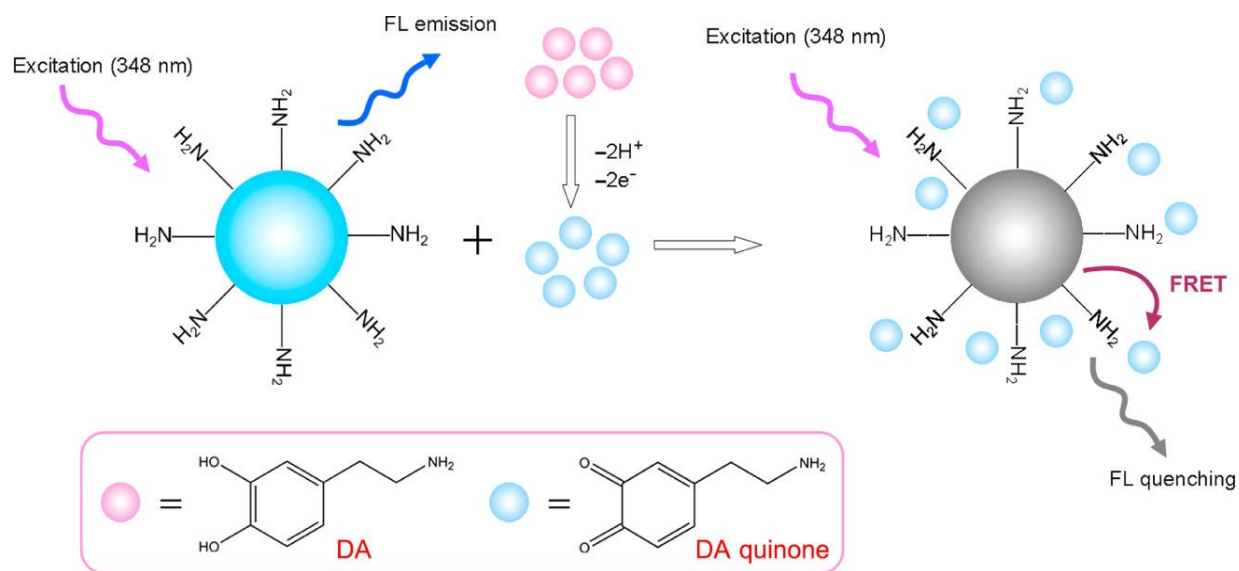


**Figure 1-19:** The proposed luminescence quenching mechanism of SiNC by dopamine. Reproduced with permission from *Anal. Chem.*, **2015**, *87*, 3360–3365 (reference 244). Copyright 2015 American Chemical Society.

Vapor and gas sensors are important today for homes and industrial use. In particular, high selectivity alcohol detection is of paramount importance for industry (*i.e.*, biomedical, chemical, and food) and breath analysis.<sup>247</sup> Multiple papers have been published incorporating porous silicon into devices for ethanol sensing; it is reasonable that SiNCs will also respond to ethanol vapors.<sup>248-</sup><sup>250</sup> Zhang and coworkers employed red luminescent SiNCs coupled to an optical fiber for the detection of ethanol.<sup>251</sup> The optical fiber was dipped into a solution of hydride terminated SiNCs and dried in ambient conditions. This procedure resulted in micron scale “clumps” of SiNCs on the end facet of the fiber. Exposure of this structure to dry flowing O<sub>2</sub>, water vapor, or ethanol resulted in predictable changes in the SiNCs luminescence (see Figure 1-20). The detection limit of ethanol using these systems was found to be 380 ppm after 15 s of exposure time of the fiber to the vapor. The detection limit for water was not reported.

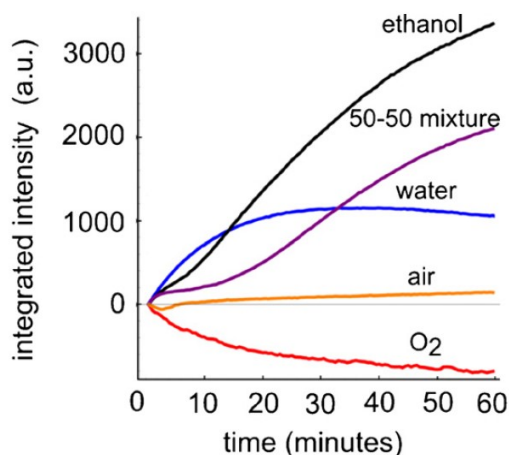


**Figure 1-20:** The integrated fluorescence intensity as a function time for a SiNC fiber sensor in O<sub>2</sub>, air, and air saturated with water, ethanol, or a 50% mixture of both. Reproduced with permission from *Sens. Actuators, B*, **2013**, *181*, 523-528 (reference 251). Copyright 2013 Elsevier.

#### 1.5.2.4 Antibiotics

The class of tetracycline antibiotics includes tetracycline (TC), a common antibiotic used to treat bacterial infections and used in the agricultural sector as a food additive.<sup>252,253</sup> Excessive use of TC is not desirable as it can lead to resistance.<sup>254</sup> In this context, monitoring TC concentrations in food is vital. This leads to a demand for straightforward, rapid, and selective detection methods. Amine functionalized porous silicon has been used in electrochemical impedance sensors sensitive to TC.<sup>255</sup> These observations indicate that other nanocrystalline silicon containing systems could be used to develop tetracycline sensing platforms.

Lin and Wang showed that the blue luminescence of amine terminated SiNCs can be quenched in the presence of tetracycline (TC), oxytetracycline (OTC) and chlorotetracycline (CTC).<sup>219</sup> A solution containing SiNCs in PBS buffer was exposed to TC, OTC or CTC and resulted in the quenching of the luminescence. The limits of detection for this method were determined to be 25.9 nM, 20.4 nM, and 28.3 nM for TC, OTC, and CTC, respectively. There was no measured change in the lifetime of the SiNCs after the addition of TC containing molecule indicating the quenching occurred by the formation of a ground state complex. The authors propose that the amine surface groups of the SiNCs interact with the tetracycline containing molecules to form ground-state complexes (Figure 1-21). It is also important to note that there was also overlap between the emissions of the SiNCs with the absorption peak of TC that could also contribute to quenching. However, the authors state that the shared emission, absorption overlap was not significant enough to induce FRET; therefore, the dynamic quenching mechanism is the dominate mechanism. To determine the applicability of the SiNCs in real life applications, the SiNCs were applied to the analysis of milk samples. The proteins and lipids were removed

from the milk samples prior to testing. After the titration of the SiNCs with the milk samples, the luminescence intensity did decrease.

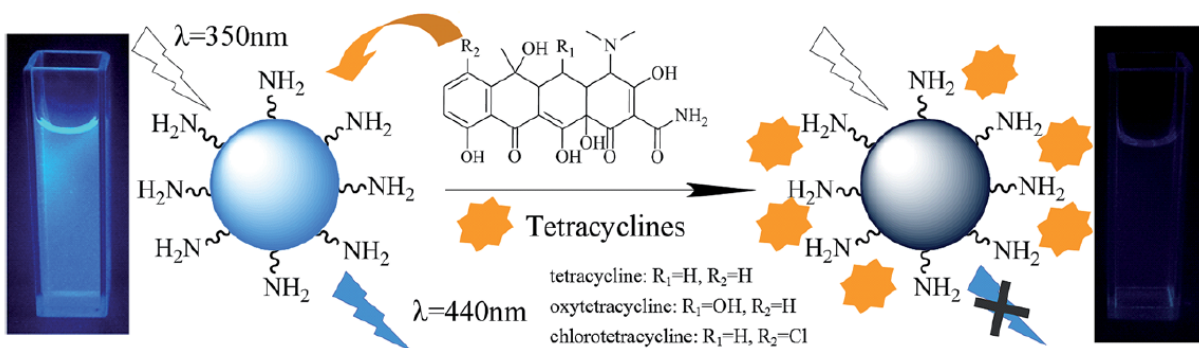


**Figure 1-21:** The proposed mechanism of SiNC fluorescence quenching by TCs. Photo: SiNCs excited by UV light at 365 nm before (left) and after (right) 10 mM of TC. Reproduced and modified with permission from *RSC Adv.*, **2015**, *5*, 27458-27463 (reference 219). Copyright 2013 Royal Society of Chemistry.

### 1.5.2.5 Pesticides

Pesticides are used all over the world in agriculture and can cause persistent contamination in the environment and accumulation in the ecosystem.<sup>256</sup> Many pesticides contain carbamate and organophosphate compounds that disrupt the cholinesterase enzymes used to regulate acetylcholinesterase (AChE),<sup>257,258</sup> this disruption can lead to respiratory paralysis and death.<sup>258</sup>

Unfortunately, many methods used to detect these pesticides are expensive, require sophisticated instrumentation and complex sample pretreatment, as well as highly skilled professionals.<sup>259</sup> Fluorescent QD sensors offer a comparatively simple detection method; however, there are toxicity concerns when using heavy metal QDs.<sup>260,261</sup> Alternatively, oxide-

coated porous silicon sensors have been developed for pesticide sensing.<sup>262,263</sup> These studies again suggest SiNCs could be used in a similar way.

The use of blue luminescent, hydride terminated SiNCs to sense pesticides has been demonstrated.<sup>259</sup> SiNCs were first dispersed into a solution containing PBS buffer, acetylcholine chloride (ACh), acetylcholinesterase (AChE), and choline oxidase (ChOx). The combination of ACh and AChE yields choline that then reacted with ChOx to produce H<sub>2</sub>O<sub>2</sub>. The H<sub>2</sub>O<sub>2</sub> (which contains an active oxygen species) present in solution can capture the conduction band electrons of the SiNCs, prohibit the recombination of the electron-hole pair, and cause luminescence quenching of the SiNCs. Carbaryl, a carbamate family pesticide, was then added to the solution and left for 15 min in the dark at 40 °C prior to luminescence analysis. The addition of carbaryl caused the inhibition of AChE, disallowing the reaction between AChE and ChOx and a decrease of H<sub>2</sub>O<sub>2</sub> production. With less H<sub>2</sub>O<sub>2</sub> present in solution, there is a decrease in the electron transfer from the SiNCs to H<sub>2</sub>O<sub>2</sub>, and therefore an increase of the SiNC luminescence (Figure 1-22). The authors determined the limits of detection of this method for the carbaryl-based pesticides carbaryl, parathion, diazinon, and phorate to be  $7.25 \times 10^{-9}$ ,  $3.25 \times 10^{-8}$ ,  $6.76 \times 10^{-8}$ , and  $1.9 \times 10^{-7}$  g/L, respectively.

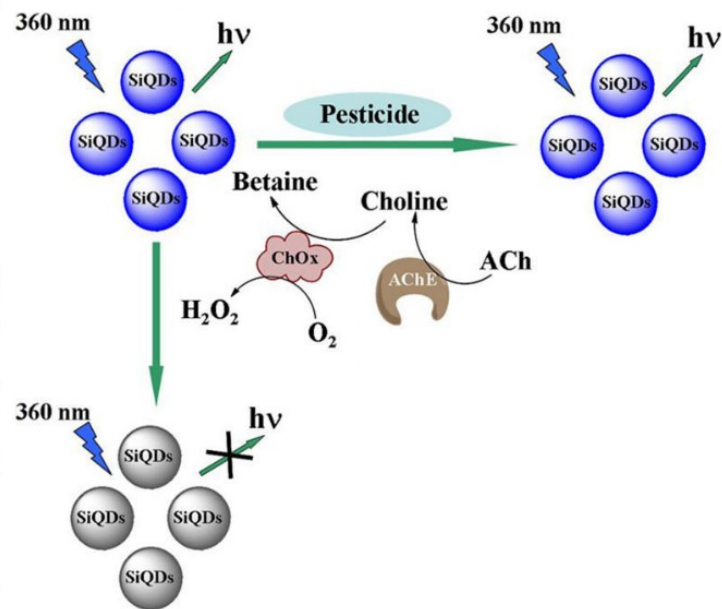


**Figure 1-22:** Mechanism of a SiNC based pesticide sensor. Reproduced and modified with permission from *Anal. Chem.*, **2013**, *85*, 11464–11470 (reference 259). Copyright 2013 American Chemical Society.

### 1.5.2.6 Environmental and Biological pH

There has been an increase of interest in materials with pH-responsive optical properties for the investigation of the environment, medicine, and biology.<sup>264</sup> Many studies have shown that QDs can be tailored for pH sensors; however, SiNCs have not been studied as thoroughly.<sup>265-268</sup> Feng and coworkers developed a pH sensor using blue luminescent, amine terminated SiNCs for water samples.<sup>269</sup> The investigation employed solutions containing SiNCs in Britton-Robinson (BR) buffer solution in the pH range of 2.01 to 11.02. It was determined that as the pH increased, the luminescence of the SiNCs increased, with luminescence stabilization occurring at pH=7.77. Also studied was the possible effect of interferents (*i.e.*,  $K^+$ ,  $Cd^{2+}$ ,  $Mg^{2+}$ ,  $Ca^{2+}$ ,  $Mg^{2+}$ ,  $NO_3^-$ ,  $SO_4^{2-}$ ,  $PO_4^{3-}$ ), which were shown to not have any significant interference effect on the SiNC sensing

system. When tested with real life water samples with varying pH, the pH values calculated with SiNCs were in close agreement with the actual pH values measured using a pH meter.

The above sections provided an overview of the different types of analytes that have been investigated using SiNCs and are summarized in Table 1-1. The majority of the sensors have used either amine or hydride terminated SiNCs with the main class of analytes being metal cations.

**Table 1-1:** Overview of the SiNC-based sensor systems discussed in Section 1.5.2.

Analyte class	Analyte	SiNC surface functionalization	LOD <sup>a</sup>	Ref. <sup>b</sup>
High Energy Material	DNT	Alkyl oligomer	18.2 ng (solid)	226
	DNT	Alkyl monolayer	6 ppb (vapor)	228
Metal Cation	TNT	3-aminopropyl	1 nM	227
	Hg <sup>2+</sup>	Amine terminated	50 nM	232
	Cu <sup>2+</sup>	Hydride	8 nM	233
	Cu <sup>2+</sup>	Silica	0.5 μM	231
	Cr <sup>4+</sup>	PAMAM-OH <sup>c</sup> coating	2.7 μM	234
Biologically Relevant Molecules	Glucose	Hydride	0.68 μM	239
		Hydride	0.05 μM	241
	Dopamine	Amine terminated	0.3 nM	244
Antibiotic	Ethanol	Hydride	380 ppm	251
	Tetracycline	Amine terminated	25.9 nM	219
	Oxytetracycline		20.4 nM	
Pesticide	Carbaryl	Hydride	28.3 nm	
			7.25 x 10 <sup>-9</sup> g/L	259
	Parathion		3.25 x 10 <sup>-8</sup> g/L	
	Diazinon		6.76 x 10 <sup>-8</sup> g/L	
	Phorate		1.9 x 10 <sup>-7</sup> g/L	
pH	pH	Amine terminated	pH range 2.01-7.7	269
<sup>a</sup> LOD means limit of detection. <sup>b</sup> Ref. means reference number cited in the main text. <sup>c</sup> PAMAM-OH is abbreviation for hydroxyl poly(amidoamine) dendrimer, 5 <sup>th</sup> generation.				

## 1.6 Thesis outline

This thesis focuses on the surface functionalization of SiNCs and the development of a series of sensor platforms based upon them. The use of radical based functionalization methods for the functionalization of SiNCs is described in Chapters 2 and 3. The method of hydrosilylation of SiNCs via thermal radical initiators, 2,2'-azobis(2-methylpropionitrile) and benzoyl peroxide, is evaluated for functional group tolerance and the possible reaction mechanism from which it proceeds is investigated in Chapter 2. Chapter 3 explores the functionalization of SiNCs with lipoic acid or dibutyl disulfide via the use of a commercial fluorescent light source for the generation of thiyl radicals.

Chapters 4 and 5 describe the integration of SiNCs into paper or polydimethylsiloxane solid substrates and subsequent use as sensing platforms. The investigation of a SiNCs paper-based sensor for the detection of higher energy compounds (*i.e.*, nitroaromatics, nitroamine, and nitrate esters) is discussed in Chapter 4. Chapter 5 explores the use of SiNCs for the detection of solution and vapor phase biogenic amines (*i.e.*, putrescene, spermidine and cadaverine) for the development of food spoilage sensors.

Finally, Chapter 6 provides a brief summary of the results outlined in Chapters 2-5 and delivers an outlook for future research directions related to surface functionalization methods and sensors.

## **Chapter 2**

# **Radical Initiated Hydrosilylation on Silicon Nanocrystal Surfaces: An evaluation of functional group tolerance and mechanistic study.<sup>2</sup>**

---

<sup>2</sup> A version of this chapter has been published:

Yang, Z.; Gonzalez, C. M.; Purkait, T. K.; Iqbal, M.; Meldrum, A.; Veinot, J. G. C. *Langmuir* **2015**, *31*, 10540-10548.

Zhenyu Yang and Christina M. Gonzalez have made equal contribution to the published paper.

## 2.1 Introduction

Nanomaterials like silicon nanocrystals (SiNCs) have attracted much attention because of their unique optoelectronic and chemical properties.<sup>50</sup> Silicon is particularly appealing because it is abundant in the Earth's crust, low in toxicity, and SiNCs exhibit size as well as surface-chemistry-dependent photoluminescence (PL).<sup>50,54,56,270,271</sup> Prototype applications of SiNCs include solar cells,<sup>272,273</sup> light-emitting diodes,<sup>274</sup> sensors,<sup>41,226,259</sup> bioimaging,<sup>275,276</sup> and batteries.<sup>277,278</sup> As is the case for all nanomaterials and their applications, developing versatile methods for tailoring particle surface chemistry is of paramount importance.<sup>56</sup>

The most common approach for modifying SiNC surfaces are all derivatives of hydrosilylation.<sup>62,132,279</sup> This class of reactions adds a Si–H bond across an unsaturated (*i.e.*, double or triple) C–C bond. Thermally activated hydrosilylation is widely employed because it proceeds regardless of particle dimension and there is no need for catalysts that can compromise material properties/purity (*vide infra*).<sup>113,137,138,181</sup> While a few exceptional cases exist,<sup>280,281</sup> thermal hydrosilylation has a high temperature requirement (upwards of 140 °C) necessary for homolytic cleavage of the Si–H. Another important shortcoming of thermally activated hydrosilylation, is the formation of SiNC surface bonded ligand oligomers that could limit future applications.<sup>158</sup>

At first inspection, photo-initiated hydrosilylation provides a viable alternative that addresses many of these challenges; it proceeds at room temperature, does not require catalysts, and provides monolayer passivation. Unfortunately, this reaction is size-dependent;<sup>144</sup> larger SiNCs (*i.e.*,  $d \geq 6$  nm) are not effectively functionalized. This alone limits the general applicability of this approach. Drawing from molecular silane chemistry, transition metal-catalyzed hydrosilylation has been explored; regrettably these catalysts can be costly, difficult to remove,

and compromise SiNC optical properties.<sup>154,190</sup> Recently, our group reported room-temperature SiNC surface hydrosilylation using borane reagents and diazonium salts, however, functional group tolerance has not been thoroughly investigated.<sup>147,152</sup> Catalyst-free, room-temperature hydrosilylation of  $\omega$ -ester- (*i.e.*, alkene–COOR) and  $\omega$ -acid-terminated alkenes (*i.e.*, alkene–COOH) have been reported;<sup>282</sup> this method was recently extended to controlled SiNC passivation with styrene monolayers.<sup>283</sup>

Radical initiators, such as 2,2'-azobis(2-methylpropionitrile) (AIBN) and peroxides promote hydrosilylation on bulk silicon surfaces.<sup>136,284,285</sup> Linford and Chidsey proposed radicals produced from the thermal decomposition of diacyl peroxides in the presence of hydride terminated bulk silicon (*i.e.*, Si(111) and Si(100)), cause homolytic cleavage of Si-H by hydride abstraction, to promote insertion of an alkene.<sup>136,181</sup> Moran and Carter also applied this general approach to graft polymers onto bulk Si (100) surfaces, however they reported the AIBN-derived radicals were not responsible for the corresponding reaction.<sup>284</sup> Nelles *et al.* also provided a brief report on radical initiated functionalization of freestanding SiNCs, however, experimental conditions and mechanistic details were scarce.<sup>146</sup> Clearly, radical initiated surface modification of SiNCs holds promise and would benefit from a systematic study. The following discussion describes an investigation of the effectiveness of two commercially available thermally activated radical initiators (*i.e.*, AIBN and benzoyl peroxide (BP)) in promoting hydrosilylation reactions on the surfaces of SiNCs. All SiNCs were comprehensively characterized using electron microscopy, X-ray photoelectron spectroscopy, <sup>1</sup>H NMR, nanostructure-assisted laser desorption/ionization mass spectrometry (NALDI-MS), optical spectroscopy (*i.e.*, photoluminescence and FT-IR), as well as thermogravimetric analysis (TGA).

## 2.2 Experimental

### 2.2.1 Reagents and Materials

Commercial hydrogen silsesquioxane (HSQ, trade name Fox-17) was purchased from Dow Corning Corporation (Midland, MI). Electronics grade hydrofluoric acid (HF, 49% aqueous solution) was purchased from J.T. Baker. Reagent grade methanol, ethanol, 1-dodecene (95%), styrene (99%), methyl-10-undecenoate (96%), 4-pentenoic acid (97%), phenylacetylene (98%), hexene (97%), octyne (98%), 2,2'-azobis(2-methylpropionitrile) (AIBN, 98%), benzoyl peroxide (98%), 2,2,6,6-tetramethyl-1-piperidinyloxy (TEMPO, 98%) were purchased from Sigma-Aldrich and used as received. Reagent grade toluene (Sigma Aldrich) was dried over molecular sieves (4Å) prior to use. All ligands were purified by passing over neutral alumina to remove inhibitors immediately prior to use.

### 2.2.2 Material Characterization and Instrumentation

Fourier Transform Infrared Spectroscopy (FT-IR) was performed using a Nicolet Magna 750 IR spectrophotometer by drop-coating a toluene dispersion of SiNCs. X-ray photoelectron spectroscopy (XPS) measurements were obtained using a Kratos Axis Ultra X-ray photoelectron spectrometer operated in energy spectrum mode at 210 W. XPS samples were prepared as a film drop-cast from SiNC toluene dispersion onto a copper foil substrate. Spectra were fitted using CasaXPS (VAMAS) software and were calibrated to the lowest binding energy component of the C 1s emission at 284.8 eV. Transmission electron microscopy (TEM) was performed on a JEOL-2010 (LaB<sub>6</sub> filament) electron microscope with an accelerating voltage of 200 keV using samples of SiNCs drop-cast onto a holey carbon coated copper grid (300 mesh, Electron Microscopy Science). High-resolution (HR) TEM images were obtained from Hitachi-9500 electron

microscope with an accelerating voltage of 300 kV. The HRTEM images were processed using Gatan Digital Micrograph software (Version 2.02.800.0).

Photoluminescence (PL) spectra were obtained using a Cary Eclipse spectrophotometer ( $\lambda_{\text{ex}} = 350 \text{ nm}$ ). PL lifetimes were acquired by illuminating a solution sample in a quartz cuvette with an argon ion laser (476 nm, ~30 mW). The laser was modulated by an acousto-optic modulator operating at 500 Hz. Emission from the SiNCs was channeled into a photomultiplier (Hamamatsu H7422P-50) connected to a photon counting card (Becker-Hickl PMS-400A). Lifetime decay data was fit to a stretched exponential function in Mathematica (Version 10) given by  $y(t) = A[\exp(-(t/\tau)^\beta)] + C$ , where  $A$  is the initial intensity,  $\tau$  is the time decay (basic lifetime),  $\beta$  is a stretching parameter that can vary between 0 and 1, and  $C$  is an offset.<sup>286-288</sup>

Nanostructured-assisted laser desorption/ionization mass spectroscopy (NALDI-MS) spectra were obtained in the positive/negative reflection mode using a Bruker Daltonics UltrafleXtreme MALDI TOF/TOF mass spectrometer. Samples were prepared by spotting 1  $\mu\text{L}$  of sample solution onto a Bruker Daltonics NALDI target and air-dried. Electron ionization mass spectroscopy (EI-MS) spectra were collected on a Kratos MS-50 (high resolution, electron impact ionization). The samples were loaded by direct probe.

Nuclear magnetic resonance spectroscopy (NMR) spectra were obtained using a Varian Unity INova Console 500 MHz NMR spectrometer. A concentrated (*ca.* 6 mg/mL) solution of functionalized SiNCs in  $\text{CD}_2\text{Cl}_2$  was used to collect the  $^1\text{H}$  NMR spectra. The obtained FID files were processed using Nuts NMR data processing software.

Thermogravimetric analysis (TGA) was performed using a Mettler Toledo Star TGA/DSC system. Functionalized SiNC samples were placed in a Pt pan and heated in an Ar atmosphere from 25 to 1000  $^\circ\text{C}$  at 10  $^\circ\text{C}/\text{min}$ .

### 2.2.3 Preparation of oxide-embedded SiNCs ( $d_{\text{avg}} = \sim 3, 5, \text{ and } 8 \text{ nm}$ )

Oxide-embedded SiNCs were prepared using well-established procedures developed in our laboratory.<sup>112</sup> Briefly, solid HSQ was placed in a quartz reaction boat, transferred to a tube furnace and heated at 1100 °C in an argon atmosphere containing 5% hydrogen. This general procedure affords an amber SiNC/SiO<sub>2</sub> composite containing 3 nm SiNCs that was subsequently crushed using an agate mortar and pestle. To obtain larger NCs (*i.e.*,  $d_{\text{avg}} = \sim 5 \text{ and } 8 \text{ nm}$ ), *ca.* 0.5 g of the SiNC/SiO<sub>2</sub> composite placed in a carbon boat, transferred to a high temperature furnace (Sentro Tech Corp.) and heated in an argon atmosphere at 1200 °C ( $d_{\text{avg}} = 5 \text{ nm}$ ) or 1300 °C ( $d_{\text{avg}} = 8 \text{ nm}$ ) for 1 h. After cooling to room temperature, the resulting composites were ground using a mortar and pestle. All composites were shaken with high-purity silica beads using a Burrell Wrist Action Shaker for 12 h.

### 2.2.4 Preparation of hydride-terminated SiNCs

SiNC/SiO<sub>2</sub> composite (0.2 g) was transferred into a polyethylene terephthalate (PET) beaker containing a Teflon coated stir bar. Ethanol (3 mL) and water (3 mL) were added and the mixture was stirred to ensure uniform wetting; this procedure afforded a brown suspension. Subsequently, a 49 % aqueous HF (3 mL) solution was added slowly with stirring. **Caution:** HF is dangerous and requires appropriate handling procedures and personal protective equipment. After 1 hour, the suspension changed appearance becoming orange/yellow. Hydrophobic hydride-terminated SiNCs (H-SiNCs) were extracted from the ethanolic aqueous layer using 3 x ~10 mL extractions into toluene. The resulting SiNC toluene suspension was divided equally amongst test tubes and centrifuged at 3000 rpm; the supernatant was decanted and the H-SiNC precipitate was used immediately in functionalization procedures (*vide infra*).

### 2.2.5 Radical initiated hydrosilylation of alkenes/alkynes by H-SiNCs

The H-SiNCs obtained from the etching procedure (*vide supra*) were redispersed into toluene (*ca.* 20 mL) that had been pre-dried over molecular sieves (4Å) and transferred to an oven-dried (125 °C) 100 mL Schlenk flask equipped with a Teflon coated magnetic stir bar and attached to an argon charged Schlenk line. The radical initiator (*i.e.*, AIBN or BP; 0.061 mmol) and surface ligand of choice (*i.e.*, 1-dodecene, 1-octyne, 4-pentenoic acid, methyl-10-undecenoate, styrene and phenylacetylene; 0.018 mol) were added to the flask and the reactant mixture was subjected to three freeze-pump-thaw cycles. The reaction mixture was subsequently heated to and maintained at 60 °C (AIBN) or 85 °C (BP) and stirred for 19 h to yield orange/yellow solutions.

Equal volumes (*ca.* 10 mL) of the orange/yellow solutions containing functionalized nanoparticles were dispensed into centrifuge tubes. For alkyl terminated particles, 1:1 methanol:ethanol anti-solvent was added to achieve a total volume of 50 mL in each tube. This procedure induced the formation of an orange precipitate that was isolated by centrifugation in a high-speed centrifuge at 14000 rpm for 0.5 h. The supernatant was decanted and the particles were redispersed in a minimal amount of toluene (*ca.* 2 mL) and re-precipitated upon addition of 1:1 methanol:ethanol. This solvent/anti-solvent purification process was repeated twice. Purification of styrene-terminated SiNCs was achieved by implementing a variation of this method using 100% ethanol as the anti-solvent. Purification of ester-terminated and carboxylic-terminated used hexanes as the anti-solvent. Finally, the purified SiNCs were redispersed in dry toluene (pre-dried over molecular sieves (4Å)), filtered through a 0.45 μm polytetrafluoroethylene (PTFE) syringe filter, and stored in vials for further use. The resulting SiNCs were analyzed using FT-IR, TEM, XPS, and PL.

## 2.2.6 Thermal functionalization of H-SiNCs

The H-SiNCs obtained from the etching procedure (*vide supra*) were redispersed into *ca.* 20 mL of 1-dodecene, transferred into an oven-dried (125 °C) Schlenk flask equipped with a Teflon coated magnetic stir bar, and attached to an argon charged Schlenk line. The flask was then evacuated and backfilled with argon three times to remove air from the solution. The solution was then heated to a temperature of 190 °C and was left stirring for 15 h resulting in a non-opalescent orange/yellow solution. This SiNC solution was purified as described above for alkyl particles and finally stored in a vial for TGA and <sup>1</sup>H NMR analysis.

## 2.2.7 Reaction of TEMPO with SiNCs

H-SiNCs (25 mg) were re-dispersed in dry toluene (pre-dried over molecular sieves (4Å)) and transferred to an oven-dried (125 °C) 100 mL Schlenk flask equipped with a Teflon coated magnetic stir bar and attached to an argon charged Schlenk line. TEMPO (0.11 mmol) and the initiator of choice (*i.e.*, AIBN or BP; 0.061 mmol) were added and the reaction mixture was subjected to three freeze-pump-thaw cycles. The cloudy reaction mixture was heated to, and maintained at 60 °C (AIBN) or 85 °C (BP) under argon atmosphere for 19 h. The reaction mixture remained cloudy with no color change consistent with negligible surface modification. No further characterization was performed.

## 2.2.8 Reaction of dodecene with radical initiators

Dodecene (0.018 mol) was dissolved in dry toluene (20 mL, pre-dried over molecular sieves (4Å)) and the radical initiator of choice (*i.e.*, AIBN or BP; 0.061 mmol) were added to an oven-dried (125 °C) Schlenk flask equipped with a Teflon coated magnetic stir bar and attached to an argon charged Schlenk line. The reaction mixture was then subjected to three freeze-pump-

thaw cycles and subsequent heating to 60 °C (AIBN) or 85 °C (BP) for 19 h and yielded a colorless solution. The resulting solution was analyzed using EI-MS.

### **2.2.9 Reaction of TEMPO and SiNCs in absence of radical initiators**

H-SiNCs (25 mg) were re-dispersed in dry toluene (pre-dried over molecular sieves (4Å)) and transferred to an oven-dried (125 °C) 100 mL Schlenk flask equipped with a Teflon coated magnetic stir bar and attached to an argon charged Schlenk line. TEMPO (0.11 mmol) was added and the reaction mixture was subjected to three freeze-pump-thaw cycles and subsequent heating to 60 °C (AIBN) or 85 °C (BP) for 19 h. The particles were isolated by centrifugation, purified using toluene as a solvent (5 mL) and methanol as the anti-solvent (40 mL). This procedure yielded an orange precipitate that was isolated by centrifugation in a high-speed centrifuge at 14000 rpm for 0.5 h. The supernatant was decanted and the particles were redispersed in a minimal amount of toluene (*ca.* 5 mL, pre-dried over molecular sieves (4Å)) and re-precipitated upon addition of methanol (40 mL). This solvent/anti-solvent purification process was repeated twice. The supernatant was discarded and the isolated solid was analyzed by FT-IR.

### **2.2.10 Evaluation of the influence of reaction time**

H-SiNCs (25 mg) were re-dispersed in dry toluene (pre-dried over molecular sieves (4Å)) and transferred to an oven-dried (125 °C) 100 mL Schlenk flask equipped with a Teflon coated magnetic stir bar and attached to an argon charged Schlenk line. 1-Dodecene (0.018 mol) and the radical initiator of choice (*i.e.*, AIBN or BP; 0.061 mmol) were added and the reaction mixture was subjected to three freeze-pump-thaw cycles. Subsequently the reaction mixture was heated to 60 °C (AIBN) or 85 °C (BP). Samples (2 mL) of the reaction mixture were extracted at intervals of 1, 2, 3, 5, and 19 h after reaction temperature stabilization. Each sample was purified using the

toluene/methanol solvent/anti-solvent procedure for alkyl functionalized SiNCs described above. The nanocrystal products were evaluated using NALDI-MS.

### 2.2.11 Estimation of surface coverage

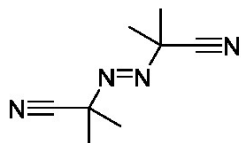
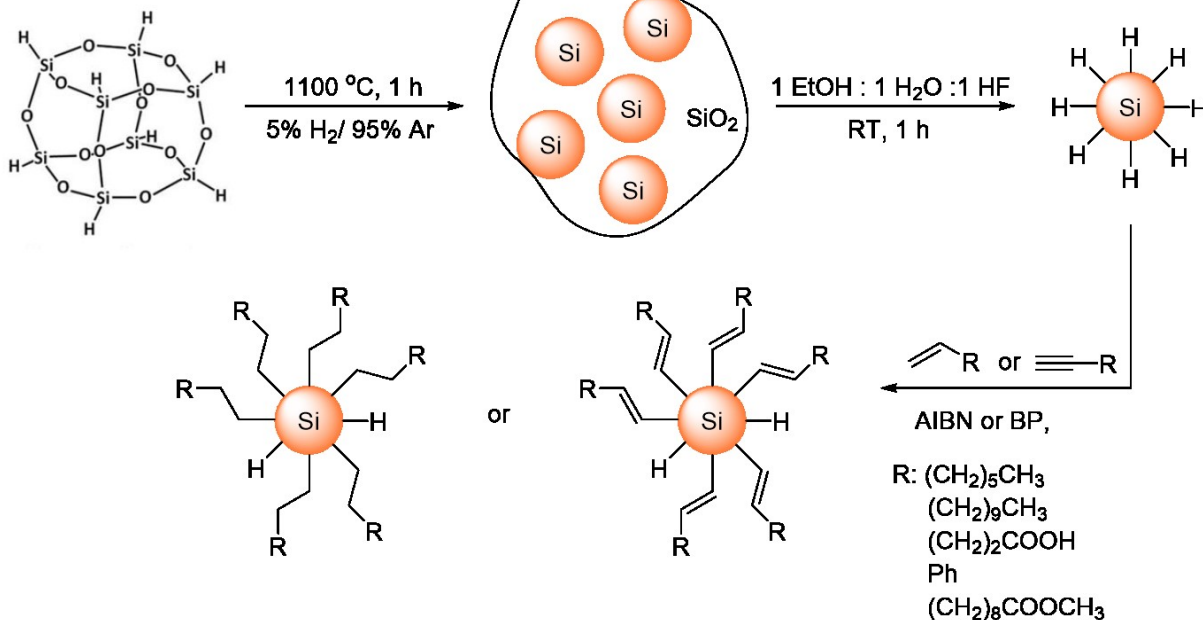
Surface coverages afforded by the present functionalization methods were evaluated for dodecyl-functionalized SiNCs using a well-established literature procedure.<sup>101</sup> Briefly, a known mass of dodecyl-functionalized SiNCs was dispersed in 1 mL CDCl<sub>3</sub> with 0.01% (v/v) tetramethylsilane (TMS). The ratios of the integrated peak area arising from dodecyl methyl protons (3 H) and the TMS protons (12 H) were determined from the <sup>1</sup>H NMR spectra. Surface coverage was also estimated from TGA traces assuming that the mass loss arises from the loss of grafted organic ligands and that there is no increase in mass due to oxidation of SiNCs.<sup>152</sup> The number of ligands per nanocrystal and surface coverage were estimated for a compact icosahedral  $d = 3.5$  nm SiNCs consisting of 1100 Si atoms and 300 surface Si atoms.<sup>289</sup> A description of the equations used for these calculations can be seen in the Appendix.

## 2.3 Results and Discussion

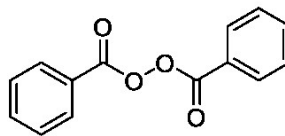
Well-defined H-SiNCs ( $d \sim 3$  nm) were obtained using an established procedure developed in the Veinot Laboratory (Scheme 2.1).<sup>112</sup> The resulting H-SiNCs were then reacted with one of two common thermally activated radical initiators (*i.e.*, AIBN and BP) and a series of alkene or alkyne terminated ligands (*i.e.*, 1-dodecene, 1-octyne, methyl-10-undecenoate, styrene and phenylacetylene). Briefly, freshly prepared H-SiNCs were combined with the ligand and initiator of choice in toluene under inert conditions (*i.e.*, argon atmosphere), degassed, and heated to an appropriate initiation temperature (*i.e.*, AIBN, 60 °C; BP 85 °C). Reaction progress was qualitatively evaluated by monitoring the reaction mixture transparency – past experience shows

SiNCs bearing well-passivated surfaces afford transparent mixtures/solutions (see Figure 2-1). A typical AIBN initiated reaction between H-SiNCs and dodecene became transparent after *ca.* 5 h. Consistent with other functionalization procedures, we also note surface passivation renders the NCs PL upon exposure to UV irradiation (Figure 2-1). Qualitatively, reactions initiated by BP proceeded more quickly than those of the equivalent reaction using AIBN. The H-SiNC suspension became transparent after 1 h of starting the reaction (Figure 2-1). It is reasonable that this difference in reaction times arises because of the different half-lives of AIBN and BP; the half-life of AIBN at 70° C and BP at 85° C in toluene are 4.8 and 1.4 h, respectively.<sup>290</sup> The shorter half-life time for BP would suggest the generation of radicals from the initiator would occur at a faster rate, allowing for hydrosilylation reactions using BP to progress at a faster rate. These observations also suggest these radical driven surface reactions proceed more quickly than analogous photochemical and thermal hydrosilylations on H-SiNCs, which require at least 15 h to reach completion.<sup>144,181</sup>

### Hydrogen Silsesquioxane



2,2'-azobis(2-methylpropionitrile)  
AIBN



benzoyl peroxide  
BP

**Scheme 2-1:** Synthesis and radical initiated functionalization of 3 nm SiNCs. Additional annealing at 1200 °C ( $d = 5\text{ nm}$ ) and 1300 °C ( $d = 8\text{ nm}$ ) prior to HF etching is required to achieve larger particles.

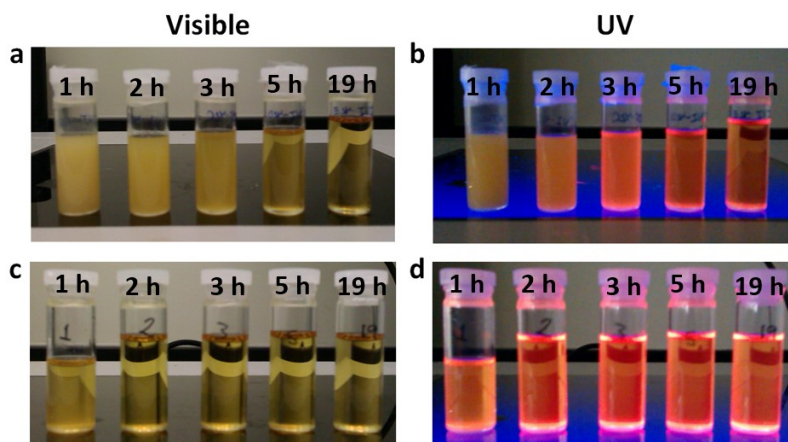


**Figure 2-1:** Photographs of suspensions/solutions of 3 nm hydride-terminated SiNCs/dodecene mixture under visible light and UV light irradiation. (a, b) AIBN and (c, d) BP are used as radical initiators. Samples were extracted from dispersions at predesigned reaction time (from left to right in each image: 1, 2, 3, 5, and 19 h).

FT-IR spectroscopy is essential when investigating SiNC surface modification. The IR spectra of functionalized SiNCs from the BP and AIBN initiated reactions are shown in Figure 2-2 and Figure 2-3, respectively. A typical spectrum of H-SiNCs shows two distinctive strong absorptions at *ca.* 2100 and 850  $\text{cm}^{-1}$ ; these are routinely attributed to Si-H<sub>x</sub> ( $x = 1-3$ ) stretching and scissoring, respectively.<sup>280,281</sup> Following hydrosilylation, the intensities of these signals are substantially reduced and features associated with new surface groups appear. For example, reactions employing n-alkenes saw the appearance of C-H<sub>x</sub> stretching and bending in the 2850-3000  $\text{cm}^{-1}$  and 1300-1450  $\text{cm}^{-1}$  regions, respectively.<sup>291</sup> Spectra acquired for n-alkyne-derivatized SiNCs showed the absorption at 1600  $\text{cm}^{-1}$  and can be confidently assigned to C=C, as well as the aliphatic C-H<sub>x</sub> stretching and bending at 2850-2930 and 1475-1365  $\text{cm}^{-1}$ , respectively. When styrene and phenyl acetylene were used, the spectra included features characteristic of phenyl ring C-H (3100-3000  $\text{cm}^{-1}$ ), C-C (1600-1585  $\text{cm}^{-1}$ ) moieties as well as phenyl ring overtones (2000-1665  $\text{cm}^{-1}$ ).<sup>280</sup> For reactions involving methyl-10-undecenoate, the spectra showed the appearance

of C=O stretching ( $\sim 1730\text{ cm}^{-1}$ ).<sup>282,292</sup> The spectra of 4-pentenoic acid reacted SiNCs showed features at  $3400\text{ cm}^{-1}$  and  $1705\text{ cm}^{-1}$  corresponding to  $\text{-OH}$  stretching and C=O groups, respectively.<sup>293</sup> In addition, the spectra of functionalized SiNCs also exhibited features at  $\sim 1130\text{-}1000\text{ cm}^{-1}$  (Si-O-Si stretching),  $\sim 2250\text{ cm}^{-1}$  ( $\text{H}_x\text{Si-O}_y$  backbonding), and at  $\sim 2100\text{ cm}^{-1}$  (Si-H stretching), indicating incomplete surface coverage of the SiNCs.<sup>294,295</sup>

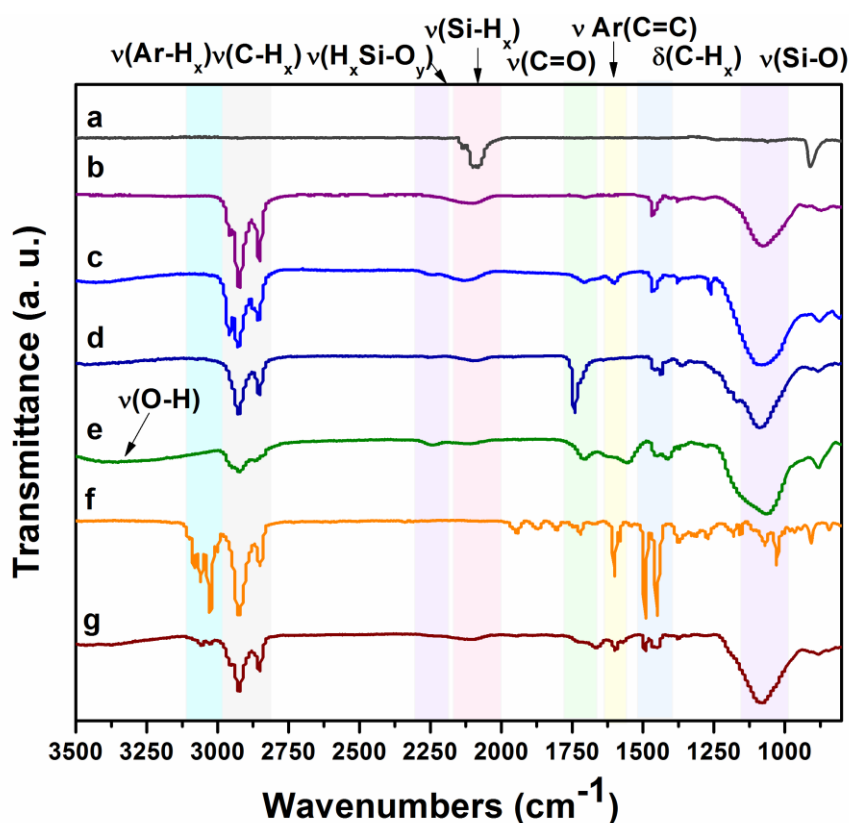


**Figure 2-2:** FT-IR spectra of 3 nm SiNCs obtained from BP initiated reactions with indicated surface functionalities: a) hydride, b) dodecene, c) octyne, d) methyl-10-undecenoate, e) pentenoic acid, f) styrene, and g) phenylacetylene.

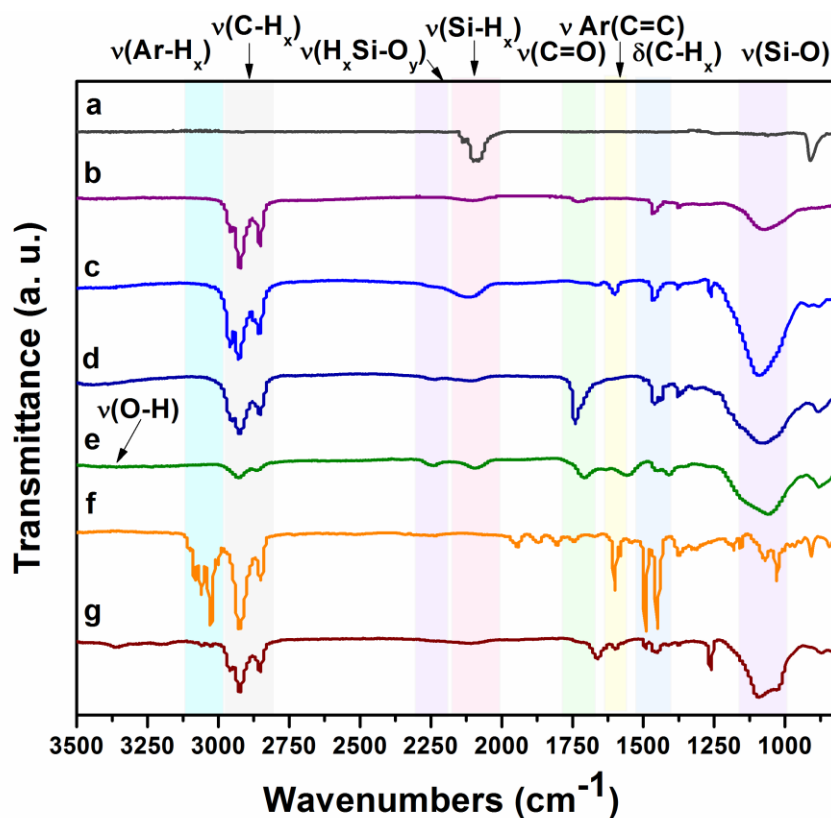


**Figure 2-3:** FT-IR spectra of 3 nm SiNCs obtained from AIBN initiated reactions with indicated surface functionalities: a) hydride, b) dodecene, c) octyne, d) methyl-10-undecenoate, e) pentenoic acid, f) styrene, and g) phenylacetylene.

The surface coverage of the SiNCs obtained from radical initiated hydrosilylation can be estimated using the  $^1\text{H}$  NMR and TGA analysis (Figures 2-4 and 2-5, Tables 2-1 and 2-2).<sup>101,152,289</sup>  $^1\text{H}$  NMR spectra of SiNCs functionalized with 1-dodecene in  $\text{CDCl}_3$  (Figure 2-4) show resonances from terminal methyl protons with a chemical shift at *ca.* 0.9 ppm and methylene chain protons in the range of *ca.* 1.1 to 1.6 ppm. From the  $^1\text{H}$  NMR spectrum, a ratio of the integrated peak areas of the surface organic groups to tetramethylsilane (TMS, an internal standard) provides an estimate of percent surface coverage. Reactions involving 1-dodecene initiated by BP provide a slightly higher surface coverage (64%) than those from the AIBN reaction (50%). The  $^1\text{H}$  NMR spectrum

of ester functionalized SiNCs shows resonances at *ca.* 1.3, 1.6, 2.3 ppm for methylene protons and at 3.6 ppm for ester methyl protons (Figure 2-5a). The spectrum of pentanoic acid functionalized NCs shows broad low intensity signals at 1.3 and 1.5 ppm due to the limited solubility of the product (Figure 2-5b). The limited solubility of the pentanoic acid SiNCs precluded reliable surface coverage estimates from NMR data. Meaningful evaluation of surface coverage on styrene and phenylacetylene functionalized NCs using NMR data was not possible because of precise integration of the low intensity and broad resonance of aromatic protons is unreliable. Based on these limitations of  $^1\text{H}$  NMR analyses, TGA was also employed to determine surface coverage (see Table 2-2). *n*-Alkane functionalities provided the highest surface coverage (64%) of the surfaces investigated here (33% for phenylacetylene, 34% for ester, and 42% for carboxylic acid).

The same surface coverage analysis of  $^1\text{H}$  NMR and TGA was also applied to thermal hydrosilylation of SiNCs with 1-dodecene. From the  $^1\text{H}$  NMR spectrum (not shown), an intense resonance of ligand protons was observed and resulted in a surface coverage of 223% (Table 2-1). TGA analysis resulted in a high weight loss (83%) and showed a similar high surface coverage of 262% (Table 2-2). This is substantially higher than the coverage of SiNCs with 1-dodecene using either AIBN or BP as radical initiators. This high surface coverage indicated the formation of oligomers on the surface of the SiNCs.<sup>158</sup>

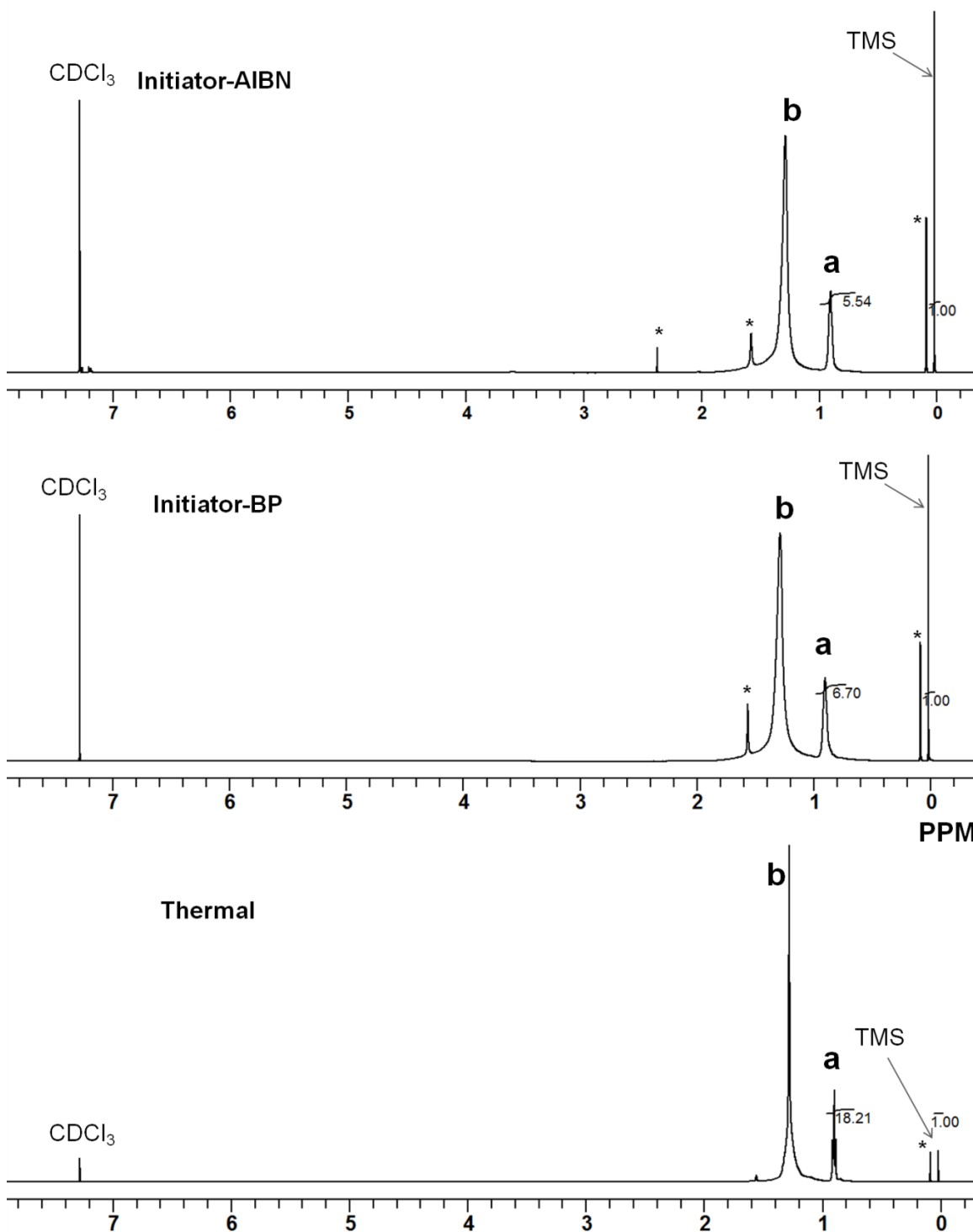


**Figure 2-4:**  $^1\text{H}$  NMR spectra in  $\text{CDCl}_3$  containing 0.01% (v/v) TMS of dodecyl-SiNCs obtained from the indicated functionalization method showing integration of dodecyl methyl protons (3H) to TMS protons (12 H). Dodecyl methyl protons and chain methylene protons denoted by a and b respectively. Solvent impurities denoted by an asterisk (\*).

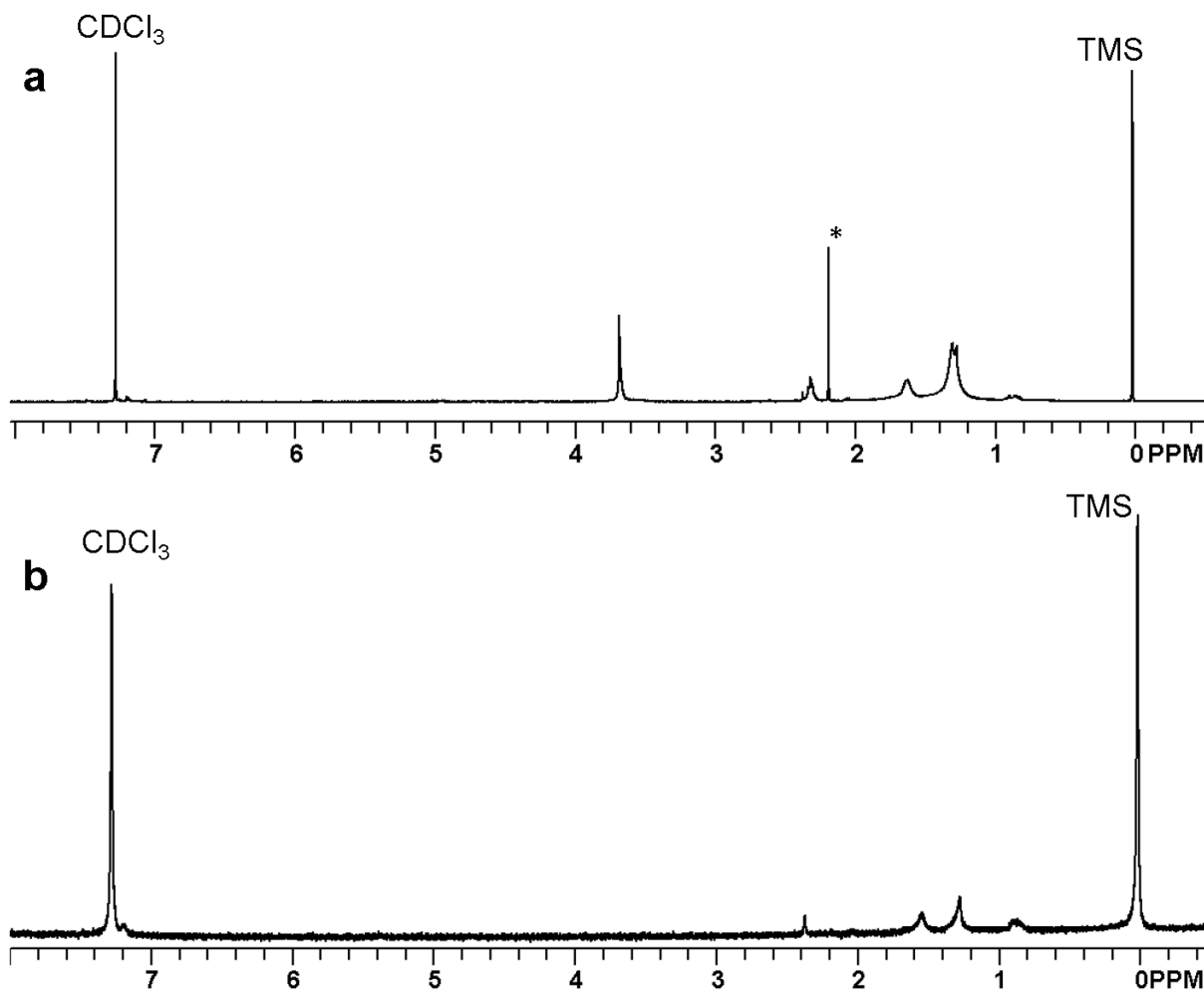


**Figure 2-5:** <sup>1</sup>H NMR spectra in CDCl<sub>3</sub> containing 0.01% (v/v) TMS of a) methyl-10-undecenoate and b) pentanoic acid functionalized SiNCs obtained from BP initiated functionalization. Solvent impurities denoted by an asterisk (\*).

**Table 2-1:** Determination of surface coverage using <sup>1</sup>H NMR.

Ligand/ Initiator	Ligand methyl to TMS Proton ratio <sup>§</sup>	Ligand to TMS mole ratio	Moles of ligand <sup>§</sup>	Moles of Si atoms <sup>§</sup>	Number of ligands per NC	%Surface coverage
Dodecene/ AIBN	0.88	3.52	2.59E-06	2.00E-05	142	47
Dodecene/ BP	1.01	4.06	2.98E-06	1.76E-05	186	62
Dodecene/ Thermal	1.58	6.33	4.66E-06	7.67E-05	668	223
Ester/ BP	0.73	2.93	2.15E-06	2.02E-05	117	39

<sup>§</sup> per 1 mg of functionalized SiNCs.

**Table 2-2:** Surface coverage metrics determined using TGA.

Ligand/ Initiator	% Mass loss	% Mole of ligand	% Mole of Si atoms	Number of ligands per NC	%Surface coverage
Dodecene/ AIBN	27.6	0.267	1.950	151	50
Dodecene/ BP	41.77	0.303	1.737	192	64
Dodecene/ Thermal	83	0.481	0.674	786	262
Ester/ BP	40.0	0.199	2.127	103	34
Acid/ BP	29.0	0.289	2.517	127	42
Phenylacetylene/ BP	25	0.244	2.659	101	34

NALDI-MS is a powerful tool that gives insight into the nature of surface bonded groups; it has been successfully applied to the evaluation of SiNC surface oligomerization.<sup>158</sup> Herein, we employ NALDI-MS to interrogate the SiNC surface groups obtained from radical initiated reactions. For convenience, 1-dodecene was chosen as the test case. Control samples, containing only AIBN or BP initiator and ligands were prepared and treated using the identical protocols, yet no mass signals corresponding to dodecene oligomers/polymers were observed (Figures 2-5 and 2-6). To evaluate SiNC modification, we performed a time-dependent study: samples were extracted from SiNC dispersions at predetermined times (*i.e.*, 1, 2, 3, 5, and 19 h), purified, and evaluated. It is known that the Si-Si linkage is the weakest of the surface bonds (*i.e.*, Si-Si, 210–250 kJ mol<sup>-1</sup>; Si-C, 369 kJ mol<sup>-1</sup>; and C-C, 292-360 kJ mol<sup>-1</sup>), and will cleave preferentially during NALDI analysis, therefore liberated groups are expected to include differing numbers of silicon atoms.<sup>131,158</sup> The fragmentation patterns of all samples are complex and conclusive identification of individual signals is not possible (Figures 2-7, 2-8, 2-9, and 2-10).<sup>158</sup> Signals from samples highlighted in green can be assigned to peaks not associated with the background signal or straightforward dodecene and dodecene oligomers. No mass fragments associated with the dodecene monomer (*i.e.*,  $m/z = 168.3$ ) were detected, consistent with effective sample purification. Also, no high molecular weight fragments separated by  $m/z = 168.3$  corresponding to dodecene oligomers/polymers were detected suggesting oligomers/polymers did not form. It was also interesting to note the differences seen in Figure 2-9 is a NALDI-MS spectra obtained from dodecene functionalized SiNCs from the use of AIBN while Figure 2-11 is NALDI-MS obtained from BP initiated reaction. However, the exact origin of this difference is unknown.

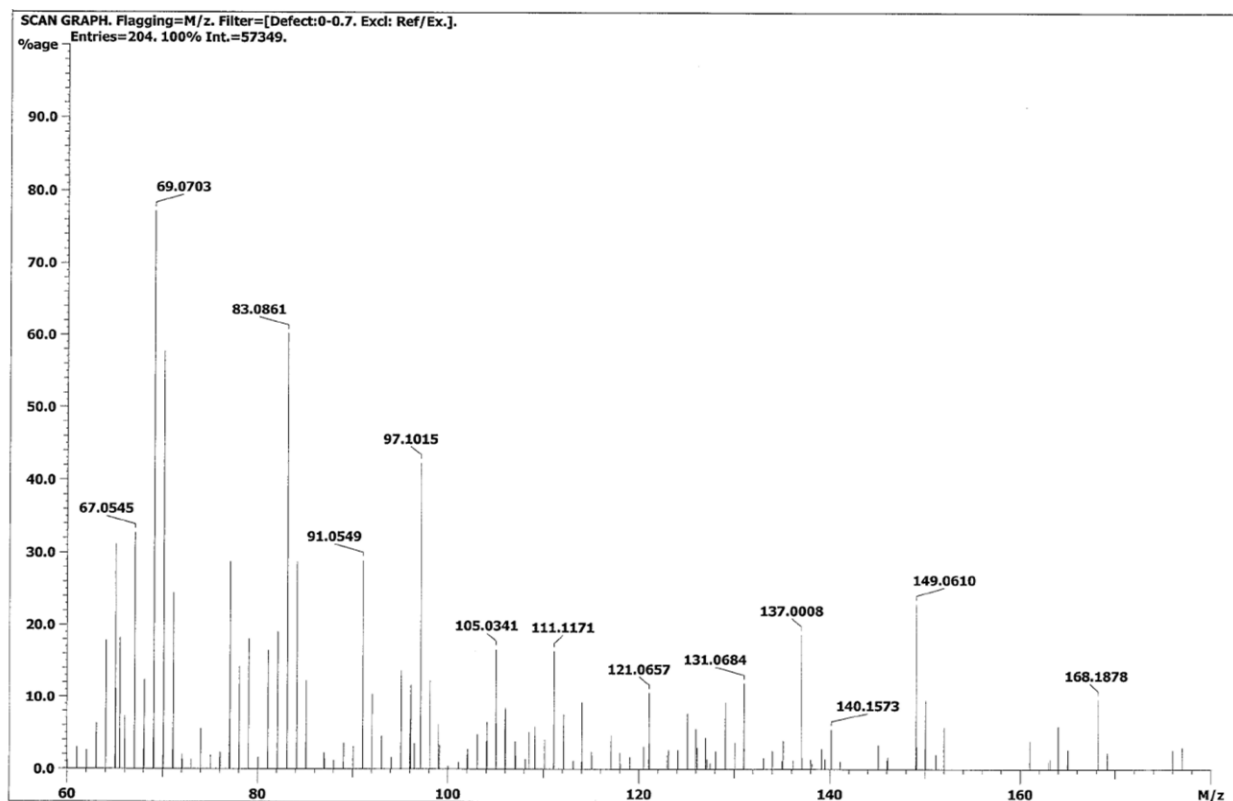


**Figure 2-6:** EI-MS taken after reaction of dodecene and AIBN. No dodecene oligomeric species were detected.

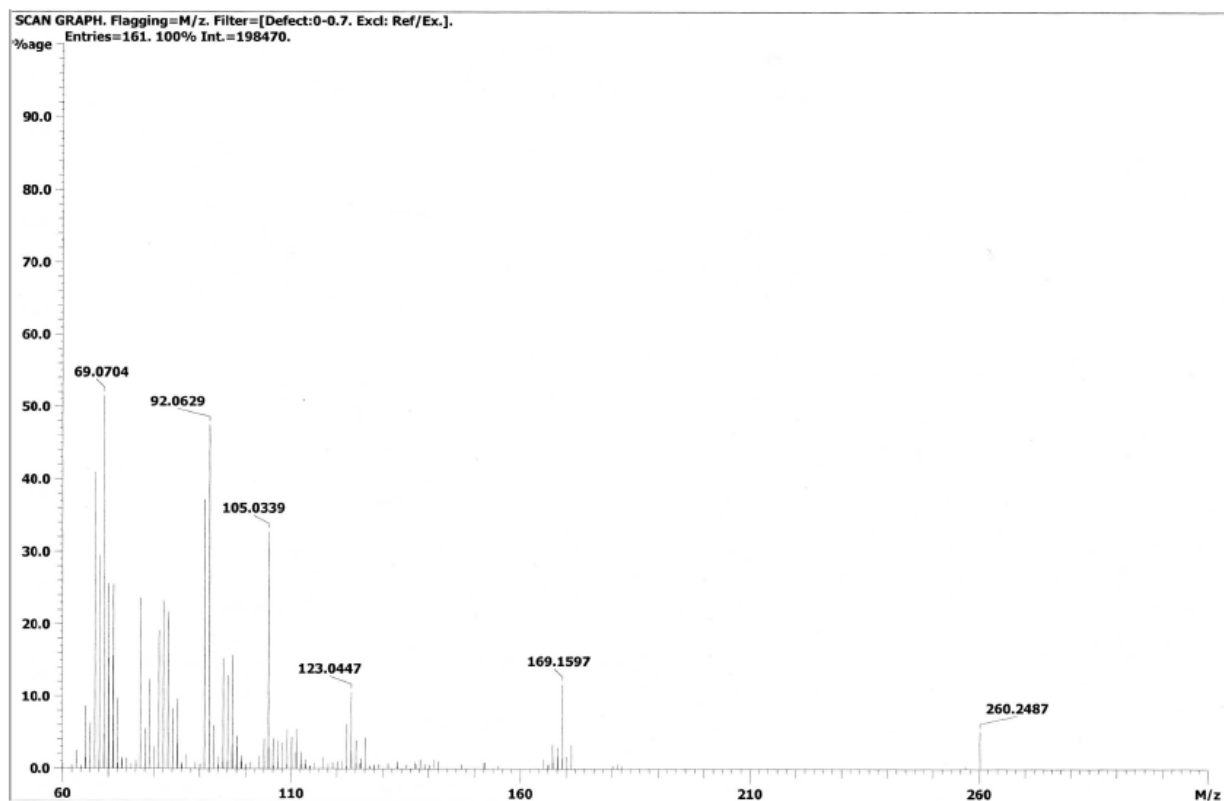


**Figure 2-7:** EI-MS taken after reaction of dodecene and BP. No dodecene oligomeric species were detected.

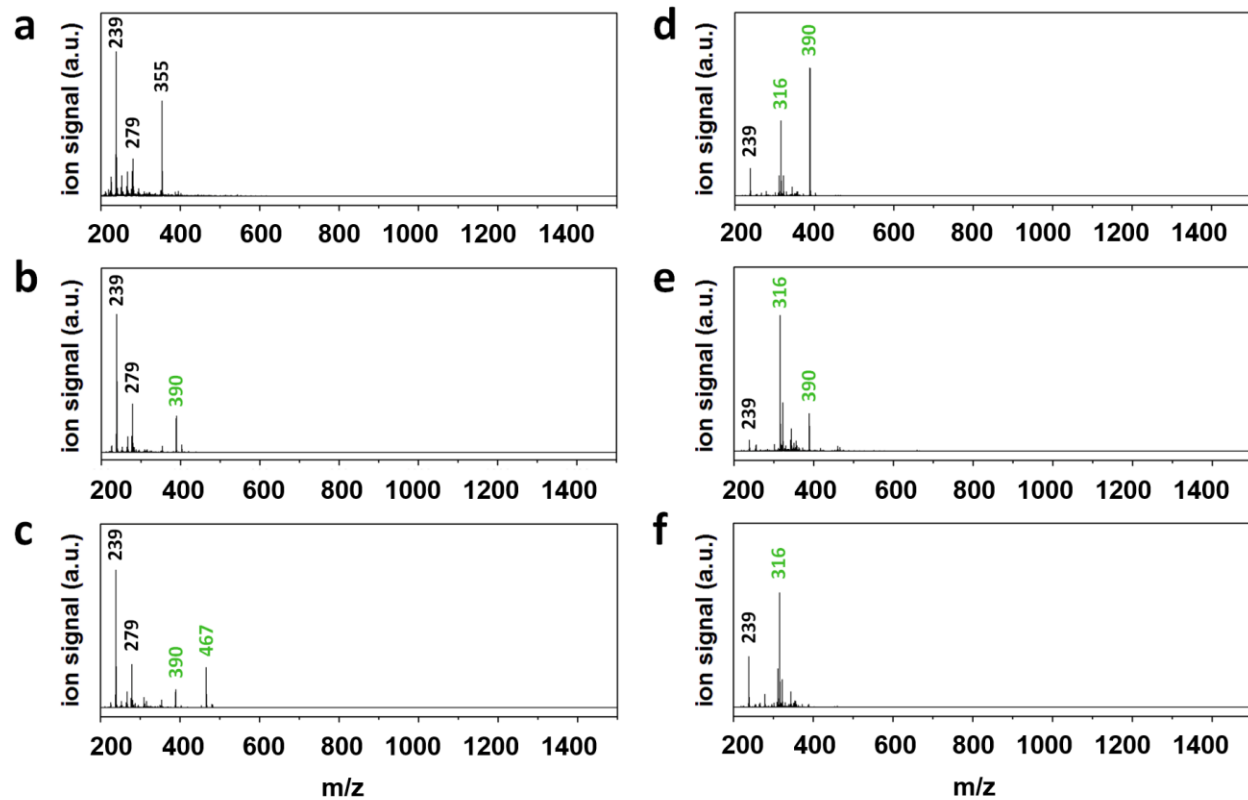


**Figure 2-8:** NALDI-MS spectra of 3 nm dodecyl-passivated SiNCs functionalized at different pre-designed reaction time using AIBN as reaction initiator: (a) background, (b) 1, (c) 2, (d) 3, (e) 5, and (f) 12 h in the range of 200-1500 m/z.

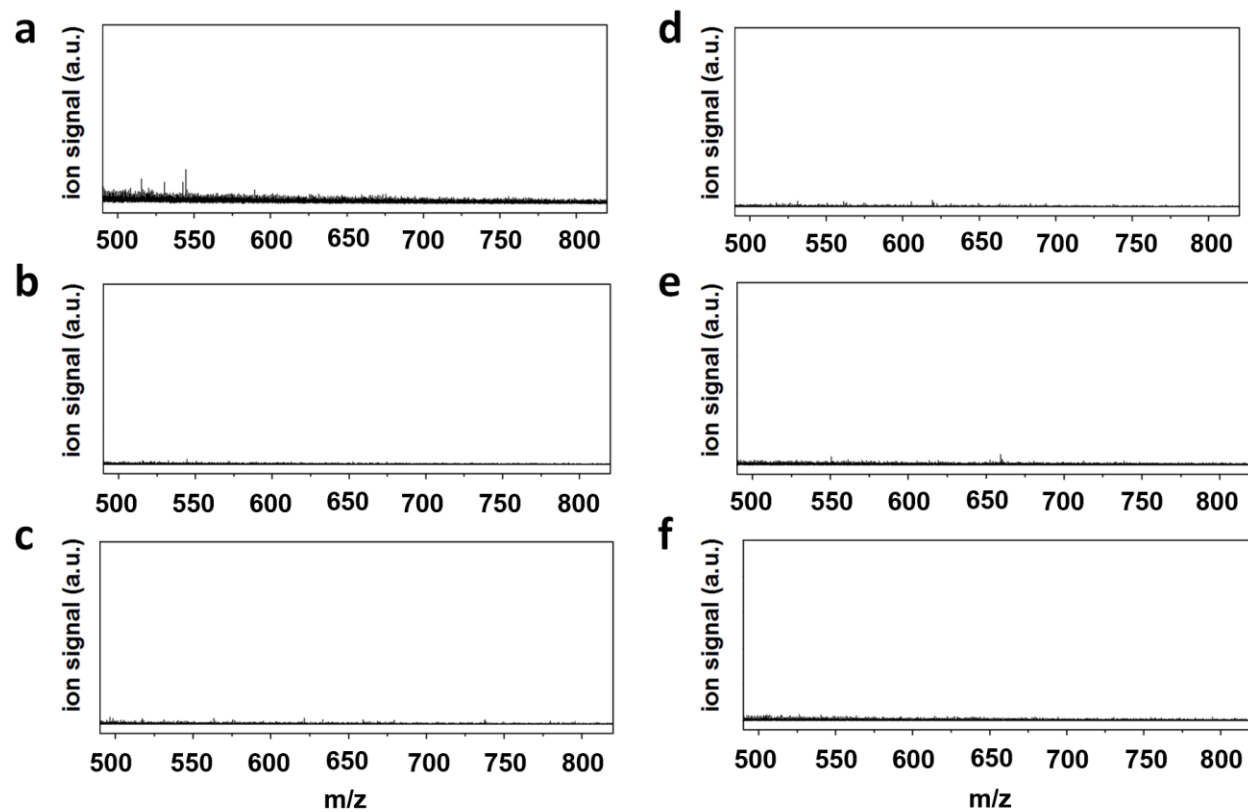


**Figure 2-9:** NALDI-MS spectra of 3 nm dodecyl-passivated SiNCs functionalized at different predesigned reaction time using AIBN as reaction initiator as: (a) background, (b) 1, (c) 2, (d) 3, (e) 5, and (f) 12 h in the range of 475-825 m/z. Note: These spectra are a “zoom-in” of those shown in Figure 2-8.

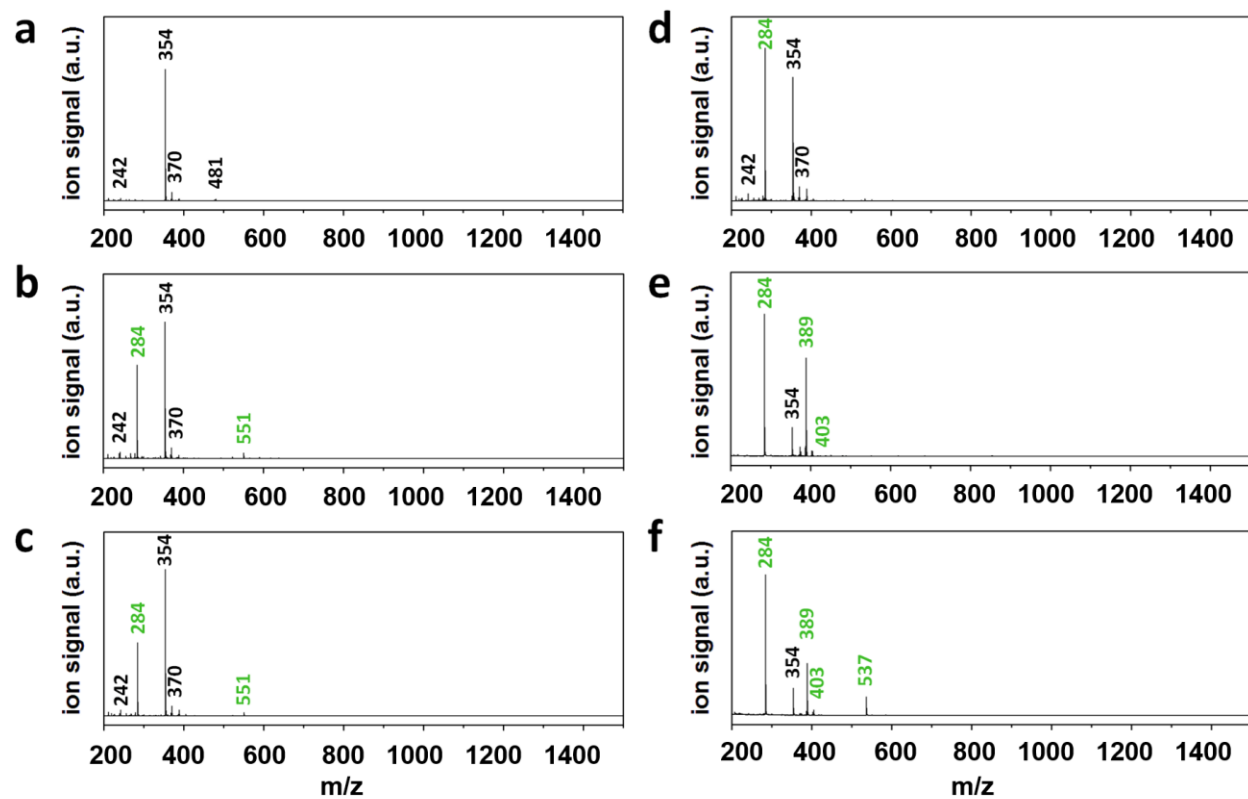


**Figure 2-10:** NALDI-MS spectra of 3 nm dodecyl-passivated SiNCs functionalized at different predesigned reaction time using BP as reaction initiator: (a) background, (b) 1, (c) 2, (d) 3, (e) 5, and (f) 12 h.

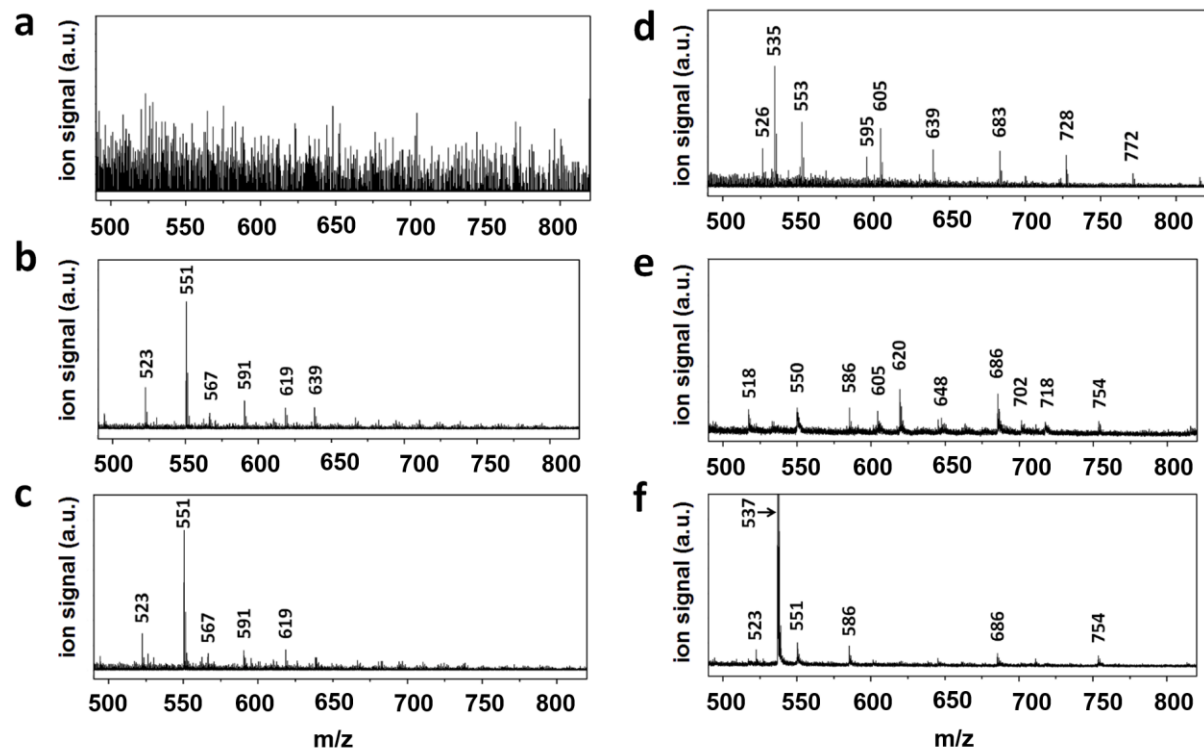


**Figure 2-11:** NALDI-MS spectra of 3 nm dodecyl-passivated SiNCs functionalized at different predesigned reaction time using BP as reaction initiator: (a) background, (b) 1, (c) 2, (d) 3, (e) 5, and (f) 12 h. Note: These spectra are a “zoom-in” of those shown in Figure 2-10.

Carter *et al.* demonstrated the formation of polystyrene brushes on bulk Si surfaces.<sup>284</sup> They suggested reactions involving bulk Si and AIBN led to solution-borne oligomers/polymers that in turn attach to Si surfaces. To investigate if this same process occurs for the present nanosystems, H-SiNCs were modified with styrene using both radical initiators (*i.e.*, AIBN or BP) and the resulting products were evaluated using NALDI-MS (Figure 2-12). No high molecular weight fragments associated with styrene oligomers or polystyrene were detected (*i.e.*, 60 or 85 °C) consistent with no oligomers attaching to the SiNC surfaces.

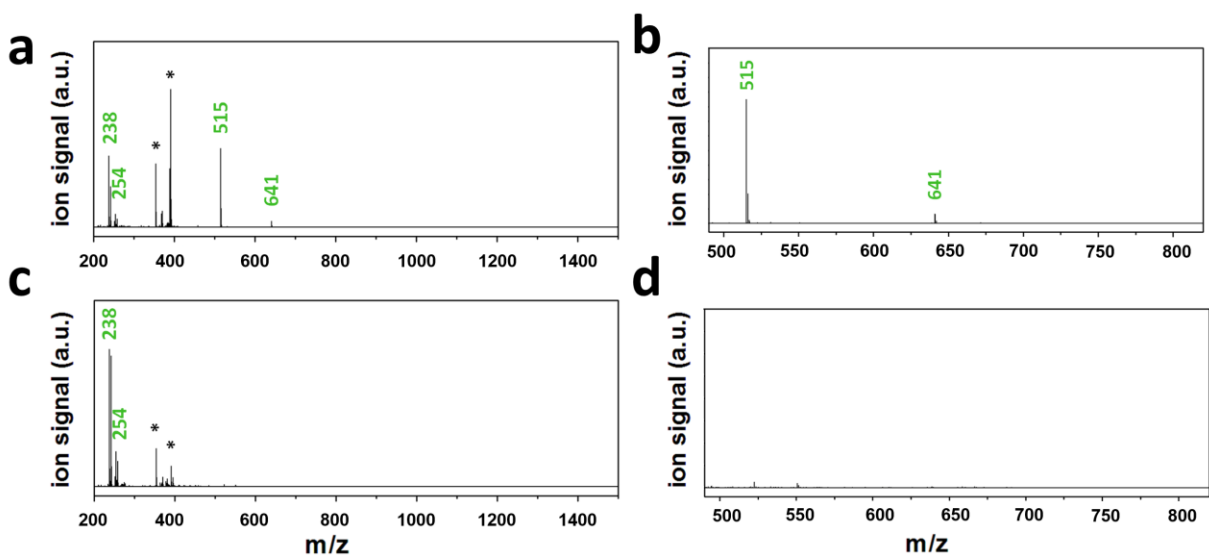


**Figure 2-12:** NALDI-MS spectra of 3 nm styrene-passivated SiNCs functionalized using (a) AIBN or (b) BP as reaction initiator. Asterisks indicate background signals.

Insight into the oxidation of SiNC surfaces is available from XPS (Figures 2-13 and 2-14). All spectra show the functionalized SiNCs contain only carbon, oxygen, and silicon at the sensitivity limit of the method. For clarity only the Si 2p<sub>3/2</sub> components of spin-orbit coupling pairs are shown. A dominant emission present at 99.3 eV in all the high resolution spectra is

readily assigned to elemental silicon (*i.e.*, Si (0)).<sup>158</sup> Other components between 100 and 102.5 eV are routinely assigned to silicon suboxides (*i.e.*, SiO<sub>x</sub>, 0 < x < 2) and functionalized silicon surfaces with Si–C features.<sup>158</sup> The component at 103.4 eV (denoted as Si (IV)) is confidently attributed to SiO<sub>2</sub>.<sup>158</sup> SiNCs functionalized with aromatic groups showed higher Si (IV) content resulting from less efficient surface passivation

Based on the results of the various surface analyses (*i.e.*, FTIR, XPS, <sup>1</sup>H NMR, and TGA), the surfaces of the functionalized SiNCs achieved by radial initiated hydrosilylation are complex. The determined ligand surface coverages are between 34-64% with the remaining SiNC surface consisting of Si-H<sub>x</sub> and SiO<sub>x</sub> species (see Figure 2-15).

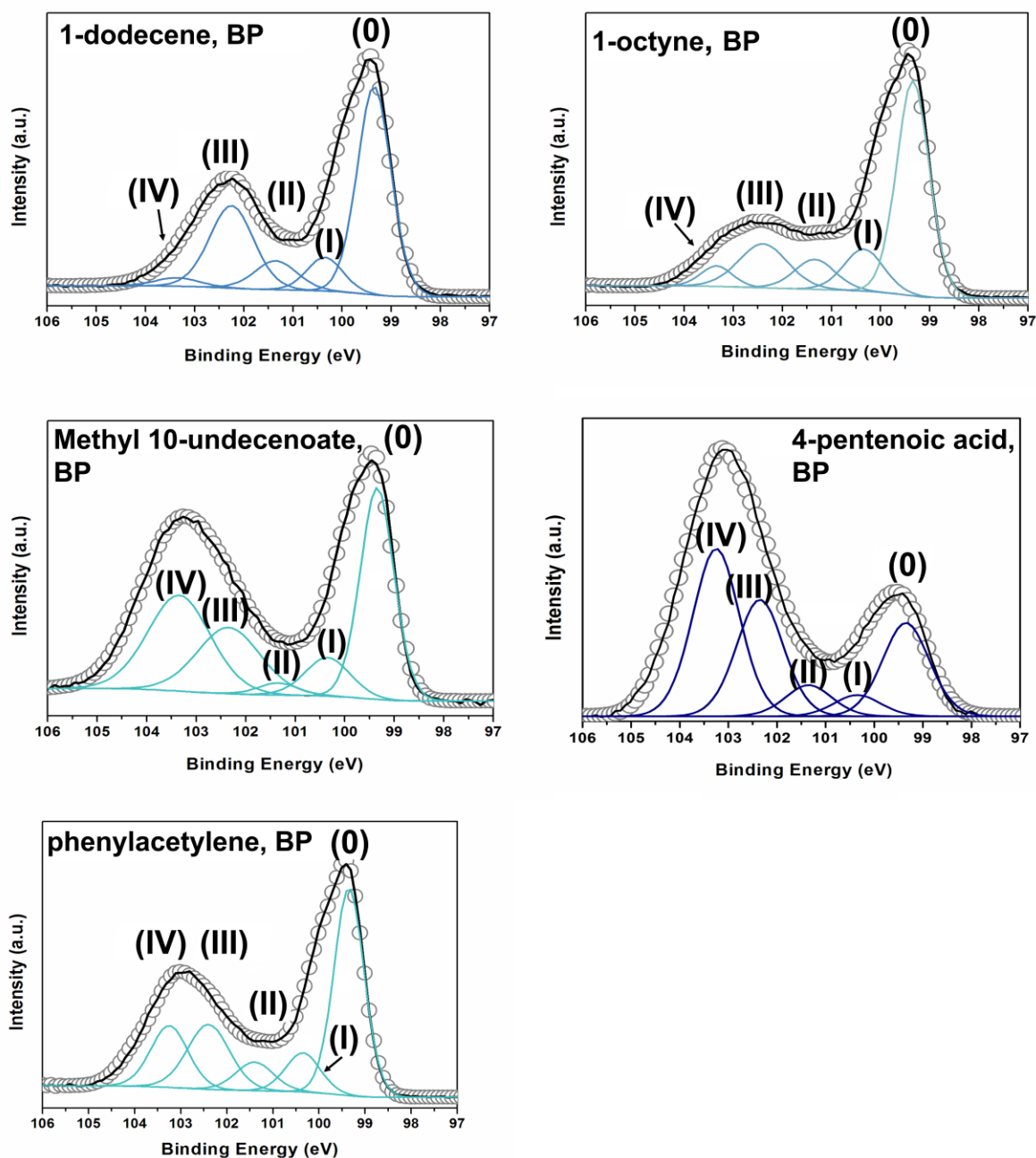


**Figure 2-13:** High-resolution XPS spectra of silicon (2p) signals for SiNCs passivated with different ligands using BP as reaction initiator. Si (0), Si (I), Si (II), Si (III), and Si (IV) are denoted as (0), (I), (II), (III), and (IV), respectively. Black curves and circles correspond to the original data and fit spectra, respectively. Fitting results are shown for the Si 2p<sub>3/2</sub> components. The Si 2p<sub>1/2</sub> signals have been omitted for clarity.

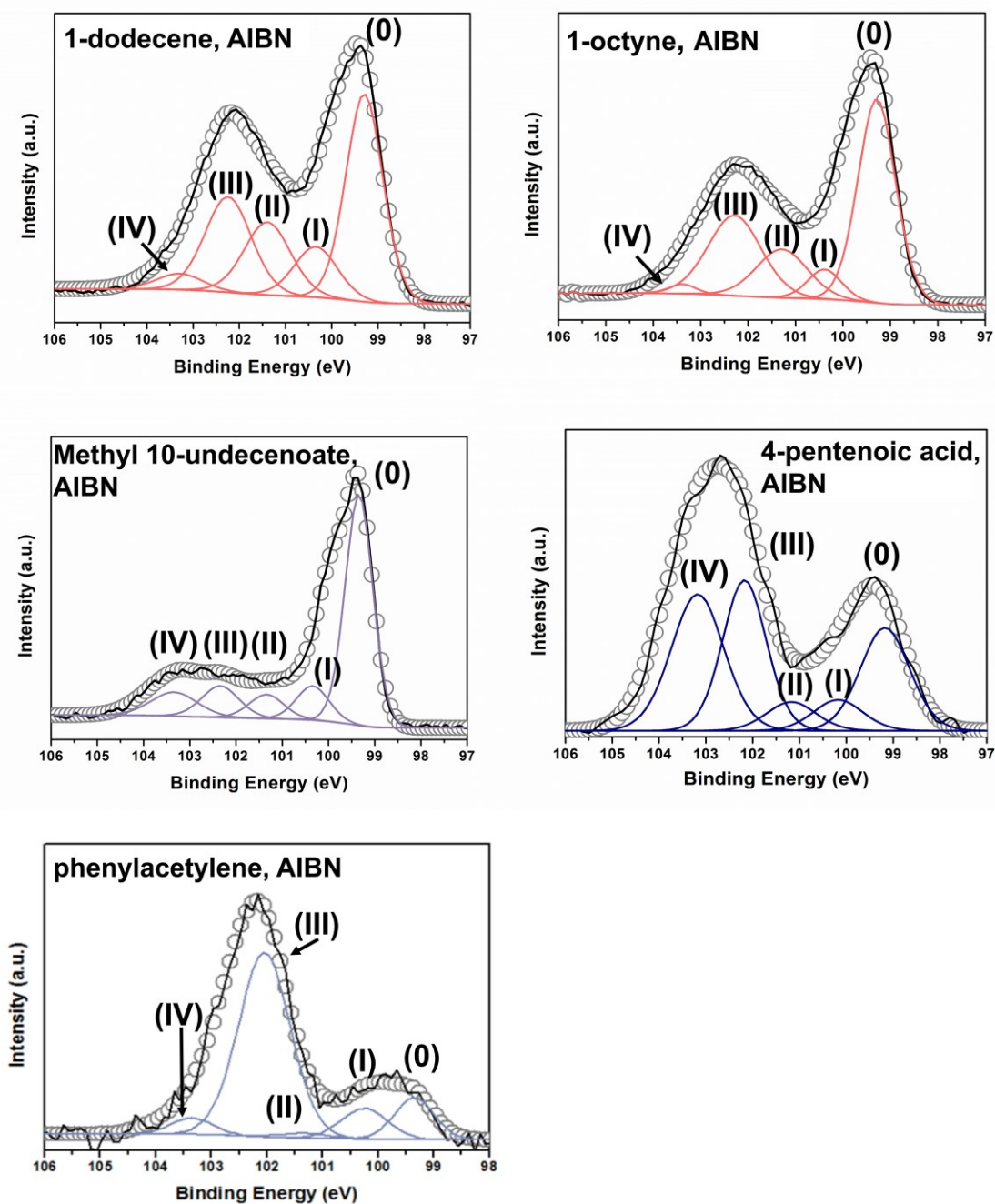


**Figure 2-14:** High-resolution XPS spectra of silicon (2p) signals for SiNCs passivated with different ligands using AIBN as reaction initiator. Si (0), Si (I), Si (II), Si (III), and Si (IV) are denoted as (0), (I), (II), (III), and (IV), respectively. Black curves and circles are correspondent to original and fit spectra, respectively. Fitting results are shown for the Si 2p<sub>3/2</sub> components. The Si 2p<sub>1/2</sub> signals have been omitted for clarity.

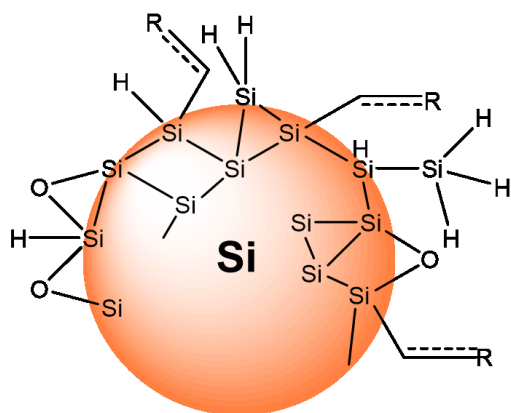


**Figure 2-15:** Representative schematic highlighting the complexity of SiNC surfaces after functionalization with an alkene or alkyne (denoted as R) via radical initiated hydrosilylation with AIBN or BP.

All of the resulting functionalized 3 nm SiNCs display PL. Table 2-3 shows the corresponding emission maxima of SiNCs functionalized with the various ligands. The maximum emission lay between 630 and 737 nm. Also of note, there is a slight shift of PL maximum for samples with styrene and phenylacetylene ligands. The radiative lifetimes of all samples were evaluated and exhibited a stretched exponential decay described by the following equation:

$$y(t) = Ae^{(-\frac{t}{\tau})^\beta} + C$$

Where  $\tau$  is the time decay,  $\beta$  is the dispersion factor and  $C$  is the constant offset. Lifetime data are summarized in Table 2-4 and were between 18-160  $\mu$ s, consistent with a band-gap based emission.<sup>289</sup> We also note that no excitation-wavelength-dependent emission was observed. The differences in PL emission from the different samples could be due to the different degree of surface oxidation (Figures 2-13 and 2-14) and slight particle size differences (Figure 2-17).

**Table 2-3:** Wavelengths of PL maxima of 3 nm SiNCs functionalized with various ligands using AIBN and BP as reaction initiators (unit: nm).

Initiator	1-octyne	1-dodecene	styrene	phenyl-acetylene	methyl-10-undecenoate	4-pentenoic acid
AIBN	729	696	633	652	737	696
BP	725	684	635	671	720	694

**Table 2-4:** Results of PL lifetime decay ( $\tau$ ) of 3 nm SiNCs functionalized with various ligands using AIBN and BP as reaction initiators (unit:  $\mu$ s).

Initiator	1-octyne	1-dodecene	styrene	phenyl-acetylene	methyl-10-undecenoate	4-pentenoic acid
AIBN	155	115	86	151	142	18
BP	151	109	85	133	160	20

To investigate any size dependence, reactions were performed with dodecene and larger H-SiNCs ( $d_{\text{avg}} = 5$  and 8 nm). Identical reactivity was observed and FT-IR spectra (Figure 2-16) indicate similar surface bonding information (*e.g.*, surface group attachment and incomplete surface coverage oxidation). The particle size and uniformity were evaluated using TEM and the purified SiNCs exhibit similar diameters for each radical reaction (Figures 2-17 and 2-18). Furthermore, PL showed a red-shift of the emission maximum with the increased particle size (Figure 2-19).

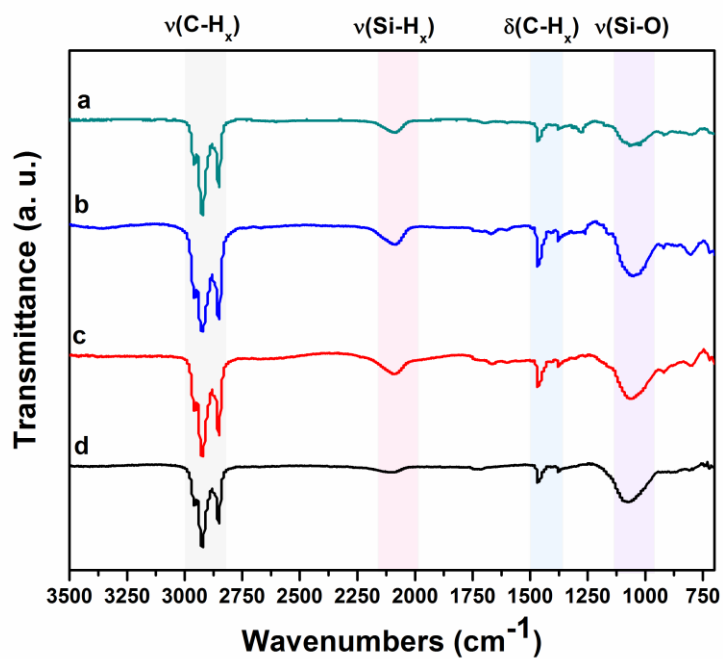


**Figure 2-16:** FT-IR spectra of a) 8 nm and b) 5 nm dodecyl-SiNCs functionalized using BP and c) 8 nm and d) 5 nm dodecyl-SiNCs functionalized using AIBN.

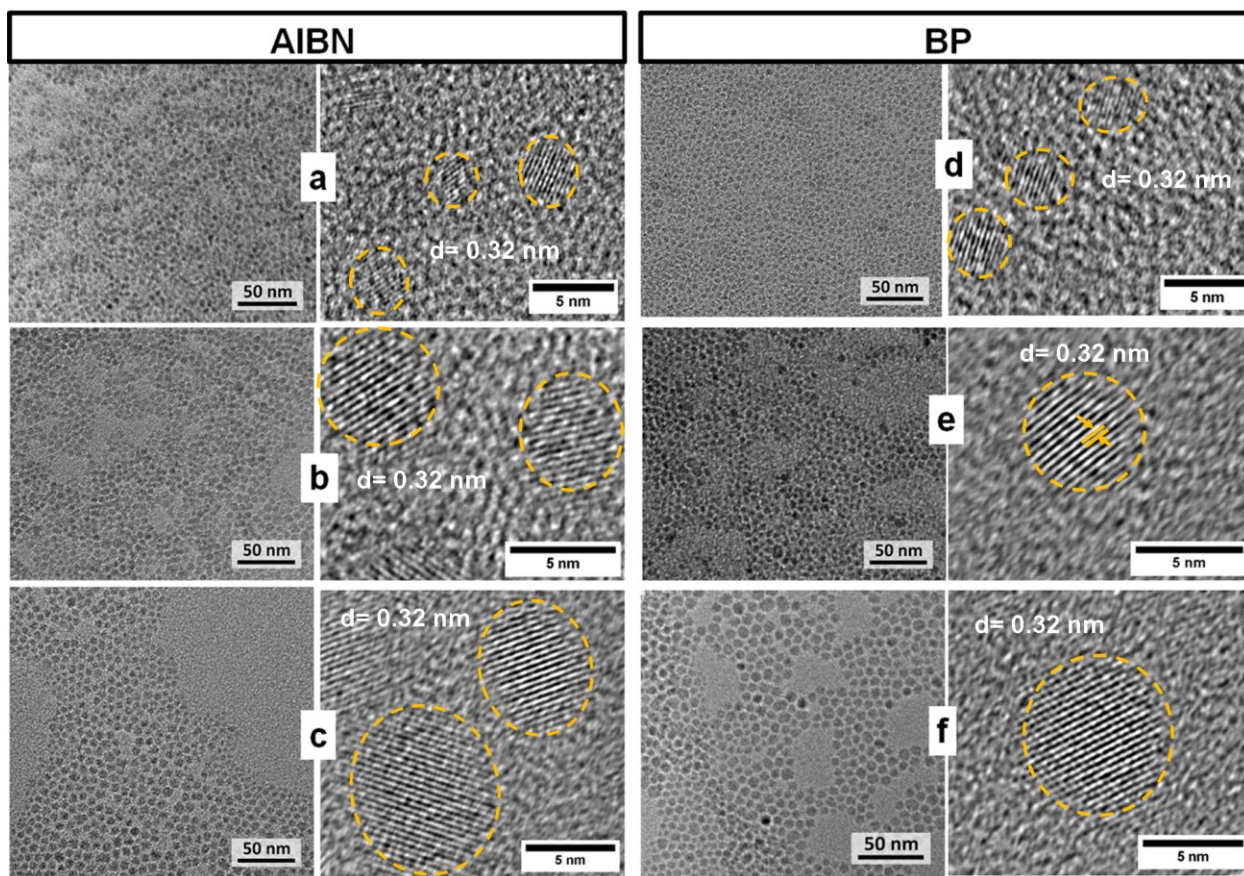


**Figure 2-17:** Bright-field TEM and HRTEM images of dodecyl-passivated SiNCs of various sizes: ((a, d) 3 nm, (b, e) 5 nm and (c, f) 8 nm) functionalized using AIBN or BP as reaction initiator.

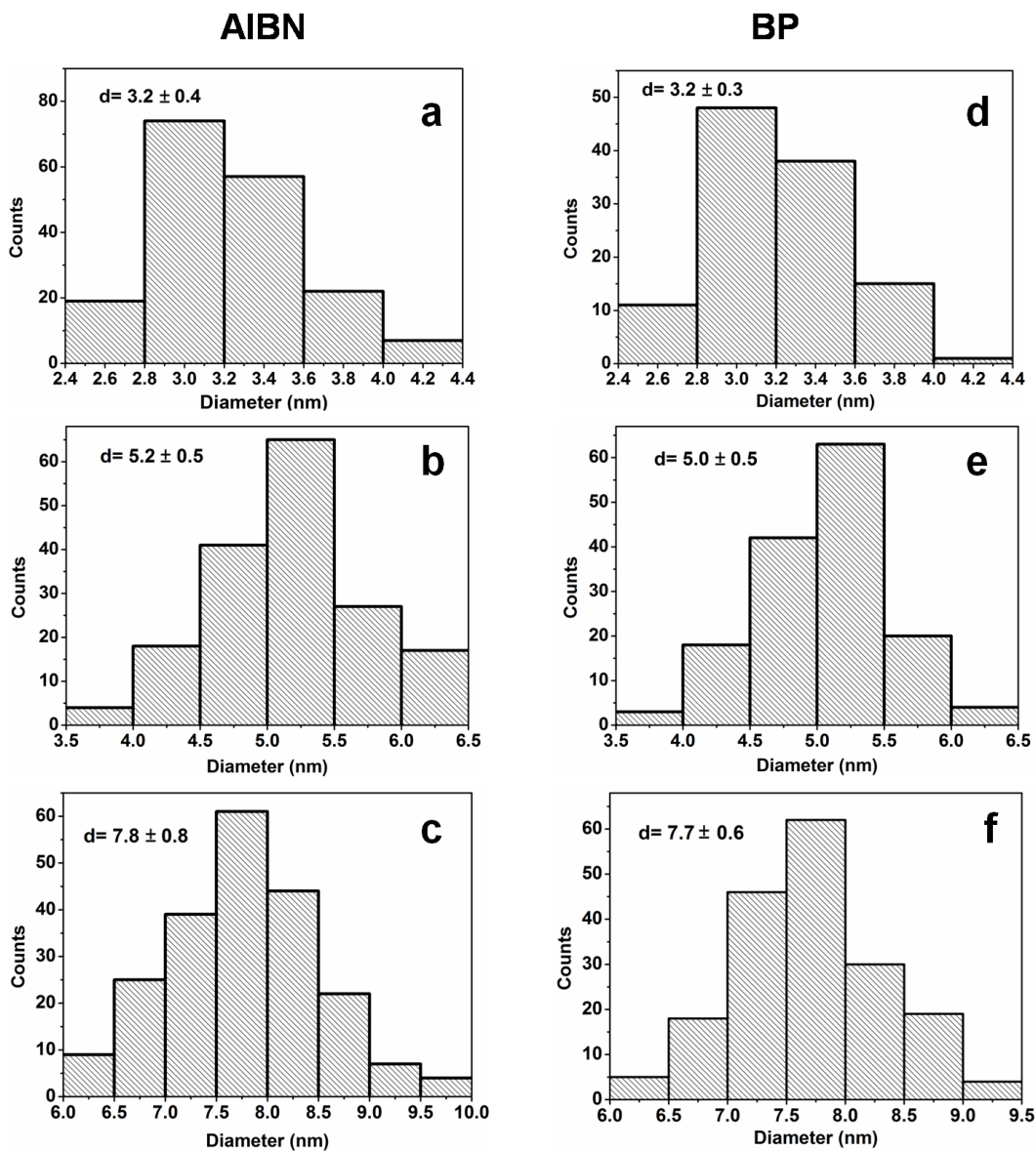


**Figure 2-18:** Size distribution of dodecyl-passivated SiNCs of various sizes: ((a, d) ~3 nm, (b, e) ~5 nm and (c, f) ~8 nm) functionalized using AIBN or BP initiator. Note: Particle size histograms were assembled by counting 200 SiNCs through the longest diameter present with Image J software.

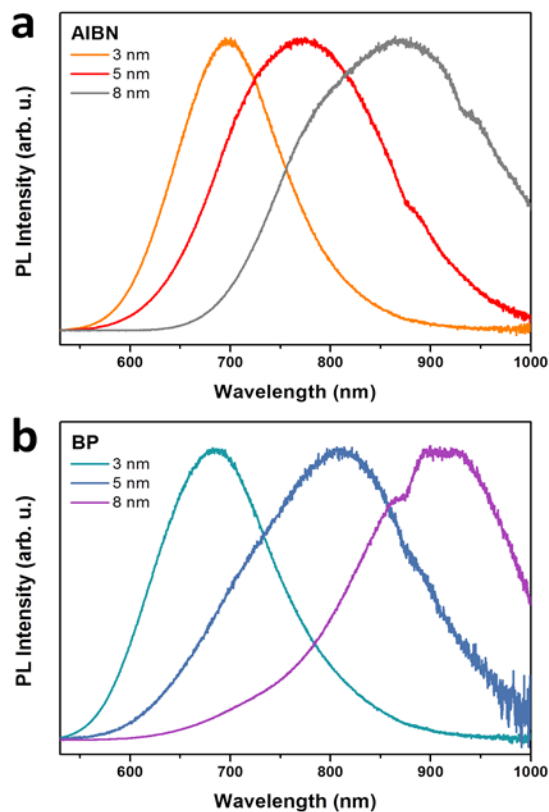


**Figure 2-19:** Size-dependent PL spectra of dodecyl-functionalized SiNCs in toluene using (a) AIBN or (b) BP as initiator. (Excitation wavelength used,  $\lambda = 476$  nm.)

To investigate the mechanism of the present radical initiated reaction, we employed a radical trap, 2,2,6,6-tetramethyl-1-piperidinyloxy (TEMPO) that has been widely used to capture dangling bonds on Si surfaces.<sup>296-298</sup> After stirring a mixture of TEMPO, 3 nm H-SiNC, ligands and radical initiator at reaction temperature for 19 h the mixture remained cloudy and the color of the mixture lightened from brown/orange to yellow; this suggests no hydrosilylation occurred between ligands and silicon surface. Control reactions involving stirring H-SiNCs with only the alkene or with the alkene and TEMPO for 12 h did not result in any change in the suspension color or transparency. Finally, a reaction of only H-SiNCs with TEMPO and radical initiators (AIBN

or BP) for 12 h provided a transparent red/yellow solution. The purified products recovered from these reactions dissolved in toluene to yield pale yellow solutions that showed yellow luminescence upon excitation at 365 nm UV irradiation. FT-IR analyses of these products (Figure 2-20) shows C–H<sub>x</sub> (2850–3000 cm<sup>-1</sup>) and Si–O (~1100 cm<sup>-1</sup>) stretching features and little evidence of Si–H<sub>x</sub> signals (~2100 cm<sup>-1</sup>) consistent with surface attachment of TEMPO onto the SiNCs. From this, we conclude TEMPO is capturing surface radicals on SiNC surfaces and preventing further reaction. This is similar to what was proposed for bulk system at high temperature.<sup>181</sup> In this context, we propose the present reactions proceed via abstraction of a hydrogen radical by the radical initiators (see Scheme 2-2) followed by reaction with solution borne species containing unsaturated C–C bonds.

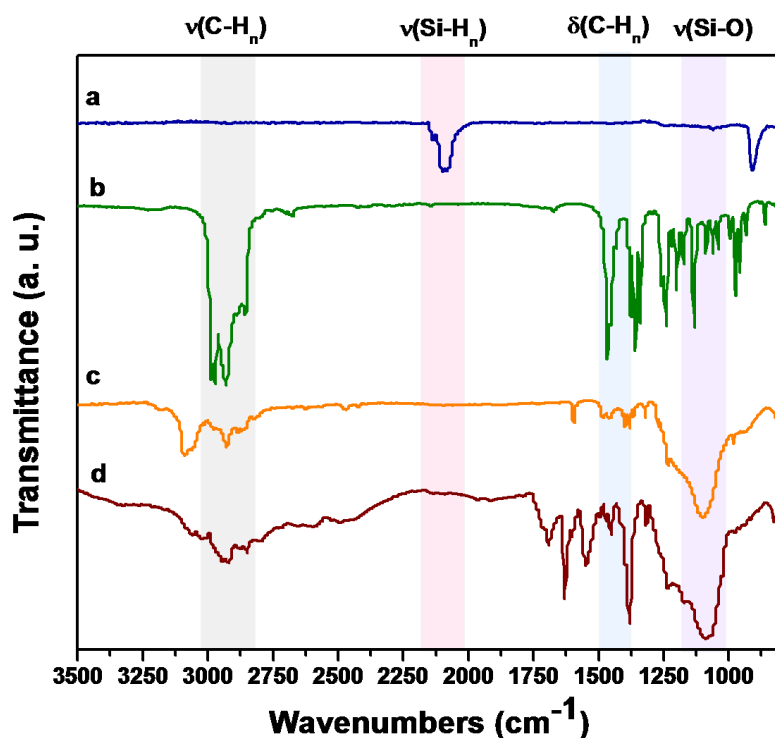
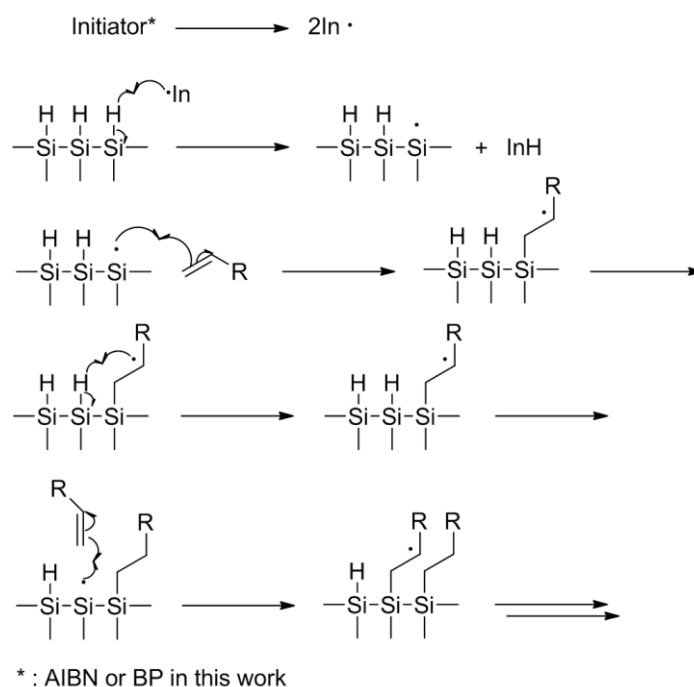


**Figure 2-20:** FT-IR spectra of a) hydride-terminated SiNCs, b) TEMPO and c) TEMPO-capped SiNCs using AIBN, and d) TEMPO-capped SiNCs using BP.



**Scheme 2-2:** Mechanism of SiNC surface hydrosilylation driven by pyrolysis of radical initiators as proposed previously by Linford and Chidsey.<sup>136,181</sup>

## 2.4 Conclusions

In this present study, SiNC surface hydrosilylation initiated by AIBN and BP were investigated. Compared with other known SiNC surface passivation approaches (*i.e.*, thermal and photochemical initiated hydrosilylation), radical initiator driven hydrosilylation offers clear advantages. The present reactions are particle size independent, accessible to terminal alkene and alkyne functional groups, and can proceed under mild conditions and short reaction times (*i.e.*, < 3 h). In addition, we have identified that radical initiated hydrosilylation on SiNCs provides monolayer passivated surfaces. We also propose the reaction proceeds via a mechanism that begins with abstraction of a surface hydride, which is similar to what has been reported on bulk silicon systems. However, characterization of the surface by FTIR, XPS, <sup>1</sup>H NMR and TGA

indicate the resulting SiNCs were not 100% functionalized with organic moieties, leading to the formation of a mixed surface on the SiNCs. Future work should be aimed at achieving more complete passivation toward oxidation.

**Chapter 3**  
**The formation of Si-S bonds on the Silicon**  
**Nanocrystal Surface via a Commercial Fluorescent**  
**Light Source.**

### 3.1 Introduction

Silicon is the primary semiconductor used in the electronics industry<sup>299,300</sup> and is an attractive material for application development as it is abundant<sup>301</sup> and low in toxicity.<sup>40-42</sup> Furthermore, both porous and nanocrystalline silicon display unique photoluminescence properties not observed for bulk silicon.<sup>50,56,302-304</sup> Freestanding silicon nanocrystals (SiNCs) have already been used for the development of a variety of prototype materials including photovoltaics,<sup>67,68</sup> electronics,<sup>66</sup> catalysis,<sup>64</sup> photonics,<sup>65</sup> and sensors.<sup>72</sup> In order to advance the incorporation of SiNCs for applications, developing multipurpose techniques for the tailoring of the SiNC surface is of the utmost importance. In doing so, desirable changes in both electronic and optical response, stability (*e.g.*, possibly resistance to oxidation), and solution-processability of SiNCs could be realized.

The most common surface modification of SiNCs involves the hydrosilylation of hydride-terminated SiNCs (H-SiNCs) surface with unsaturated C=C or C=O bonds.<sup>126,132,148,152,181,305-307</sup> Despite the similarities in the reactivity of bulk and nanosilicon surfaces, important reactivity differences are also observed, such as size dependent reactivity<sup>144</sup> and oligomerization.<sup>158</sup> Also of interest, is the development of methods that could lead to alternative surfaces linkages (*e.g.*, Si-chalcogenides) that could influence the electronic structure of the NC. For example, Gergel-Hackett and co-workers demonstrated that an alkythiol monolayer passivated bulk silicon surface can be employed to design a complementary metal-oxide-semiconductor (CMOS) compatible electronic device that demonstrated a significant reduction in barrier height during charge transport.<sup>308</sup> In addition, ligand exchange using SiNCs with surfaces consisting of Si-S<sup>125</sup> and Si-O<sup>126</sup> have been recently shown, with the Si-S being the more labile/reactive bond.

As previously discussed in Section 1.4.1.2, the formation of Si-S surface bonds via solution methods is still in its infancy.<sup>125,174-180</sup> Recently, Buriak and co-workers have demonstrated the passivation of porous silicon with alkylthiols through the activation of dialkyl disulfides (*i.e.*, RS-SR) upon activation with diazonium-based radical initiator<sup>180</sup> or thermal initiation.<sup>174</sup> Korgel and co-workers passivated the SiNCs surface with alkylthiols through thermal activation of alkanethiols.<sup>125</sup> In both cases, the involvement of surface silyl radicals, have been considered the primary driving force for the observed reactivity.

It is well known that the disulfide moiety of lipoic acid can be activated in the presence of UV irradiation to produce thiyl radicals.<sup>309</sup> These radicals can lead to the formation of polylipoic acid.<sup>310-312</sup> Polylipoic acid can further degrade under exposure to light, yielding a complex mixture of oligomers and monomer.<sup>310,311,313</sup> Recently, Mattousi and co-workers, exploited this reactivity for the bidentate ligation of lipoic acid-based ligands onto CdSe-ZnS core-shell quantum dots under UV or sunlight irradiation.<sup>314-316</sup> Since the disulfide bond can be activated under very mild conditions (*i.e.*, sunlight) to produce thiyl radicals, we postulate that these radicals in the presence of H-SiNCs, can abstract the hydrogen from the H-SiNC surface, to produce surface-based silyl radicals. The surface silyl radicals can then combine to the free thiyl radicals to form alkylthiol passivation on the SiNC surfaces.

For this study, a cyclic disulfide (lipoic acid, LA) and a linear disulfide (dibutyl disulfide, DBDS) were investigated as model ligands in the functionalization of a series of SiNCs ( $d \sim 3, 6,$  or 8 nm). The reactions were promoted using a commercial fluorescence light source (18 W).

## 3.2 Experimental

### 3.2.1 Reagents and Materials

Commercial hydrogen silsesquioxane (HSQ, trade name Fox-17) was purchased from Dow Corning Corporation (Midland, MI). Electronics grade hydrofluoric acid (HF, 49% aqueous solution) was purchased from J.T. Baker. Reagent grade ( $\pm$ )- $\alpha$ -lipoic acid (LA,  $\geq 98\%$ ) and dibutyl disulfide (DBDS, 97%) were purchased from Sigma-Aldrich. Dibutyl disulfide was dried over 3 Å molecular sieves prior to use. Tetrahydrofuran (THF), hexanes, toluene, and acetonitrile solvents were collected from Pure-Solv purification system prior to use.

### 3.2.2 Material Characterization and Instrumentation

Fourier Transform Infrared Spectroscopy (FT-IR) was completed using a Nicolet Magna 750 IR spectrophotometer by drop-coating a THF (for lipoic acid surface functionalized SiNCs, LA-SiNCs) or toluene (for dibutyl disulfide surface functionalized SiNCs, DBDS-SiNCs) dispersion of SiNCs. Transmission electron microscopy (TEM) was performed on a JEOL-2010 (LaB<sub>6</sub> filament) electron microscope with an accelerating voltage of 200 kV using samples of post functionalized SiNCs drop-cast onto a holey carbon coated copper grid (300 mesh, Electron Microscopy Science). High-resolution (HR) TEM images were obtained from a Hitachi-9500 electron microscope with an accelerating voltage of 300 kV. The HRTEM images were processed using Gatan Digital Micrograph software (Version 2.02.800.0). X-ray photoelectron spectroscopy (XPS) measurements were acquired using a Kratos Axis Ultra X-ray photoelectron spectrometer operated in energy spectrum mode at 210 W. XPS samples were prepared inside a glove box as a film drop-cast from a SiNC THF or toluene dispersion onto a copper foil substrate and placed in an air sensitive sample holder prior to acquisition. The resulting spectra were fitted using CasaXPS

(VAMAS) software and were calibrated to the lowest binding energy component of the C 1s emission at 284.8 eV.

Photoluminescence (PL) spectra of the SiNCs were obtained using a Cary Eclipse spectrophotometer ( $\lambda_{\text{ex}} = 350$  nm). PL samples were prepared inside a glove box by transferring a solution sample of SiNC into an air sensitive quartz cuvette. PL lifetimes were collected by illuminating the solution sample with an argon ion laser (476 nm, ~30 mW). The laser was modulated by an acousto-optic modulator operating at 500 Hz. Emission from the SiNCs was channeled into a photomultiplier (Hamamatsu H7422P-50) connected to a photon counting card (Becker-Hickl PMS-400A). Lifetime decay data was fit to a stretched exponential function in Mathematica (Version 10) given by  $y(t) = A[\exp(-(t/\tau)^\beta)] + C$ , where  $A$  is the initial intensity,  $\tau$  is the time decay (basic lifetime),  $\beta$  is a stretching parameter that can vary between 0 and 1, and  $C$  is an offset.<sup>286-288</sup>

Nanostructured-assisted laser desorption/ionization mass spectroscopy (NALDI-MS) spectra were obtained in the positive/negative reflection mode using a Bruker Daltonics UltrafleXtreme NALDI TOF/TOF mass spectrometer. Samples were prepared by spotting 1  $\mu\text{L}$  of sample solution onto a Bruker Daltonics NALDI target and air-dried.

Proton nuclear magnetic resonance spectroscopy ( $^1\text{H}$  NMR) solution samples were prepared inside the glove box and sealed prior to data collection.  $^1\text{H}$  NMR spectra were obtained using a Varian Unity INova Console 500 MHz NMR spectrometer. A concentrated (*ca.* 6 mg/mL) solution of LA-SiNCs or neat LA in  $\text{CD}_2\text{Cl}_2$  was used to collect the  $^1\text{H}$  NMR spectra. The resulting FID files were processed using Nuts NMR data processing software.

Thermogravimetric analysis (TGA) samples of functionalized SiNCs in hexanes were kept in the glove box prior to analysis. TGA was performed using a Mettler Toledo Star TGA/DSC

system. LA- or DBDS-SiNC samples were placed in a Pt pan and heated in an Ar atmosphere from 30 to 700 °C at 10 °C/min.

Dynamic Light Scattering (DLS) measurements were performed using a Malvern Zetasizer Nano S equipped with a 633 nm laser. All samples were filtered using a 0.45 µm PTFE syringe filter and equilibrated to 25 °C prior to data acquisition. A refractive index of 1.460 was used for all measurements with each measurement consisting of an average minimum of 10 scans.

### 3.2.3 Preparation of oxide-embedded SiNCs ( $d_{\text{avg}} = 3, 5, \text{ and } 8 \text{ nm}$ )

Oxide-embedded SiNCs were prepared using well-established protocols developed in our laboratory.<sup>112</sup> In brief, solid HSQ was put in a quartz reaction boat, placed into a tube furnace, and heated at 1100 °C in a 95% argon/5% hydrogen atmosphere for 1 h. This process affords an amber colored SiNC/SiO<sub>2</sub> composite containing 3 nm SiNCs that was then crushed using an agate mortar and pestle. Larger NCs (*i.e.*,  $d_{\text{avg}} = \sim 5$  and 8 nm) were achieved by placing *ca.* 0.5 g of the SiNC/SiO<sub>2</sub> composite in a carbon boat, transferred to a high temperature furnace (Sentro Tech Corp.), and heated at 1200 °C ( $d_{\text{avg}} = 5 \text{ nm}$ ) or 1300 °C ( $d_{\text{avg}} = 8 \text{ nm}$ ) for 1 h in an argon atmosphere. The resulting composites were ground to a powder at room temperature using a mortar and pestle. All composites were shaken with high-purity silica beads using a Burrell Wrist Action Shaker for 12 h.

### 3.2.3 Preparation of hydride-terminated SiNCs

To liberate SiNC from the oxide matrix, the SiNC/SiO<sub>2</sub> composite (0.2 g) was first transferred into a polyethylene terephthalate (PET) beaker containing a Teflon coated stir bar with 100% Ethanol (2 mL) and water (2 mL) and stirred to ensure uniform wetting. Next, a 49% aqueous HF (2 mL) solution was added slowly to the brown suspension while stirring. **Caution:**

HF is dangerous and requires appropriate handling procedures and personal protective equipment. Following ~1 h, the brown suspension changed appearance becoming orange/yellow. Hydrophobic, hydride-terminated SiNCs (H-SiNCs) were extracted from the aqueous layer using 3 x ~10 mL extractions into toluene. The resulting SiNC/toluene suspension was divided equally between test tubes and centrifuged at 3000 rpm; the supernatant was decanted and the H-SiNC precipitate was used directly in functionalization procedures (*vide infra*).

### 3.2.4 Commercial fluorescent light induced functionalized of H-SiNCs

The H-SiNCs obtained from the etching procedure (*vide supra*) were redispersed in THF (*ca.* 5 mL) that had been collected from the solvent system and transferred to an oven-dried (125 °C) 100 mL Schlenk flask equipped with a Teflon coated magnetic stir bar and attached to an argon charged Schlenk line. Lipoic acid (LA, 1.2 mmol) or dibutyl disulfide (DBDS, 7.9 mmol) was added to the flask and the reactant mixture was subjected to three freeze-pump-thaw cycles. The reaction mixture was then placed in a water bath with a commercial compact fluorescent light (Luminus, model P-17718NT, 18 W, color temperature 3500 K) and the assembly was covered with foil. The emission spectrum is shown in Figure 3-1. The exposure times investigated included 90 - 120 min, 90 - 150 min, and 24 - 36 h for reactions involving LA and 3, 6, and 8 nm diameter SiNCs, respectively. For reactions using DBDS, the exposure times were 60 - 120 min and 9 - 12 h for 3 and 6 nm diameter SiNCs, respectively. All reactions yielded orange/yellow solutions.

After the predefined reaction time, the reaction flask was transferred into a nitrogen filled glove box for purification. Equal volumes (*ca.* 5 mL) of the orange/yellow solutions containing functionalized nanoparticles were dispensed into centrifuge tubes. For LA functionalized SiNCs (LA-SiNCs), hexane (*ca.* 35 mL) was added as an anti-solvent to achieve a total volume of 40 mL

in each tube. The tubes were capped and parafilm prior to the removal of the samples from the glovebox. This resulted in the generation of an orange precipitate that was isolated by centrifugation in a high-speed centrifuge at 11000 rpm for 0.25 h. The centrifuge tube was returned into the glove box, the supernatant was decanted, and the particles were re-dispersed in a minimal amount of THF (*ca.* 2 mL) and re-precipitated upon addition of hexane (*ca.* 25 mL). This solvent/anti-solvent purification process was repeated twice. Purification of DBDS functionalized SiNCs (DBDS-SiNCs) was achieved by implementing a variation of this method using toluene and acetonitrile as the solvent and anti-solvent, respectively. Finally, the purified SiNCs were redispersed in THF (LA-SiNCs) or toluene (DBDS-SiNCs), filtered through a 0.45  $\mu\text{m}$  polytetrafluoroethylene (PTFE) syringe filter, and stored in vials in the glove box for further use. The resulting SiNCs were analyzed using FT-IR, TEM, XPS, NMR, TGA, DLS and PL.

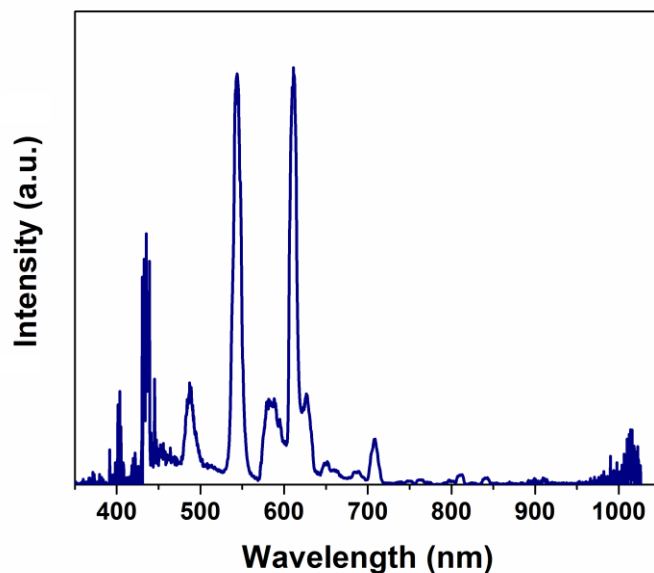


**Figure 3-1:** Emission spectrum of compact fluorescent light source.

### **3.2.5 Reaction of H-SiNCs with lipoic acid in the absence of heat and light**

H-SiNCs ( $d = 3$  nm, 25 mg) were dispersed in dry THF (taken from the solvent system) and transferred to an oven-dried ( $125$  °C) 100 mL Schlenk flask equipped with a Teflon coated magnetic stir bar and attached to an argon charged Schlenk line. LA (1.2 mmol) was added to the flask and the reactant mixture was subjected to three freeze-pump-thaw cycles. The reaction flask was then covered in foil and stirred for 42 h. The reaction mixture remained cloudy with no detectable color change. The reaction mixture was stored in a vial without purification and left on the bench top and exposed to ambient light for 2 weeks. No further characterization was performed.

### **3.2.6 Thermal reaction of H-SiNCs with lipoic acid**

H-SiNCs ( $d = 3$  nm, 25 mg) were re-dispersed in dry THF (obtained from the solvent system) and transferred to an oven-dried ( $125$  °C) 100 mL Schlenk flask equipped with a Teflon coated magnetic stir bar and attached to an argon charged Schlenk line. LA (1.2 mmol) was added to the flask and the reactant mixture was subjected to three freeze-pump-thaw cycles. The reaction flask was then heated in an oil bath at  $45$  °C in the dark for 42 h. The reaction mixture remained cloudy with no color change consistent with negligible surface modification. The reaction solution was stored in a vial without purification and left on the bench top and exposed to ambient light for 2 weeks. No further characterization was performed.

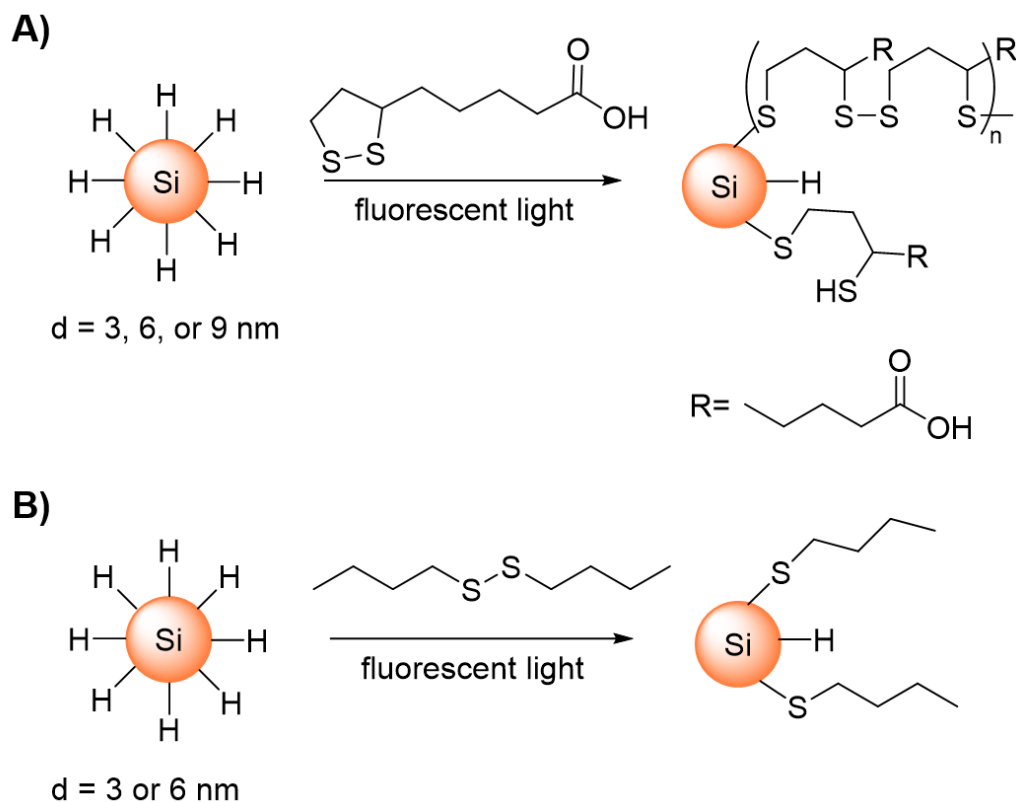
### **3.2.7 Reaction of H-SiNCs with lipoic acid in the presence of trace water**

H-SiNCs (25 mg) were re-dispersed in 5 mL of benzene and transferred to an oven-dried ( $125$  °C) 100 mL Schlenk flask equipped with a Teflon coated magnetic stir bar and attached to a Schlenk line for freeze drying. The reaction solution was frozen using a liquid nitrogen charged

dewar while under high vacuum. After the solution was frozen solid, the liquid nitrogen dewar was removed and the flask was left under vacuum for 1 h. Then LA (1.2 mmol) was added to the flask and the reactant mixture was subjected to three freeze-pump-thaw cycles. The reaction flask was placed in a water bath and then exposed to fluorescent light for 2 h. There was no apparent change in the solution mixture after 2 h, and water (150  $\mu$ L) was added over a period of 5 h and left to react for an additional 16 h. No functionalized SiNCs were recovered post purification.

### 3.3 Results and discussion

H-SiNCs (d~3, 6, 8 nm) were produced from established Veinot Laboratory protocol (Scheme 1)<sup>112</sup> and were reacted with lipoic acid (LA) or dibutyl disulfide (DBDS) in the presence of a commercial compact fluorescent light (18 W, 3500 K). In a typical experiment, fresh H-SiNCs (~20 mg) were combined with either LA (1.2 mmol) or DBDS (7.9 mmol) in an argon atmosphere and exposed to the emission of a common compact fluorescent light (18 W, emission spectra Figure 3-1 above, Scheme 3-1). During the reaction, the flask was submerged into a water-bath to ensure the effect of the heat generated from the light source was minimal. The reaction progress was qualitatively evaluated by monitoring the transparency of the reaction mixture.<sup>148</sup> For reactions with LA, transparent solutions were obtained in 90 - 120 min, 90 - 150 min, and 24 - 36 h for reactions involving 3, 6, and 8 nm diameter SiNCs, respectively. While the longer reaction time for larger sized particles is consistent with size dependent reactivity of SiNCs,<sup>144</sup> the variation in reaction time for a given particle size is currently not well understood. For reactions involving DBDS, transparent solutions were obtained within 60 - 120 min for 3 nm and 9 h - 12 h for 6 nm SiNCs. Studies involving SiNCs with d = 8 nm did not produce a transparent mixture. This observation may be the result of the established need for longer surface groups to render larger particles soluble. However, no further characterization was performed.



**Scheme 3-1:** Fluorescent light induced functionalization of H-SiNCs with A) lipionic acid or B) dibutyl disulfide.

FT-IR spectroscopy was employed to evaluate the modification of the SiNC surfaces (Figure 3-2). Prior to reaction, H-SiNCs displayed characteristic strong absorption modes at *ca.* 2100 and 850  $\text{cm}^{-1}$  arising from Si-H<sub>x</sub> ( $x = 1-3$ ) stretching and scissoring, respectively.<sup>317,318</sup> Following the reaction of SiNCs with LA (Figure 3-2A) and DBDS (Figure 3-2B), the intensities of the Si-H<sub>x</sub> signals decreased considerably (attributed to incomplete surface coverage), and various new signals appeared indicating surface modification indeed occurred. For both ligands investigated, features emerged related to the alkyl C-H<sub>x</sub> stretching and bending in the 2850-3000 and 1300-1450  $\text{cm}^{-1}$  regions.<sup>291</sup> For LA-SiNCs, the appearance of features at 3400  $\text{cm}^{-1}$  and 1705

$\text{cm}^{-1}$  corresponding to the carboxylic acid group of LA was observed.<sup>293</sup> In addition, a weak feature in the spectrum of the LA-SiNC at  $2575 \text{ cm}^{-1}$  related to S-H stretching was noted.<sup>319,320</sup> Additionally, the spectra of all functionalized SiNCs displayed features at  $\sim 1130\text{-}1000 \text{ cm}^{-1}$  related to Si-O stretching arising from residual surface oxidation though the degree varied with particle size.<sup>101,294</sup> A more intense Si-O feature was observed for 3 and 6 nm LA-SiNCs compared to their 8 nm counterpart LA-SiNCs. This difference in the size dependent oxidation may be due to the smaller SiNCs having a higher surface area to volume ratio, as well as more irregular shapes that provide reactive high energy facets.

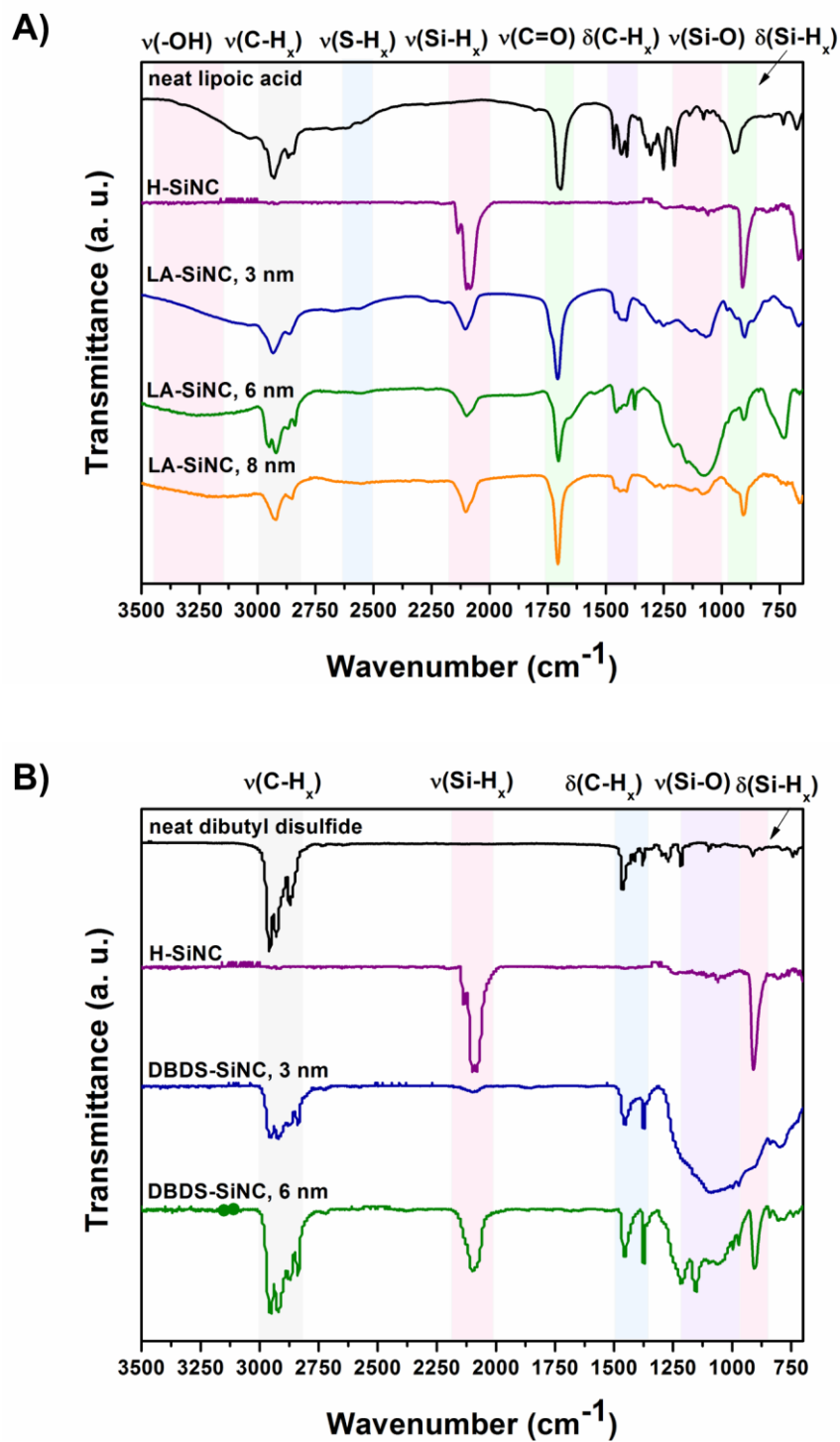


**Figure 3-2:** A) FT-IR spectra of neat lipoic acid, H-SiNCs and LA-SiNCs (3 nm, 6 nm, and 8 nm).  
 B) FT-IR spectra of neat dibutyl disulfide, H-SiNCs and DBDS SiNCs (3 nm and 6 nm).

XPS was employed to gain further insight into the oxidation states of the functionalized SiNCs. Many reports show post functionalization silicon surfaces with only the Si(0) component present in the Si 2p spectral region.<sup>174-177,179,180,321</sup> A representative example is found in the work by Hung et al. in which oxide free Si(111) surfaces were functionalized with 1-octadecanethiol using white light.<sup>179</sup> The Si 2p XPS of these samples showed an intense signal at 99.8 eV with no higher oxidation states being present. Post functionalization oxidation of the thiol bearing Si(111) surface in air lead to the appearance of a broad signal at 104 eV indicative of silicon oxides. Similar observations were noted by Hacker<sup>175</sup> as well as Sano and co-workers.<sup>176</sup> This functionalization approach was extended to porous silicon by the Buriak group, who reported similar Si 2p XP spectra with the major Si(0) components occurring at 99.5 - 99.9 eV; no higher energy features above 102 eV related to silicon oxides were observed.<sup>174,180</sup>

In contrast, the Korgel group extended thiol surface functionalization to freestanding SiNCs.<sup>125</sup> The Si 2p spectral region of these NCs after functionalization with dodecanethiol SiNCs is starkly different from the previous reports noted above. A component assigned to Si(0) appears at 99.8 eV; other components were observed at 100.4, 101.5, 102.6, and 103.7 eV that were assigned to Si(I), Si(II), Si(III), and Si(IV) oxides. An additional feature not present in previous investigations appears at 101.9 eV and was assigned to Si-S bonding. In the context of the bulk and porous-Si reports noted above, this assignment is questionable and could result from complex surface oxide species.

The S 2p spectral region is also of interest when studying the formation of Si-S surfaces. The representative S 2p<sub>3/2</sub> spectrum includes doublets at ~163.5 eV for bound sulfur<sup>178-180,322</sup> and in some cases a doublet at ~163.2 eV for unbound/free sulfur.<sup>174</sup>

Figures 3-3 and 3-4 display the high resolution spectra of the Si 2p and S 2p spectral region for LA-SiNCs and DBDS-SiNCs, respectively. The Si 2p<sub>3/2</sub> emission in the high resolution spectra of all functionalized SiNCs examined displayed a component attributed to Si(0) at 99.3 eV.<sup>158</sup> The components between 100 and 102.5 eV are assigned to silicon sub-oxides (*i.e.*, Si(I), Si(II), Si(III)) and the component at 103.4 eV (denoted as Si (IV)) is confidently attributed to SiO<sub>2</sub>.<sup>158</sup> Of important note, the Si 2p region of 3 and 6 nm LA-SiNCs showed greater contributions from higher binding energy components. This may result from surface oxidation and/or functionalization. Consistent with the FT-IR analysis described above (Figure 3-2A), the Si 2p<sub>3/2</sub> emission for 8 nm lipoic acid functionalized particles shows limited oxidation. As mentioned earlier, the origin of the apparent size dependence of the degree of surface oxidation may be the result of the smaller SiNCs having a higher surface area to volume ratio and more irregular shapes that provide reactive high energy facets.

The S 2p emission consists of two features<sup>323</sup> at 161.9 eV<sup>174,180,324,325</sup> and 164.0 eV,<sup>174,326</sup> that are readily attributed to the bound thiolate and unbound disulfide, respectively. For LA-SiNCs, the later component may arise from surface-bonded or free polymeric lipoic acid (*vide supra*). The unbound sulfur peak seen in 6 nm DBDS-SiNCs may be a result of residual DBDS.

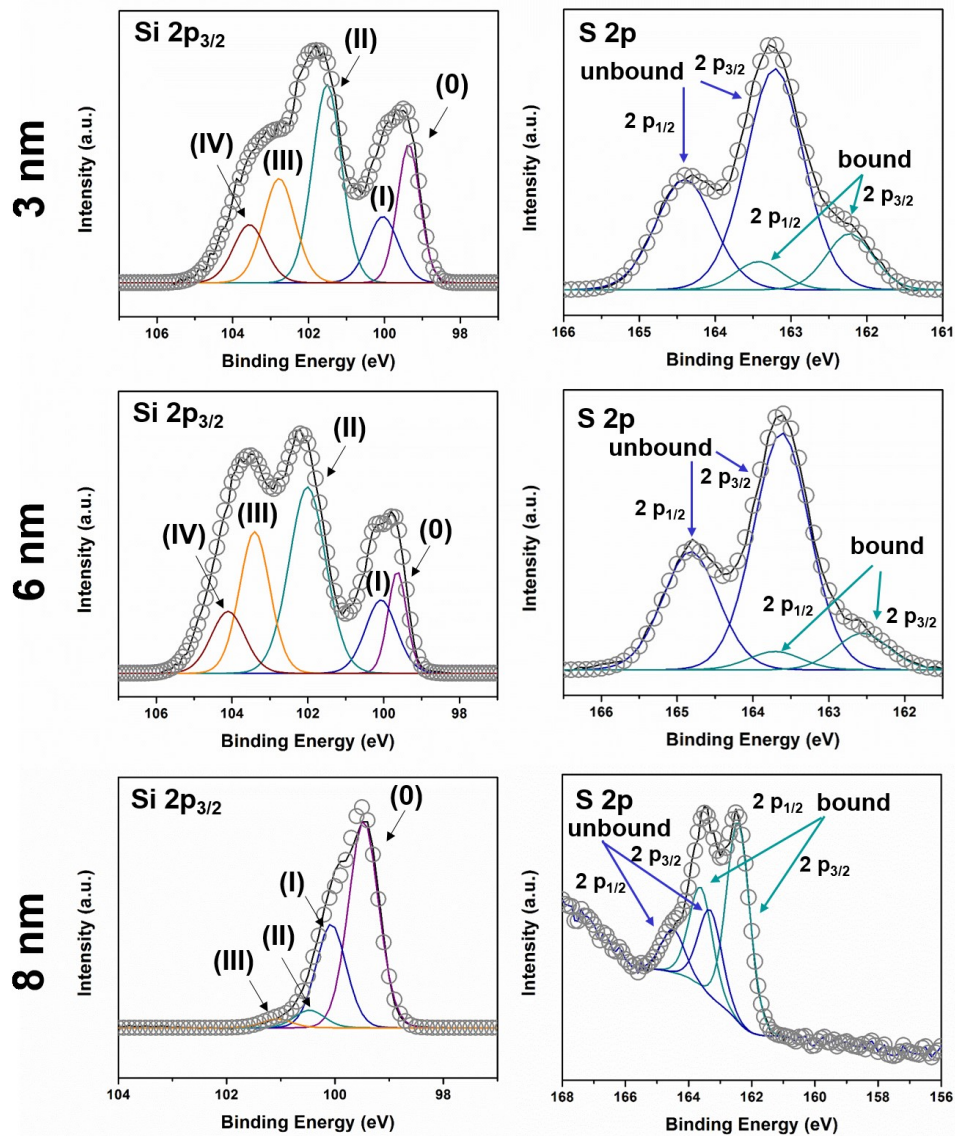


**Figure 3-3:** High-resolution XPS spectra of silicon ( $2p_{3/2}$ ) and sulfur ( $2p$ ) signals for 3, 6, and 8 nm LA-SiNCs. Fitting results for Si  $2p$  are shown for the Si  $2p_{3/2}$  components while Si  $2p_{1/2}$  signals have been omitted for clarity. Si (0), Si (I), Si (II), Si (III), and Si (IV) are denoted as (0), (I), (II), (III), and (IV), respectively. For S  $2p$  spectra, ‘bound’ refers to Si-S and ‘unbound’ indicates free sulfur. For all spectra, black curves and circles correspond to the original data and fit spectra, respectively.

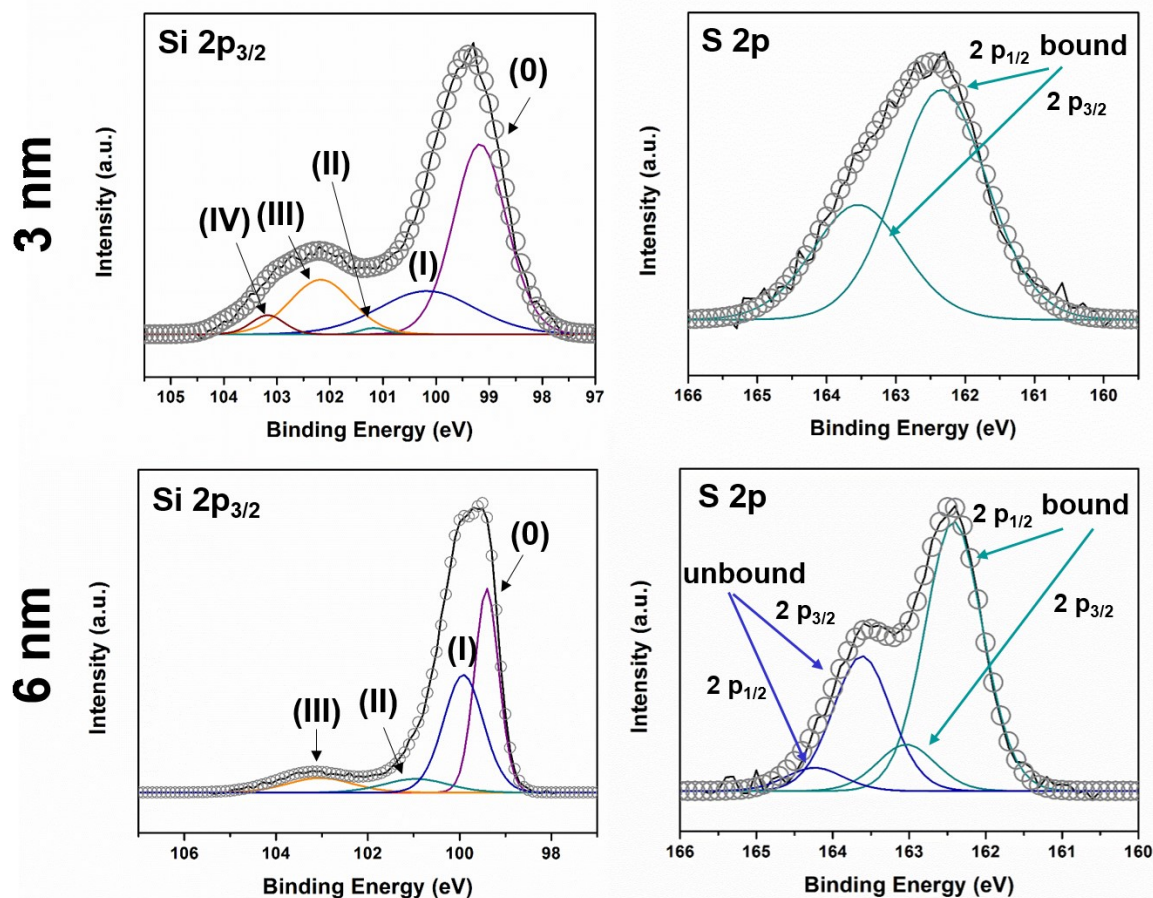


**Figure 3-4:** High-resolution XPS spectra of silicon ( $2p_{3/2}$ ) and sulfur ( $2p$ ) signals for 3 and 6 nm DBDS-SiNCs. Fitting results are shown for the Si  $2p_{3/2}$  components. Si  $2p_{1/2}$  signals have been omitted for clarity. Si (0), Si (I), Si (II), Si (III), and Si (IV) are denoted as (0), (I), (II), (III), and (IV), respectively. For S  $2p$  spectra, ‘bound’ refers to Si-S and ‘unbound’ indicates free sulfur. For all spectra, black curves and circles correspond to the original data and fit spectra, respectively.

UV irradiation of lipoic acid can lead to polymerization. This process occurs because of the homolytic cleavage of the S-S bond<sup>184,327</sup> (bond dissociation energy, BDE, S-S = 53-57 kcal/mol),<sup>328</sup> that produces thiyl radicals that initiates polymerization.<sup>309,312</sup> To determine if surface ligands were oligomeric in nature on the LA-SiNC surface, NALDI-MS was employed; this technique has been applied previously to identify the presence of oligomers on SiNC surfaces.<sup>158</sup> Recall (Section 2.3), the resulting fragmentation patterns obtained from this technique can be complex due to the various bond strengths at the SiNC surface (Si-Si, 210–250 kJ mol<sup>-1</sup>; Si-C, 369 kJ mol<sup>-1</sup>; and C-C, 292-360 kJ mol<sup>-1</sup>).<sup>131</sup>

SiNCs with  $d = 3, 6,$  or  $8$  nm were investigated and the resulting data were evaluated by identifying a series of signals separated by  $m/z = 206$ , the loss of a repeat unit from an oligomer or polymer of lipoic acid (Figure 3-5). There were no fragments associated with lipoic acid ( $m/z = 206$ ) for all samples investigated. For 3 and 6 nm SiNCs, fragments showed a distinct series of mass peaks separated by  $m/z = 206$ . For 8 nm lipoic acid functionalized SiNCs, no evidence of oligomers was detected. This difference may arise from the established photodegradation of the polymer and is the subject of ongoing investigation.<sup>310,313</sup> The origin of this size dependent reactivity is unclear. To isolate if the SiNCs were responsible for the observed oligomerization, a sample of LA exposed to the emission of the fluorescent light was evaluated (Figure 3-5D) and oligomers made up of LA units were detected. For reactions involving DBDS, the S-S bond is not held together by a bridging ring as the lipoic acid S-S bond, and no oligomerization is expected. Therefore, NALDI-MS was not employed for DBDS-SiNCs.

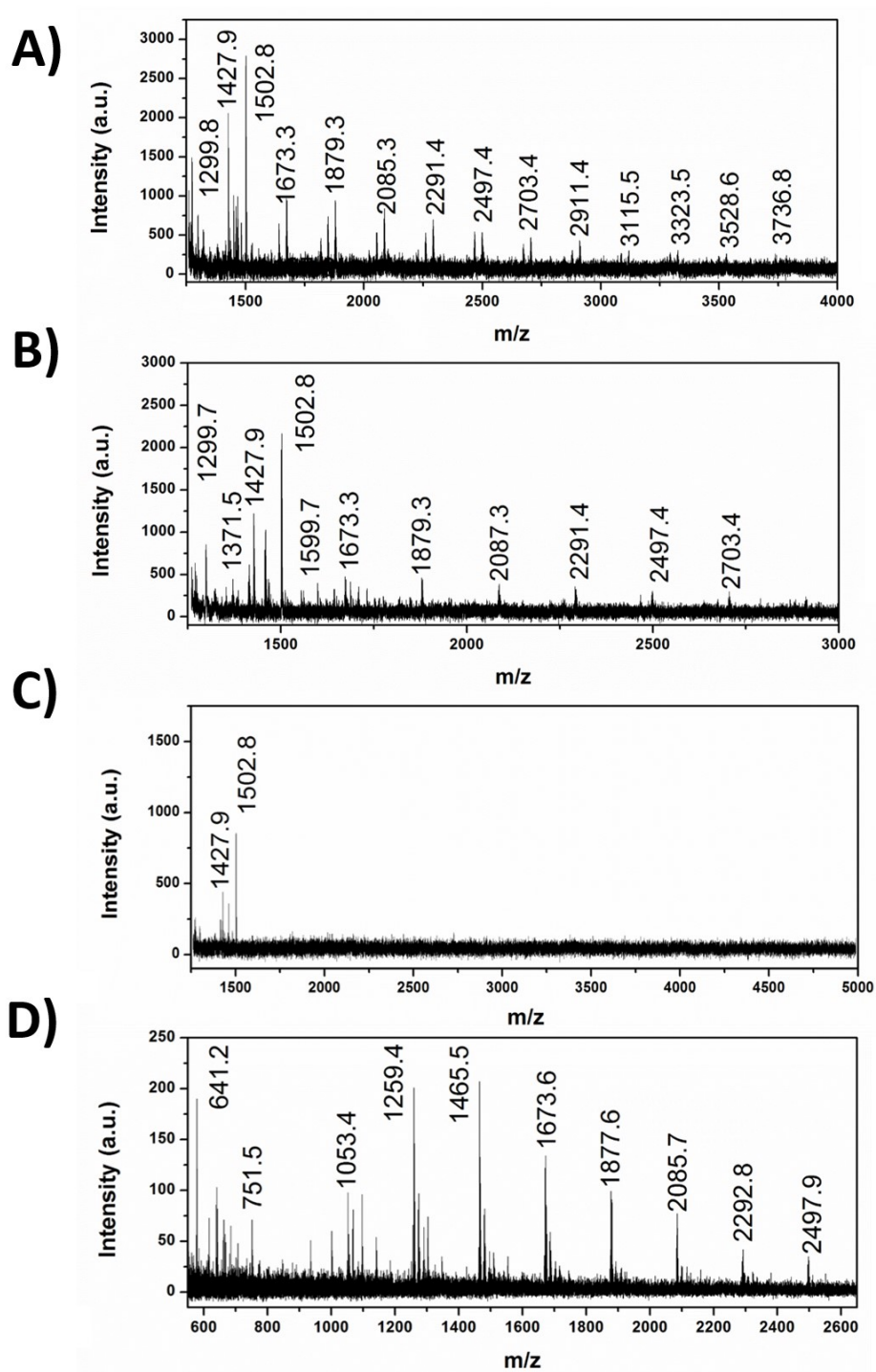


**Figure 3-5:** NALDI-MS spectra of A) 3 nm, B) 6 nm, C) 8 nm LA-SiNCs D) NALDI-MS spectrum of lipoic acid after exposure to fluorescent light.

To further interrogate the nature of the surface ligand, TGA was performed (Figure 3-6). The TGA traces reveal a significant weight loss of occurring at 150 - 600 °C for 3, 6, and 8 nm LA-SiNCs when heating, and occurs in a similar temperature range to that previously reported for polymeric lipoic acid.<sup>313</sup> While quantitative identification of the species present is not possible, the appearance of several weight loss events suggests a mixture (*e.g.*, free and surface bonded oligomers, oligomers of varied molecular weights). TGA analysis was also used to evaluate DBDS-SiNCs. In this case, a mass increase was observed as the sample was being heated, rather than a weight loss (Figure 3-7). The origin of this behavior is not obvious and may be related to the weak Si-S surface linkage<sup>320</sup> as well as a possible gas leak in the TGA that came to light post analysis. Due to the interest of time, this measurement was not repeated.

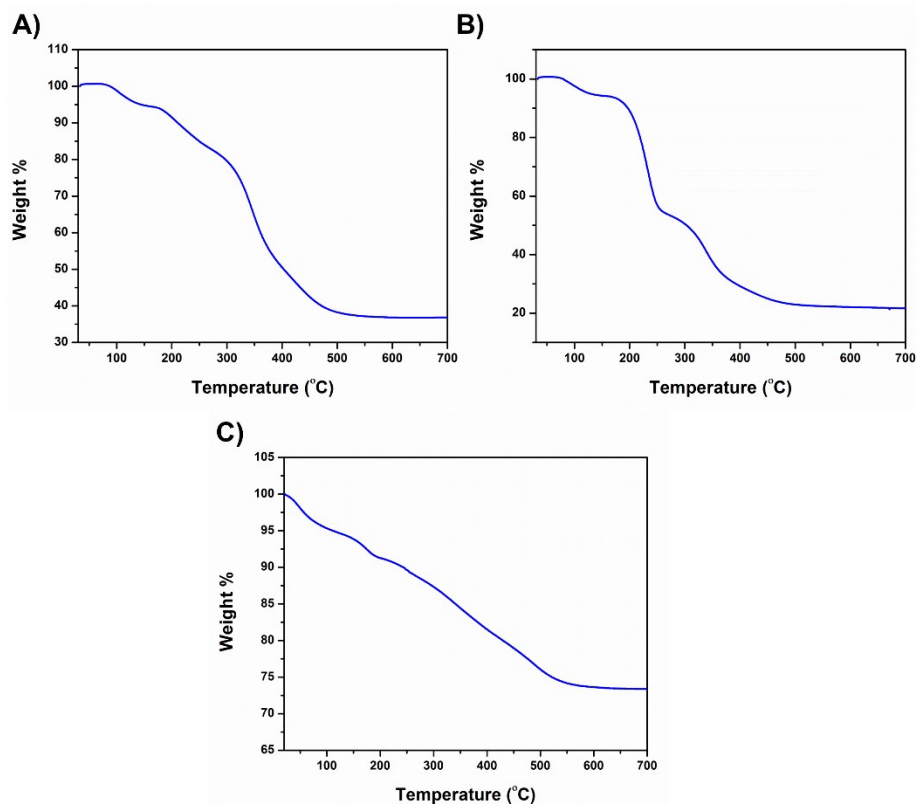


**Figure 3-6:** TGA curves of LA-SiNCs with  $d =$  (A) 3 nm, (B) 6 nm, and (C) 8 nm.

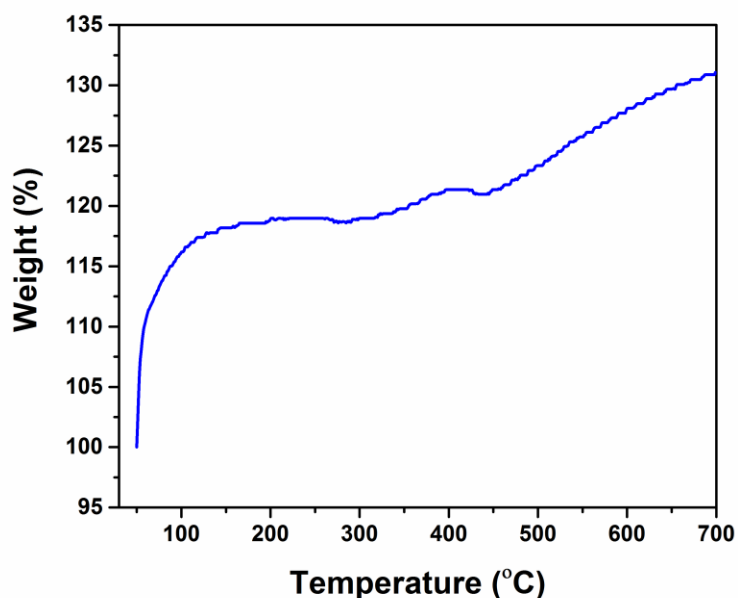


**Figure 3-7:** TGA curve of DBDS-SiNC with  $d = 3$  nm.

The LA-SiNCs were further probed by  $^1\text{H}$  NMR spectroscopy (in  $\text{THF-d}_8$ ) to obtain complimentary information related to the nature of the surface ligands (Figure 3-8). The resonances corresponding to alkyl (1.4 – 3.0 ppm) and acidic protons ( $\sim 10.8$  ppm) on the surface ligands of functionalized particles exhibit significant broadening compared to those noted for free lipoic acid.<sup>313</sup> This broadening has been noted previously for surface bonded species and results from the long relaxation times due to the slow/restricted rotation of the ligand.<sup>329</sup> The polymeric nature of the surface ligand might also contribute to the observed broadening of the  $^1\text{H}$  NMR spectra.<sup>310,313</sup> Unfortunately,  $^1\text{H}$  NMR spectroscopy could not be obtained for DBDS-SiNCs due to limited solubility.

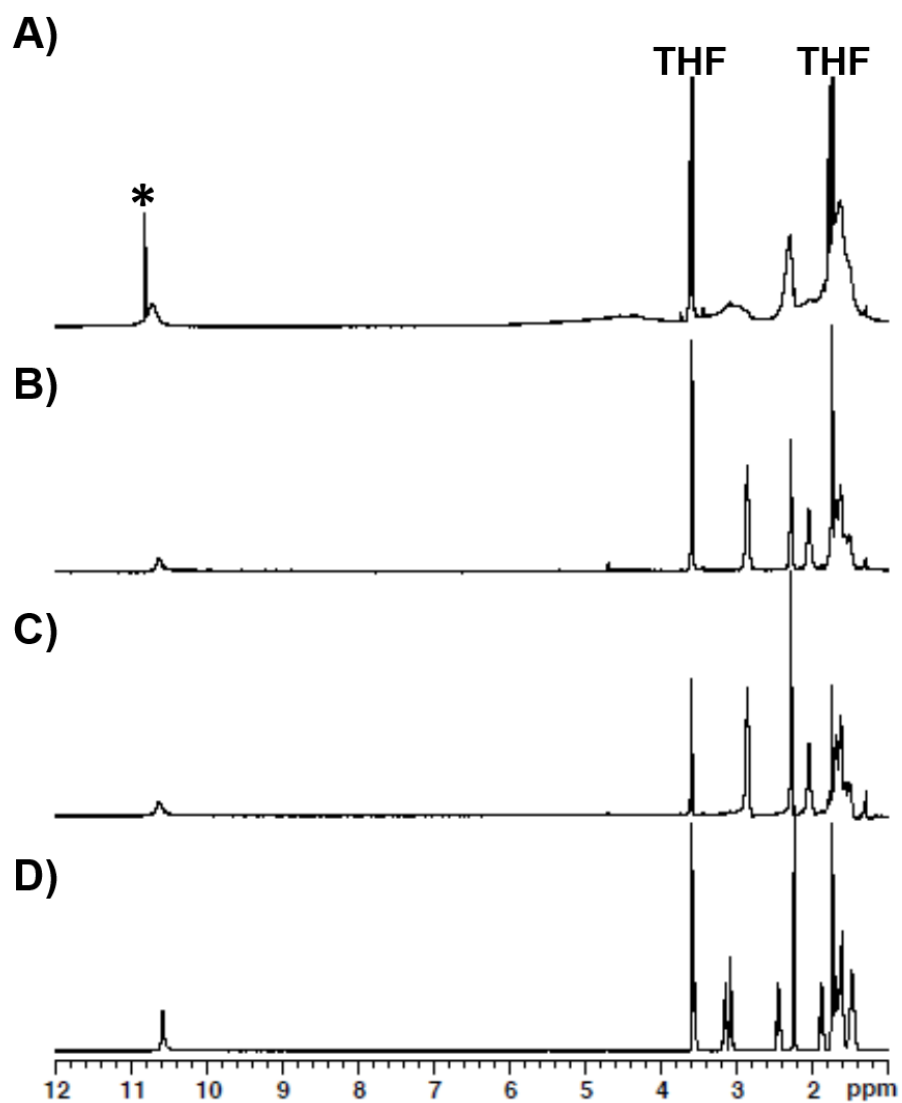


**Figure 3-8:**  $^1\text{H}$  NMR spectra of A) 8 nm, B) 6 nm, and C) 3 nm LA-SiNCs. D)  $^1\text{H}$  NMR spectra of neat lipoic acid. \* Denotes free lipoic acid and/or trace impurities.

Based on the FTIR (Figure 3-2), XPS (Figures 3-3 and 3-4), NALDI-MS (Figure 3-5), TGA (Figure 3-6), and  $^1\text{H}$  NMR (Figure 3-8) analyses, the surfaces of the functionalized SiNCs are complex. It is reasonable surface groups include LA (monomer or polymeric dependent on

SiNC size) or DBDS ligands attached, as well as residual Si-H (from unreacted surface sites) complex oxides denoted as Si-O-Si (from oxidation) (See Figure 3-9).

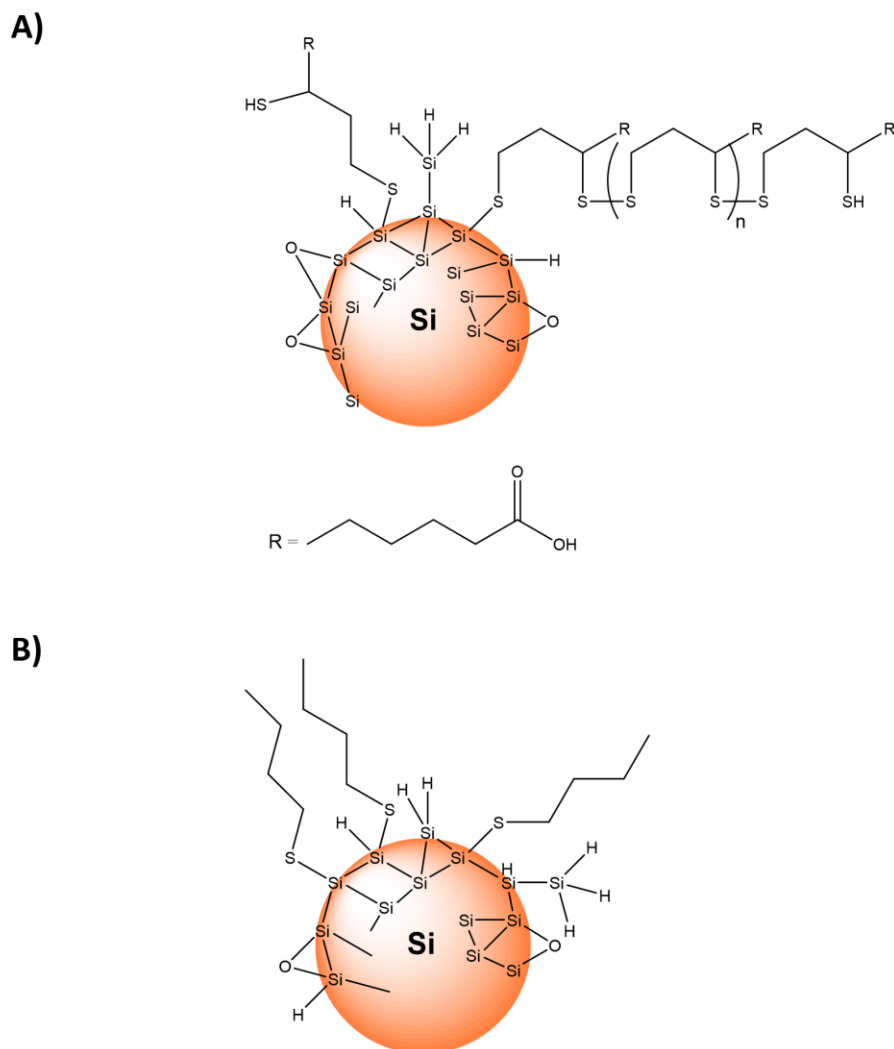


**Figure 3-9:** Representative schematic of the surface of SiNCs after reactions with A) lipic acid or B) dibutyl disulfide.

The particle size and morphology of all functionalized SiNCs were evaluated using TEM (Figure 3-10a-e). For images of LA-SiNCs (Figure 3-10a-c), aggregation was observed consistent with interparticle interactions involving carboxylic acid groups of the lipic acid surface ligands

(*e.g.*, H-bonding and dimerization). The TEM images of DBDS-SiNCs (Figure 3-10d-e) also showed evidence of aggregation. As a consequence of this aggregation, a detailed size analysis from TEM images could not be achieved. The HRTEM (Figure 3-10f) of 8 nm LA-SiNCs shows lattice fringes resulting from Si (111) lattice spacing ( $d$ -spacing = 0.32 nm) indicating the Si core remained intact throughout the functionalization procedure. Further evaluation of the hydrodynamic radius of the SiNCs was performed using DLS, however, no clear trends were observed and may be the result of solution borne oligomers complicating the analysis (data not shown).

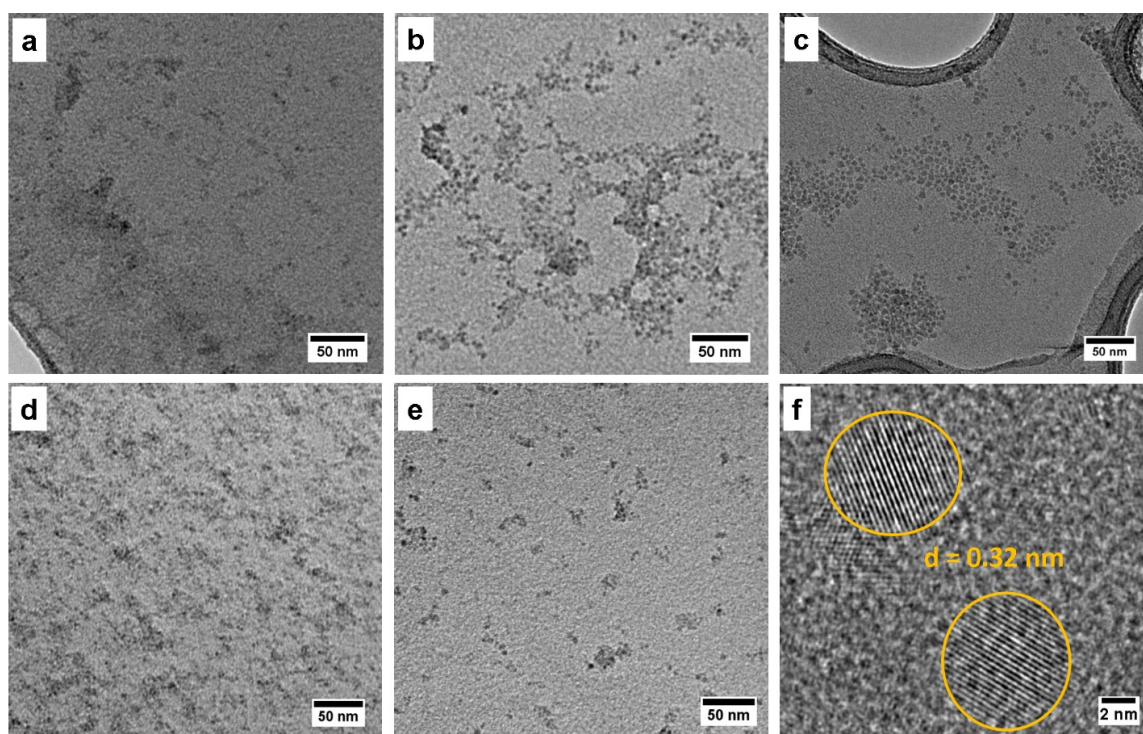


**Figure 3-10:** TEM images LA-SiNCs with diameter: (a) 3 nm, (b) 6 nm, (c) 8 nm. TEM images of DBDS-SiNCs with diameter: (d) 3 nm, (e) 6 nm. (f) HRTEM image of LA-SiNCs with diameter 8 nm.

All functionalized SiNCs are photoluminescent (PL, Figure 3-11) and exhibit PL maxima occurring at 618, 619 and 659 nm for 3, 6, and 8 nm for LA-SiNCs, respectively (Figure 3-10A).

DBDS-SiNCs displayed emission maxima at 719 and 725 nm for 3 and 6 nm SiNCs, respectively (Figure 3-10C). A slight blue-shift in the PL emission was observed for all sizes of LA-SiNCs compared to that of DBDS-SiNCs. The origin of this behavior is unclear, however, it may be related to the degree of surface oxidation of the LA-SiNCs that could reduce particle size or introduce surface states (Figures 3-2 and 3-3).<sup>56,330</sup> In attempts to elucidate the role of surface and core states in the observed PL, the radiative lifetimes of all functionalized SiNCs were also measured. The resulting data were evaluated by fitting to a stretched exponential decay by the following equation:

$$y(t) = Ae^{(-\frac{t}{\tau})^\beta} + C$$

Where  $\tau$  is the time decay,  $\beta$  is the dispersion factor and  $C$  is the constant offset. The measured lifetimes were 26, 17, and 113  $\mu\text{s}$  for 3, 6, and 8 nm LA-SiNCs, respectively. For 3 and 6 nm DBDS-SiNCs, the determined lifetimes were 45 and 75  $\mu\text{s}$ , respectively. All measured lifetimes are consistent with a band-gap based emission.<sup>289</sup>

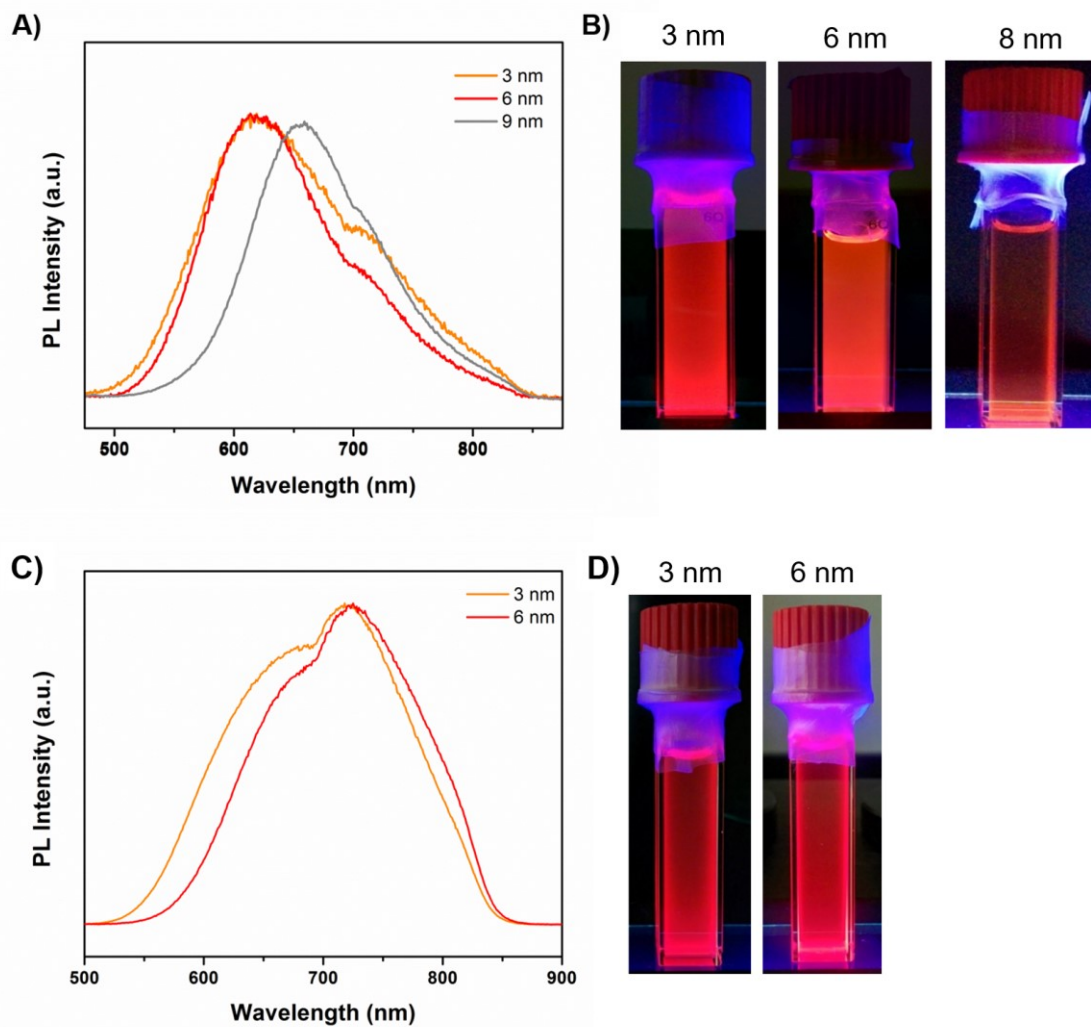


**Figure 3-11:** A) Photoluminescence spectra of LA-SiNCs (d = 3, 6, or 8 nm) functionalized with lipoic acid upon excitation at 350 nm. B) Photographs of LA-SiNCs (d = 3, 6, 8 nm) upon exposure to 365 nm light. C) Photoluminescence spectra of DBDS-SiNCs (d = 3 or 6 nm) upon excitation at 350 nm. D) Photographs of DBDS-SiNCs (d = 3, 6 nm) upon excitation at 365 nm.

### 3.3.1 Investigation the origin of the reactivity

To determine if the light was driving the observed reactivity, a series of experiments designed to isolate its potential role were performed using 3 nm H-SiNCs. First, to determine if heat generated from the light source initiated the reaction, H-SiNCs (~20 mg) and LA (1.2 mmol) were heated to 45 °C for 42 h in an Ar atmosphere. This treatment resulted in no qualitative change consistent with no reaction occurring (Figure 3-12A-i). To investigate the role of light, H-SiNCs (~20 mg) and LA (1.2 mmol) were stirred in the subdued light (*i.e.*, the reaction flask was wrapped in aluminum foil) for 42 h in an Ar atmosphere. Again, no reaction was observed (Figure 3-12A-ii). Both reaction mixtures were stored in ambient light for 2 weeks after which the mixtures were less cloudy suggesting a slow reaction leading to surface modification may have occurred (Figure 3-12B). This reaction may have been initiated by the low intensity irradiation from overhead fluorescent lights that have a similar spectral profile to that of the compact fluorescent bulb used herein, however, no further evaluation was performed.<sup>184</sup> To determine if trace water promotes the reaction of SiNCs with lipoic acid, a sample of freeze-dried SiNCs was combined with LA (1.2 mmol) and exposed to the emission of a compact fluorescent light while being maintained under an Ar atmosphere. After two hours no change was observed. To investigate if residual water remaining after extraction from the HF etching influenced reactivity, trace water was added; after 16 h, the reaction mixture was qualitatively unchanged indicating water did not play a role.

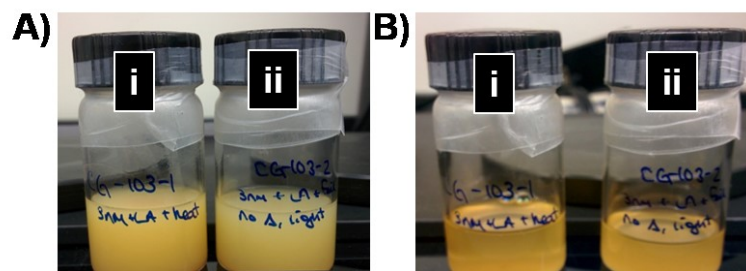


**Figure 3-12:** Vials containing reaction mixtures A) immediately after B) and two weeks after the reactions of i) H-SiNCs ( $d = 3$  nm) and lipionic acid heated to  $45$  °C and ii) H-SiNCs ( $d = 3$  nm) and lipionic acid in subdued light and heat.

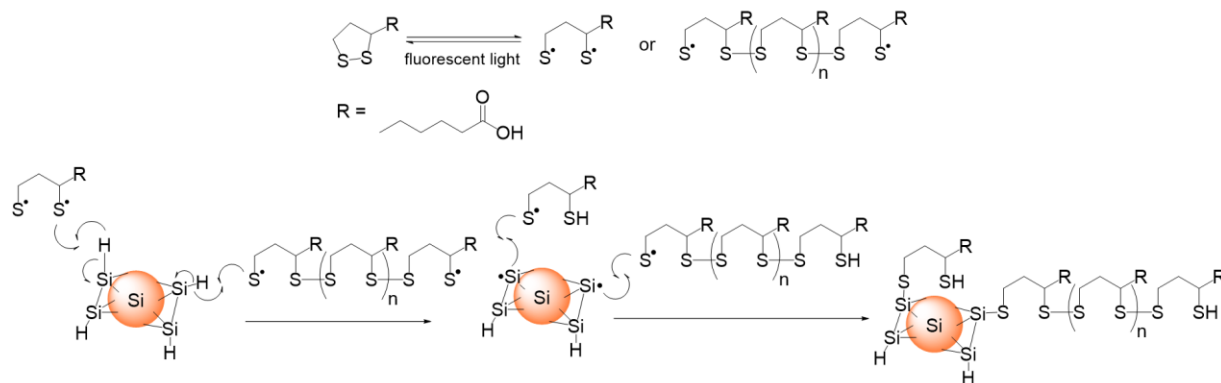
### 3.3.2 Proposed Reaction Mechanism

Previous studies indicated irradiation of lipionic acid (*i.e.*, the disulfide bond) can induce thiyl radicals that can induce the formation of oligomeric and polymeric lipionic acid.<sup>309-312</sup> It is also well established that thiyl radicals are useful in the generation of silyl radicals from organosilanes.<sup>184,327,331-333</sup> NALDI-MS analysis of the lipionic acid functionalized SiNCs shows the formation of oligomers. This was further supported by TGA. Based upon these observations, and the known reactivity of H-SiNCs, it is reasonable that thiyl radicals could be activating the SiNC surface.<sup>146,148,149</sup> In this context, we propose that irradiation of lipionic acid leads to the generation of thiyl radicals (Scheme 3-2a) that abstract a surface hydride of the H-SiNCs or forms oligomeric lipionic acid chains.<sup>184</sup> The silyl radical on the SiNC further reacts with additional thiyl radicals present in solution, finally resulting in the surface functionalization of the SiNCs with either monomer or oligomer lipionic acid units.

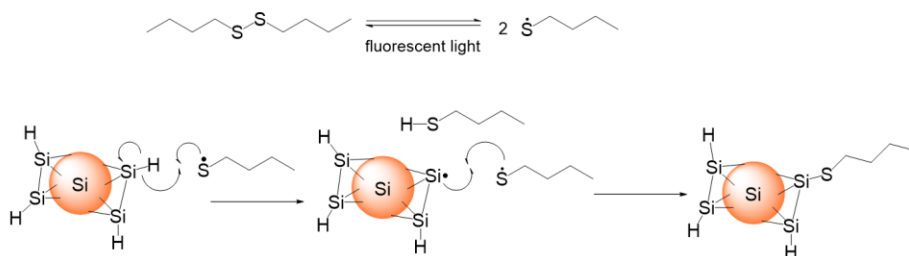
For reactions involving DBDS, the S-S bond is not held together by a bridging ring as the lipionic acid S-S bond, as described above, and no oligomerization is expected. A similar reaction mechanism (Scheme 3-2b) is proposed in which irradiation causes the breakage of the S-S bond

resulting in a thiyl radical capable of hydride abstraction from the H-SiNC surface. Again, the remaining silyl radical on the surface can then react with the additional thiols in solution, resulting in surface functionalization.

(a) Lipoic Acid Functionalization



(b) Dibutyl disulfide Functionalization



**Scheme 3-2:** Proposed reaction mechanisms for H-SiNCs reacted with a) lipoic acid or b) dibutyl disulfide via a compact fluorescent light.

### 3.4 Conclusion

In conclusion, the work outlined in this chapter presents an alternative reaction method to functionalize SiNC surfaces with S-S containing molecules (*i.e.*, lipoic acid and dibutyl disulfide) via a compact fluorescent light source to generate Si-S surface linkages. The mild reaction

conditions used are available to SiNCs  $d = 3, 6, \text{ or } 8$  nm for lipoic acid or  $d = 3$  or  $6$  nm for dibutyl disulfide, exhibit PL, and display long radiative lifetimes under inert atmosphere conditions. NALDI-MS/MALDI-MS and TGA analysis suggests the formation of oligomers/polymers of lipoic acid on the SiNC surface. We also propose the reaction proceeds via a mechanism that begins with abstraction of a surface hydride, similarly to what has been reported on bulk silicon systems.

## **Chapter 4**

# **Detection of High-Energy Compounds Using Photoluminescent Silicon Nanocrystal Paper Based Sensors.<sup>3</sup>**

---

<sup>3</sup> A portion of this chapter has been published:  
Gonzalez, C. M.; Iqbal, M.; Dasog, M.; Piercey, D. G.; Lockwood, R.; Klapoetke, T. M.; Veinot,  
J. G. C. *Nanoscale* **2014**, *6*, 2608-2612.

## 4.1 Introduction

As previously discussed in Chapter 1, sensing high energy materials (*i.e.*, explosives) has received substantial attention because of the obvious importance to security and forensics; detection of these materials is also crucial because many are toxic and pose environmental risks.<sup>222,223,334</sup> Modern methods for detecting explosives include gas chromatography coupled with mass spectrometry, ion mobility spectrometry, surface enhanced Raman spectroscopy, and energy dispersive X-ray spectroscopy.<sup>335-338</sup> Unfortunately, all of the methods are infrastructure intensive and cannot be readily implemented in the field or outside a laboratory setting.<sup>339</sup> There is a concerted push to develop sensing technologies that are cost effective. One approach has been to use paper substrates as sensing motifs. For example, paper-based Surface Enhanced Raman Spectroscopy substrates for explosive detection have also been developed.<sup>340,341</sup> In this context, development of complementary techniques for straightforward, rapid, on-site detection is of paramount importance.

An attractive approach toward realizing this goal is the development of fluorescent sensors that respond to these compounds. These sensors are usually comparatively simple, require minimal infrastructure, are cost-effective, and exhibit adequate sensitivity, as well as response times.<sup>8</sup> Recently, luminescent nanomaterials (*e.g.*, Cd-based quantum dots (QDs)) have been explored as fluorescent sensors because of their exquisite tunability.<sup>15,342,343</sup> Freeman and coworkers successfully employed fluorescent, functionalized CdSe/ZnS QDs to detect trace quantities of trinitrotoluene (TNT) and cyclotrimethylenetrinitramine (RDX).<sup>210</sup> In efforts to render these systems portable and increase their compatibility with field applications, researchers interfaced the active nanomaterials with common filter paper to afford a detection system. Zhang and coworkers coated filter paper with dual-emission CdTe QDs that luminesce different colours

in the presence of TNT.<sup>344</sup> Similarly, Ma and coworkers used the molecular emitter 8-hydroxyquinoline aluminum and nanospheres to detect 2,4,6-trinitrophenol (TNP).<sup>345</sup>

Quantum dots have the clear advantages over molecule-based emitters given that they are less susceptible to photobleaching, however, CdSe and CdTe QDs are toxic.<sup>211</sup> Furthermore, regulations exist or are pending in numerous jurisdictions that limit their widespread use in industrial and consumer applications – new materials must be explored.<sup>211</sup> Silicon nanocrystals (SiNCs) are an attractive alternative material that maintains all the advantages of Cd-based quantum dots (*e.g.*, tailorability and photostability) with the clear benefit of being less toxic. The Sailor group showed the photoluminescence of hydride terminated porous silicon films was quenched upon exposure to dinitrotoluene (DNT), TNT, and nitrobenzene (NB) vapors.<sup>224</sup> These quenching processes are believed to occur via a reversible electron transfer mechanism or irreversible chemical oxidation depending on the duration of vapor exposure.<sup>224</sup> The authors noted these findings are in agreement with the work by Fauchet and McLendon, that showed nitroaromatics could participate in electron transfer if the quencher redox level lies below the conduction band edge of porous silicon.<sup>346</sup> However, hydride terminated porous silicon surface is readily oxidized upon exposure to air and is fragile, thus making it impractical for field applications. Germanenko and coworkers demonstrated the red luminescence of web-like agglomerated silicon nanocrystals ( $d \sim 5\text{-}6\text{ nm}$ ) bearing a 1-2 nm oxide surface layer was quenched when exposed to nitroaromatic compounds.<sup>225</sup> Again, an electron transfer quenching mechanism is proposed, as observed with porous silicon. Unfortunately, the luminescence of these materials was not affected by explosives-related compounds NB and mononitrotoluene (MNT) that are common degradation products of nitro class explosives typically found in landmines.<sup>347</sup> These early reports demonstrate the promise of Si-based nanomaterials and suggest photoluminescent

SiNCs could be used as sensors for nitro containing explosives. To the best of our knowledge, no study has been reported that employed well-defined freestanding alkyl terminated surface silicon nanocrystals as a nitroaromatic, nitroamine or nitrate ester explosives detection system.

In this chapter, we describe the detection of a series of nitroaromatic compounds (*i.e.*, mononitrotoluene (MNT), nitrobenzene (NB), dinitrotoluene (DNT), and trinitrotoluene (TNT)), as well as the nitroamine RDX and nitrate ester pentaerythritol tetranitrate (PETN) by exploiting the optical response of dodecyl functionalized SiNCs in solution. We subsequently extend this investigation and outline the fabrication and application of an air-stable, fluorescent, paper detector based upon these particles. This paper-based system showed rapid detection of nitroaromatics, nitroamine, and nitrate esters by luminescent quenching in solution, vapor and solid phase at nanogram levels. We then further investigated the coupling of pentanoic acid functionalized SiNCs to non-fluorescent thin layer chromatography (TLC) plates for the separation of MNT and DNT.

## 4.2 Experimental

### 4.2.1 Chemicals/Reagents and Materials

Hydrogen silsesquioxane (HSQ, trade name Fox-17, sold commercially as a solution in methyl isobutyl ketone) was purchased from Dow Corning Corporation (Midland, MI). Hydrofluoric acid (HF, 49% aqueous solution) was purchased from J.T. Baker. Reagent grade methanol, ethanol, toluene, 1-dodecene (95%), 2,4-dinitrotoluene (DNT), and mononitrotoluene (MNT), 2,2'-azobis(2-methylpropionitrile) (AIBN, 98%), 4-(dimethylamino)pyridine (DMAP, 95%), *N,N'*-dicyclocarbodiimide (DCC, 99%), pentenoic acid (97%, dried over molecular sieves (3 Å) prior to use) dichloromethane, and acetone were purchased from Sigma Aldrich.

Nitrobenzene (NB, 99%) was received from Alfa Aesar. 2,4,6-trinitrotoluene (TNT), pentaerythritol tetranitrate (PETN), and cyclotrimethylenetrinitramine (RDX) were synthesized using established literature procedures.<sup>348</sup> Silica gel on TLC aluminum foils (silica gel 60 matrix, without fluorescence indicator, L x W 5 cm x 7.5 cm, product number 55811) were purchased from Sigma Aldrich.

#### 4.2.2 Preparation of hydride-terminated Si nanocrystals

A composite consisting of SiNCs embedded within a SiO<sub>2</sub>-like matrix was prepared via thermal processing of HSQ as described previously.<sup>112</sup> Briefly, solid HSQ was placed in a quartz reaction boat and heated at 1100°C in a tube furnace for 1 h under reducing conditions (*i.e.*, 95% Ar/5% H<sub>2</sub>). This procedure yields SiNCs (diameter *ca.* 3.7 nm) within a protective oxide. After cooling to room temperature, the composite was crushed using an agate mortar and pestle to form a fine brown powder. Additional grinding was performed upon shaking with high-purity silica beads with a Burrell Wrist Action Shaker for 12 h. The resulting SiNC/SiO<sub>2</sub> composite was chemically etched to liberate hydride-terminated SiNCs. 0.4 g of ground composite powder was transferred into a polypropylene beaker with a stir bar. 5 mL of water and 5 mL of ethanol were added to the beaker with mechanical stirring. 5 mL of 49% HF solution (**Caution!** HF must be handled with extreme care) was then slowly added to the beaker and the mixture was stirred for 1 h. The hydride-terminated SiNCs (H-SiNCs) were extracted from the aqueous layer into *ca.* 30 mL (*i.e.*, 3x 10 ml) of toluene. The cloudy yellow SiNC toluene suspension was transferred into test tubes and centrifuged at 3000 rpm to isolate the SiNCs for immediate dodecyl functionalization (*vide infra*).

### 4.2.3 Synthesis of dodecyl functionalized silicon nanocrystals

The toluene supernatant was decanted and H-SiNCs were immediately dispersed in *ca.* 30 mL dodecene and transferred to a flame dried Schlenk flask that was equipped with a magnetic stir bar. The flask was attached to a Schlenk line and evacuated and backfilled with argon three times to remove air. The reaction mixture was heated to 190 °C and stirred for 12 h to yield a transparent orange-yellow solution. The resulting solution was cooled to room temperature and mixed with 105 mL of a 1:1 methanol:ethanol mixture and placed in a high-speed centrifuge at 14000 rpm for 0.5 h. The supernatant was decanted and 10 mL of toluene was added to redisperse the particles. 35 mL of 1:1 methanol:ethanol solution was then added and the centrifugation/decanting/redispersion procedure was repeated twice. The purified particles were finally redispersed in toluene (10 mL), filtered through a 0.45 µm PTFE syringe filter, and stored in vials under ambient conditions for future use. The SiNCs were characterized using FT-IR and TEM.

### 4.2.4 Synthesis of carboxylic acid functionalized silicon nanocrystals

Again, the toluene supernatant was decanted, the H-SiNCs were dispersed in 10 mL of toluene and transferred to an argon charged, oven dried Schlenk flask equipped with a magnetic stir bar. Pentenoic acid (0.018 mol) dried over molecular sieves (3 Å) was then added to this solution along with 0.061 mmol of AIBN. The mixture was then subjected to three cycles of freeze-pump-thaw, heated to 60 °C and stirred for 19 h. The resulting SiNCs were isolated by centrifugation at 3000 rpm for 10 min. The supernatant was then decanted and the remaining SiNCs were redispersed in 95% ethanol and pentane was used as the anti-solvent. This solvent/anti-solvent mixture was then centrifuged at 14000 rpm for 20 min. This procedure was

repeated an additional two times. The purified SiNCs were then stored in vials under ambient conditions until further use. The SiNCs were characterized using FT-IR and TEM.

#### **4.2.5 Coupling of carboxylic acid functionalized silicon nanocrystals to TLC plates**

Carboxylic acid functionalized SiNCs (~20 mg) were dispersed in 25 mL of dry toluene in a dry argon charged Schlenk flask and subjected to three freeze-pump-thaw cycles. Then the non-fluorescent TLC plates (1.5 x 5 cm, previously dried in vacuum overnight prior to use) were strung through a metal wire and placed into the Schlenk flask containing the SiNC solution (Figure 4-11, below). A solution mixture of DCC (0.08 mmol) and DMAP (0.12 mmol) was added to the Schlenk flask under ice cooling. The reaction mixture was left under ice for 10 min and then at room temperature overnight. The SiNC coupled TLC (SiNC-TLC) plates were then washed with dichloromethane and acetone to remove remove excess reagents and were dried under vacuum prior to use.

#### **4.2.6 Material Characterization and Instrumentation**

Fourier Transform Infrared Spectroscopy (FT-IR) of functionalized SiNCs was performed using a Nicolet Magna 750 IR spectrophotometer by drop coating a toluene dispersion of SiNCs. Transmission Electron Microscopy (TEM) analysis was performed using a JEOL-2010 (LaB<sub>6</sub> filament) electron microscope with an accelerating voltage of 200 keV. TEM samples were prepared by drop casting a toluene solution of SiNCs onto a 200  $\mu\text{m}$  mesh carbon coated copper grid and allowing the solvent to evaporate under vacuum prior to imaging. Size information was obtained by counting no fewer than 200 particles using Image J program. Photoluminescence (PL)

spectra were acquired using a Cary Eclipse spectrophotometer ( $\lambda_{\text{ex}} = 350 \text{ nm}$ ). All solution-based quenching studies were performed using toluene solutions of functionalized SiNCs (1 mg/mL).

#### 4.2.7 Solution phase PL quenching studies

Stock solutions of NB, MNT, and DNT were prepared in toluene at appropriate concentrations. The working solutions were then stirred thoroughly prior to fluorescent measurements for a minimum of 5 min each. The solution samples were then transferred to a spectrophotometer quartz cuvette and fluorescent measurements were then taken at room temperature. The final concentration of nitroaromatic compounds analyzed are listed in Table 4.1 below.

#### 4.2.8 Solution phase PL lifetime studies

Photoluminescence lifetimes were acquired by shining a modulated argon ion laser (476 nm, ~30mW) into the quartz cuvette containing the as prepared solutions and then coupled to a fiber optic system. The laser was modulated by an acousto-optic modulator operating at 500 Hz. Light from the SiNCs was channeled into a photomultiplier (Hamamatsu H7422P-50) connected to a photon counting card (PMS-400A). Lifetime decay data was fit to a stretched exponential function in Mathematica given by  $y(t) = A[\exp(-(t/\tau)^\beta)] + C$ , where  $A$  is the initial intensity,  $\tau$  is the time decay (basic lifetime),  $\beta$  is a stretching parameter that can vary between 0 and 1, and  $C$  is an offset.<sup>286-288</sup>

As the concentration of nitroaromatic compounds (*i.e.*, NB, MNT, DNT) increased, the values of  $\tau$  decreased, indicating that the SiNCs were quenched by fast, non-radiative, processes.<sup>225</sup> Additionally,  $\beta$  decreased indicating that the lifetime distribution grew due to the presence of non-

radiative relaxation pathways with NB, MNT, and DNT.<sup>349</sup> The final concentration of nitroaromatic compounds analyzed for lifetime measurements are listed in Table 4.1.

**Table 4-1:** Concentrations of nitroaromatics (*i.e.*, NB, MNT and DNT) used for PL and lifetime measurements.

<b>PL measurements (mM)</b>	<b>PL lifetime measurements (mM)</b>
0	0
0.05	0.05
0.075	0.075
0.25	0.25
0.5	0.5
0.75	0.75
1	1
1.5	1.5
2.5	2.5
5	5
7.5	-
10	-
25	-

#### 4.2.9 SiNCs paper sensor for visual detection of nitroaromatic compounds

A piece of filter paper (Fisherbrand, qualitative P4) was cut into small rectangles and dipped into a beaker containing a 5 mg/mL solution of dodecyl functionalized SiNCs for 10 min. The filter paper was then removed and dried under N<sub>2</sub> for 2 min. This indicator paper displayed red-orange luminescence when exposed to a hand held UV lamp ( $\lambda = 365$  nm). To display the potential application as a fluorescent paper sensor, solutions of nitroaromatic compounds were spotted onto the paper directly by pipette, “fingerprinted” with solid nitroaromatic compounds onto the paper, or exposed to nitrobenzene vapor. Finally, the paper was imaged under the UV lamp ( $\lambda = 365$  nm) and photos were taken by a digital camera.

For cotton swab residue studies, 2  $\mu\text{L}$  of varying concentrations (0.0125, 0.05, 0.25 mM) of DNT were drop coated onto cotton swab tips. These swabs were then left to dry and should result in residues of 4.5, 18.2, 91.1 ng of DNT present on the swab. A blank swab was prepared by drop coating 2  $\mu\text{L}$  of toluene onto the cotton swab tips and left to dry. All of the prepared swabs were then pressed onto the filter paper to observe if quenching of luminescence would occur.

For solid residue testing, 0.5 mg of DNT was weighed in a plastic tray, and then a gloved finger tapped onto the solid DNT sample. The excess solid was brushed off until there was no visible solid present on the glove. The gloved finger was then pressed four times successively on the filter paper. The paper was then viewed under the UV lamp to determine if quenching was achieved. Further solid residue testing was performed by swiping a gloved finger into the empty plastic tray where the DNT was once present. The gloved finger was then pressed onto the filter paper 4 times, and observed under a UV lamp. A similar procedure was followed to test if the filter paper could detect DNT solid residue that was present on cotton fabric. 0.5 mg of DNT was applied to cotton fabric, brushed off, and then the filter paper was rubbed onto the fabric, and finally observed under a UV lamp.

Vapor testing of nitrobenzene was performed by placing the prepared sensor paper over the mouth of a bottle containing concentrated NB and leaving for 3 min. The resulting paper was then removed and imaged under UV lamp. To check if the filter paper sensor was reusable, it was then placed under a  $\text{N}_2$  airstream for 2 min to evaporate off NB, then removed and imaged under UV lamp.

#### **4.2.10 TLC separation of nitroaromatic compounds**

A SiNC-TLC plate was first spotted with 2  $\mu\text{L}$  of MNT (0.1 M) and 2  $\mu\text{L}$  of DNT (0.1 M) in separate lanes. The TLC plate was then developed in a beaker containing a 50:50 mixture of

CH<sub>2</sub>Cl<sub>2</sub>:acetone. A second SiNC-TLC plate was spotted with 2 μL of MNT (0.1 M) and then spotted with 2 μL of DNT (0.1 M) in the same lane. Again, the TLC plate was then developed in a beaker containing a 50:50 mixture of CH<sub>2</sub>Cl<sub>2</sub>:acetone. The TLC plates were then exposed to a handheld UV lamp ( $\lambda = 365$  nm) for observation and analysis.

## 4.3 Results and Discussion

### 4.3.1 Characterization of dodecyl functionalized SiNCs

Oxide-embedded SiNCs were obtained from the thermally induced disproportionation of HSQ.<sup>112</sup> After etching with HF, red-emitting, hydride terminated SiNCs were obtained and immediately functionalized with dodecene via thermally induced hydrosilylation as reported previously.<sup>112</sup> Material characterization is summarized in Figure 4-1. The FTIR spectrum (Figure 4-1A) shows features characteristic of alkyl terminated surfaces at 2920 cm<sup>-1</sup> (C-H stretching) and 1450 cm<sup>-1</sup> (-C-H bending) consistent with dodecyl functionalization.<sup>142</sup> Features observed at 2110 and 1050 cm<sup>-1</sup> indicate small amounts of SiH<sub>x</sub> and Si-O-Si functionalities, respectively, remain following alkyl modification. The PL spectrum of the dodecyl functionalized SiNCs in toluene (Figure 4-1B) shows a peak intensity maximum at 643 nm. Morphology of the functionalized SiNCs was evaluated using transmission electron microscopy (Figure 4-1C) which indicates the particles are pseudospherical with an average diameter of 3.7 ± 0.4 nm (Figure 4-1D).

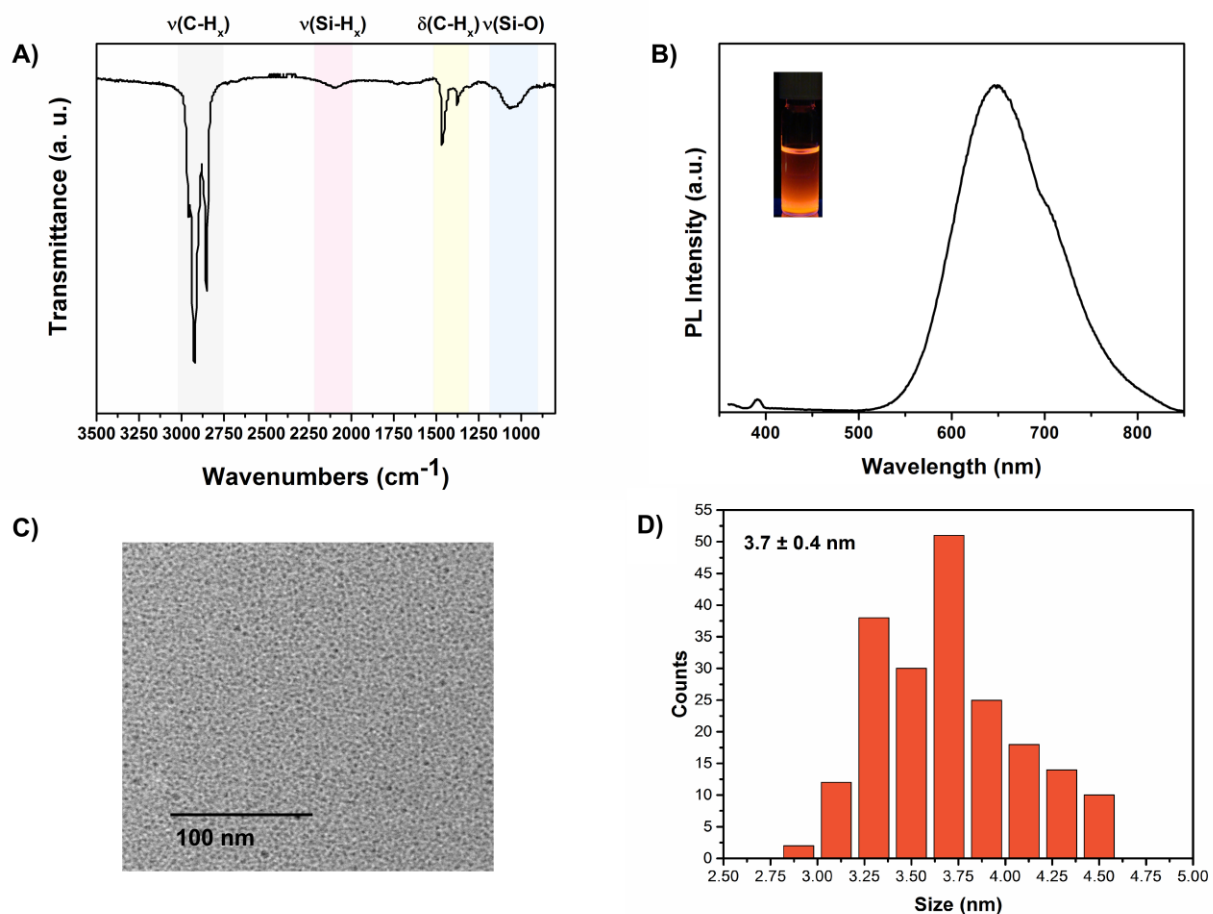


**Figure 4-1:** Characterization of dodecyl functionalized SiNCs. (A) FTIR spectrum of SiNCs. (B) Fluorescence spectrum of SiNCs with an inset of the nanocrystals displaying the red-orange luminescence atop UV benchtop. (C) TEM image of resulting nanocrystals and (D) the particle size distribution analysis of the SiNCs. Note: Particle size histograms were assembled by counting 200 SiNCs through the longest diameter present with Image J software.

### 4.3.2 Fluorescence quenching by nitroaromatic compounds

Upon the addition of nitroaromatic compounds (*i.e.*, NB, MNT, and DNT) to solutions of dodecyl functionalized SiNCs, luminescence was quenched. Figure 4-2A-C shows titration curves of the fluorescence peak intensity of toluene solutions containing 1 mg/mL SiNCs as a function of nitroaromatic (*i.e.*, NB, MNT, and DNT) concentration ranging from 0.05 to 25 mM. Consistent

with previous reports, the degree of SiNCs PL quenching was proportional to the concentration of nitroaromatic (*i.e.*, higher the nitroaromatic concentration, the more efficient the quenching). In addition, no shift in PL maximum or changes in the line shape of the PL spectrum resulted.

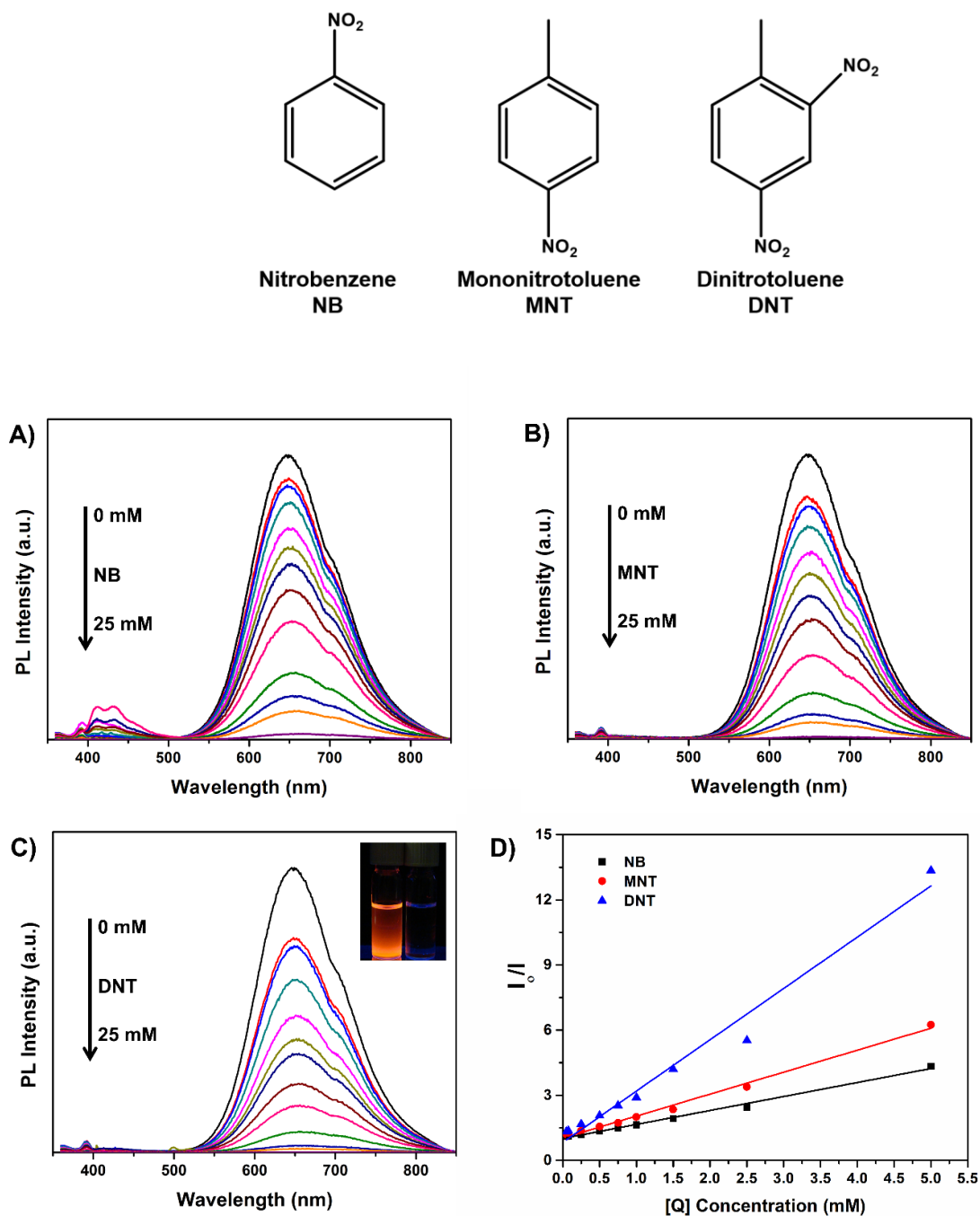
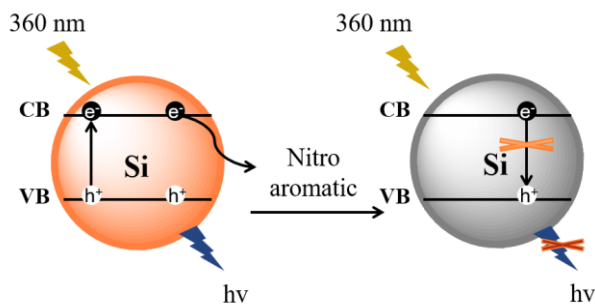


**Figure 4-2:** Fluorescence quenching spectra of SiNCs by increasing concentrations of (A) NB, (B) MNT, (C) DNT in solution with an inset showing the quenching effect with 0 and 25 mM DNT atop bench-top UV-lamp. (D) The Stern-Volmer plot for the quenching efficiencies of NB, MNT and DNT at different concentrations.

To gain a more complete understanding of the quenching behaviour induced by NB, MNT, and DNT on dodecyl functionalized SiNCs PL data was evaluated using the Stern-Volmer equation:

$$I_0/I = K_{sv}[Q] + 1$$

Where,  $I_0$  and  $I$  are the luminescence intensity in the absence and presence of nitroaromatic compounds (analyte), respectively.  $[Q]$  is the nitroaromatic compound (analyte) concentration, and  $K_{sv}$  is the luminescence quenching constant. Figure 4-2D shows the relationship of  $I_0/I$  vs. nitroaromatic compound (NB, MNT, DNT) concentration. In the range of 0.05-5 mM, NB, MNT, and DNT display linear behaviour indicative of the quenching arising from a dynamic process such as an electron transfer.<sup>350</sup> It has been proposed, based upon the correlation of reduction potentials in nitroaromatic compounds, that luminescence quenching of both porous silicon and oxide terminated web-like aggregates of SiNCs proceeds via an electron transfer pathway (Scheme 4-1).<sup>224,225,346</sup> Suggestions have been made that the electron transfer occurs from the Si nanomaterial conduction band to the vacant  $\pi^*$  orbital of the nitroaromatic compound, resulting in photoluminescence quenching.<sup>225,351</sup> If this is the case for the present systems, considering the known reduction potentials of NB, MNT, and DNT (*i.e.*, -1.15 V, -1.19 V, and -0.9 V vs NHE in acetonitrile, respectively),<sup>224,346</sup> the PL quenching efficiency should decrease for more negative redox potentials. As such, DNT should be the most efficient quencher of the three tested here. The  $K_{sv}$  values determined from the analysis presented in Figure 4-1B are  $6.44 \text{ (mM)}^{-1}$ ,  $1.01 \text{ (mM)}^{-1}$ , and  $2.36 \text{ (mM)}^{-1}$  for NB, MNT, and DNT, respectively. Unfortunately, this trend does not hold true for NB and MNT  $K_{sv}$  values, however DNT was the most efficient quencher.



**Scheme 4-1:** Proposed electron transfer quenching mechanism of SiNCs by nitroaromatic compounds, where  $e^-$ ,  $h^+$ , CB and VB represent an electron, hole, conduction band and the valence band, respectively.

To further verify the quenching mechanism is a dynamic process, the PL lifetime of the SiNCs as a function for each of the nitroaromatic quenchers (*i.e.*, NB, MNT, DNT) concentration in the range of 0.05 - 5 mM was studied. If the PL lifetime is independent of the quencher concentration, the quenching mechanism is static and is governed by the formation of a ground state nanoparticle-analyte complex.<sup>352</sup> Alternatively, if the quenching process is dynamic there will be a decrease in the lifetime because of additional deactivation pathways (*e.g.*, electron transfer) that will shorten the lifetime.<sup>352</sup> For the present system, increasing the concentration of the nitroaromatic compound resulted in a decrease of lifetime decays (Figure 4-3A-C). These results were then plotted as  $\tau_0/\tau$  vs. nitroaromatic compound (NB, MNT, DNT) concentration where  $\tau_0$  and  $\tau$  are the PL lifetimes in the absence and presence of nitroaromatic compounds (analyte), respectively (Figure 4-3D). Unfortunately, due to time and instrument availability, only one data set was collected and no statistical analysis could be performed. As expected, DNT was the most efficient lifetime quencher of all nitroaromatic compounds tested. These results further support the quenching mechanism is a dynamic process via electron transfer.

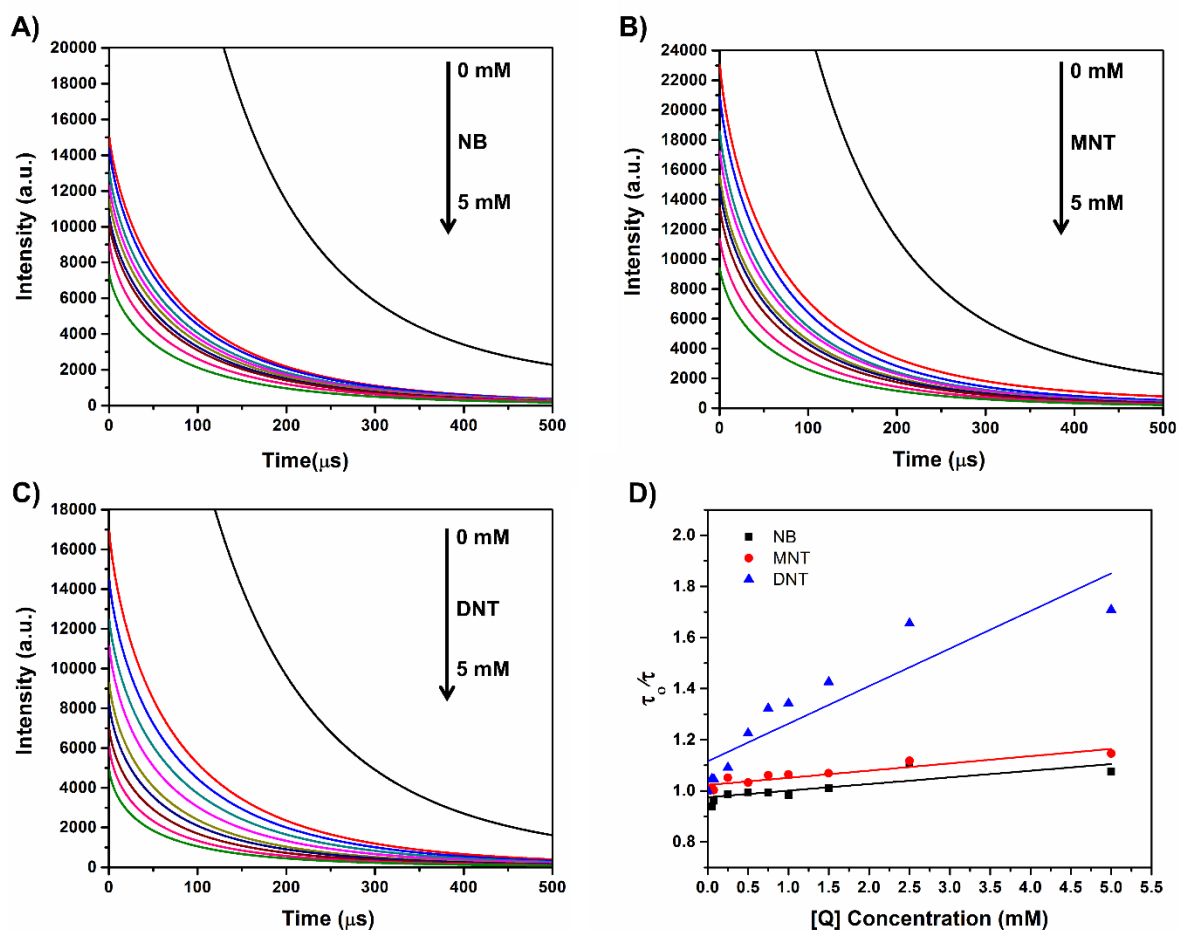


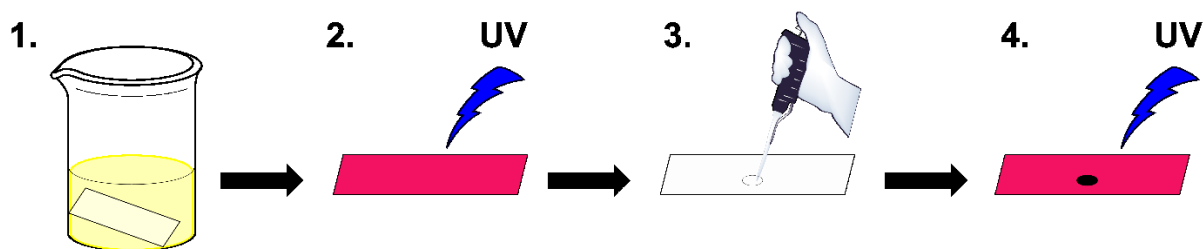
**Figure 4-3:** The PL lifetimes of SiNCs with varying concentrations of (A) NB, (B) MNT, and (C) DNT in solution. (D) The Stern-Volmer plot for the PL lifetime decays of SiNCs of NB, MNT, and DNT at different concentrations.

To determine the limit of detection (LOD) for PL quenching that functionalized SiNCs display for toluene solutions of NB, MNT, and DNT, the PL quenching arising from analyte concentrations of the range 0.05 - 5 mM was evaluated. The LOD for nitroaromatic compounds in toluene was determined using the  $3\sigma$  criteria and were calculated to be 1.54, 0.995, and 0.341 mM (*i.e.*, 184.6, 136.5, and 62.1 ppm, respectively) for NB, MNT, and DNT, respectively.<sup>353,354</sup> Unfortunately, solution phase LODs in toluene are not as sensitive as previous reports.<sup>355</sup> The

origin of the decreased LODs is unclear, however, it may result from the influence of the alkyl surface termination and is the subject of ongoing investigations. Fortunately, these solution LODs do not preclude the practical usefulness of this SiNCs detection system, which can be extended to solid residue and vapor detection (*vide infra*). Furthermore, it is also reasonable LODs will be improved by appropriate tailoring the surface functional groups.

#### 4.3.4 Visual Detection using paper supported SiNCs

Extending the potential utility of the present SiNCs sensing motif, we prepared filter paper impregnated with luminescent SiNCs by dip-coating in a toluene solution of the NCs (Scheme 4-2). The resulting paper displayed red-orange photoluminescence characteristic of the SiNCs upon exposure to a standard handheld UV ( $\lambda = 365 \text{ nm}$ ) lamp. To test the sensitivity of this new detection system, 2  $\mu\text{L}$  of stock solutions (0.25, 5, and 25 mM) of NB, MNT, and DNT were spotted onto the prepared paper (Scheme 4-2). Photographs of the exposed papers are shown in Figure 4-4.



**Scheme 4-2:** Schematic representation of the preparation and use of SiNC based sensor paper. (1) A piece of filter paper is dip coated in a solution of concentrated SiNCs, (2) the resulting paper is fluorescent under UV light ( $\lambda = 365 \text{ nm}$ ), (3) nitroaromatic solution is spotted onto the sensing paper, and (4) quenching of the spot is observed under UV light ( $\lambda = 365 \text{ nm}$ ).

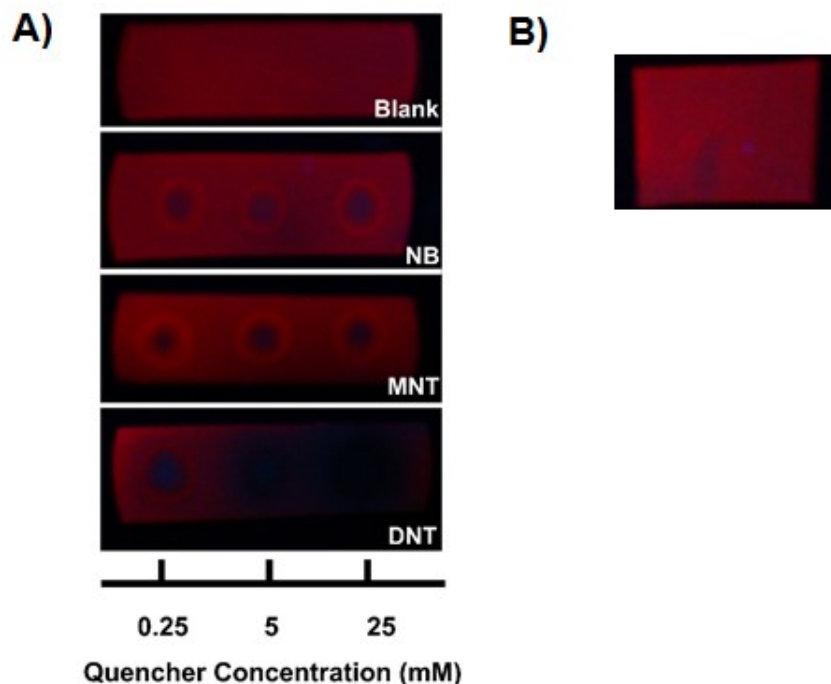


**Figure 4-4:** Solution spot tests of A) nitroaromatics NB, MNT, and DNT (left to right: 2  $\mu$ L aliquots of 0.25, 5 and 25 mM, in toluene) or B) toluene (2  $\mu$ L).

All concentrations tested resulted in complete quenching of the area spotted for every compound. The results indicate the filter paper is more effective at 0.25 and 5 mM concentration than solution-phase measurement by the fluorometer where complete quenching at these concentrations was not achieved. There was no visible difference in the quenched spots for all concentrations of NB and MNT. It should be noted that a bright is observed ring around the quenched spots; this could result from limited mobility of the SiNCs in the presence of toluene (Figure 4-4B). However, DNT displayed a dramatic quenching increase in the area surrounding the initial spot of the compound. As seen in solution, DNT is the most effective of the nitroaromatics tested. To further test the application of the filter paper, 25  $\mu$ L of 0.01 mM solutions of explosives TNT, RDX, and PETN were spotted onto the filter paper, and the fluorescence was rapidly and completely quenched for all compounds (Figure 4-5). This study showed the filter

paper is not only sensitive to nitroaromatics, but also to nitroamines and nitrate esters, and points to the scope of such this sensor motif in real-world applications.

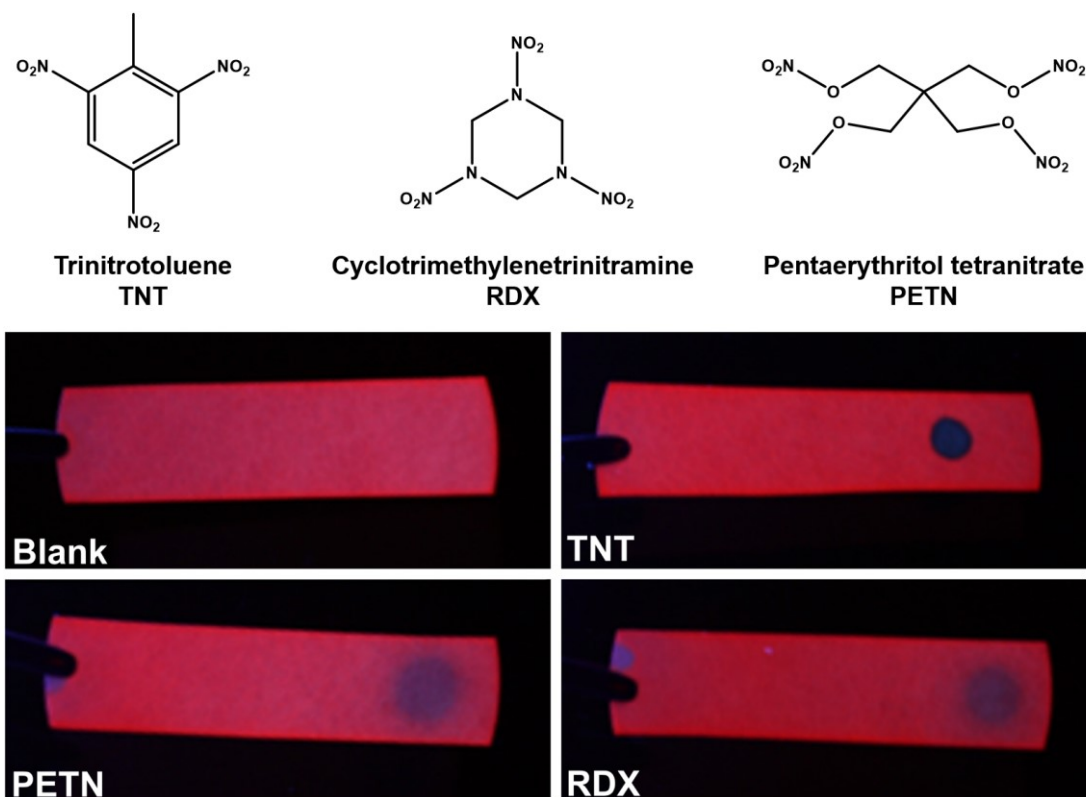


**Figure 4-5:** Images of SiNC coated filter paper under a handheld UV-lamp without the presence of nitrocompounds and in the presence of solutions of TNT, PETN, and RDX as indicated.

This same filter paper detector can also be applied in the detection of chemical residues. Placing known quantities of DNT residues (*i.e.*, 4.5, 18.2, 91.1 ng) on cotton swabs and exposing the filter paper to the residue indicated the present system can detect as little as 18 ng of DNT (Figure 4-6A). The detection of trace residues of DNT on the surfaces of a plastic tray and cotton fabric were also tested. Contact of the exposed surface with the filter detection paper resulted in quenching of the SiNC luminescence (Figure 4-6B-C). Further testing was carried out by wiping

a gloved finger that had been previously exposed to solid DNT. Pressing the finger onto the paper successively 4 times resulted in subsequent quenching (Figure 4-7). Although the exact quantity of DNT residue on the glove decreased with successive printing, the qualitative signal to noise ratio between the first and last print appears to remain unchanged.<sup>356</sup>

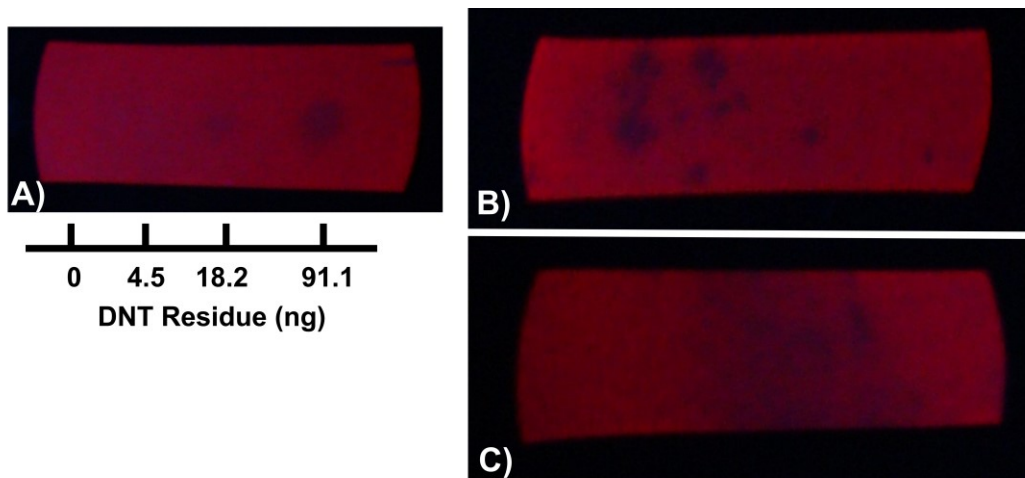


**Figure 4-6:** Solid DNT residue testing onto SiNC filter paper by (A) cotton swab tips having different amounts of DNT, the DNT residue left after visibly brushing off 0.5 mg DNT from a (B) plastic tray and a (C) cotton fabric, respectively.

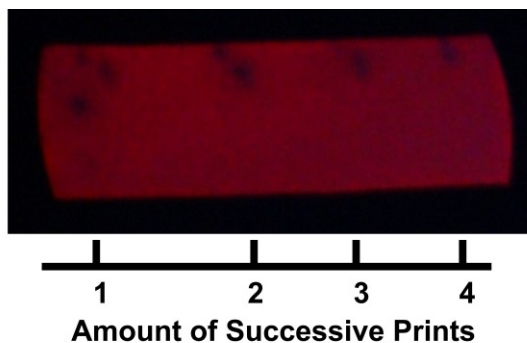


**Figure 4-7:** Solid DNT residue testing on glove. The gloved finger was “finger-printed” successively onto the luminescent filter paper up to four times.

Solid TNT was similarly tested using the glove method, where the contaminated finger was placed on the luminescent area of the detector paper; the luminescence was quenched where the finger was placed (Figure 4-8). Of important note, control tests (not shown) with a gloved finger, an ungloved finger, and a finger of someone who recently smoked a cigarette provided no quenching.

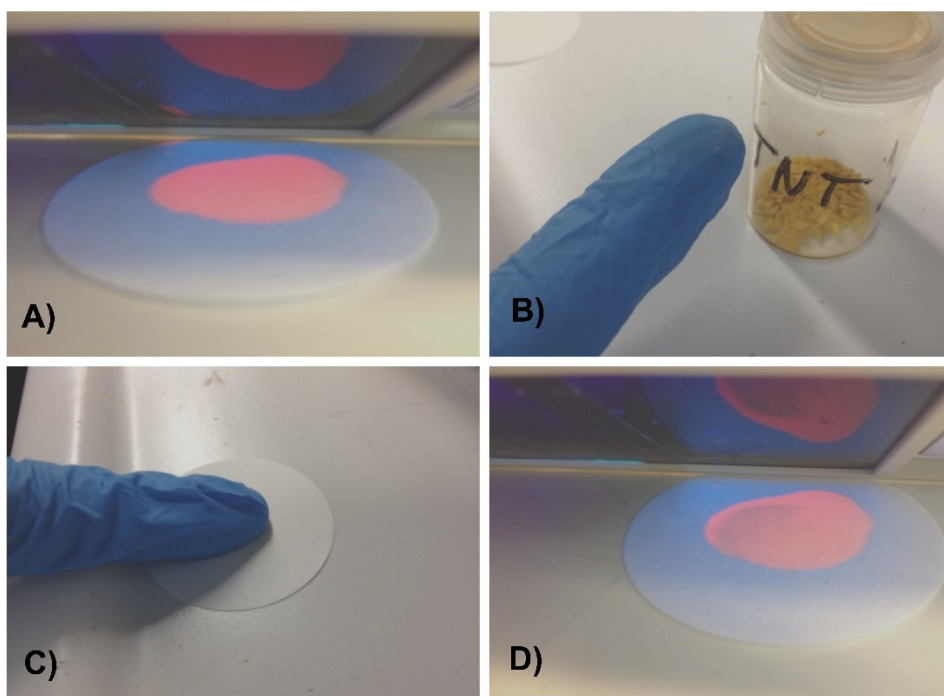


**Figure 4-8:** Images of (A) a spotted filter paper with SiNCs, (B) a gloved finger with trace amounts of solid TNT, (C) application of solid TNT to the coated filter paper, and (D) observed quenching of luminescent filter paper after contact with the solid TNT residue.

To further explore the versatility of the present detection system for nitro-compounds in the vapor-phase, indicator paper was exposed to the headspace above NB. Exposure to NB vapors, completely quenched the SiNCs within 3 minutes (Figure 4-9) and quenching was reversed upon

exposure to a stream of flowing N<sub>2</sub>. These results are similar to those reported by Content and coworkers using hydride terminated porous silicon,<sup>224</sup> and confirm the present paper motif offers detection of nitroaromatics in solution as well as the vapor and solid phases. The paper-based system may be best adapted as a reliable frontline screening method for on-site detection where rapid detection of explosives and related compounds could prove useful in areas such as landmines, airport and border security, *etc.*<sup>357</sup>

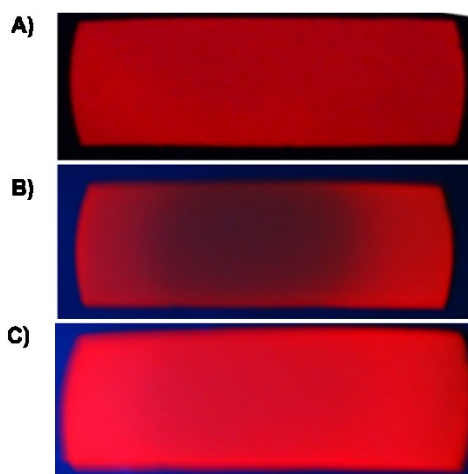


**Figure 4-9:** Images of SiNC impregnated filter paper under a handheld UV-lamp (A) without the presence of nitrobenzene vapor, (B) after quenching with nitrobenzene vapor, and (C) the quenched filter paper after 2 min in N<sub>2</sub> airmass.

#### **4.3.5 Separation of nitroaromatics via SiNCs coupled to TLC plates by esterification**

While the paper-based system is capable of detecting nitroaromatics, nitroamine, and nitrate ester compounds, one limitation of the platform is it is not able to separate/distinguish between the molecules. One possible way to do this is through thin layer chromatography (TLC).

As previously shown by the Trogler group, luminescent organosilicon copolymers could be covalently linked to a non-fluorescent silica gel TLC plate, rendering the plate fluorescent, and subsequently used for the TLC separation of high energy compounds.<sup>358</sup> Covalent coupling of SiNCs to a TLC plate could also remove possible mobility problems as seen in Figure 4-4. This approach of using TLC as a support platform could be applied to SiNCs, however, the surface functional group would have to be modified from an alkyl chain. An esterification reaction between carboxylic acid functionalized SiNCs and the hydroxyl groups of a non-fluorescent silica gel TLC plate would generate a luminescent TLC plate covalently linked to the SiNCs. It is believed that carboxylic acid functionalized SiNCs will still display luminescence quenching when exposed to the nitroaromatic compounds as carboxylic acid groups have been previously shown to increase adhesive forces between explosive compounds on solid substrates.<sup>359</sup>

H-SiNCs were first functionalized with pentenoic acid using AIBN as a radical initiator, resulting in carboxylic acid terminated SiNCs.<sup>148</sup> Surface modification was analysed using FTIR (Figure 4-10A). The broad -OH stretch at 3500-3000  $\text{cm}^{-1}$ , the C=O stretch at 1710  $\text{cm}^{-1}$  and occurrence of features at 2930-2845  $\text{cm}^{-1}$  and 1475-1405  $\text{cm}^{-1}$  of due to  $-\text{CH}_x$  stretching and bending, respectively, indicate surface modification was achieved.<sup>293</sup> Again, the presence of stretching at 2250-2100  $\text{cm}^{-1}$  and 1086  $\text{cm}^{-1}$  result from Si- $\text{H}_x$  and Si-O, respectively due to incomplete surface coverage. The resulting SiNCs displayed luminescence with the peak intensity maximum appearing at 617 nm (Figure 4-10B). The pentanoic acid functionalized SiNCs were then assessed using TEM (Figure 4-10C). Unfortunately, the SiNCs shown in the resulting TEM image appear to be aggregated. This could be due to the hydrogen bonding interactions between the carboxylic groups of the SiNCs.

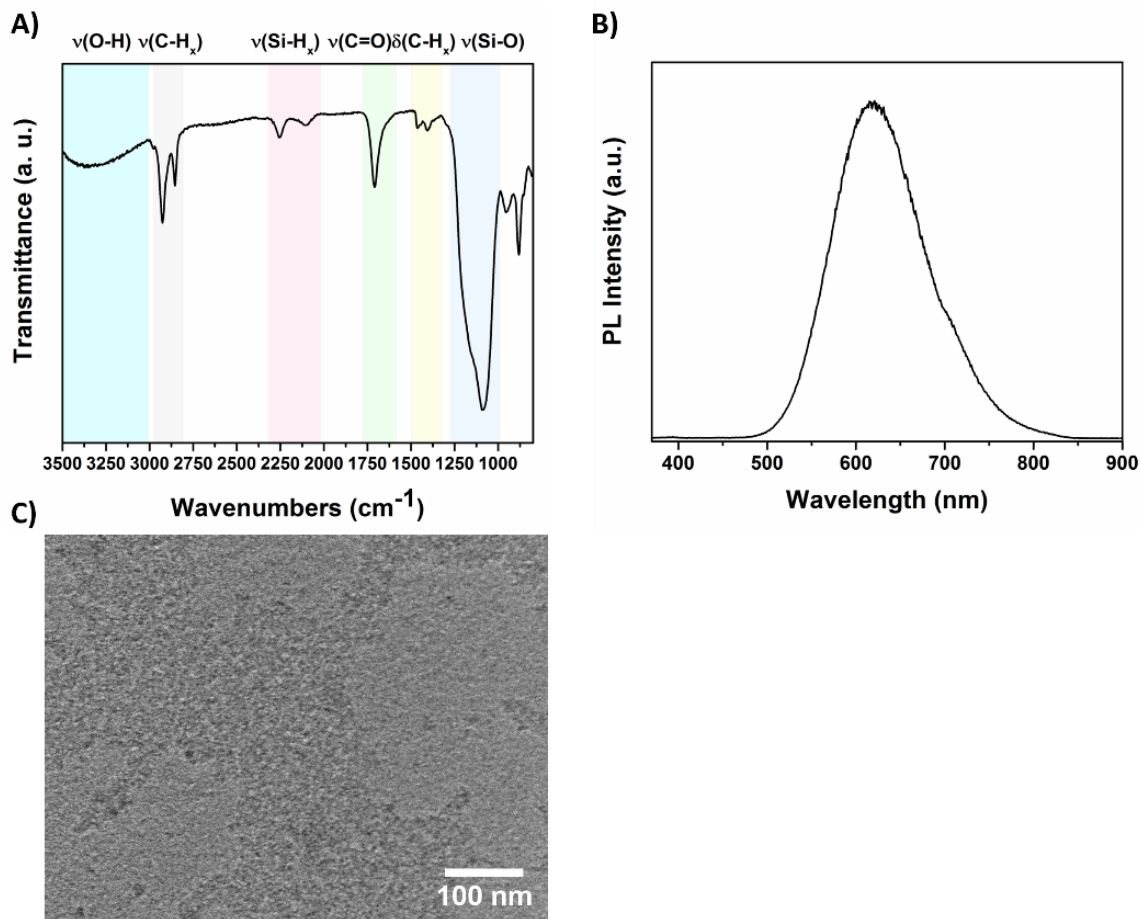


**Figure 4-10:** Characterization of pentanoic acid functionalized SiNCs. (A) FTIR spectrum of SiNCs. (B) Fluorescence spectrum of SiNCs. (C) TEM image of resulting nanocrystals.

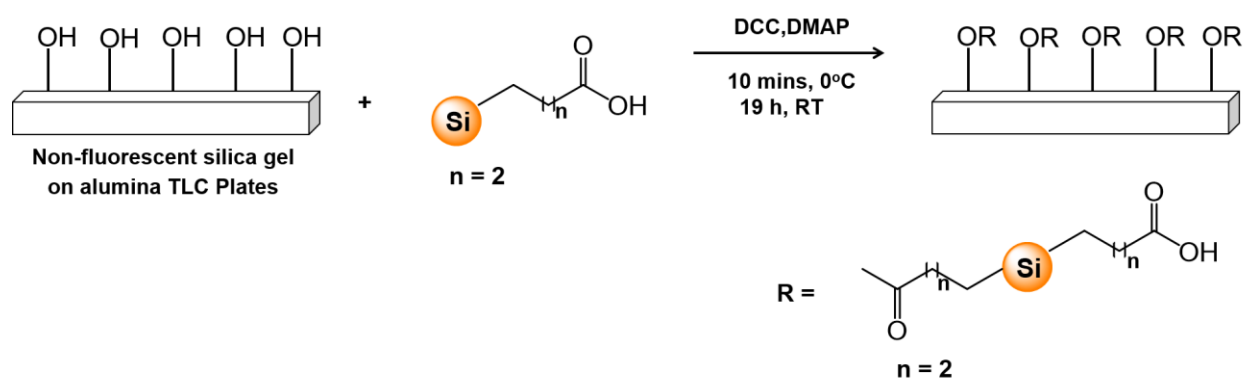
The pentanoic acid functionalized SiNCs were then coupled to non-fluorescent TLC plates via a Steglich esterification reaction (Scheme 4-3) using the experimental setup seen in Figure 4-11.<sup>360</sup> In brief, non-fluorescent TLC plates (Figure 4-12A) were strung through a metal wire and hung into a Schlenk flask containing a solution of ~20 mg of SiNCs and 25 mL toluene under an argon atmosphere. A solution mixture of DCC and DMAP was added to the Schlenk flask under ice cooling. The reaction mixture was left under ice for 10 min and then at room temperature overnight. The TLC plates were then washed with dichloromethane and acetone to remove remove

excess reagents and were dried under vacuum prior to use. The resulting TLC plates were then observed under a handheld UV lamp ( $\lambda = 365 \text{ nm}$ ) and displayed characteristic red-orange luminescence throughout the plate indicating the SiNCs were anchored on the TLC plate (Figure 4-12B).

The SiNC coupled TLC (SiNC-TLC) plates were then investigated for the separation of the nitroaromatics MNT and DNT, both at concentration of 0.1 M. The SiNC-TLC plates were first spotted with MNT and DNT in separate lanes and then resolved/developed in a solvent mixture of  $\text{CH}_2\text{Cl}_2$ :hexanes (1:1). It was observed that both the MNT and DNT moved on the plate while the SiNCs remained stationary indicating the covalent linkage between the TLC plate and SiNCs was successful (Figure 4-12C). MNT and DNT were then spotted onto the TLC plate as a mixture and again resolved with a mixture of 1:1  $\text{CH}_2\text{Cl}_2$ :hexanes (Figure 4-12D). The retention factors ( $R_f$ ) for MNT and DNT were 0.6 and 0.8, respectively. The difference in  $R_f$  results from the differences in the polarity differences in the structures of MNT and DNT. MNT has one nitro group in its chemical structure while DNT has two nitro groups. The MNT molecule was able to move further up the TLC plate than DNT resulting in the differences of  $R_f$  values. Based on these results and the previous demonstrations that the PL of SiNCs quench upon the addition of TNT, RDX and PETN, it is reasonable to believe this TLC separation will work for these compounds of interest as well.



**Figure 4-11:** Reaction setup for esterification of pentanoic acid functionalized SiNCs to non-fluorescent TLC plates.



**Scheme 4-3:** Steglich esterification of pentanoic acid functionalized SiNCs with non-fluorescent TLC plates

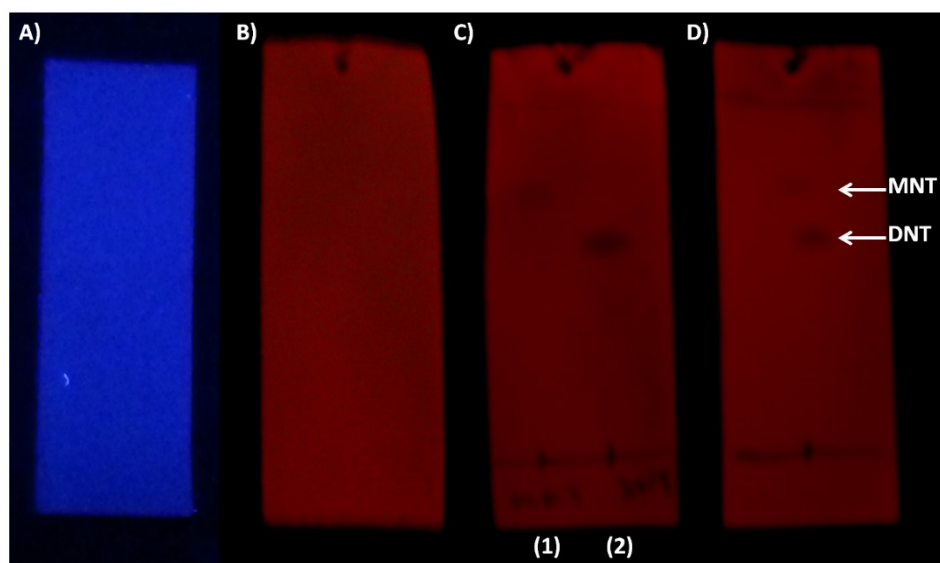


**Figure 4-12:** UV illumination images of (A) non-fluorescent TLC plate before modification with SiNCs, (B) luminescent TLC plate after surface modification with SiNCs, (C) multilane image of developed TLC plate lanes (1) MNT and (2) DNT using a mixture of 1:1 of  $\text{CH}_2\text{Cl}_2$ : hexanes (D) separation of a mixture of MNT and DNT using a mixture of 1:1 of  $\text{CH}_2\text{Cl}_2$ : hexanes.

## 4.4 Conclusions

In conclusion, the present study demonstrates that luminescent dodecyl functionalized SiNCs are quenched in the presence of nitroaromatic, nitroamine, and nitrate ester explosive compounds. When tested in solution, the fluorescence intensity decreased with increasing amount of nitroaromatic introduced. The applicability of these SiNCs was tested by coating them onto a filter paper to generate a luminescent paper-sensor. The paper-sensor successfully detects solution, solid and vapor phase nitroaromatic compounds through visualization of fluorescent quenching under a handheld UV lamp ( $\lambda = 365 \text{ nm}$ ). The versatility was further expanded to the sensing of nitroamines and nitrate esters (*i.e.*, RDX and PETN). The method described here offers a non-toxic, portable, rapid, and straightforward sensing system for on-site detection of nitro group

containing explosives. Additional studies were investigated by covalently linking carboxylic acid terminated SiNCs to non-fluorescent TLC plates rendering them luminescent post reaction. These SiNC anchored TLC plates were then shown to be capable platforms for the separation of MNT and DNT. Further testing and development using different surface functional groups other than dodecene could be performed to increase sensitivity and selectivity towards nitroaromatic, nitroamine and nitrate ester explosives or for the detection of other molecules.

**Chapter 5**  
**Silicon Nanocrystals for the Development of Biogenic**  
**Amine Sensing Platforms.**

## 5.1 Introduction

The quality control of meat and seafood has gained increasing interest over the years for both health and economic reasons.<sup>361-363</sup> It has been recently reported by the CBC that some retailers were changing the labels of food packaging in order to fool the consumer into buying products that are not as fresh.<sup>364</sup> One marker of meat spoilage is the formation of biogenic amines, which are organic bases that can consist of aliphatic (putrescine, cadaverine, spermidine, spermine, spermidine), aromatic (tyramine, phenylethylamine) or heterocyclic (histamine, tryptamine) structures and can be seen in Figure 5-1.<sup>365</sup> These compounds are formed by the microbial enzymatic decarboxylation of amino acids and by amination of carbonyls.<sup>366,367</sup> The consumption of biogenic amines can lead to food poisoning and hypertension.<sup>365</sup> In this context, their detection is of crucial importance.

Previous methods for detecting biogenic amines include capillary electrophoresis,<sup>367,368</sup> high-performance liquid chromatography,<sup>369</sup> and gas chromatography.<sup>370</sup> Unfortunately, these methods are not practical for straightforward, rapid and portable detection. An alternative is the development of luminescence-based detection systems. Previous examples of this include the use of responsive organic dyes,<sup>371</sup> polymers,<sup>372</sup> and Ru and Ln complexes,<sup>373</sup> however, limitations of these materials include photobleaching, cost, and toxicity.

## Biogenic Amines

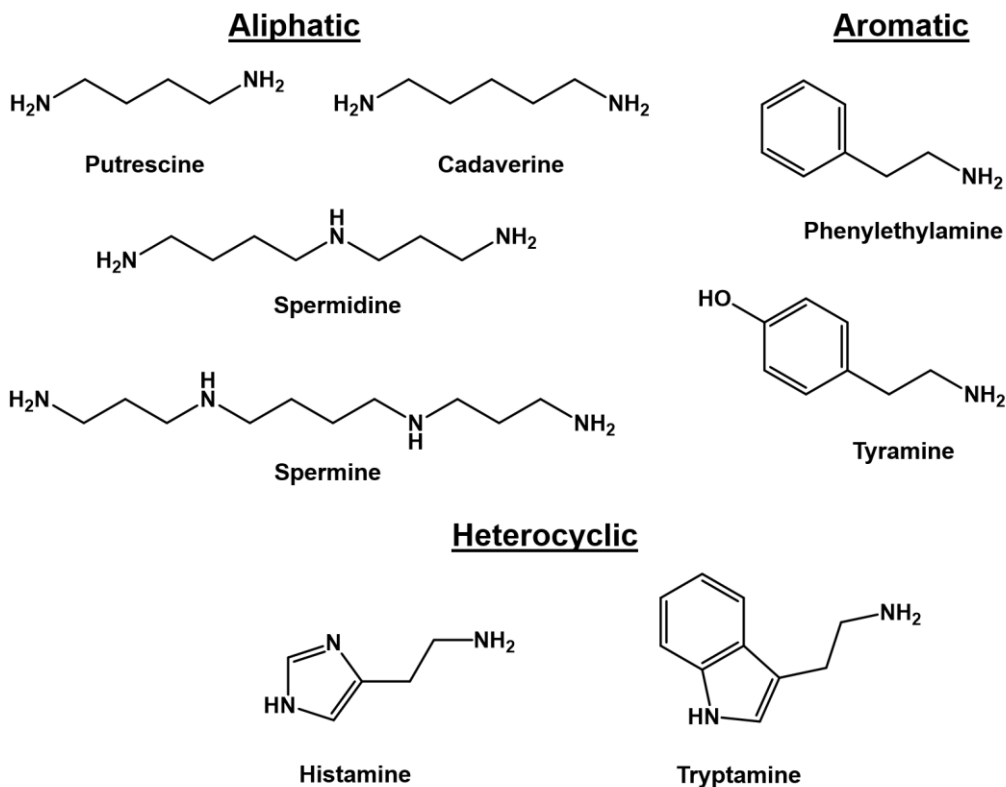


**Figure 5-1:** Various types of biogenic amines.

An alternative material to implement for luminescence-based detection of biogenic amines is silicon nanocrystals (SiNCs). They have been previously implemented in sensing platforms as described in Section 1.5 and Chapter 4 of this thesis. Rho and Pinizzotto showed the photoluminescence of porous silicon derived from p- and n-type substrates, as well as silicon nanocrystallites (obtained via ultrasonic extraction from p-type porous silicon) was quenched in the presence *n*-propylamine and ethylenediamine.<sup>374</sup> They proposed the quenching process resulted from a chelate effect in which the Lewis bases interacted with acidic sites on the silicon surface. However, photoluminescence lifetime measurements were not reported that would have

shed light on the possibility of an active electron transfer mechanism. In addition, the silicon nanocrystallite surface explored consisted primarily of a hydride and oxide surface, prone to oxidation and not ideal for sensor development. However, this report suggests that SiNCs with a more stable surface ligand could be used as a sensor for aliphatic biogenic amines.

In this study, we investigated the use of SiNCs for the optical detection of aliphatic biogenic amines. First, solution-based studies implementing SiNCs bearing three different surface groups (*i.e.*, alkyl oligomer, alkyl monolayer, or ester monolayer) was performed to evaluate which surface group showed the greatest response upon exposure to a model amine compound (*i.e.*, allylamine). Having identified ester monolayer functionalized SiNCs as the preferred candidate, they were tested in solution for response to aliphatic biogenic amines (*i.e.*, putrescine, cadaverine, spermidine). The SiNCs were then incorporated into solid-state polymer films as well as a porous sponge network and explored as potential putrescine vapor sensing media using pure biogenic amine samples. Finally, the effects raw meat had on the optical properties of the solid-state supports were evaluated.

## **5.2 Experimental and Methods**

### **5.2.1 Materials**

Commercial hydrogen silsesquioxane (HSQ, trade name FOx-17) was purchased from Dow Corning Corporation (Midland, MI). Electronics grade hydrofluoric acid (HF, 49% aqueous solution) was purchased from J.T. Baker. Reagent grade methanol, ethanol, 1-dodecene (95%), methyl-10-undecenoate (96%), acetone, 2,2'-azobis(2-methylpropionitrile) (AIBN, 98%), putrescine (98.5%), histamine (97%), spermidine (99%), cadaverine (95%), and allylamine (98%) were purchased from Sigma-Aldrich and used as received. SYLGARD 184 Silicone Elastomer

Kit for the generation of polydimethylsiloxane (PDMS) was purchased from Dow Corning and used as received. Reagent grade toluene (Sigma Aldrich) was dried over molecular sieves (4Å) prior to use. Cover glass slides (48x60 mm) were purchased from Gold Seal. Commercial sugar cubes (Rogers Sugar, Lantic Inc.) were used directly from the package.

## 5.2.2 Material Characterization and Instrumentation

Fourier Transform Infrared Spectroscopy (FT-IR) was performed using a Nicolet Magna 750 IR spectrophotometer. Samples were prepared by drop-coating a toluene dispersion of SiNCs onto a KBr plate. Transmission electron microscopy (TEM) was performed on a JEOL-2010 (LaB<sub>6</sub> filament) electron microscope with an accelerating voltage of 200 keV using samples of SiNCs drop-cast onto a holey carbon coated copper grid (300 mesh, Electron Microscopy Science). Scanning electron microscopy (SEM) was carried out with a JEOL 6301F field emission SEM operated at an acceleration voltage of 5 kV. Samples were prepared by attaching the solid samples onto carbon tape.

Photoluminescence (PL) spectra for solution based samples were obtained using a Cary Eclipse spectrophotometer ( $\lambda_{\text{ex}} = 350 \text{ nm}$ ). The steady-state spectroscopy PL measurements used a 405 nm LED operated at a surface power density of  $\sim 1.3 \text{ W m}^{-2}$  as the excitation source for vapor based (*i.e.*, putrescine, water and 100% ethanol) and raw meat studies. Additionally, for vapor studies, the PDMS prepared samples were placed in a sealed chamber that facilitated controlled exposure to flowing gases (*i.e.*, putrescine, water or 100% ethanol).

The PL was then collected by an optical fiber (numerical aperture 0.21) passed through a longpass filter (550 nm) to eliminate scattered excitation light, and collected by an Ocean Optics mini-USB spectrometer. The spectral response was calibrated using a blackbody light source (Optics LS1). The PL lifetimes were acquired by illuminating a solution sample in a quartz cuvette

with an argon ion laser (476 nm, ~30 mW). The laser was modulated by an acousto-optic modulator operating at 500 Hz. Emission from the SiNCs was channeled into a photomultiplier (Hamamatsu H7422P-50) connected to a photon counting card (Becker-Hickl PMS-400A). Lifetime decay data was fit to a stretched exponential function in Mathematica (Version 10) given by  $y(t) = A[\exp(-(t/\tau)^\beta)] + C$ , where  $A$  is the initial intensity,  $\tau$  is the time decay (basic lifetime),  $\beta$  is a stretching parameter that can vary between 0 and 1, and  $C$  is an offset.<sup>286-288</sup>

### 5.2.3 Preparation of oxide-embedded SiNCs

Oxide-embedded SiNCs ( $d_{\text{avg}} = 3.5$  nm) were prepared using established Veinot group protocols.<sup>112</sup> Briefly, solid HSQ was placed in a quartz reaction boat and transferred to a tube furnace, and then heated to 1100 °C in a 95% argon/5% hydrogen atmosphere for 1 h. The resulting amber colored SiNC/SiO<sub>2</sub> composite was then crushed using an agate mortar and pestle and finally shaken with high-purity silica beads using a Burrell Wrist Action Shaker for 12 h.

### 5.2.4 Preparation of hydride-terminated SiNCs

The SiNC were removed from the oxide matrix by hydrofluoric acid (HF) etching. The SiNC/SiO<sub>2</sub> composite (0.4 g) was first placed into a polyethylene terephthalate (PET) beaker containing a Teflon coated stir bar with 100% Ethanol (4 mL) and water (4 mL) and stirred to ensure uniform wetting and a brown suspension. A 49 % aqueous HF (4 mL) solution was then slowly added to the suspension while stirring and left for 1 h. **Caution:** HF is dangerous and requires appropriate handling procedures and personal protective equipment. Following a 1 h stir period, the brown suspension became orange/yellow. The hydrophobic, hydride-terminated SiNCs (H-SiNCs) were extracted from the aqueous layer using 2 x ~20 mL extractions into toluene. The obtained SiNC/toluene suspension was then divided equally between test tubes and

centrifuged at 3000 rpm. After centrifugation, the supernatant was decanted and the H-SiNC precipitate was immediately used in various functionalization procedures (*vide infra*) described below.

### 5.2.5 Preparation of alkyl oligomer SiNCs

The H-SiNCs obtained from the etching procedure (*vide supra*) were redispersed into *ca.* 20 mL of 1-dodecene, transferred into an oven-dried (125 °C) Schlenk flask equipped with a Teflon coated magnetic stir bar, and attached to an argon charged Schlenk line. The flask was then evacuated and backfilled with argon three times to remove air from the solution. The solution was then heated to a temperature of 190 °C and was left stirring for 15 h resulting in a transparent orange/yellow solution.

### 5.2.6 Preparation of alkyl and ester monolayer SiNCs

Freshly obtained H-SiNCs from the etching procedure (*vide supra*) were redispersed into toluene (*ca.* 20 mL, pre-dried over molecular sieves (4Å)), transferred to an oven-dried (125 °C) 100 mL Schlenk flask equipped with a Teflon coated magnetic stir bar, and attached to an argon charged Schlenk line. The radical initiator, AIBN (0.061 mmol) and surface ligand of choice (*i.e.*, 1-dodecene or methyl-10-undecenoate, 0.018 mol) were added to the flask and the reactant mixture was subjected to three freeze-pump-thaw cycles.<sup>148</sup> The reaction mixture was subsequently heated to and maintained at 60 °C (AIBN) and stirred for 19 h to yield transparent orange/yellow solutions.

### 5.2.7 Purification and preparation of SiNC stock solutions

For alkyl terminated SiNCs, equal volumes (*ca.* 10 mL) of the orange/yellow solutions containing functionalized nanoparticles were dispensed into 50 mL polytetrafluoroethylene (PTFE) centrifuge tubes. A 1:1 methanol:ethanol anti-solvent was added to achieve a total volume of 50 mL in each tube. This caused the formation of an orange precipitate that was isolated by centrifugation at 12000 rpm for 0.5 h. The supernatant was decanted and the particles were redispersed in a minimal amount of toluene (*ca.* 2 mL) and re-precipitated upon addition of 1:1 methanol:ethanol. This solvent/anti-solvent purification process was repeated twice. Finally, the purified SiNCs were redispersed in dry toluene (pre-dried over molecular sieves (4Å)), and filtered through a 0.45  $\mu\text{m}$  PTFE syringe filter. The resulting SiNCs were then dried under vacuum, dispersed in toluene to yield a 1 mg/mL suspension and were stored under ambient conditions for analysis (FTIR, TEM, XPS, and PL) and solution based studies.

For ester monolayer SiNCs, purification was achieved by implementing a variation of solvent/anti-solvent method described above. In this case, hexane was used as the anti-solvent. Finally, the purified SiNCs were redispersed in dry toluene (pre-dried over molecular sieves (4Å)), filtered through a 0.45  $\mu\text{m}$  PTFE syringe filter, and dried under vacuum. The SiNCs were finally dispersed in toluene to generate a 1 mg/mL stock solution and stored under ambient conditions for analysis (FTIR, TEM, and PL) and use for solution based studies and PDMS incorporation.

### 5.2.8 PDMS film containing ester monolayer functionalized SiNCs

A PDMS film containing ester monolayer SiNCs were added in a ratio of 1 mL of SiNCs (1 mg/mL) to 3 mL of the PDMS elastomer based and mixed (the luminescence appeared to be homogenous throughout the mixture when viewed atop a benchtop UV lamp,  $\lambda=365$  nm), followed

the addition of 0.3 mL of the curing agent. The ratio of base to curing agent (10:1) was followed as per the supplier instructions listed on the bottle. The obtained mixture was then drop coated on a glass slide (pre-treated with 100% ethanol to remove impurities from the surface) and left to cure for 24 h (as directed by supplier). The resulting film displayed red-orange luminescence when exposed to a hand held UV lamp ( $\lambda=365$  nm). The luminescent film was stored in a petri dish under ambient conditions for analysis (SEM, luminescence) and future use (vapor and raw meat studies).

### **5.2.9 PDMS sponge containing ester monolayer functionalized SiNCs**

First, a homogenous mixture of ester terminated SiNCs and PDMS was prepared as described in section 5.2.8. The freshly prepared solution mixture was then drop coated over a sugar cube (template) that had been placed in a quartz reaction boat. The mixture was absorbed into the pores of the sugar cube (evaluated qualitatively) and the quartz boat was transferred to a tube furnace, and heated to 120 °C in a 95% argon/5% hydrogen atmosphere for 15 min.<sup>375</sup> After cooling to room temperature, the PDMS/sugar cube material was then placed in a beaker of deionized water for 24 h to dissolve and remove the sugar cube template from the PDMS. The water was changed twice during this process. The resulting material was then dried under a high vacuum Schlenk line to remove any trace water. The final obtained material displayed red-orange luminescence when exposed to a hand held UV lamp ( $\lambda=365$  nm) and stored in vials under ambient condition for analysis (SEM, luminescence) and future use (vapor and raw food studies).

### **5.2.10 Solution Phase PL Studies of Titrations of SiNCs with Amines**

Stock solutions of allylamine, putrescine, cadaverine, and spermidine were prepared in toluene at various concentrations (*i.e.*, 0-5 M, allyamine, 0-100 ppm, putrescine, cadaverine, and

spermidine). The SiNC stock solutions prepared as outlined above were first titrated with allylamine. This was achieved by adding a known volume (*i.e.*, 300  $\mu$ L) of SiNC stock solution to a predetermined volume of amine solutions of a known concentration. The resulting solutions mixtures consisted of allylamine concentrations in the range of 0 to 0.5 M. The photoluminescence of these mixtures were evaluated and ester monolayer functionalized SiNCs were used for the titration of the biogenic amines (*i.e.*, putrescence, cadaverine and spermidine), and evaluated after one minute of exposure.

### **5.2.11 Vapor Phase Studies Experimental Setup**

To investigate the luminescent response of PDMS films or sponges containing SiNCs, a custom chamber (Figure 5-8 below) was designed and built. It has the capacity to deliver amine vapor from a bubbler to a sealed gas chamber containing the PDMS/SiNC substrates. An argon gas cylinder was attached to quarter-inch poly-vinyl chloride (PVC) tubing that was split into two lines with independent flow controllers. Line 1 passed through a bubbler containing the solution phase analyte of interest (*i.e.*, putrescine, 100% ethanol, or distilled water). For putrescine measurements, the bubbler was submerged in a water bath maintained at 27 °C (melting point of putrescine). Line 2 did not pass through the bubbler and carried only argon gas. The two lines flowed into the sealed gas chamber containing the PDMS film or sponge containing SiNCs.

The PL response was collected by an optical fiber (numerical aperture 0.21) coupled directly into the sample chamber. The fiber was also passed through a 550 nm longpass filter to eliminate scattered excitation light and brought to an Ocean Optics USB spectrometer. The spectrometer was calibrated by a blackbody light source (Ocean Optics LS1) prior to PL measurement collection.

### **5.2.12 PDMS film or sponge containing SiNCs luminescence studies with Ar vapor**

A sample of PDMS film or sponge containing SiNCs was placed in the sealed gas chamber and exposed to argon vapor (4 L/min) for a period of 60 min while under continuous excitation from the LED (405 nm, surface power density of  $3.3 \text{ W m}^{-2}$ ). The luminescence spectrum was collected every 3 seconds during this time period. The results were then analyzed as a function of the temporal change of maximum PL intensity.

### **5.2.13 PDMS film or sponge containing SiNCs luminescence bleaching and recovery studies**

A sample of PDMS film or sponge containing SiNCs was placed in the sealed gas chamber and exposed to argon vapor (4 L/min) for 60 min. Throughout this period, the LED (405 nm surface power density of  $3.3 \text{ W m}^{-2}$ ) excitation source was cycled on and off periodically every 10 min, with the excitation source turned off during first 10 min of collection time. The luminescence spectrum was collected every 3 seconds during this time period. The spectral response (*i.e.*, maximum PL intensity) was evaluated as a function of time.

### **5.2.14 PDMS film or sponge containing SiNCs luminescence studies with putrescine vapor**

A sample of PDMS film or sponge containing SiNCs was placed in the sealed gas chamber and exposed to Ar vapor (4 L/min) for a period of 20 - 30 min to account for any possible photobleaching from the excitation source prior to putrescine vapor exposure. After 20 - 30 min interval, the Ar vapor line was closed, and the putrescine vapor line was opened (4 L/min) for 40 min under excitation from the LED (405 nm, surface power density of  $3.3 \text{ W m}^{-2}$ ). The

luminescence spectrum was collected every 3 seconds during this time period. The results were then analyzed as a function of the change of maximum PL intensity over time.

### **5.2.15 PDMS film or sponge containing SiNCs luminescence studies with water or ethanol vapor**

A sample of PDMS film or sponge containing SiNCs was placed in the sealed gas chamber and exposed to Ar vapor (4 L/min) for 15 min to account for any possible photobleaching from the excitation source prior to analyte (water or 100 % ethanol) exposure. After the 15 min interval, the Ar vapor line was closed, and the analyte vapor line was opened (4 L/min) for 20 min under excitation from the LED (405 nm, surface power density of  $3.3 \text{ W m}^{-2}$ ). The luminescence spectrum was collected every 3 seconds during this time period. The results were then analyzed as a function of the change of maximum PL intensity over time.

### **5.2.16 PDMS film or sponge containing SiNCs luminescence studies after exposure with raw food**

A sample of PDMS film or sponge containing SiNCs was placed atop 1 g of raw meat aliquots (*i.e.*, pork, chicken, salmon, and pickerel) in vials. Two samples for each type of meat were prepared: one stored for 4 days at room temperature and the second stored for 4 days at  $4 \text{ }^{\circ}\text{C}$  in the refrigerator. The PL of the PDMS samples were monitored after 0, 1, 2, 3, and 4 days of raw meat exposure by placing the sensor in a sample holder than exposing it to a LED (405 nm, surface power density of  $\sim 3.3 \text{ W m}^{-2}$ ). The PL was then collected by an optical fiber and passed through a 550 nm longpass filter to eliminate scattered excitation light and brought to an Ocean Optics mini-USB spectrometer.

### 5.2.17 Visual Monitoring SiNC to Raw Meat

A sample of PDMS film or sponge containing SiNCs was placed on top of 1 g of raw meat aliquots (*i.e.*, pork, chicken, salmon, and pickerel) and wrapped in commercial plastic wrap. The samples were then placed in a cardboard box to block out as much surrounding light as possible. A handheld UV light ( $\lambda = 365$  nm) and digital camera (Canon PowerShot ELPH 300 HS, equipped with a 550 nm longpass filter over the lens) were clamped above the samples for monitoring. Photographs of the samples after 0 and 24 h of exposure of the PDMS substrates to the meat were taken under UV light ( $\lambda = 365$  nm). Note: The UV light was only turned on while the photograph was being acquired. The digital photographs were split into red, green, and blue components using Image J software. The red component was then evaluated qualitatively for PL intensity changes.

## 5.3 Results and Discussion

H-SiNCs were first prepared by a well-known procedure established in the Veinot Laboratory.<sup>112</sup> The H-SiNCs were then further modified with three surface groups: alkyl oligomer, alkyl monolayer, or ester monolayer termination. The alkyl oligomer SiNCs were obtained by combining H-SiNCs and 1-dodecene in a Schlenk flask under an argon atmosphere, degassed, and heated to 190 °C for 19 h. To achieve alkyl monolayer and ester monolayer SiNCs, H-SiNCs were combined with 1-dodecene or 10-methyl-undecenoate and AIBN (0.061 mol) in toluene under an argon atmosphere and heated to 60 °C for 19 h.<sup>148</sup> Surface modification was evaluated using FT-IR (Figure 5-2A). The FTIR spectra for all three surface functionalized SiNCs investigated show features at 2921 - 2850  $\text{cm}^{-1}$  and 1300 - 1450  $\text{cm}^{-1}$  consistent with C-H<sub>x</sub> stretching and bending, respectively.<sup>142,376</sup> A signal at 1736  $\text{cm}^{-1}$  was observed corresponding to C=O stretching for ester monolayer functionalized SiNCs.<sup>282,292</sup> Additional features appearing at ~1130-1000  $\text{cm}^{-1}$  and

2100  $\text{cm}^{-1}$  related to Si–O and Si–H<sub>x</sub> stretching, respectively, are consistent with incomplete surface coverage, and were observed for all three surface functionalities.<sup>294</sup> The PL spectra of all 3 surface groups can be seen in Figure 5-2B, with the peak intensity maxima occurring at 672, 723, and 663 nm for alkyl oligomer, alkyl monolayer, and ester monolayer functionalized SiNCs, respectively, consistent with band gap emitting SiNCs.<sup>289</sup> Minor differences in luminescence maximum amongst the three surface groups could be attributed to a different degree of surface oxidation and slight variation in particle size. The particle size of all SiNCs was evaluated using TEM (Figure 5-3). The brightfield images show all SiNC samples were all pseudospherical with average diameters of  $3.7 \pm 0.4$ ,  $3.4 \pm 0.9$ , and  $4.1 \pm 1.1$  nm for alkyl oligomer, alkyl monolayer, and ester monolayer functionalized SiNCs, respectively.

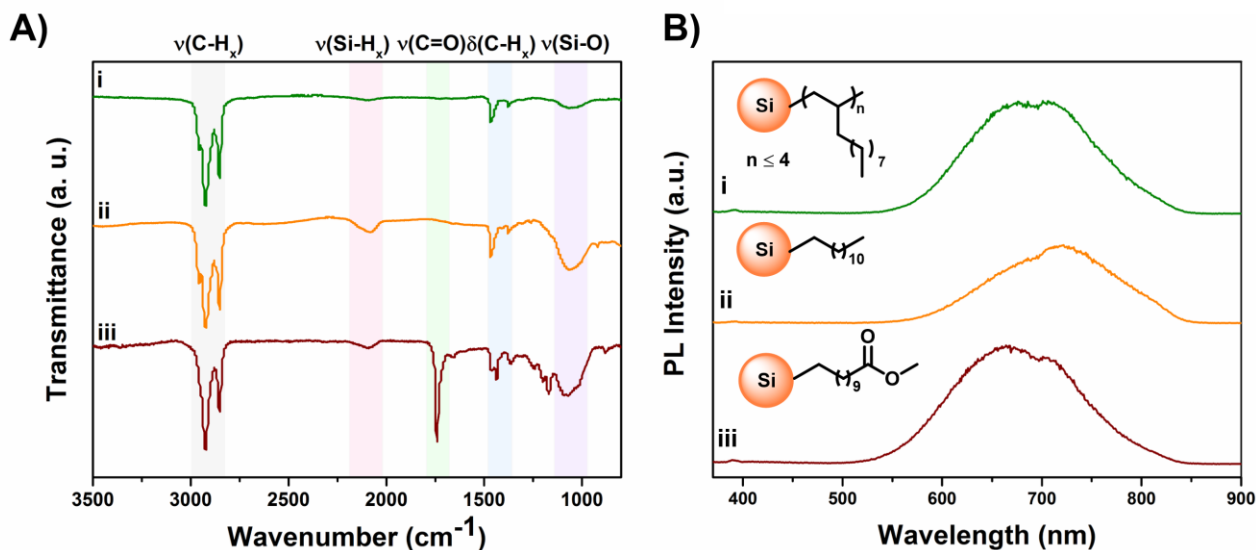


**Figure 5-2:** FT-IR (A) and photoluminescence (B) spectra for i) alkyl oligomer, ii) alkyl monolayer and iii) ester monolayer functionalized SiNCs.

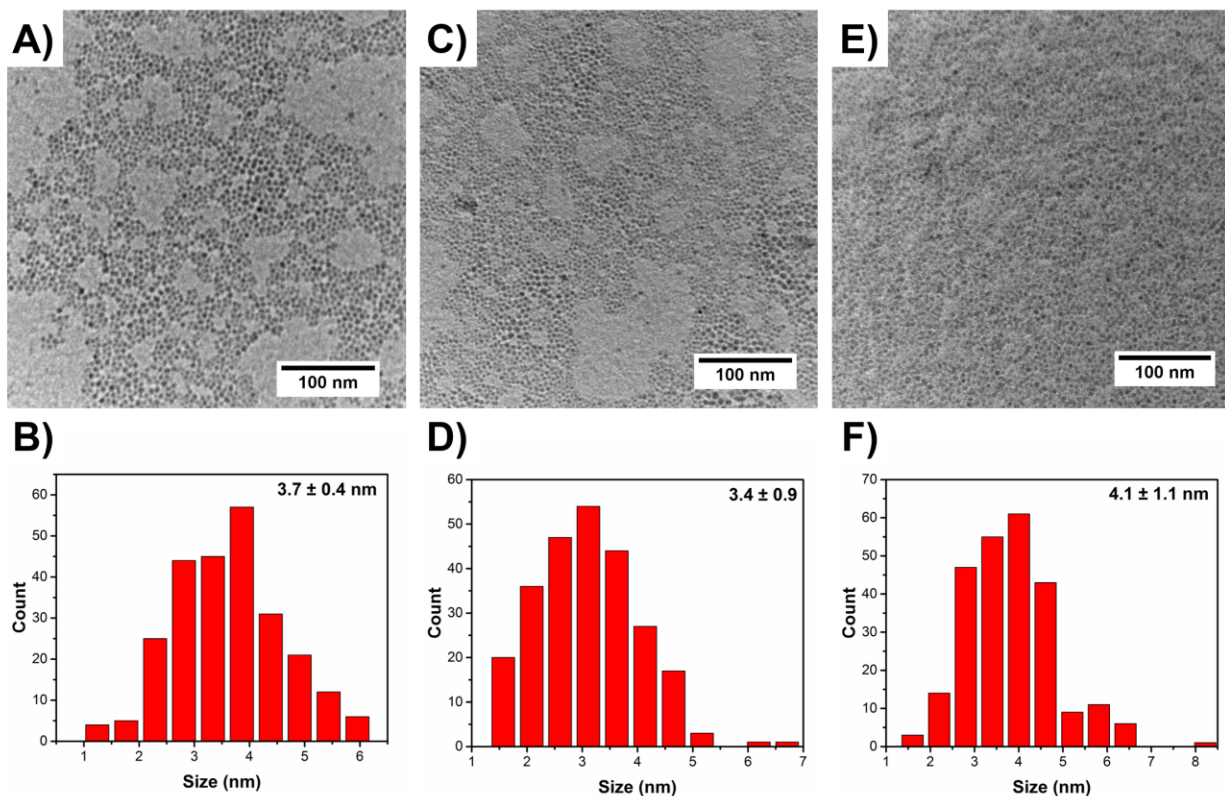


**Figure 5-3:** TEM and particle size distribution for alkyl oligomer (A-B), alkyl monolayer (C-D), and ester monolayer (E-F) functionalized SiNCs. Note: Particle size histograms were assembled by counting 200 SiNCs through the longest diameter present with Image J software.

To qualitatively evaluate the appropriateness of SiNCs bearing different surface groups, stock solutions (1 mg/mL in toluene) of alkyl oligomer, alkyl monolayer, or ester monolayer functionalized SiNCs were titrated with the model biogenic amine allylamine to achieve final amine concentrations ranging from 0.00 - 0.5 M. Figure 5-3 shows all SiNCs examined displayed a decrease in the luminescent intensity proportional to the concentration of allylamine added (*i.e.*, the higher the allylamine concentration, the more efficient the quenching). However, the extent of the quenching varied depending on the SiNC surface. Qualitatively, the alkyl oligomer functionalized SiNCs are least responsive (Figure 5-4A), the alkyl monomer SiNCs is intermediate

(Figure 5-4B), and the ester terminated SiNCs are most responsive (Figure 5-4C). While both alkyl-based surfaces respond to amine exposure, it is reasonable the oligomeric species may prevent access of the allylamine molecule to the SiNC surface, thus limiting the interactions that induce luminescence quenching.<sup>72</sup> This finding is consistent with the recent work of Nguyen and coworkers that showed alkyl oligomer functionalized SiNCs can be less responsive in sensing analytes of interest when an electron quenching mechanism is involved.<sup>228</sup> The ester monolayer functionalized SiNCs displayed the greatest spectral response toward allylamine with a marked quenching at the highest allylamine concentration (0.5 M). This behavior may arise because the ester surface moieties that may promote interaction with allylamine. For example, oxygen atoms may participate in H-bonding with the amines. Such interactions could increase the effective amine concentration and the probability of amine molecules reaching the SiNC surface; this would be expected to promote processes such as electron transfer or fluorescence resonance energy transfer. In addition to decreased PL intensity, the photoluminescence maximum of ester monolayer modified particles blue-shifted. This spectral shift may arise because of direct modification of the SiNC surfaces by allylamine. Similar, although more pronounced, spectral changes have been noted when red-emitting hydride-terminated SiNC surfaces have been exposed to amines.<sup>129</sup> In addition, surface accessibility on ester modified SiNCs may be enhanced because particles prepared in this way possess at least 10% less surface coverage than equivalent alkyl functionalized SiNCs (See Chapter 2).<sup>148</sup> Based on these initial experiments, all future experiments were performed using ester monolayer functionalized SiNCs.

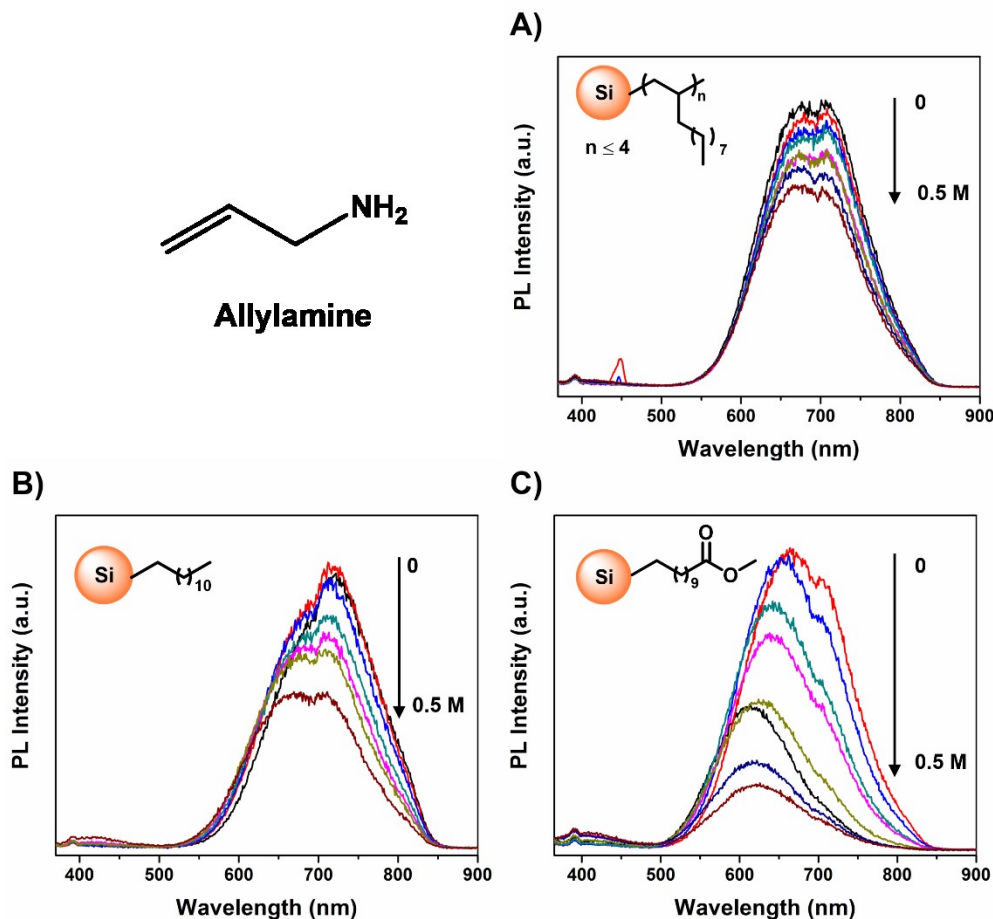


**Figure 5-4:** Photoluminescence quenching spectra of SiNCs functionalized with A) alkyl oligomer, B) alkyl monomer, or C) ester monolayer by increasing concentrations of allylamine in solution in the range of 0 and 0.5 M.

In an attempt to interrogate the mechanism of luminescence quenching, solutions of ester monolayer functionalized SiNCs (1 mg/mL) were titrated with the biogenic amines (*i.e.*, putrescine, spermidine and cadaverine) with final concentrations ranging from 0 - 100 ppm (Figure 5-5). As expected, the addition of the biogenic amines induced quenching of the SiNC luminescence that increased with amine concentration. Somewhat surprisingly, putrescine and spermidine caused no shift in the luminescence maxima or line shape of the spectra. In contrast,

higher concentrations of cadaverine caused the appearance of an additional luminescence feature at 400 nm. This may be attributed to the direct modification of the SiNC surfaces by cadaverine or the luminescence of the toluene solvent (Figure 4-2A).

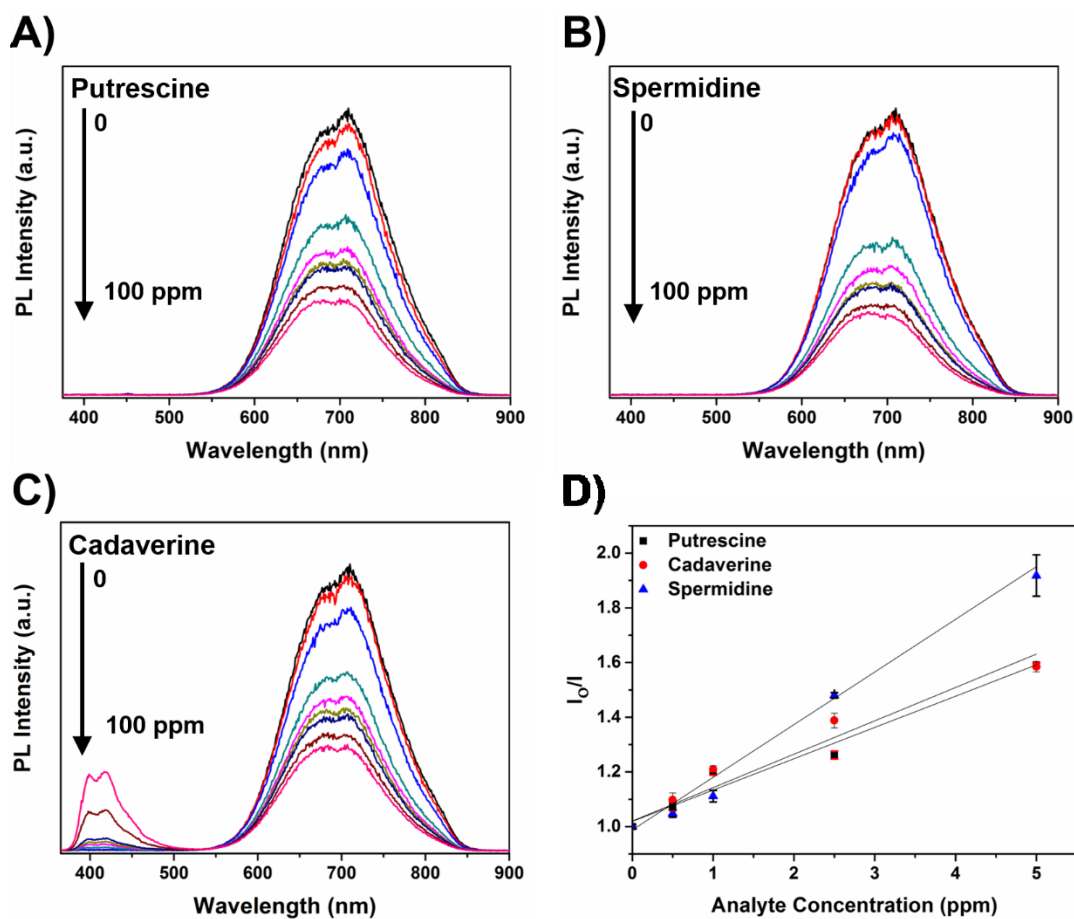
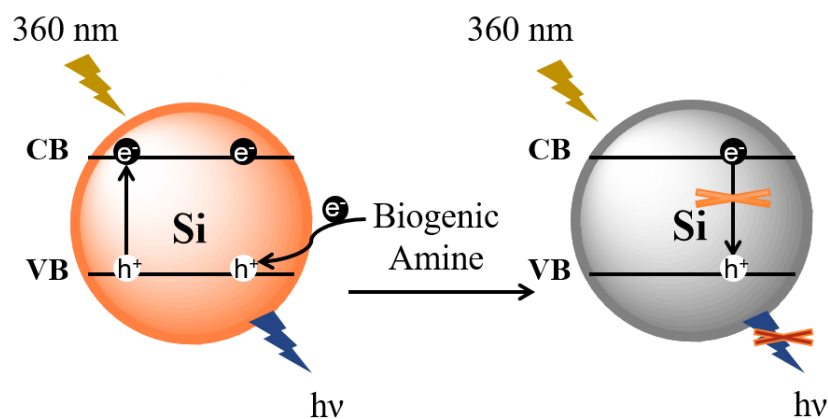


**Figure 5-5:** Photoluminescence quenching spectra of SiNCs with increasing concentrations of (A) putrescine, (B) spermidine, and (C) putrescine (D) A Stern-Volmer plot for the quenching efficiencies of putrescine, spermidine and cadaverine.

The quenching behavior resulting from the addition of putrescine, spermidine, or cadaverine to solutions of SiNCs was assessed by using the Stern-Volmer equation:

$$I_0/I = K_{sv}[Q] + 1$$

Where,  $I_0$  and  $I$  are the fluorescence intensity in the absence and presence of the amine compounds, respectively.  $[Q]$  is the concentration of the amine of interest, and  $K_{sv}$  is the fluorescence quenching constant. Figure 5-5D displays the relationship of  $I_0/I$  vs. biogenic amine molecule (*i.e.*, putrescine, spermidine, cadaverine) concentration in the concentration range of 0.5 - 100 ppm. The linear behaviour in the range of 0.5 - 5 ppm of putrescine, spermidine, and cadaverine, indicates the quenching may be resulting from a dynamic process such as electron transfer.<sup>72,350</sup> In the case of an electron transfer quenching mechanism, it is reasonable that an electron from the amine group (electron donor) could transfer to the vacant hole in the conduction band of the SiNCs (electron acceptor), preventing the recombination of the electron-hole pair, and finally resulting in luminescence quenching (Scheme 5-1).<sup>377,378</sup>



**Scheme 5-1:** Proposed electron transfer quenching mechanism of SiNCs by biogenic amine compounds, where  $e^-$ ,  $h^+$ , CB and VB represent an electron, hole, conduction band and the valence band, respectively.

The  $K_{sv}$  values (Table 5-1) determined from this analysis are 0.11, 0.12, and 0.19  $\text{ppm}^{-1}$  for putrescine, cadaverine, and spermidine, respectively. This trend can be tentatively related to the chemical structures of the biogenic amines investigated. Spermidine has one additional nitrogen than putrescine and cadaverine that could increase its quenching efficiency leading to its higher  $K_{sv}$ . The putrescine and cadaverine molecules only very slightly resulting in near-identical  $K_{sv}$  values.

**Table 5-1:** The determination of  $K_{sv}$  ( $\text{ppm}^{-1}$ ) and the limit of detection (ppm) based on the Stern-Volmer analysis of photoluminescence quenching in ester monolayer functionalized SiNCs after exposure to biogenic amines. Also shown is the reported oral toxicity levels<sup>379</sup> for comparison to limit of detection.

<b>Biogenic Amine</b>	<b><math>K_{sv}</math> (<math>\text{ppm}^{-1}</math>)</b>	<b>Linear Regression <math>R^2</math></b>	<b>Limit of detection (ppm)</b>	<b>Reported Oral toxicity levels (ppm)<sup>379</sup></b>
<b>Putrescine</b>	0.11	0.969	8.4	2000
<b>Cadaverine</b>	0.12	0.939	7.9	2000
<b>Spermidine</b>	0.19	0.982	4.9	600

The excited state luminescent lifetime of the ester monolayer functionalized SiNCs was evaluated as a function of biogenic amine (*i.e.*, putrescine, spermidine, cadaverine) concentration. If no change in the PL lifetime is detected upon addition of the quenching analyte, it suggests the quenching mechanism is static and may be caused by the formation of a ground state nanoparticle-analyte complex.<sup>352</sup> Alternatively, if the luminescence lifetime decreases the process is deemed

dynamic, and occurs because of additional deactivation pathways (e.g., electron transfer).<sup>352</sup> For the present system, increasing the concentration of the biogenic amine compounds resulted in a decrease of lifetimes (Table 5-2). These results (Table 5-2) were plotted as  $\tau_0/\tau$  vs. biogenic amine concentration where  $\tau_0$  and  $\tau$  are the luminescence lifetimes in the absence and presence of biogenic amine compounds, respectively (Figure 5-6). Unfortunately, due to time and instrument availability, only one data set was collected, as opposed to at least 3 trials. While no linear relationship was observed during this initial trial, the general observation is the luminescence lifetimes decrease with biogenic amine concentration providing additional evidence the quenching mechanism follows a dynamic electron transfer process (Scheme 5-1).

**Table 5-2:** Luminescence lifetimes of SiNCs after exposure to biogenic amines (*i.e.*, putrescine, spermidine, cadaverine) in the concentration range of 0.5 - 5 ppm.

<b>Concentration (ppm)</b>	<b>0</b>	<b>0.5</b>	<b>1</b>	<b>2.5</b>	<b>5</b>
<b>Putrescine <math>\tau</math> (<math>\mu</math>sec)</b>	37.05	35.27	36.16	36.97	34.66
<b>Spermidine <math>\tau</math> (<math>\mu</math>sec)</b>	37.05	37.20	36.54	35.89	34.06
<b>Cadaverine <math>\tau</math> (<math>\mu</math>sec)</b>	37.05	37.29	36.08	35.31	33.21

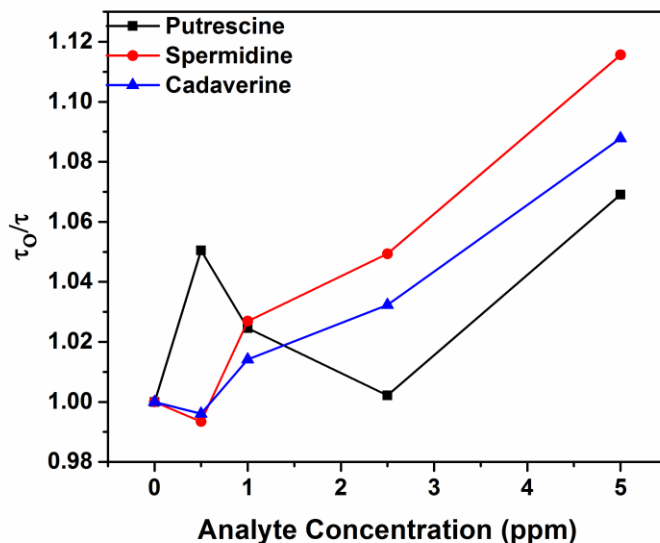
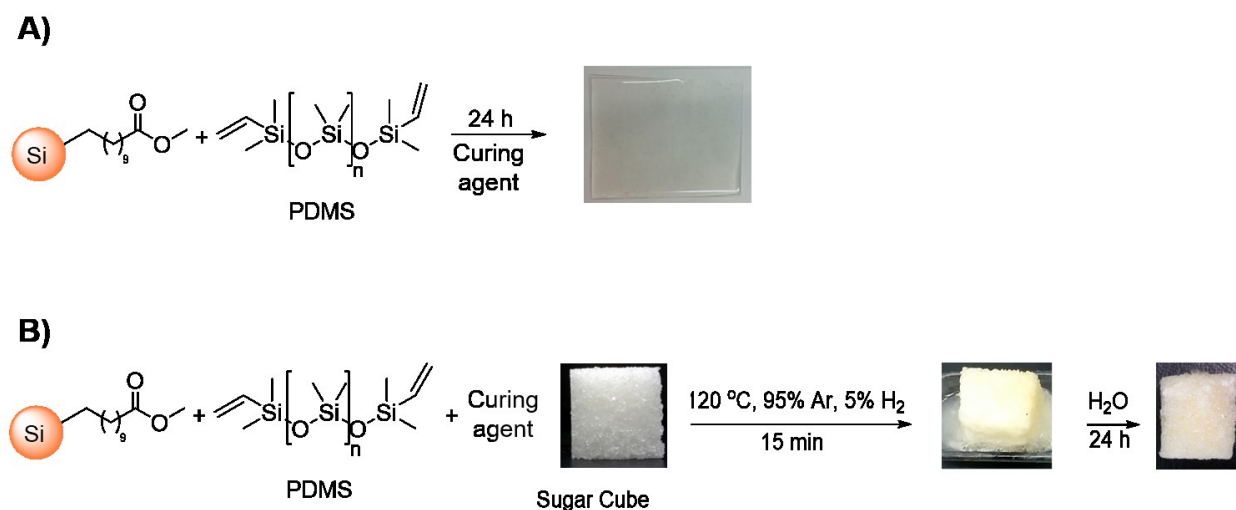


**Figure 5-6:** The Stern-Volmer plot for the quenching efficiencies of putrescine, spermidine and cadaverine at different concentrations.

The solution limit of detection (LOD) for luminescence quenching of the ester monolayer functionalized SiNCs by putrescine, spermidine and cadaverine in the range of 0.5 - 5 ppm were determined using the  $3\sigma$  criteria and are 8.4, 7.9 and 4.9 ppm for putrescine, cadaverine, and spermidine, respectively.<sup>353,354</sup> Again, the NC luminescence was most sensitive to spermidine. These LOD values far exceed the oral toxicity levels for putrescine, spermidine, and cadaverine (*i.e.*, 2000, 600, 2000 ppm, respectively) suggesting the present NCs may be a promising candidate for sensing motifs.<sup>379</sup>

If the present ester monolayer functionalized SiNCs are to find practical applications in areas such as food packaging, a solid-state substrate suitable for vapor detection must be developed. In this context we evaluated polydimethylsiloxane (PDMS), as a non-toxic, inert, and non-flammable polymer support.<sup>380</sup> To incorporate the SiNCs into the polymer, two polymer

morphologies were explored: 1. PDMS films containing SiNCs and 2. PDMS sponges containing SiNCs (Scheme 5-2).<sup>375</sup> It was expected that differences in response of these two morphologies would result from changes in porosity.<sup>373</sup> To prepare the polymer precursor mixtures, ester modified SiNCs were homogenously mixed with the commercial PDMS elastomer base, followed by the addition of the curing agent. This mixture was drop coated onto a glass slide/membrane and cured for 24 h to produce a film (Scheme 5-2A) or was integrated into the pores of a sugar cube template and heated (Scheme 5-2B).<sup>375</sup> The sugar cube template was subsequently removed upon dissolution with distilled water, and the PDMS material was dried in vacuum. The resulting PDMS structure consisted of a sponge-like network of pores (Scheme 5-2B). Both the PDMS film and PDMS sponge displayed characteristics of SiNC red-orange luminescence when exposed to a benchtop UV lamp ( $\lambda = 365$  nm, Figure 5-7A-B). SEM analysis of the structures (Figure 5-7C-D) indicated the film was uniform (Figure 5-7C) while the sponge consisted of a porous network (Figure 5-7D).



**Scheme 5-2:** Preparation of A) PDMS films containing SiNCs and B) PDMS sponges containing SiNCs.

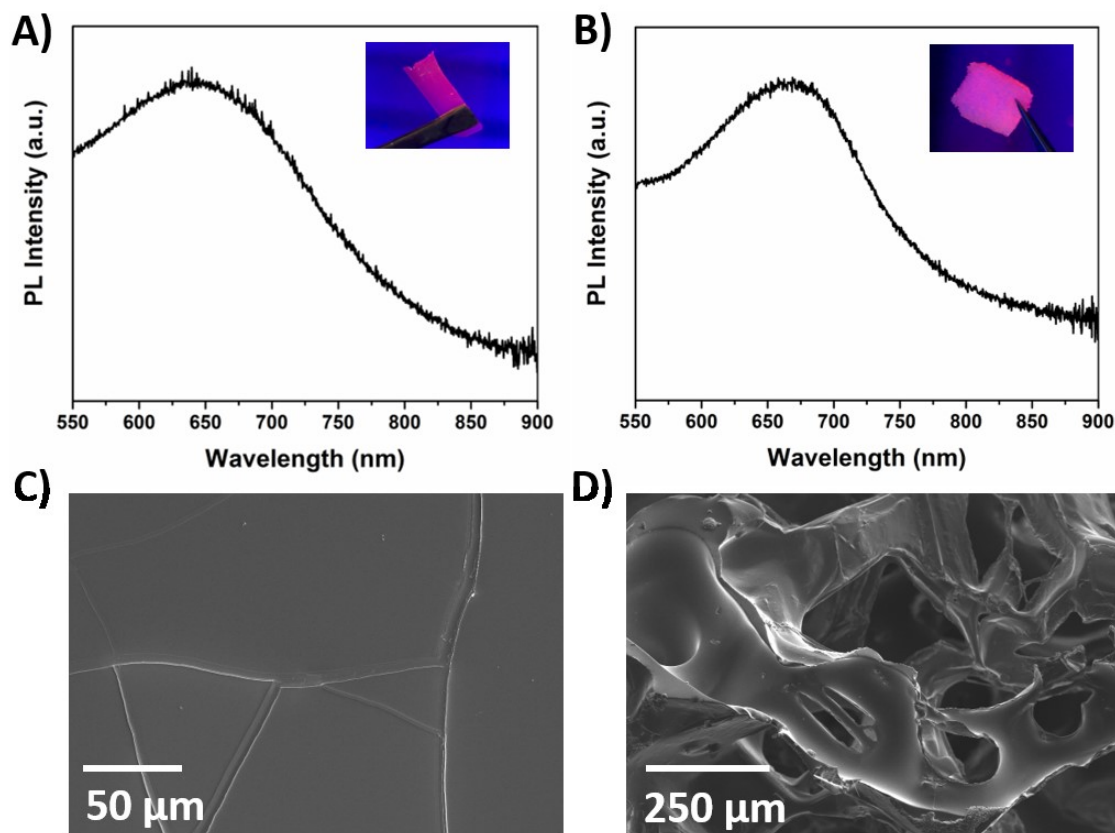


**Figure 5-7:** Photoluminescence spectra of PDMS A) film and B) sponge containing SiNCs. Insets are images of materials upon exposure to a benchtop UV lamp. SEM images of PDMS C) film containing SiNCs and D) sponge containing SiNCs.

The two structural motifs of PDMS/SiNC hybrids were evaluated as potential amine sensing materials using a custom apparatus consisting of two independent gas lines carrying the amine of interest and argon gas feeding into a sealed gas chamber (Figure 5-8). The PDMS SiNC hybrids were placed in the gas chamber, exposed to a LED excitation source (405 nm), and the luminescence was collected by a fiber after passing through a 550 nm long pass filter. Both structural motifs were evaluated under an argon gas flow rate of 4 L/min (Figure 5-9A-B) a non-linear decrease in the luminescence intensity that stabilized within 20 - 30 min. This decrease in

PL intensity may result from photobleaching or emission intermittency (also known as “blinking”). Photobleaching in quantum dots is the permanent loss of emission after continuous illumination by a light source over time and is usually confined to their absorption region.<sup>381-384</sup> Blinking is the switching of a quantum emitter between bright (on) and dark (off) states or even between more states when continuously illuminated.<sup>33,385,386</sup>

To further investigate the PL intensity over time during irradiation and excitation of the LED, the LED excitation source was turned off and on in ten min increments under an argon gas flow rate at 4 L/min for a period of 60 min (Figure 5-9C-D). For both motifs, the luminescence intensity would decrease during LED exposure and then partially recover after the LED was turned off. These observations suggest the LED may be causing both photobleaching and blinking. Unfortunately, evaluating the absorption of PDMS/SiNCs is non-trivial (*i.e.*, the spectrum is featureless), thus preventing definitive determination of photobleaching. The luminescence recovery noted may be attributed to blinking where the emitter was falling into a trap state that caused the emitter to stay in the off state for a very long time during irradiation time and was eventually recovered when the source was off.<sup>386</sup>

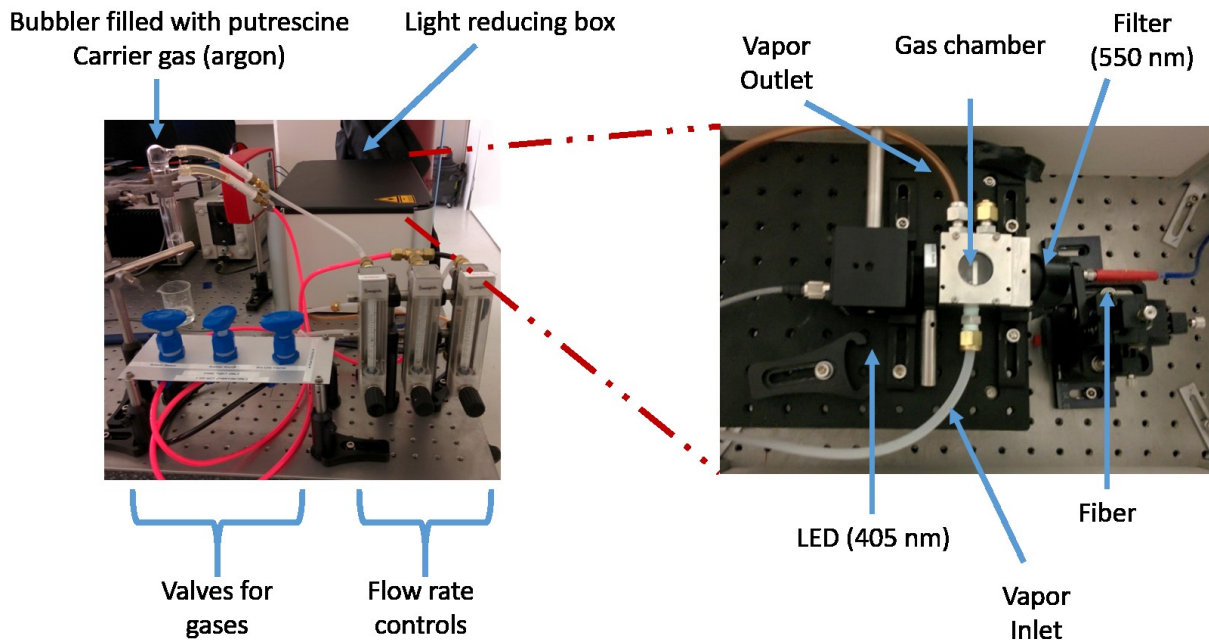


**Figure 5-8:** Custom vapor sensing experimental setup. The bubbler filled with analyte of interest is connected to a carrier gas (argon), that is then passed through the gas chamber holding the PDMS film sponge containing SiNCs sensor. The sensor is excited by the LED ( $\lambda = 405 \text{ nm}$ ) and the luminescence is first passed through a longpass filter ( $\lambda = 550 \text{ nm}$ ) before collection by the optical fiber.

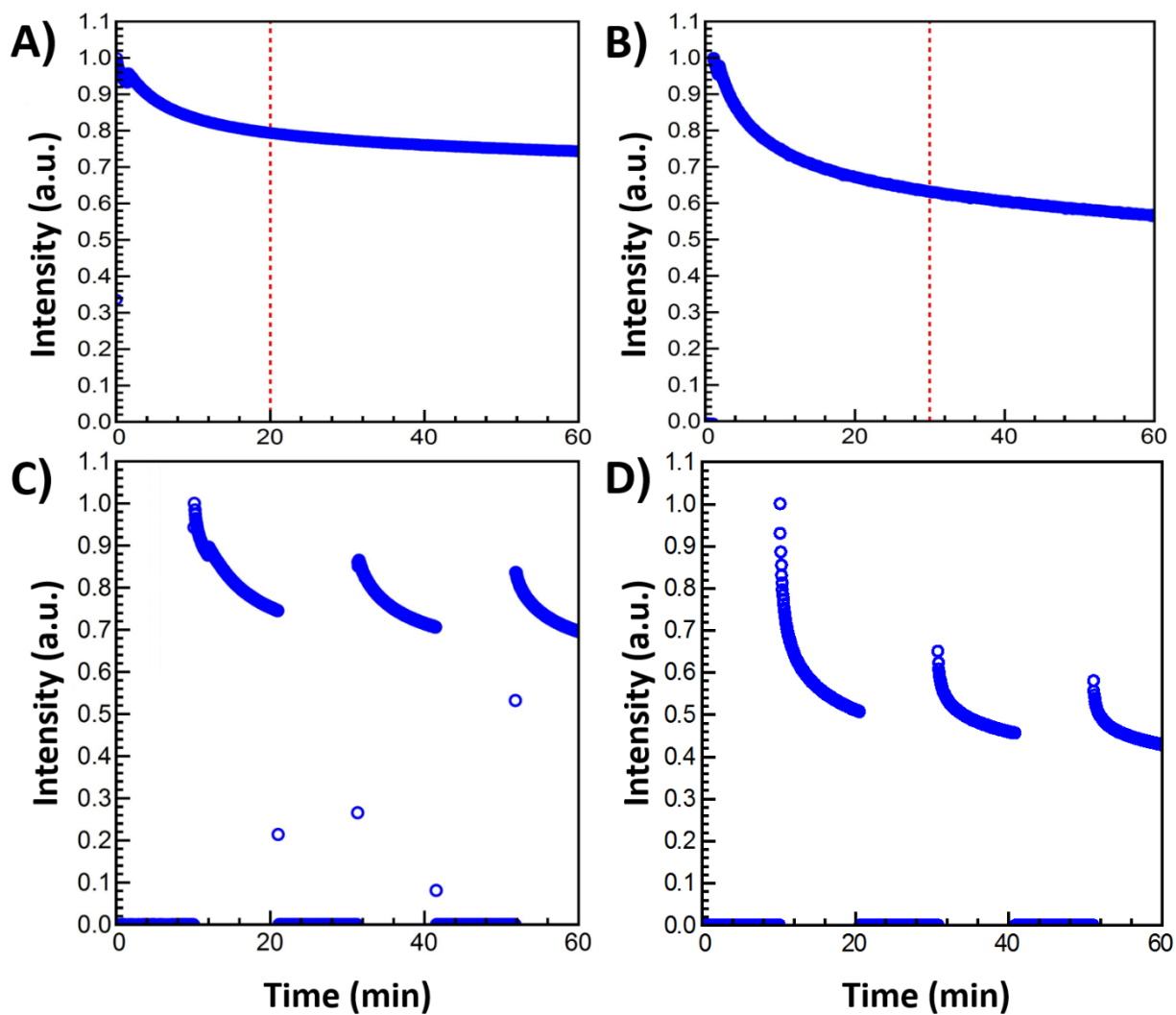


**Figure 5-9:** PDMS A) film B) sponge containing SiNCs luminescence intensity after exposure to LED excitation source (405 nm) under argon gas (4 L/min). PDMS C) film D) sponge containing SiNCs luminescence intensity over time after exposure to LED excitation source in 10 min intervals under argon gas (4 L/min).

The PDMS/SiNCs were then tested for sensitivity toward the vapors of biogenic amine. For these measurements, putrescine was chosen as the biogenic amine of interest. To account for the changes in PL response noted above, the PDMS/SiNC substrates were exposed to LED excitation prior to introduction of putrescine vapor (*i.e.*, 20 min for film and 30 min for sponge). After vapor introduction, the luminescence intensity of both samples decreased (Figure 5-10A-B) and levels off after ~ 5 min of exposure. This may be the result of surface saturation. A similar biogenic vapor response in which the fluorescent quenching occurs within the first 50 sec of exposure to a thin film sample has been previously reported.<sup>377</sup> In order to estimate the change of luminescence induced by the putrescine vapor, a line of best fit was performed (Figure 5-10A-B). The change in intensity was determined by the following equation:

$$\Delta Intensity = I_{meas}(x \text{ min}) - I_{calc}(x \text{ min})$$

Where  $\Delta Intensity$  is the change in intensity,  $I_{meas}$  is the intensity measured at the time of putrescine introduction and  $I_{calc}$  is the intensity calculated from the line of best fit at the time of putrescine introduction. The  $\Delta Intensity$  for the PDMS film and PDMS sponge containing SiNCs are 0.057 and 0.017, respectively. These preliminary studies indicate that both types of solid-state substrate are responsive towards putrescine vapor and paves the way for future investigation of the influence of pore size.

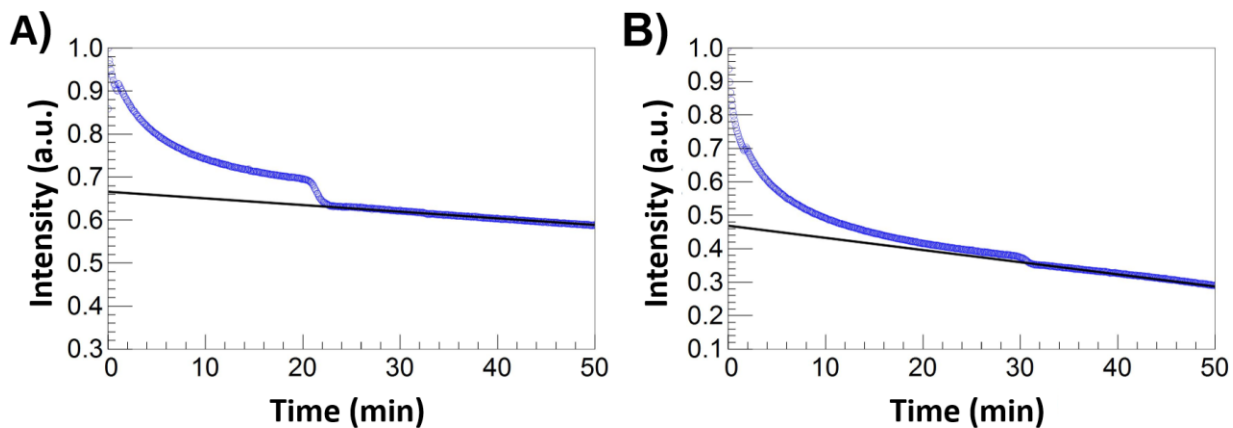


**Figure 5-10:** PDMS film (A) and PDMS sponge (B) containing SiNCs luminescence intensity over time after exposure to putrescine vapor (4 L/min). The line of best fit of PDMS film (A) and PDMS sponge (B) is shown as the black line.

In addition to exploring the impact of biogenic amines on PL response, possible interferents (*i.e.*, water and 100% ethanol vapors) were examined using the same protocols applied to biogenic amines on the PDMS substrates. Figure 5-11 shows the response to water and ethanol vapor. Qualitatively, the sponge motif PL was affected more than that of the film. However, variations in sample thickness preclude a quantitative analysis. It has been previously shown that the introduction of water or ethanol vapors to SiNCs can cause quenching or blue-shifts of the PL maxima, therefore these results are not completely unexpected.<sup>204,251,320,387,388</sup>

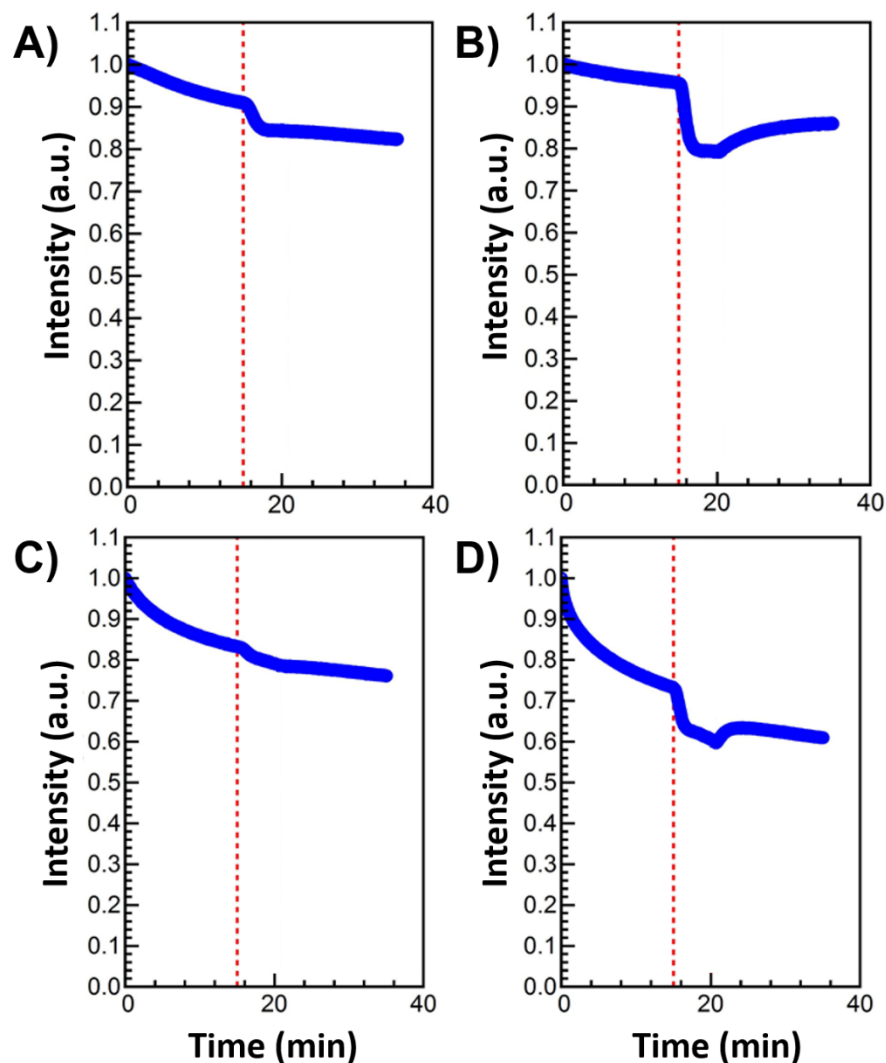


**Figure 5-11:** PDMS film (A) and PDMS sponge (B) containing SiNCs luminescence intensity over time after exposure to water vapor (4 L/min). PDMS film (C) and PDMS sponge (D) containing SiNCs luminescence intensity over time after exposure to 100 % ethanol vapor (4 L/min). The dashed red line indicates the time at which water or ethanol vapor was introduced into the system.

While the present PDMS/SiNC hybrids are not optimized, it is useful to qualitatively evaluate their response upon exposure to raw meat. To do so, raw meat pieces (*i.e.*, salmon, pickerel, pork or chicken, 1 g) were placed in a vial with a small piece of PDMS/SiNC substrate

and sealed. The samples were stored at room temperature or in the fridge (4 °C) and the luminescence response of the substrate was recorded once a day over a period of 4 days. The results of this preliminary study are presented in Figure 5-12.

It was anticipated that room temperature raw meat samples would have a quenching effect on the PL of the PDMS substrates indicating the formation of biogenic amines and quenching efficiency would increase with aging. Conversely, the samples kept in the fridge would not spoil (as rapidly), therefore no (or minimal) generation of biogenic amines would occur, and the PDMS substrates PL would remain unaffected. A similar study by the Swager group previously showed this trend using chemiresistive detectors.<sup>389</sup> Unfortunately, no clear trends were noted. There are many factors that could have led to this result. For example, PDMS substrates may not be selective for biogenic amines, water could be impacting the PL, the luminescent NCs may not be uniformly distributed in the substrate, sampling errors, *etc.* Due to the complexity of the results and poor sensing performance, the experiment was not repeated, and no statistical analysis was performed or shown in Figure 5-12.

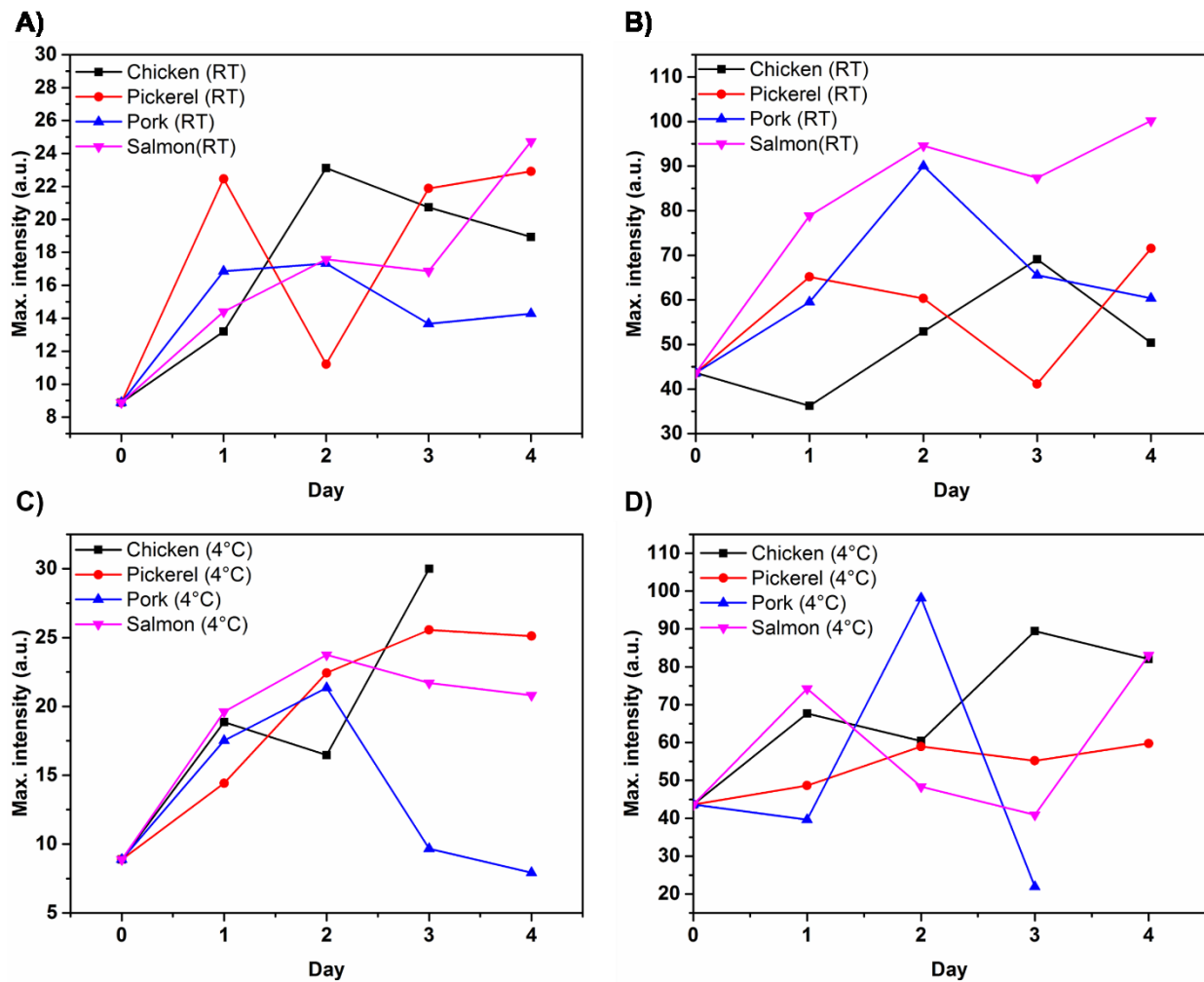


**Figure 5-12:** PDMS film (A) and PDMS sponge (B) containing SiNCs maximum luminescence intensity over period of 4 days at room temperature after raw food exposure. PDMS film (C) and PDMS sponge (D) containing SiNCs maximum luminescence intensity over period of 4 days at 4 °C after raw food exposure.

Since the first trial of the PDMS substrates resulted in inconclusive results that may be attributed to experimental setup, an alternative method was used to evaluate the response of the PDMS substrates to raw meat over a 24-hour time period. In this setup, the PDMS substrates (films or sponges) were placed directly on top 1 g aliquots of raw meat (*i.e.*, pork, salmon, chicken,

beef or pickerel) and wrapped in commercial polyethylene plastic wrap to mimic store packaging of meat (Figure 5-13). A digital camera (equipped with a 550 nm longpass filter over the lens) was positioned and clamped above the samples to collect photos of the PDMS substrates at 0 and 24 h of exposure to meat at room temperature. A hand held UV lamp ( $\lambda = 365$  nm) was also positioned slightly above the samples and was only turned on at the time of photo collection. Photos were taken at either ambient or UV light at 0 and 24 hours of sample exposure to raw meat.

Sensing of biogenic amines through digital camera images by studying the red-green-blue readouts have been previously reported.<sup>390</sup> This concept has also been extended to SiNC PL intensities under UV light by Ngyuen and coworkers to study nitroaromatic quenching on paper substrates.<sup>228</sup> Therefore, this idea was applied to the current system (Figure 5-13) in which the digital image acquired under UV light was split into the red-green-blue components, with evaluation of the red component. It could be seen in Figure 5-13 that there was a decrease in the PL of the PDMS substrates over the 24 h period for all samples examined. However, this PL change was also observed in the blank samples, indicating the generation of biogenic amines may not be causing the PL quenching selectively.

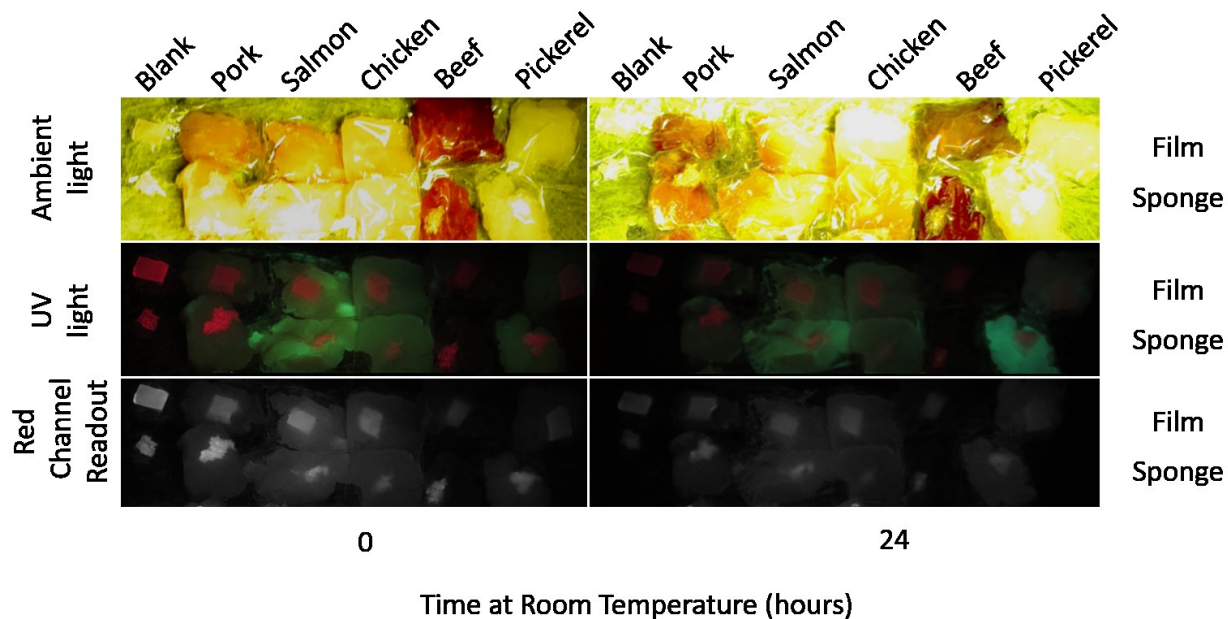


**Figure 5-13:** Digital images of PDMS film and PDMS sponge containing SiNCs substrates exposed to raw pork, salmon, chicken, beef or pickerel for 0 - 24 h at room temperature. (Note: Ambient light passed through 550 nm filter, UV light,  $\lambda=365$  nm)

## 5.4 Conclusions

SiNCs of various surface groups (*i.e.*, alkyl oligomer, alkyl monolayer, and ester monolayer) were first tested for possible luminescence quenching with allylamine. It was determined the ester monolayer functionalized SiNCs displayed the greatest response towards this amine molecule and used for biogenic amine studies. Solution based photoluminescence studies indicated that the quenching proceeds via an electron transfer mechanism. The solution based LODs were determined to be 8.4, 7.9 and 4.9 ppm for the biogenic amines putrescine, cadaverine, and spermidine, respectively, indicating SiNCs of interest for the development of a possible sensor. The SiNCs were then successfully incorporated into PDMS film and sponge substrates and then

were further used to study the detection of putrescine vapors and raw food monitoring. It was found that the PDMS samples displayed quenching in the presence of putrescine vapor, however, a response towards water and ethanol vapors were also observed, indicating the created sensor was not selective. Furthermore, when testing the measured PL of PDMS substrate samples upon exposure to raw food, no correlation could be found between the samples at room temperature and at 4 °C. When measuring the PL response of the PDMS samples with a digital camera, a PL quenching response was also observed. However, this response was also observed for PDMS samples that were not exposed to raw meat under the sample conditions, again, indicating the current system is not selective towards biogenic amines. While these materials may be promising for biogenic amine sensors for food packaging, further investigation is still needed to overcome experimental setup concerns, as well as the influence of common interferents such as water vapor.

# **Chapter 6**

## **Conclusions and Future Directions**

## 6.1 Conclusions

Quantum dots (QDs) have proven to be a major advancement in the field of materials science, due to their optical properties. However, there is a need for abundant and non-toxic QDs. Less toxic, luminescent silicon nanocrystals (SiNCs) may be the solution. However, the surface chemistry of SiNCs is far less developed than that of other QDs, limiting the examples of incorporation of these materials into prototype devices such as sensors. The aim of the research outlined in this thesis was to explore the surface chemistry and potential sensing capabilities of SiNCs. The work presented in Chapters 2 and 3 explored the surface functionalization of SiNC surfaces either through the use of thermal radical initiators or a commercially available compact fluorescent light source, while Chapters 4 and 5 investigated the development of potential sensing platforms based upon SiNCs.

Chapter 2 provided an investigation of the functional group tolerance of the thermal radical initiated hydrosilylation of SiNCs method using two common thermal radical initiators (*i.e.*, 2,2'-azobis(2-methylpropionitrile) (AIBN) and benzoyl peroxide), and a series of alkene or alkyne terminated ligands (*i.e.*, 1-dodecene, 1-octyne, methyl-10-undecenoate, styrene, pentenoic acid and phenylacetylene). This approach resulted in the successful hydrosilylation of SiNCs under mild reaction temperatures (60 - 85 °C) and was shown to be size independent (SiNCs  $d = 3, 6, \text{ or } 9 \text{ nm}$ ). An additional benefit of this method, was the formation of monolayer passivated surfaces. These conditions are advantageous when compared to that of thermal hydrosilylation (requires temperatures  $> 150 \text{ }^\circ\text{C}$ , formation of oligomeric surfaces)<sup>148</sup> and photochemical hydrosilylation (not effective for larger SiNCs).<sup>142</sup> Reducing the reaction temperature allows for the hydrosilylation of SiNCs with lower boiling point ligands and opens the door for expanding the surface chemistry of SiNCs. Furthermore, monolayer passivated SiNCs would be advantageous

in the development of sensing systems where processes like electron transfer rely on close proximity of the analyte to the SiNC core to occur.<sup>15</sup> In contrast to the work done by Moran and Carter where AIBN was used for the polymerization of monomers, followed by grafting of the polymer onto silicon surfaces,<sup>284</sup> we showed through the use of the radical trap 2,2,6,6-tetramethyl-1-piperidinyloxy (TEMPO), that AIBN promoted the abstraction of the SiNC surface hydride.

Chapter 3 investigates the functionalization of SiNCs with S-S bond containing molecules (*i.e.*, lipoic acid and dibutyl disulfide) through the use of a commercial fluorescent light source (18 W). The mild reaction conditions (fluorescent light, no heat) used generated monolayer (dibutyl disulfide) or oligomer (lipoic acid) Si-S passivated surfaces, however, differences were observed between the two ligands investigated. For example, SiNCs of sizes  $d = 3, 6, \text{ or } 8 \text{ nm}$  were investigated and lipoic acid was successfully attached for all SiNCs sizes investigated. However, reactions with dibutyl disulfide were only successful for smaller SiNCs ( $d = 3 \text{ or } 6 \text{ nm}$ ). Another observation related to SiNC size was the length of time required for complete reaction. Reactions involving lipoic acid require reaction times of 90 - 120 min, 90 - 150 min, and 24 - 36 h those involving 3, 6, and 8 nm SiNCs, respectively. Alternatively, reactions using dibutyl disulfide occurred within 60 - 120 min and 9 - 12 h for 3 and 6 nm SiNCs, respectively. While it is reasonable longer reaction times would be required for increasing particle size, the cause for the observed time range in which reactions proceeded is still unknown. We postulate the reaction proceeds first by cleavage of the S-S bond by the fluorescent light source, generating two thiyl radicals which could then abstract a surface hydride.<sup>184</sup> The resulting siyl radical could then combine with thiyl radicals in solution to generate Si-S surface bonds.

The development of a paper-based SiNC sensor was described in Chapter 4. Dodecyl functionalized SiNCs prepared via thermal hydrosilylation were tested for their optical response

toward nitroaromatics (*i.e.*, nitrobenzene (NB), mononitrotoluene (MNT), and dinitrotoluene (DNT)) in solution. The addition of any of the tested nitroaromatics resulted in a proportional decrease in luminescence intensity and lifetime with increasing concentration of nitroaromatics. Based on these observations, it was proposed the luminescence quenching mechanism was caused by the electron transfer from the SiNC conduction band to the vacant  $\pi^*$  orbital of the nitroaromatic compound. To take further advantage of the SiNC luminescence quenching caused by the introduction of nitroaromatics, a paper-based sensor was developed by dip-coating a piece of filter paper into a solution containing SiNCs. The resulting paper was then shown to be responsive towards vapor, solutions and solid nitroaromatics. Of particular interest was the observation of the sensor to quench in the presence of known explosive compounds (*i.e.*, trinitrotoluene (TNT), nitramine cyclotrimethylenetrinitramine (RDX) and the nitrate ester pentaerythritol tetranitrate (PETN)). The method developed here offers a non-toxic, portable, rapid, and straightforward sensing system for on-site detection of nitro group containing explosives. Further investigation into the use of SiNCs for explosive detection was conducted by covalently linking carboxylic acid terminated SiNCs to non-fluorescent thin layer chromatography (TLC) plates to obtain luminescent TLC plates. These SiNC-TLC plates were able to separate MNT and DNT, an advantage over the dip-coated paper-based sensor which cannot distinguish between compounds of interest.

Finally, the investigation of the use of SiNCs for the detection of biogenic amines was explored in Chapter 5. After initial screening of SiNCs with three different surface groups (*i.e.*, alkyl oligomer, alkyl monolayer, or ester monolayer) toward model amine compound, allyamine, the ester monolayer functionalized SiNCs displayed the most significant quenching response. These SiNCs were further tested for their response towards aliphatic biogenic amines (*i.e.*,

putrescine, cadaverine, spermidine) in solution. Both luminescence intensity and lifetime decreased with the addition of biogenic amines, and it was proposed an electron was being transferred from the biogenic amine to a vacancy in the valence band of the SiNCs. To further evaluate the SiNCs for the detection of amine vapors for the future development of food packaging sensors, the ester monolayer functionalized SiNCs were incorporated into either porous or non-porous (polydimethylsiloxane) PDMS supports. While studies conducted with the prepared PDMS sensors with putrescence vapors displayed a decreased in luminescence intensity, the materials were not selective and quenched in the presence of either water or ethanol vapors. Also, experiments set up to mimic raw meat packaging with the PDMS sensors proved to be inconclusive.

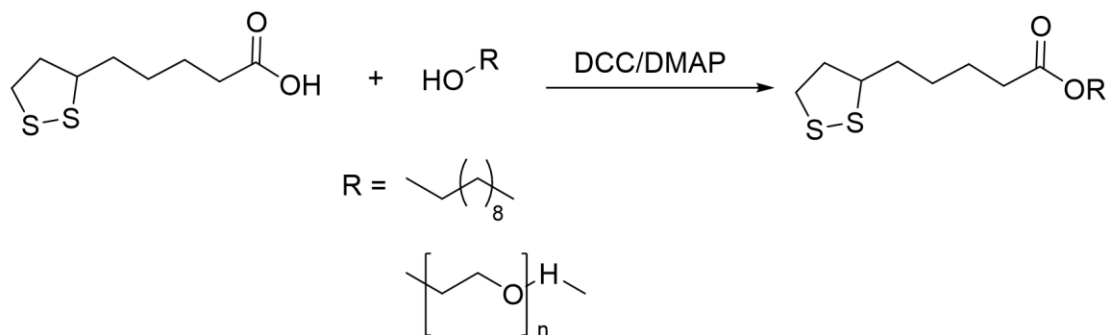
## **6.2 Future Directions**

### **6.2.1 Exploration of solubility with lipoic acid based ligands**

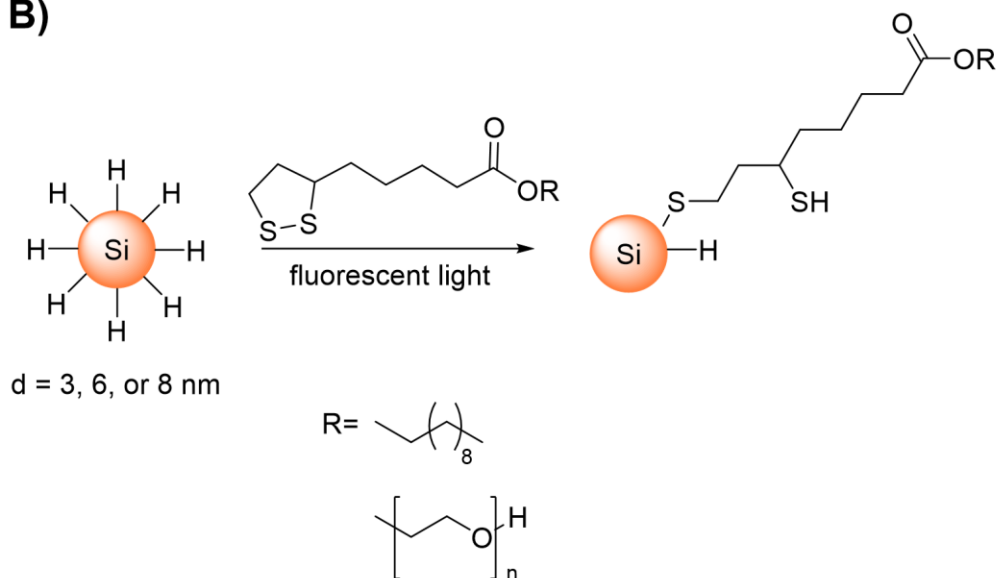
A current challenge in the surface passivation of SiNCs is the dispersibility of the SiNCs in various solvents. Of particular importance is aqueous soluble SiNCs that can be used in sensing and biological applications. In Chapter 3, functionalization of SiNCs with lipoic acid generated the polymeric form of lipoic acid; a polymer that is unstable under continuous light exposure.<sup>313</sup> Though long term irradiation of the SiNCs was not studied, this may prove to be a limitation of the SiNCs with this surface group. One way to build upon the S-S bond chemistry investigated in this thesis is to modify the lipoic acid ligand prior to SiNC functionalization. Research done by the Mattoussi group has shown that modification of lipoic acid with various polyethylene glycol (PEG) polymers resulted in the successful photoligation of the QD surface, rendering them soluble in methanol.<sup>315,316</sup> Therefore, it can be postulated that the chemistry of a modified lipoic acid

ligand (*i.e.*, cyclic disulfide group intact) would be compatible with the method described in Chapter 3 (Scheme 6-1). The resulting functionalized SiNCs may show increased stability as well as be soluble in solvents such as methanol or toluene.

**A)**



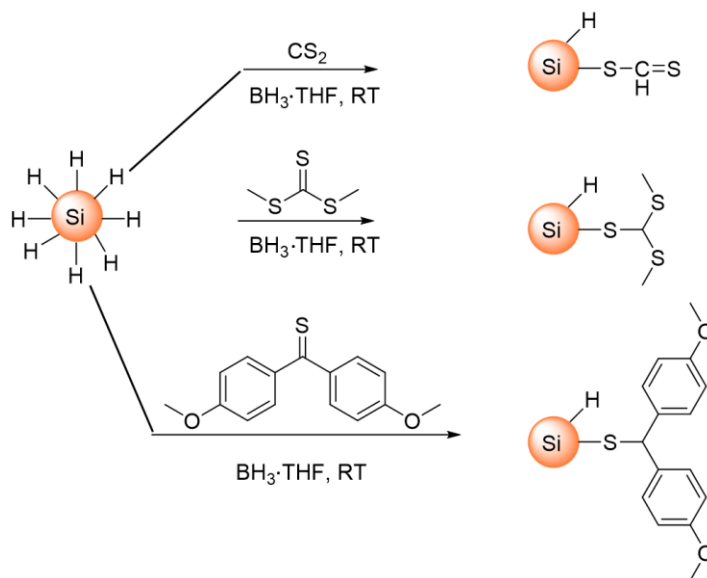
**B)**



**Scheme 6-1:** A) The modification of lipoic acid with dodecanol or polyethylene glycol by Steglich Esterification using *N,N'*-dicyclocarbodiimide (DCC) and 4-(dimethylamino)pyridine (DMAP).<sup>360</sup> B) The functionalization of SiNCs with modified lipoic acid molecules by a fluorescent light source.

## 6.2.2 Functionalization of SiNCs using thioketones

As described in Chapter 1, the study and development of methods to functionalize SiNCs with chalcogenides is still in its infancy. An alternative method to generate Si-S surfaces, would be the use of the borane-catalyst  $\text{BH}_3 \cdot \text{THF}$ . This reagent has been shown to catalyze the hydrosilylation of hydride terminated SiNCs (H-SiNCs) with alkenes and alkynes at room temperature.<sup>152</sup> Furthermore,  $\text{BH}_3 \cdot \text{THF}$  has been shown to activate Si-O SiNC surfaces allowing for ligand exchange with alkenes and alkynes.<sup>126</sup> These previous reports indicate this reagent is very reactive towards SiNC surfaces. Additionally, the work of the Rosenberg group has shown that molecular silanes can undergo borane-catalyzed hydrosilylation in the presence of thioketones.<sup>391,392</sup> It is proposed that  $\text{BH}_3 \cdot \text{THF}$  could be used as a catalyst for the hydrosilylation of H-SiNCs with thioketones to produce Si-S surface bonds (Scheme 6-2). The use of this method could expand the library of possible Si-S surface ligands.

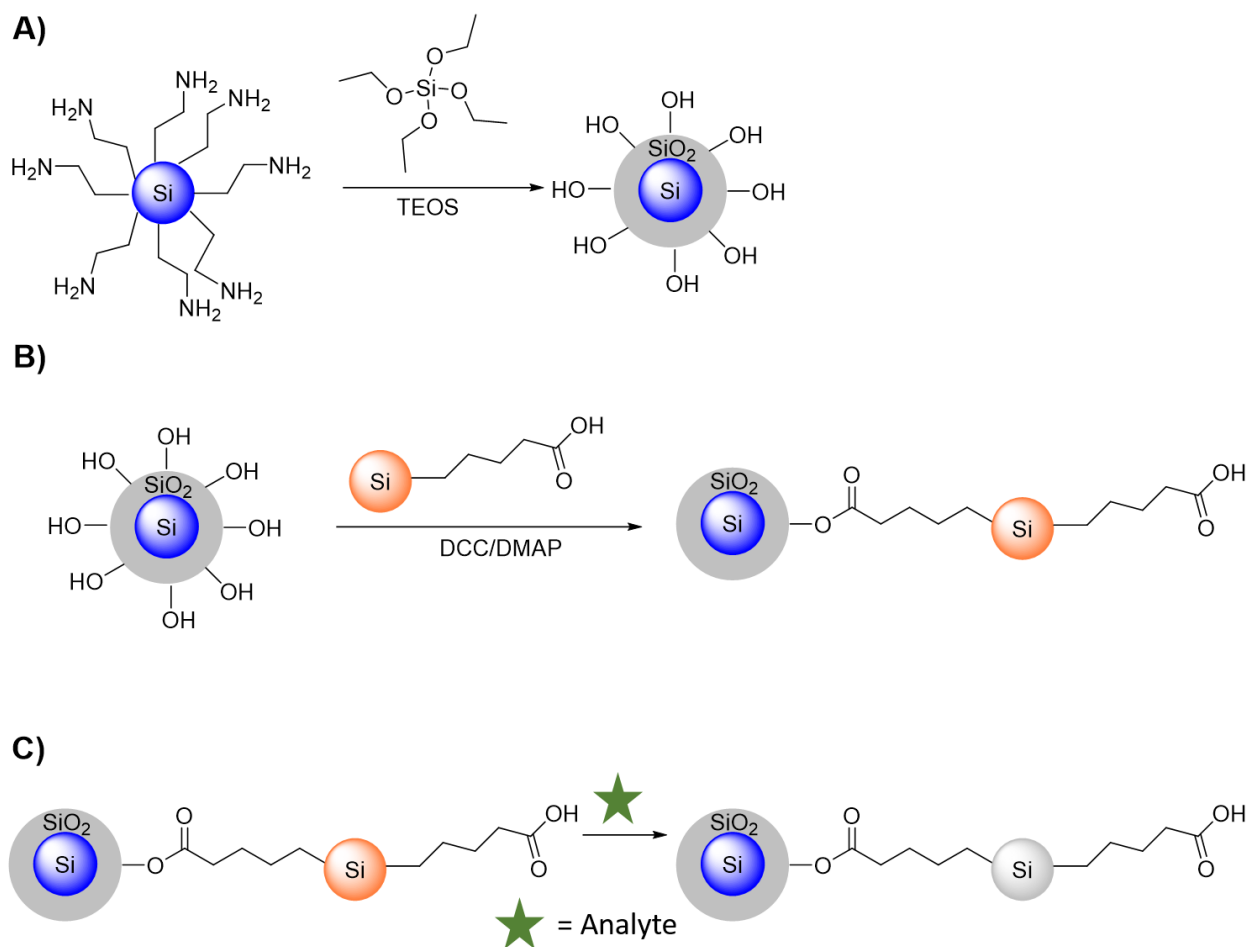


**Scheme 6-2:** Reaction of SiNCs with various thioketones at room temperature (RT).

Preliminary results using this reaction method indicate the presence of Si-S bonds. Further studies using  $\text{BH}_3 \cdot \text{THF}$  as a reagent to activate Si-S SiNCs surfaces for ligand exchange reactions are the subject of ongoing investigation.

### 6.2.3 Development of a ratiometric sensor

The development of QD-based ratiometric sensors and their advantages was briefly discussed in Chapter 1, Section 1.5.1.3.<sup>216</sup> To date, SiNC based ratiometric sensors have not been reported. As described in Chapter 1, Sections 1.3 and 1.4, multiple preparation and surface passivation methods can generate SiNCs with tunable luminescence. The incorporation of these various luminescent SiNCs to generate a SiNC-based ratiometric sensing platform could be possible. Previous ratiometric sensors using Cd-based QDs have been developed in which a QD emitting one wavelength is encapsulated in a non-porous silica shell, while a QD emitting a different wavelength is tethered to the outside of the silica shell.<sup>344,393</sup> Once exposed to the analyte of interest, the QD luminescence on the outside of the shell is quenched while the silica encapsulated QD luminescence remains unchanged. This concept may be extended to SiNCs (Scheme 6-3). One possible route to explore would be the encapsulation of blue-emitting SiNCs into a non-porous silica shell (SiNC@SiO<sub>2</sub>, Scheme 6-3A). The encapsulation of SiNCs into a mesoporous silica shell has been previously shown in the Veinot group.<sup>394,395</sup> A similar method could be implemented in the absence of a surfactant (*i.e.*, cetyltrimethylammonium bromide, CTAB) to generate a non-porous silica shell. Next a red-emitting SiNC could be coupled to the surface of SiNC@SiO<sub>2</sub> (Scheme 6-3B). The resulting material could then be exposed to an analyte of interest (*e.g.*, nitroaromatics, biogenic amines, metal cations, *etc.*), effectively making a SiNC ratiometric sensor (Scheme 6-3C).



**Scheme 6-3:** Proposed reaction scheme to generate a SiNC ratiometric sensor. A) Reaction of blue-emitting  $\text{NH}_2$  terminated SiNCs<sup>83</sup> reacted with tetraethyl orthosilicate (TEOS) to generate silica coated SiNCs ( $\text{SiNC@SiO}_2$ ).<sup>395</sup> B) Coupling of  $\text{SiNC@SiO}_2$  with acid terminated SiNCs to achieve sensor material.<sup>148,360</sup> C) Use of prepared sensor in the presence of an analyte.

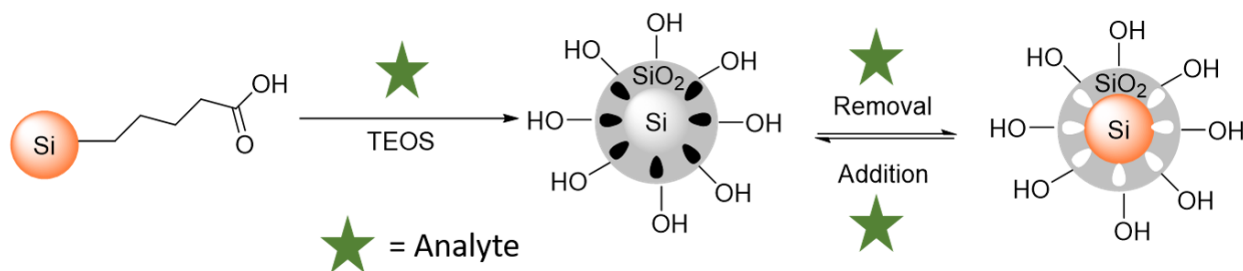
### 6.2.4 Exploration of SiNCs embedded within porous structures for sensing

While the use of SiNCs as sensors is on the rise, a challenge that must be overcome is selectivity. As seen in Chapter 4, the additional use of TLC had to be implemented for the separation and identification of nitroaromatic compounds. Moreover, the apparent research trend of SiNCs sensors is for the development of solution based sensors. Currently, there are limited

examples of SiNCs used for vapor sensing.<sup>251,387,388</sup> While the SiNC/PDMS sensors studied for biogenic amine vapor sensing in Chapter 5 did quench upon putrescine vapor exposure, the materials were susceptible to quenching in the presence of water and ethanol vapor interferents. One possible way to increase the selectivity of SiNCs or develop vapor sensing platforms is through incorporating SiNCs with/within porous structures such as molecularly imprinted polymers (MIPs) or aerogels.

#### 6.2.4.1 Development of SiNCs coated with MIPs

MIPs result from a molecular imprinting technique that involves the copolymerization of functional monomers and cross linkers in the presence of target analytes which act as template molecules.<sup>396</sup> Following the removal of the template, recognition sites complementary in size, shape, and chemical functionality to the template molecule remain.<sup>396,397</sup> This concept has been used to generate luminescent MIP capped QDs (QD@MIP) for optical sensors.<sup>396,398,399</sup> These studies compared the use of a QD@MIP material and uncapped QD optical response towards analytes such as TNT<sup>396</sup> and norepinephrine.<sup>399</sup> These studies showed the QD@MIP materials had a higher response towards the target analyte than the QD counterpart. Furthermore, Xu and coworkers reported the QD@MIP was selective to TNT over other competitive molecules (*i.e.*, dinitrophenol, 4-nitrophenol, phenol and DNT).<sup>396</sup> The authors stated the imprinting cavities was a contributing factor towards selectivity as the other molecules examined had different shapes and volumes than TNT. This concept could be further extended to SiNCs to create a SiNC@MIP sensor (Scheme 6-4) to increase selectivity towards target analytes (*i.e.*, nitroaromatics or biogenic amines).



**Scheme 6-4:** Schematic for the preparation of SiNC@MIP and the sensing mechanism.

#### 6.2.4.2 Development of SiNC vapor sensors through the use of aerogel hybrids

Aerogels are three-dimensional solid networks comprised of nanometer scale building blocks and have the characteristic advantages of high internal surface areas, low density, and an extensive pore network.<sup>400</sup> Silica aerogels for example, display high optical transparency and the permeability of the gel network could lead to the detection of small molecule vapors.<sup>400</sup> The incorporation of CdSe QDs during aerogel fabrication or carbon dots post aerogel fabrication has led to luminescent aerogel hybrid materials that were used as sensing platforms for the detection of trimethylamine and NO<sub>2</sub> vapors, respectively.<sup>400,401</sup> These successful reports of aerogel hybrid materials as optical vapor sensors indicate this is an avenue worth exploring with SiNCs. The successful incorporation of SiNCs into silica aerogels to create a hybrid material has been previously shown.<sup>402-404</sup> Recently our group has shown the successful incorporation of SiNCs into silica aerogels that retain the high optical transparency of the silica gel and the SiNC luminescence.<sup>404</sup> This hybrid aerogel displayed rapid luminescence quenching upon exposure to NB (Figure 6-1) in a similar manner discussed in Chapter 4.<sup>226,404</sup> This observed quenching indicates the SiNCs are still chemically accessible within the silica aerogel, making these hybrid materials promising sensing platforms.

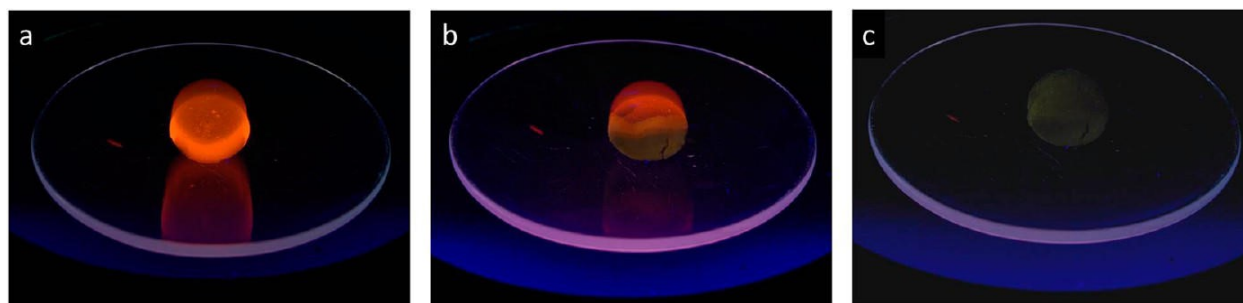


**Figure 6-1:** Images of a SiNC-silica aerogel hybrid material a) before, b) partial and c) complete exposure to nitrobenzene. Image reproduced with permission from *Chem. Mater.*, **2016**, *28*, 3877-3886 (reference 404). Copyright 2016 American Chemical Society.

While the limit of detection was not reported, it would be interesting to study how this hybrid material compares to other reported limit of detection using SiNCs for nitrobenzene, to demonstrate the influence of porosity on the sensing capability. Furthermore, these SiNC aerogel hybrid materials could also be ideal sensing platform candidates for various gases (*e.g.*, NO<sub>2</sub>, NH<sub>3</sub>, *etc.*).

# Appendix

## Appendix: Surface Coverage Calculation

Surface coverage estimates of surface passivated silicon nanocrystals (SiNCs) described in Chapter 2 were determined by either proton nuclear magnetic resonance ( $^1\text{H}$  NMR)<sup>101,152</sup> or thermogravimetric analysis (TGA).<sup>152</sup>

### Surface coverage determination through $^1\text{H}$ NMR.

A  $^1\text{H}$  NMR was taken from a sample prepared from a known mass (minimum 5 mg) of surface passivated SiNCs dispersed in 1 mL  $\text{CDCl}_3$  with 0.01% (v/v) tetramethylsilane (TMS). The ratios of the integrated peak area arising from ligand protons to the peak arising from TMS proton were determined from the  $^1\text{H}$  NMR spectrum. The coverage is estimated for a compact icosahedral, where SiNCs of  $d = 3.5$  nm contains a total of 1100 Si atoms and 300 surface Si atoms.<sup>289</sup>

$$\text{ligand to TMS proton ratio} = \frac{\text{ligand proton integrated peak area}}{\text{TMS proton peak area}}$$

$$\text{ligand to TMS proton ratio per 1 mg SiNC} = \frac{\text{ligand to TMS proton ratio}}{\text{mass of SiNC sample}}$$

$$\begin{aligned} &\text{Ligand to TMS mole ratio} \\ &= \frac{\text{ligand to TMS proton ratio per 1 mg SiNC} \times \text{number of protons ligand}}{\text{number of protons TMS}} \end{aligned}$$

$$\begin{aligned} &\text{moles of ligand in 1 mg sample} \\ &= \frac{\text{Ligand to TMS mole ratio}}{\text{number of moles of TMS in 1 mL } \text{CDCl}_3 \text{ with 0.03\% TMS}} \end{aligned}$$

$$\begin{aligned} &\text{wt of ligand in 1 mg sample} \\ &= \text{molecular weight ligand} \left( \frac{\text{mg}}{\text{mol}} \right) \times \text{moles of ligand in 1 mg sample} \end{aligned}$$

$$\text{mole fraction of ligand} = \frac{\text{wt of ligand in 1 mg sample}}{\text{molecular weight ligand}}$$

$$\text{wt of Si in 1 mg of sample} = 1 \text{ mg} - \text{wt of ligand in 1 mg sample}$$

$$\text{moles of Si in 1 mg sample} = \frac{\text{wt of Silicon in 1 mg of sample}}{\text{atomic weight of Si}}$$

$$\text{number of ligands per nanocrystal} = \frac{\text{mole fraction of ligand}}{\text{moles of Si}} \times 1100 \text{ Si atoms}$$

$$\% \text{ surface coverage} = \frac{\text{number of ligands per SiNC}}{300 \text{ Si surface atoms}} \times 100$$

### Surface coverage of SiNCs using TGA.

This calculation uses the percentage weight loss (% wt. loss) determined by TGA measurement.

The coverage is estimated for a compact icosahedral, where SiNCs of  $d = 3.5 \text{ nm}$  contains a total of 1100 Si atoms and 300 surface Si atoms.<sup>289</sup>

$$\% \text{ mole of ligand} = \frac{\% \text{ wt loss}}{\text{molecular weight ligand (g/mol)}}$$

$$\% \text{ mole of Si atoms} = \frac{100 - \% \text{ mole of ligand}}{\text{weight silicon (g/mol)}}$$

$$\text{number of ligands per nanocrystal} = \frac{\% \text{ mole of ligand}}{\% \text{ mole of Si atoms}} \times 1100 \text{ Si atoms}$$

$$\% \text{ surface coverage} = \frac{\text{number of ligands per nanocrystal}}{300 \text{ surface Si atoms}} \times 100$$

## References

- (1) Feynman, R. *Eng. Sci.* **1960**, *23*, 22.
- (2) Fahlman, B. D. *Materials Chemistry*; 1 ed.; Springer Netherlands: Mount Pleasant, MI, USA, 2007.
- (3) Xia, Y.; Yang, P.; Sun, Y.; Wu, Y.; Mayers, B.; Gates, B.; Yin, Y.; Kim, F.; Yan, H. *Adv. Mater.* **2003**, *15*, 353.
- (4) Eustis, S.; El-Sayed, M. A. *Chem. Soc. Rev.* **2006**, *35*, 209.
- (5) Moon, H. K.; Lee, S. H.; Choi, H. C. *ACS Nano* **2009**, *3*, 3707.
- (6) Zhang, G.; Li, B. *Nanoscale* **2010**, *2*, 1058.
- (7) Henglein, A. *Chem. Rev.* **1989**, *89*, 1861.
- (8) Weller, H. *Adv. Mater.* **1993**, *5*, 88.
- (9) Alivisatos, A. P. *J. Phys. Chem.* **1996**, *100*, 13226.
- (10) Gubin, S. P.; Koksharov, Y. A.; Khomutov, G. B.; Yurkov, G. Y. *Russ. Chem. Rev.* **2005**, *74*, 489.
- (11) Lu, A.-H.; Salabas, E. L.; Schüth, F. *Angew. Chem., Int. Ed.* **2007**, *46*, 1222.
- (12) Reed, M. A.; Randall, J. N.; Aggarwal, R. J.; Matyi, R. J.; Moore, T. M.; Wetsel, A. E. *Phys. Rev. Lett.* **1988**, *60*, 535.
- (13) Brus, L. E. *J. Chem. Phys.* **1983**, *79*, 5566.
- (14) Brus, L. E. *J. Chem. Phys.* **1984**, *80*, 4403.
- (15) Freeman, R.; Willner, I. *Chem. Soc. Rev.* **2012**, *41*, 4067.
- (16) Kamat, P. V.; Scholes, G. D. *J. Phys. Chem. Lett.* **2016**, *7*, 584.
- (17) Murray, C. B.; Norris, D. J.; Bawendi, M. G. *J. Am. Chem. Soc.* **1993**, *115*, 8706.
- (18) Dabbousi, B. O.; Rodriguez-Viejo, J.; Mikulec, F. V.; Heine, J. R.; Mattoussi, H.; Ober, R.; Jensen, K. F.; Bawendi, M. G. *J. Phys. Chem. B* **1997**, *101*, 9463.
- (19) Chen, H.-S.; Lo, B.; Hwang, J.-Y.; Chang, G.-Y.; Chen, C.-M.; Tasi, S.-J.; Wang, S.-J. *J. Phys. Chem. B* **2004**, *108*, 17119.
- (20) Nozik, A. J.; Uchida, H.; Kamat, P. V.; Curtis, C. *Isr. J. Chem.* **1993**, *33*, 15.
- (21) Yu, P.; Beard, M. C.; Ellingson, R. J.; Ferrere, S.; Curtis, C.; Drexler, J.; Luiszer, F.; Nozik, A. J. *J. Phys. Chem. B* **2005**, *109*, 7084.
- (22) Cao; Banin, U. *J. Am. Chem. Soc.* **2000**, *122*, 9692.
- (23) Mičić, O. I.; Cheong, H. M.; Fu, H.; Zunger, A.; Sprague, J. R.; Mascarenhas, A.; Nozik, A. J. *J. Phys. Chem. B* **1997**, *101*, 4904.

- (24) Kelly, J. A.; Henderson, E. J.; Veinot, J. G. C. *Chem. Commun.* **2010**, *46*, 8704.
- (25) Heath, J. R.; Shiang, J. J.; Alivisatos, A. P. *J. Chem. Phys.* **1994**, *101*, 1607.
- (26) Xu, Y.; Al-Salim, N.; Bumby, C. W.; Tilley, R. D. *J. Am. Chem. Soc.* **2009**, *131*, 15990.
- (27) Deepa, K. G.; Nagaraju, J. *Mater. Sci. Eng. B* **2012**, *177*, 1023.
- (28) Ellingson, R. J.; Beard, M. C.; Johnson, J. C.; Yu, P. R.; Micic, O. I.; Nozik, A. J.; Shabaev, A.; Efros, A. L. *Nano Lett.* **2005**, *5*, 865.
- (29) Hoffmann, R. *Angew. Chem., Int. Ed.* **1987**, *26*, 846.
- (30) Roduner, E. *Chem. Soc. Rev.* **2006**, *35*, 583.
- (31) Brus, L. E.; Szajowski, P. F.; Wilson, W. L.; Harris, T. D.; Schuppler, S.; Citrin, P. H. *J. Am. Chem. Soc.* **1995**, *117*, 2915.
- (32) Freeman, R.; Girsh, J.; Willner, I. *ACS Appl. Mater. Interfaces* **2013**, *5*, 2815.
- (33) Resch-Genger, U.; Grabolle, M.; Cavaliere-Jaricot, S.; Nitschke, R.; Nann, T. *Nat. Meth.* **2008**, *5*, 763.
- (34) Sun, Q.; Wang, Y. A.; Li, L. S.; Wang, D.; Zhu, T.; Xu, J.; Yang, C.; Li, Y. *Nat. Photon.* **2007**, *1*, 717.
- (35) Michalet, X.; Pinaud, F. F.; Bentolila, L. A.; Tsay, J. M.; Doose, S.; Li, J. J.; Sundaresan, G.; Wu, A. M.; Gambhir, S. S.; Weiss, S. *Science* **2005**, *307*, 538.
- (36) Graeme Md, K. A.; Pollack Jr, M. D. F. C. V. *J. Emerg. Med.* **1998**, *16*, 45.
- (37) Graeme, K. A.; Pollack, C. V. *J. Emerg. Med.* **1998**, *16*, 171.
- (38) Godt, J.; Scheidig, F.; Grosse-Siestrup, C.; Esche, V.; Brandenburg, P.; Reich, A.; Groneberg, D. A. *J. Occup. Med. Toxicol.* **2006**, *1*, 1.
- (39) Exley, C. *J. Inorg. Biochem.* **1998**, *69*, 139.
- (40) Bhattacharjee, S.; Rietjens, I. M. C. M.; Singh, M. P.; Atkins, T. M.; Purkait, T. K.; Xu, Z.; Regli, S.; Shukaliak, A.; Clark, R. J.; Mitchell, B. S.; Alink, G. M.; Marcelis, A. T. M.; Fink, M. J.; Veinot, J. G. C.; Kauzlarich, S. M.; Zuilhof, H. *Nanoscale* **2013**, *5*, 4870.
- (41) Erogbogbo, F.; Yong, K.-T.; Roy, I.; Xu, G.; Prasad, P. N.; Swihart, M. T. *ACS Nano* **2008**, *2*, 873.
- (42) Park, J. H.; Gu, L.; von Maltzahn, G.; Ruoslahti, E.; Bhatia, S. N.; Sailor, M. J. *Nat. Mater.* **2009**, *8*, 331.
- (43) Parkhutik, V. *J. Porous Mat.* **2000**, *7*, 363.
- (44) Canham, L. T. *Appl. Phys. Lett.* **1990**, *57*, 1046.

- (45) Jane, A.; Dronov, R.; Hodges, A.; Voelcker, N. H. *Trends Biotechnol.* **2009**, *27*, 230.
- (46) Ottow, S.; Lehmann, V.; Föll, H. *J. Electrochem. Soc.* **1996**, *143*, 385.
- (47) Kobayashi, K.; Harraz, F. A.; Izuo, S.; Sakka, T.; Ogata, Y. H. *Phys. Status Solidi A* **2007**, *204*, 1321.
- (48) Harraz, F. A. *Sens. Actuators, B* **2014**, *202*, 897.
- (49) Kane, E. O. *Phys. Rev.* **1966**, *146*, 558.
- (50) Brus, L. *J. Phys. Chem.* **1994**, *98*, 3575.
- (51) Kasap, S. O. *Principles of Electronic Materials and Devices*; 2nd ed.; McGraw-Hill: New York, 2002.
- (52) Sa'ar, A. *Phys. Status Solidi C* **2011**, *8*, 1764.
- (53) Hybertsen, M. S. *Phys. Rev. Lett.* **1994**, *72*, 1514.
- (54) Hessel, C. M.; Reid, D.; Panthani, M. G.; Rasch, M. R.; Goodfellow, B. W.; Wei, J.; Fujii, H.; Akhavan, V.; Korgel, B. A. *Chem. Mater.* **2012**, *24*, 393.
- (55) Wolf, O.; Dasog, M.; Yang, Z.; Balberg, I.; Veinot, J. G. C.; Millo, O. *Nano Lett.* **2013**, *13*, 2516.
- (56) Dasog, M.; De los Reyes, G. B.; Titova, L. V.; Hegmann, F. A.; Veinot, J. G. C. *ACS Nano* **2014**, *8*, 9636.
- (57) Okamoto, H.; Kumai, Y.; Sugiyama, Y.; Mitsuoka, T.; Nakanishi, K.; Ohta, T.; Nozaki, H.; Yamaguchi, S.; Shirai, S.; Nakano, H. *J. Am. Chem. Soc.* **2010**, *132*, 2710.
- (58) Sugiyama, Y.; Okamoto, H.; Mitsuoka, T.; Morikawa, T.; Nakanishi, K.; Ohta, T.; Nakano, H. *J. Am. Chem. Soc.* **2010**, *132*, 5946.
- (59) Holmes, J. D.; Johnston, K. P.; Doty, R. C.; Korgel, B. A. *Science* **2000**, *287*, 1471.
- (60) Qi, J.; White, J. M.; Belcher, A. M.; Masumoto, Y. *Chem. Phys. Lett.* **2003**, *372*, 763.
- (61) Karbassian, F.; Mousavi, B. K.; Rajabali, S.; Talei, R.; Mohajerzadeh, S.; Asl-Soleimani, E. *J. Electron. Mater.* **2014**, *43*, 1271.
- (62) Veinot, J. G. C. *Chem. Commun.* **2006**, 4160.
- (63) Cheng, X.; Lowe, S. B.; Reece, P. J.; Gooding, J. J. *Chem. Soc. Rev.* **2014**, *43*, 2680.
- (64) Islam, M. A.; Purkait, T. K.; Veinot, J. G. C. *J. Am. Chem. Soc.* **2014**, *136*, 15130.
- (65) Walters, R. J.; Bourianoff, G. I.; Atwater, H. A. *Nat. Mater.* **2005**, *4*, 143.
- (66) Ding, Y.; Dong, Y.; Bapat, A.; Nowak, J. D.; Carter, C. B.; Kortshagen, U. R.; Campbell, S. A. *IEEE Trans. Electron Devices* **2006**, *53*, 2525.

- (67) Perez-Wurfl, I.; Hao, X.; Gentle, A.; Kim, D. H.; Conibeer, G.; Green, M. A. *Appl. Phys. Lett.* **2009**, *95*, 153506.
- (68) Priolo, F.; Gregorkiewicz, T.; Galli, M.; Krauss, T. F. *Nat. Nanotechnol.* **2014**, *9*, 19.
- (69) Iqbal, M.; Purkait, T. K.; Goss, G. G.; Bolton, J. R.; Gamal El-Din, M.; Veinot, J. G. C. *ACS Nano* **2016**, *10*, 5405.
- (70) McVey, B. F. P.; Tilley, R. D. *Acc. Chem. Res.* **2014**, *47*, 3045.
- (71) Manhat, B. A.; Brown, A. L.; Black, L. A.; Ross, J. B. A.; Fichter, K.; Vu, T.; Richman, E.; Goforth, A. M. *Chem. Mater.* **2011**, *23*, 2407.
- (72) Gonzalez, C. M.; Veinot, J. G. C. *J. Mater. Chem. C* **2016**, 4836.
- (73) Belomoin, G.; Therrien, J.; Smith, A.; Rao, S.; Twesten, R.; Chaieb, S.; Nayfeh, M. H.; Wagner, L.; Mitas, L. *Appl. Phys. Lett.* **2002**, *80*, 841.
- (74) Nayfeh, M. H.; Akcikir, O.; Belomoin, G.; Barry, N.; Therrien, J.; Gratton, E. *Appl. Phys. Lett.* **2000**, *77*, 4086.
- (75) Nayfeh, M. H.; Barry, N.; Therrien, J.; Akcikir, O.; Gratton, E.; Belomoin, G. *Appl. Phys. Lett.* **2001**, *78*, 1131.
- (76) Heintz, A. S.; Fink, M. J.; Mitchell, B. S. *Adv. Mater.* **2007**, *19*, 3984.
- (77) Heintz, A. S.; Fink, M. J.; Mitchell, B. S. *Appl. Organomet. Chem.* **2010**, *24*, 236.
- (78) Chaudhary, A.-L.; Sheppard, D. A.; Paskevicius, M.; Saunders, M.; Buckley, C. E. *RSC Adv.* **2014**, *4*, 21979.
- (79) Heath, J. R. *Science* **1992**, *258*, 1131.
- (80) Arul Dhas, N.; Raj, C. P.; Gedanken, A. *Chem. Mater.* **1998**, *10*, 3278.
- (81) Baldwin, R. K.; Pettigrew, K. A.; Ratai, E.; Augustine, M. P.; Kauzlarich, S. M. *Chem. Commun.* **2002**, 1822.
- (82) Wilcoxon, J. P.; Samara, G. A.; Provencio, P. N. *Phys. Rev. B* **1999**, *60*, 2704.
- (83) Warner, J. H.; Hoshino, A.; Yamamoto, K.; Tilley, R. D. *Angew. Chem., Int. Ed.* **2005**, *44*, 4550.
- (84) Tilley, R. D.; Yamamoto, K. *Adv. Mater.* **2006**, *18*, 2053.
- (85) Wang, J.; Sun, S.; Peng, F.; Cao, L.; Sun, L. *Chem. Commun.* **2011**, *47*, 4941.
- (86) Medintz, I. L.; Uyeda, H. T.; Goldman, E. R.; Mattoussi, H. *Nat. Mater.* **2005**, *4*, 435.
- (87) Mayeri, D.; Phillips, B. L.; Augustine, M. P.; Kauzlarich, S. M. *Chem. Mater.* **2001**, *13*, 765.

- (88) Bley, R. A.; Kauzlarich, S. M. *J. Am. Chem. Soc.* **1996**, *118*, 12461.
- (89) Yang, C.-S.; Bley, R. A.; Kauzlarich, S. M.; Lee, H. W. H.; Delgado, G. R. *J. Am. Chem. Soc.* **1999**, *121*, 5191.
- (90) Liu, Q.; Kauzlarich, S. M. *Mater. Sci. Eng. B* **2002**, *96*, 72.
- (91) Pettigrew, K. A.; Liu, Q.; Power, P. P.; Kauzlarich, S. M. *Chem. Mater.* **2003**, *15*, 4005.
- (92) Nolan, B. M.; Henneberger, T.; Waibel, M.; Fässler, T. F.; Kauzlarich, S. M. *Inorg. Chem.* **2015**, *54*, 396.
- (93) Dasog, M.; Kehrlé, J.; Rieger, B.; Veinot, J. G. C. *Angew. Chem., Int. Ed.* **2016**, *55*, 2322.
- (94) Murthy, T. U. M. S.; Miyamoto, N.; Shimbo, M.; Nishizawa, J. *J. Cryst. Growth* **1976**, *33*, 1.
- (95) Cannon, W. R.; Danforth, S. C.; Flint, J. H.; Haggerty, J. S.; Marra, R. A. *J. Am. Ceram. Soc.* **1982**, *65*, 324.
- (96) Cannon, W. R.; Danforth, S. C.; Haggerty, J. S.; Marra, R. A. *J. Am. Ceram. Soc.* **1982**, *65*, 330.
- (97) Ledoux, G.; Gong, J.; Huisken, F.; Guillois, O.; Reynaud, C. *Appl. Phys. Lett.* **2002**, *80*, 4834.
- (98) Ledoux, G.; Gong, J.; Huisken, F. *Appl. Phys. Lett.* **2001**, *79*, 4028.
- (99) Huisken, F.; Kohn, B.; Paillard, V. *Appl. Phys. Lett.* **1999**, *74*, 3776.
- (100) Li, X.; He, Y.; Swihart, M. T. *Langmuir* **2004**, *20*, 4720.
- (101) Hua, F.; Swihart, M. T.; Ruckenstein, E. *Langmuir* **2005**, *21*, 6054.
- (102) Tang, Z.; Palafox-Hernandez, J. P.; Law, W.-C.; E. Hughes, Z.; Swihart, M. T.; Prasad, P. N.; Knecht, M. R.; Walsh, T. R. *ACS Nano* **2013**, *7*, 9632.
- (103) Kortshagen, U. *J. Phys. D* **2009**, *42*.
- (104) Pi, X. D.; Liptak, R. W.; Nowak, J. D.; Wells, N. P.; Carter, C. B.; Campbell, S. A.; Kortshagen, U. *Nanotechnology* **2008**, *19*, 245.
- (105) Shimizu-Iwayama, T.; Kurumado, N.; Hole, D. E.; Townsend, P. D. *J. Appl. Phys.* **1998**, *83*, 6018.
- (106) Shimizu-Iwayama, T.; Nakao, S.; Saitoh, K.; Itoh, N. *J. Phys.: Condens. Matter* **1994**, *6*, L601.
- (107) Dusane, S.; Bhave, T.; Hullavard, S.; Bhoraskar, S. V.; Lokhare, S. *Solid State Commun.* **1999**, *111*, 431.

- (108) Calleja, W.; Falcony, C.; Torres, A.; Aceves, M.; Osorio, R. *Thin Solid Films* **1995**, *270*, 114.
- (109) Zhang, Q.; Bayliss, S. C.; Hutt, D. A. *Appl. Phys. Lett.* **1995**, *66*, 1977.
- (110) Liu, S.-M.; Yang; Sato, S.; Kimura, K. *Chem. Mater.* **2006**, *18*, 637.
- (111) Liu, S.-m.; Sato, S.; Kimura, K. *Langmuir* **2005**, *21*, 6324.
- (112) Hessel, C. M.; Henderson, E. J.; Veinot, J. G. C. *Chem. Mater.* **2006**, *18*, 6139.
- (113) Yang, Z.; Dobbie, A. R.; Cui, K.; Veinot, J. G. C. *J. Am. Chem. Soc.* **2012**, *134*, 13958.
- (114) Yang, Z.; Dobbie, A. R.; Veinot, J. G. C. *MRS Conf. Proc.* **2013**, *1536*, 207.
- (115) *Silicon Nanocrystals: Fundamentals, Synthesis and Applications*; Pavesi, L.; Turan, R., Eds.; Wiley-VCH: Weinheim, 2010.
- (116) Pavesi, L.; Dal Negro, L.; Mazzoleni, C.; Franzo, G.; Priolo, F. *Nature* **2000**, *408*, 440.
- (117) Kim, S.; Fisher, B.; Eisler, H.-J.; Bawendi, M. *J. Am. Chem. Soc.* **2003**, *125*, 11466.
- (118) Zhu, H.; Song, N.; Lian, T. *J. Am. Chem. Soc.* **2010**, *132*, 15038.
- (119) Talapin, D. V.; Lee, J.-S.; Kovalenko, M. V.; Shevchenko, E. V. *Chem. Rev.* **2010**, *110*, 389.
- (120) Dubois, F.; Mahler, B.; Dubertret, B.; Doris, E.; Mioskowski, C. *J. Am. Chem. Soc.* **2007**, *129*, 482.
- (121) Yu, W. W.; Chang, E.; Falkner, J. C.; Zhang, J.; Al-Somali, A. M.; Sayes, C. M.; Johns, J.; Drezek, R.; Colvin, V. L. *J. Am. Chem. Soc.* **2007**, *129*, 2871.
- (122) Lin, C.-A. J.; Sperling, R. A.; Li, J. K.; Yang, T.-Y.; Li, P.-Y.; Zanella, M.; Chang, W. H.; Parak, W. J. *Small* **2008**, *4*, 334.
- (123) Gaponik, N.; Talapin, D. V.; Rogach, A. L.; Hoppe, K.; Shevchenko, E. V.; Kornowski, A.; Eychmüller, A.; Weller, H. *J. Phys. Chem. B* **2002**, *106*, 7177.
- (124) Shavel, A.; Gaponik, N.; Eychmüller, A. *J. Phys. Chem. B* **2006**, *110*, 19280.
- (125) Yu, Y.; Rowland, C. E.; Schaller, R. D.; Korgel, B. A. *Langmuir* **2015**, *31*, 6886.
- (126) Purkait, T. K.; Iqbal, M.; Islam, M. A.; Mobarok, M. H.; Gonzalez, C. M.; Hadidi, L.; Veinot, J. G. C. *J. Am. Chem. Soc.* **2016**.
- (127) Zou, J.; Baldwin, R. K.; Pettigrew, K. A.; Kauzlarich, S. M. *Nano Lett.* **2004**, *4*, 1181.
- (128) Reboredo, F. A.; Galli, G. *J. Phys. Chem. B* **2005**, *109*, 1072.
- (129) Dasog, M.; Yang, Z.; Regli, S.; Atkins, T. M.; Faramus, A.; Singh, M. P.; Muthuswamy, E.; Kauzlarich, S. M.; Tilley, R. D.; Veinot, J. G. C. *ACS Nano* **2013**, *7*, 2676.

- (130) Dasog, M.; Bader, K.; Veinot, J. G. C. *Chem. Mater.* **2015**, *27*, 1153.
- (131) Buriak, J. M. *Chem. Rev.* **2002**, *102*, 1271.
- (132) Buriak, J. M. *Chem. Mater.* **2014**, *26*, 763.
- (133) *Silicon in Organic, Organometallic, and Polymer Chemistry*; Brook, M. A., Ed.; Wiley-Interscience, 1999.
- (134) Hunger, R.; Jaegermann, W.; Merson, A.; Shapira, Y.; Pettenkofer, C.; Rappich, J. *J. Phys. Chem. B* **2006**, *110*, 15432.
- (135) Yang, Z., University of Alberta, 2014.
- (136) Linford, M. R.; Chidsey, C. E. D. *J. Am. Chem. Soc.* **1993**, *115*, 12631.
- (137) Bateman, J. E.; Eagling, R. D.; Worrall, D. R.; Horrocks, B. R.; Houlton, A. *Angew. Chem., Int. Ed.* **1998**, *37*, 2683.
- (138) Boukherroub, R.; Morin, S.; Bensebaa, F.; Wayner, D. D. M. *Langmuir* **1999**, *15*, 3831.
- (139) Boiadjev, V. I.; Brown, G. M.; Pinnaduwege, L. A.; Goretzki, G.; Bonnesen, P. V.; Thundat, T. *Langmuir* **2005**, *21*, 1139.
- (140) Huck, L. A.; Buriak, J. M. *Langmuir* **2012**, *28*, 16285.
- (141) Cicero, R. L.; Linford, M. R.; Chidsey, C. E. D. *Langmuir* **2000**, *16*, 5688.
- (142) Kelly, J. A.; Veinot, J. G. C. *ACS Nano* **2010**, *4*, 4645.
- (143) Stewart, M. P.; Buriak, J. M. *J. Am. Chem. Soc.* **2001**, *123*, 7821.
- (144) Kelly, J. A.; Shukaliak, A. M.; Fleischauer, M. D.; Veinot, J. G. C. *J. Am. Chem. Soc.* **2011**, *133*, 9564.
- (145) Sun, Q. Y.; de Smet, L. C. P. M.; van Lagen, B.; Wright, A.; Zuilhof, H.; Sudhölter, E. J. R. *Angew. Chem., Int. Ed.* **2004**, *43*, 1352.
- (146) Nelles, J.; Sendor, D.; Ebbers, A.; Petrat, F.; Wiggers, H.; Schulz, C.; Simon, U. *Colloid Polym. Sci.* **2007**, *285*, 729.
- (147) Höhle, I. M. D.; Kehrlé, J.; Helbich, T.; Yang, Z.; Veinot, J. G. C.; Rieger, B. *Chem. - Eur. J.* **2014**, *20*, 4212.
- (148) Yang, Z.; Gonzalez, C. M.; Purkait, T. K.; Iqbal, M.; Meldrum, A.; Veinot, J. G. C. *Langmuir* **2015**, *31*, 10540.
- (149) Wheeler, L. M.; Anderson, N. C.; Palomaki, P. K. B.; Blackburn, J. L.; Johnson, J. C.; Neale, N. R. *Chem. Mater.* **2015**, *27*, 6869.
- (150) Wang, D.; Buriak, J. M. *Langmuir* **2006**, *22*, 6214.

- (151) Buriak, J. M.; Stewart, M. P.; Geders, T. W.; Allen, M. J.; Choi, H. C.; Smith, J.; Raftery, D.; Canham, L. T. *J. Am. Chem. Soc.* **1999**, *121*, 11491.
- (152) Purkait, T. K.; Iqbal, M.; Wahl, M. H.; Gottschling, K.; Gonzalez, C. M.; Islam, M. A.; Veinot, J. G. C. *J. Am. Chem. Soc.* **2014**, *136*, 17914.
- (153) Sieval, A. B.; Linke, R.; Sieval, H. A. B.; Sudhölter, E. J. R. *Adv. Mater.* **2000**, *12*, 1457.
- (154) Tilley, R. D.; Warner, J. H.; Yamamoto, K.; Matsui, I.; Fujimori, H. *Chem. Commun.* **2005**, 1833.
- (155) Sugimura, H.; Mo, S.; Yamashiro, K.; Ichii, T.; Murase, K. *J. Phys. Chem. C* **2013**, *117*, 2480.
- (156) Liu, F.; Lubber, E. J.; Huck, L. A.; Olsen, B. C.; Buriak, J. M. *ACS Nano* **2015**, *9*, 2184.
- (157) Ciampi, S.; Harper, J. B.; Gooding, J. J. *Chem. Soc. Rev.* **2010**, *39*, 2158.
- (158) Yang, Z.; Iqbal, M.; Dobbie, A. R.; Veinot, J. G. C. *J. Am. Chem. Soc.* **2013**, *135*, 17595.
- (159) Terry, J.; Linford, M. R.; Wigren, C.; Cao, R.; Pianetta, P.; Chidsey, C. E. D. *Appl. Phys. Lett.* **1997**, *71*, 1058.
- (160) Effenberger, F.; Gotz, G.; Bidlingmaier, B.; Wezstein, M. *Angew. Chem., Int. Ed.* **1998**, *37*, 2462.
- (161) Stewart, M. P.; Buriak, J. M. *Angew. Chem., Int. Ed.* **1998**, *37*, 3257.
- (162) Lewis, L. N. *J. Am. Chem. Soc.* **1990**, *112*, 5998.
- (163) Zazzera, L. A.; Evans, J. F.; Deruelle, M.; Tirrell, M.; Kessel, C. R.; McKeown, P. J. *Electrochem. Soc.* **1997**, *144*, 2184.
- (164) Terry, J.; Linford, M. R.; Wigren, C.; Cao, R.; Pianetta, P.; Chidsey, C. E. D. *J. Appl. Phys.* **1999**, *85*, 213.
- (165) Effenberger, F.; Götz, G.; Bidlingmaier, B.; Wezstein, M. *Angew. Chem., Int. Ed.* **1998**, *37*, 2462.
- (166) Wang, X.; Ruther, R. E.; Streifer, J. A.; Hamers, R. J. *J. Am. Chem. Soc.* **2010**, *132*, 4048.
- (167) Eves, B. J.; Lopinski, G. P. *Langmuir* **2006**, *22*, 3180.
- (168) Cicero, R. L.; Chidsey, C. E. D.; Lopinski, G. P.; Wayner, D. D. M.; Wolkow, R. A. *Langmuir* **2002**, *18*, 305.
- (169) Coulter, S. K.; Schwartz, M. P.; Hamers, R. J. *J. Phys. Chem. B* **2001**, *105*, 3079.
- (170) Lai, Y.-H.; Yeh, C.-T.; Yeh, C.-C.; Hung, W.-H. *J. Phys. Chem. B* **2003**, *107*, 9351.
- (171) Zhu, Z.; Srivastava, A.; Osgood, R. M. *J. Phys. Chem. B* **2003**, *107*, 13939.

- (172) Balakumar, A.; Lysenko, A. B.; Carcel, C.; Malinovskii, V. L.; Gryko, D. T.; Schweikart, K.-H.; Loewe, R. S.; Yasseri, A. A.; Liu, Z.; Bocian, D. F.; Lindsey, J. S. *J. Org. Chem.* **2004**, *69*, 1435.
- (173) Yasseri, A. A.; Syomin, D.; Loewe, R. S.; Lindsey, J. S.; Zaera, F.; Bocian, D. F. *J. Am. Chem. Soc.* **2004**, *126*, 15603.
- (174) Hu, M.; Liu, F.; Buriak, J. M. *ACS Appl. Mater. Interfaces* **2016**, *8*, 11091.
- (175) Hacker, C. A. *Solid-State Electronics* **2010**, *54*, 1657.
- (176) Sano, H.; Ohno, K.; Ichii, T.; Murase, K.; Sugimura, H. *Japanese Journal of Applied Physics* **2010**, *49*, 01AE09.
- (177) Lam, H. Y.; Nadine, G.-H.; Christopher, D. Z.; Christina, A. H.; Curt, A. R.; James, G. K. *J. Phys.: Condens. Matter* **2008**, *20*, 374114.
- (178) Lou, J. L.; Shiu, H. W.; Chang, L. Y.; Wu, C. P.; Soo, Y.-L.; Chen, C.-H. *Langmuir* **2011**, *27*, 3436.
- (179) Huang, Y.-S.; Chen, C.-H.; Chen, C.-H.; Hung, W.-H. *ACS Appl. Mater. Interfaces* **2013**, *5*, 5771.
- (180) Buriak, J. M.; Sikder, M. D. H. *J. Am. Chem. Soc.* **2015**, *137*, 9730.
- (181) Linford, M. R.; Fenter, P.; Eisenberger, P. M.; Chidsey, C. E. D. *J. Am. Chem. Soc.* **1995**, *117*, 3145.
- (182) de Smet, L. C. P. M.; Zuilhof, H.; Sudhölter, E. J. R.; Lie, L. H.; Houlton, A.; Horrocks, B. R. *J. Phys. Chem. B* **2005**, *109*, 12020.
- (183) Chatgililoglu, C. *Helv. Chim. Acta* **2006**, *89*, 2387.
- (184) Dénès, F.; Pichowicz, M.; Povie, G.; Renaud, P. *Chem. Rev.* **2014**, *114*, 2587.
- (185) Song, J. H.; Sailor, M. J. *J. Am. Chem. Soc.* **1998**, *120*, 2376.
- (186) Höhle, I. M. D.; Angi, A.; Sinelnikov, R.; Veinot, J. G. C.; Rieger, B. *Chem. - Eur. J.* **2015**, *21*, 2755.
- (187) Ang, A.; Sinelnikov, R.; Meldrum, A.; Veinot, J. G. C.; Balberg, I.; Azulay, D.; Millo, O.; Rieger, B. *Nanoscale* **2016**, *8*, 7849.
- (188) Yang, Z.; Wahl, M. H.; Veinot, J. G. C. *Can. J. Chem.* **2014**, *92*, 951.
- (189) Ojima, I.; Clos, N.; Donovan, R. J.; Ingallina, P. *Organometallics* **1990**, *9*, 3127.
- (190) Holland, J. M.; Stewart, M. P.; Allen, M. J.; Buriak, J. M. *J. Solid State Chem.* **1999**, *147*, 251.

- (191) Li, Y.-H.; Buriak, J. M. *Inorg. Chem.* **2006**, *45*, 1096.
- (192) Dasog, M.; Veinot, J. G. C. *Phys. Status Solidi B* **2014**, *251*, 2216.
- (193) Bansal, A.; Li, X.; Lauermann, I.; Lewis, N. S.; Yi, S. I.; Weinberg, W. H. *J. Am. Chem. Soc.* **1996**, *118*, 7225.
- (194) Bansal, A.; Lewis, N. S. *J. Phys. Chem. B* **1998**, *102*, 1067.
- (195) Zhai, Y.; Dasog, M.; Snitynsky, R. B.; Purkait, T. K.; Aghajamali, M.; Hahn, A. H.; Sturdy, C. B.; Lowary, T. L.; Veinot, J. G. C. *J. Mater. Chem. B* **2014**, *2*, 8427.
- (196) Li, S. T.; Silvers, S. J.; ElShall, M. S. *J. Phys. Chem. B* **1997**, *101*, 1794.
- (197) Bell, J. P.; Cloud, J. E.; Cheng, J.; Ngo, C.; Kodambaka, S.; Sellinger, A.; Ratanathanawongs Williams, S. K.; Yang, Y. *RSC Adv.* **2014**, *4*, 51105.
- (198) Wang, L.; Li, Q.; Wang, H.-Y.; Huang, J.-C.; Zhang, R.; Chen, Q.-D.; Xu, H.-L.; Han, W.; Shao, Z.-Z.; Sun, H.-B. *Light Sci Appl* **2015**, *4*, e245.
- (199) Wolkin, M. V.; Jorne, J.; Fauchet, P. M.; Allan, G.; Delerue, C. *Phys. Rev. Lett.* **1999**, *82*, 197.
- (200) Kanemitsu, Y.; Ogawa, T.; Shiraishi, K.; Takeda, K. *Phys. Rev. B* **1993**, *48*, 4883.
- (201) Puzder, A.; Williamson, A. J.; Grossman, J. C.; Galli, G. *Phys. Rev. Lett.* **2002**, *88*, 097401.
- (202) Koch, F.; Petrova-Koch, V.; Muschik, T. *J. Lumin.* **1993**, *57*, 271.
- (203) O'Reilly, E. P.; Robertson, J. *Phys. Rev. B* **1983**, *27*, 3780.
- (204) DeBenedetti, W. J. I.; Chiu, S.-K.; Radlinger, C. M.; Ellison, R. J.; Manhat, B. A.; Zhang, J. Z.; Shi, J.; Goforth, A. M. *J. Phys. Chem. C* **2015**, *119*, 9595.
- (205) Anc, M. J.; Pickett, N. L.; Gresty, N. C.; Harris, J. A.; Mishra, K. C. *ECS J. Solid State Sci. Technol.* **2013**, *2*, R3071.
- (206) Biju, V.; Itoh, T.; Anas, A.; Sujith, A.; Ishikawa, M. *Anal. Bioanal. Chem.* **2008**, *391*, 2469.
- (207) Medintz, I. L.; Clapp, A. R.; Mattoussi, H.; Goldman, E. R.; Fisher, B.; Mauro, J. M. *Nat. Mater.* **2003**, *2*, 630.
- (208) Lou, Y.; Zhao, Y.; Chen, J.; Zhu, J.-J. *J. Mater. Chem. C* **2014**, *2*, 595.
- (209) Wu, P.; Zhao, T.; Wang, S.; Hou, X. *Nanoscale* **2014**, *6*, 43.
- (210) Freeman, R.; Finder, T.; Bahshi, L.; Gill, R.; Willner, I. *Adv. Mater.* **2012**, *24*, 6416.
- (211) Derfus, A. M.; Chan, W. C. W.; Bhatia, S. N. *Nano Lett.* **2004**, *4*, 11.
- (212) Sailor, M. J.; Wu, E. C. *Adv. Funct. Mater.* **2009**, *19*, 3195.
- (213) *Principles of Fluorescence Spectroscopy*; 3rd ed.; Lakowicz, J. R., Ed.; Springer US, 2006.

- (214) Silvi, S.; Credi, A. *Chem. Soc. Rev.* **2015**, *44*, 4275.
- (215) Yue, Z.; Lisdat, F.; Parak, W. J.; Hickey, S. G.; Tu, L.; Sabir, N.; Dorfs, D.; Bigall, N. C. *ACS Appl. Mater. Interfaces* **2013**, *5*, 2800.
- (216) Wu, P.; Hou, X.; Xu, J.-J.; Chen, H.-Y. *Nanoscale* **2016**.
- (217) Goswami, S.; Das, A. K.; Aich, K.; Manna, A.; Maity, S.; Khanra, K.; Bhattacharyya, N. *Analyst* **2013**, *138*, 4593.
- (218) Qian, J.; Wang, K.; Wang, C.; Hua, M.; Yang, Z.; Liu, Q.; Mao, H.; Wang, K. *Analyst* **2015**, *140*, 7434.
- (219) Lin, J.; Wang, Q. *RSC Adv.* **2015**, *5*, 27458.
- (220) Lowe, S. B.; Dick, J. A. G.; Cohen, B. E.; Stevens, M. M. *ACS Nano* **2012**, *6*, 851.
- (221) Wu, C.-S.; Khaing Oo, M. K.; Fan, X. *ACS Nano* **2010**, *4*, 5897.
- (222) Germain, M. E.; Knapp, M. J. *Chem. Soc. Rev.* **2009**, *38*, 2543.
- (223) Salinas, Y.; Martinez-Manez, R.; Marcos, M. D.; Sancenon, F.; Costero, A. M.; Parra, M.; Gil, S. *Chem. Soc. Rev.* **2012**, *41*, 1261.
- (224) Content, S.; Trogler, W. C.; Sailor, M. J. *Chem. - Eur. J.* **2000**, *6*, 2205.
- (225) Germanenko, I. N.; Li, S.; El-Shall, M. S. *J. Phys. Chem. B* **2001**, *105*, 59.
- (226) Gonzalez, C. M.; Iqbal, M.; Dasog, M.; Piercey, D. G.; Lockwood, R.; Klapotke, T. M.; Veinot, J. G. C. *Nanoscale* **2014**, *6*, 2608.
- (227) Ban, R.; Zheng, F.; Zhang, J. *Anal. Methods* **2015**, *7*, 1732.
- (228) Nguyen, A.; Gonzalez, C. M.; Sinelnikov, R.; Newman, W.; Sun, S.; Lockwood, R.; Veinot, J. G.; Meldrum, A. *Nanotechnology* **2016**, *27*, 105501.
- (229) Laughland, O.; Felton, R. In *The Guardian* 2016.
- (230) Sam, S. S.; Chazalviel, J.-N. J. N.; Gouget-Laemmel, A. C. A. C.; Ozanam, F. F.; Etcheberry, A. A.; Gabouze, N.-e. N. *Nanoscale Res. Lett.* **2011**, *6*, 1.
- (231) Shtenberg, G.; Massad-Ivanir, N.; Segal, E. *Analyst* **2015**, *140*, 4507.
- (232) Zhang, J.; Yu, S.-H. *Nanoscale* **2014**, *6*, 4096.
- (233) Zhao, J.; Deng, J.; Yi, Y.; Li, H.; Zhang, Y.; Yao, S. *Talanta* **2014**, *125*, 372.
- (234) Campos, B. B.; Algarra, M.; Alonso, B.; Casado, C. M.; Jiménez-Jiménez, J.; Rodríguez-Castellón, E.; Esteves da Silva, J. C. G. *Talanta* **2015**, *144*, 862.
- (235) Liao, B.; Wang, W.; Deng, X.; He, B.; Zeng, W.; Tang, Z.; Liu, Q. *RSC Adv.* **2016**, *6*, 14465.

- (236) Radhakumary, C.; Sreenivasan, K. *Anal. Chem.* **2011**, *83*, 2829.
- (237) Palestino, G.; Agarwal, V.; Aulombard, R.; Pérez, E.; Gergely, C. *Langmuir* **2008**, *24*, 13765.
- (238) López-García, J.; Martín-Palma, R. J.; Manso, M.; Martínez-Duart, J. M. *Sens. Actuators, B* **2007**, *126*, 82.
- (239) Yi, Y.; Deng, J.; Zhang, Y.; Li, H.; Yao, S. *Chem. Commun.* **2013**, *49*, 612.
- (240) Wu, P.; He, Y.; Wang, H.-F.; Yan, X.-P. *Anal. Chem.* **2010**, *82*, 1427.
- (241) Chen, Q.; Liu, M.; Zhao, J.; Peng, X.; Chen, X.; Mi, N.; Yin, B.; Li, H.; Zhang, Y.; Yao, S. *Chem. Commun.* **2014**, *50*, 6771.
- (242) Robinson, D. L.; Hermans, A.; Seipel, A. T.; Wightman, R. M. *Chem. Rev.* **2008**, *108*, 2554.
- (243) Yu, C.; Luo, M.; Zeng, F.; Zheng, F.; Wu, S. *Chem. Commun.* **2011**, *47*, 9086.
- (244) Zhang, X.; Chen, X.; Kai, S.; Wang, H.-Y.; Yang, J.; Wu, F.-G.; Chen, Z. *Anal. Chem.* **2015**, *87*, 3360.
- (245) Mu, Q.; Xu, H.; Li, Y.; Ma, S.; Zhong, X. *Analyst* **2014**, *139*, 93.
- (246) Jackowska, K.; Kryszinski, P. *Anal. Bioanal. Chem.* **2012**, *405*, 3753.
- (247) Liu, J.; Wang, X.; Peng, Q.; Li, Y. *Adv. Mater.* **2005**, *17*, 764.
- (248) Gao, J.; Gao, T.; Sailor, M. J. *Appl. Phys. Lett.* **2000**, *77*, 901.
- (249) Baratto, C.; Comini, E.; Faglia, G.; Sberveglieri, G.; Di Francia, G.; De Filippo, F.; La Ferrara, V.; Quercia, L.; Lancellotti, L. *Sens. Actuators, B* **2000**, *65*, 257.
- (250) Min, H.-K.; Yang, H.-S.; Cho, S. M. *Sens. Actuators, B* **2000**, *67*, 199.
- (251) Zhang, Z. H.; Lockwood, R.; Veinot, J. G. C.; Meldrum, A. *Sens. Actuators, B* **2013**, *181*, 523.
- (252) Verma, R.; Gupta, B. D. *Analyst* **2013**, *138*, 7254.
- (253) Gan, T.; Shi, Z.; Sun, J.; Liu, Y. *Talanta* **2014**, *121*, 187.
- (254) van den Bogaard, A. E.; Stobberingh, E. E. *Int. J. Antimicrob. Agents* **2000**, *14*, 327.
- (255) Zhang, J.; Wu, Y.; Zhang, B.; Li, M.; Jia, S.; Jiang, S.; Zhou, H.; Zhang, Y.; Zhang, C.; Turner, A. P. F. *Anal. Lett.* **2012**, *45*, 986.
- (256) Yang, F.; Wild, J. R.; Russell, A. J. *Biotechnol. Prog.* **1995**, *11*, 471.
- (257) Chen, H.; Zuo, X.; Su, S.; Tang, Z.; Wu, A.; Song, S.; Zhang, D.; Fan, C. *Analyst* **2008**, *133*, 1182.

- (258) Gong, J.; Miao, X.; Zhou, T.; Zhang, L. *Talanta* **2011**, *85*, 1344.
- (259) Yi, Y.; Zhu, G.; Liu, C.; Huang, Y.; Zhang, Y.; Li, H.; Zhao, J.; Yao, S. *Anal. Chem.* **2013**, *85*, 11464.
- (260) Du, D.; Chen, S.; Song, D.; Li, H.; Chen, X. *Biosens. Bioelectron.* **2008**, *24*, 475.
- (261) Gao, X.; Tang, G.; Su, X. *Biosens. Bioelectron.* **2012**, *36*, 75.
- (262) Rotiroti, L.; Stefano, L. D.; Rendina, I.; Moretti, L.; Rossi, A. M.; Piccolo, A. *Biosens. Bioelectron.* **2005**, *20*, 2136.
- (263) De Stefano, L.; Moretti, L.; Rendina, I.; Rotiroti, L. *Sens. Actuators, B* **2005**, *111–112*, 522.
- (264) Qu, F.; Li, N. B.; Luo, H. Q. *Langmuir* **2013**, *29*, 1199.
- (265) Tomasulo, M.; Yildiz, I.; Raymo, F. M. *J. Phys. Chem. B* **2006**, *110*, 3853.
- (266) Snee, P. T.; Somers, R. C.; Nair, G.; Zimmer, J. P.; Bawendi, M. G.; Nocera, D. G. *J. Am. Chem. Soc.* **2006**, *128*, 13320.
- (267) Dennis, A. M.; Rhee, W. J.; Sotto, D.; Dublin, S. N.; Bao, G. *ACS Nano* **2012**, *6*, 2917.
- (268) Tang, R.; Lee, H.; Achilefu, S. *J. Am. Chem. Soc.* **2012**, *134*, 4545.
- (269) Feng, Y.; Liu, Y.; Su, C.; Ji, X.; He, Z. *Sens. Actuators, B* **2014**, *203*, 795.
- (270) Heitmann, J.; Müller, F.; Zacharias, M.; Gösele, U. *Adv. Mater.* **2005**, *17*, 795.
- (271) Pi, X. D.; Liptak, R. W.; Deneen Nowak, J.; Wells, N. P.; Carter, C. B.; Campbell, S. A.; Kortshagen, U. *Nanotechnology* **2008**, *19*, 245603.
- (272) Liu, C. Y.; Holman, Z. C.; Kortshagen, U. R. *Nano Lett.* **2009**, *9*, 449.
- (273) Pi, X.; Zhang, L.; Yang, D. *J. Phys. Chem. C* **2012**, *116*, 21240.
- (274) Cheng, K.-Y.; Anthony, R.; Kortshagen, U. R.; Holmes, R. J. *Nano Lett.* **2010**, *10*, 1154.
- (275) Zhong, Y.; Peng, F.; Bao, F.; Wang, S.; Ji, X.; Yang, L.; Su, Y.; Lee, S.-T.; He, Y. *J. Am. Chem. Soc.* **2013**, *135*, 8350.
- (276) Borsella, E.; D'Amato, R.; Falconieri, M.; Trave, E.; Panariti, A.; Rivolta, I. *J. Mater. Res.* **2013**, *28*, 193.
- (277) Kim, H.; Seo, M.; Park, M.-H.; Cho, J. *Angew. Chem., Int. Ed.* **2010**, *49*, 2146.
- (278) Graetz, J.; Ahn, C. C.; Yazami, R.; Fultz, B. *Electrochem. Solid-State Lett.* **2003**, *6*, A194.
- (279) Wang, R.; Pi, X.; Yang, D. *J. Phys. Chem. C* **2012**, *116*, 19434.
- (280) Weeks, S. L.; Macco, B.; van de Sanden, M. C. M.; Agarwal, S. *Langmuir* **2012**, *28*, 17295.

- (281) Jariwala, B. N.; Dewey, O. S.; Stradins, P.; Ciobanu, C. V.; Agarwal, S. *ACS Appl. Mater. Interfaces* **2011**, *3*, 3033.
- (282) Yu, Y.; Hessel, C. M.; Bogart, T. D.; Panthani, M. G.; Rasch, M. R.; Korgel, B. A. *Langmuir* **2013**, *29*, 1533.
- (283) Yu, Y.; Korgel, B. A. *Langmuir* **2015**.
- (284) Moran, I. W.; Carter, K. R. *Langmuir* **2009**, *25*, 9232.
- (285) Lee, M. V.; Scipioni, R.; Boero, M.; Silvestrelli, P. L.; Ariga, K. *Phys. Chem. Chem. Phys.* **2011**, *13*, 4862.
- (286) Linnros, J.; Lalic, N.; Galeckas, A.; Grivickas, V. *J. Appl. Phys.* **1999**, *86*, 6128.
- (287) Berberan-Santos, M. N.; Bodunov, E. N.; Valeur, B. *Chem. Phys.* **2005**, *315*, 171.
- (288) van Driel, A. F.; Nikolaev, I. S.; Vergeer, P.; Lodahl, P.; Vanmaekelbergh, D.; Vos, W. L. *Phys. Rev. B: Condens. Matter Mater. Phys.* **2007**, *75*, 035329.
- (289) Avramov, P. V.; Fedorov, D. G.; Sorokin, P. B.; Chernozatonskii, L. A.; Gordon, M. S. *Los Alamos Natl. Lab., Prepr. Arch., Condens. Matter* **2007**, *1*.
- (290) Odian, G. *Principles of Polymerization*, 2004.
- (291) Smith, B. C. *Infrared Spectral Interpretation: A Systematic Approach*, 1998.
- (292) Sieval, A. B.; Demirel, A. L.; Nissink, J. W. M.; Linford, M. R.; van der Maas, J. H.; de Jeu, W. H.; Zuilhof, H.; Sudhölter, E. J. R. *Langmuir* **1998**, *14*, 1759.
- (293) Clark, R. J.; Dang, M. K. M.; Veinot, J. G. C. *Langmuir* **2010**, *26*, 15657.
- (294) Delpuech, N.; Mazouzi, D.; Dupré, N.; Moreau, P.; Cerbelaud, M.; Bridel, J. S.; Badot, J. C.; De Vito, E.; Guyomard, D.; Lestriez, B.; Humbert, B. *J. Phys. Chem. C* **2014**, *118*, 17318.
- (295) O'Keefe, P.; Aoyagi, Y.; Komuro, S.; Kato, T.; Morikawa, T. *Appl. Phys. Lett.* **1995**, *66*, 836.
- (296) Pitters, J. L.; Piva, P. G.; Tong, X.; Wolkow, R. A. *Nano Lett.* **2003**, *3*, 1431.
- (297) Guisinger, N. P.; Greene, M. E.; Basu, R.; Baluch, A. S.; Hersam, M. C. *Nano Lett.* **2004**, *4*, 55.
- (298) Pitters, J. L.; Wolkow, R. A. *J. Am. Chem. Soc.* **2005**, *127*, 48.
- (299) Ball, P. *Nat. Mater.* **2005**, *4*, 119.
- (300) Cava, R. J. *Nature* **2006**, *444*, 427.
- (301) Michl, J. *Chem. Rev.* **1995**, *95*, 1135.

- (302) Cullis, A. G.; Canham, L. T. *Nature* **1991**, 353, 335.
- (303) Li, X.; He, Y.; Talukdar, S. S.; Swihart, M. T. *Langmuir* **2003**, 19, 8490.
- (304) Kocevski, V.; Eriksson, O.; Rusz, J. *Phys. Rev. B* **2013**, 87, 245401.
- (305) Veinot, J. G. C. *Chem. Commun.* **2006**, 4160.
- (306) Warner, J. H.; Hoshino, A.; Yamamoto, K.; Tilley, R. D. *Angew. Chem., Int. Ed.* **2005**, 44, 4550.
- (307) Hua, F.; Swihart, M. T.; Ruckenstein, E. *Langmuir* **2005**, 21, 6054.
- (308) Gergel-Hackett, N.; Zangmeister, C. D.; Hacker, C. A.; Richter, L. J.; Richter, C. A. *J. Am. Chem. Soc.* **2008**, 130, 4259.
- (309) Barltrop, J. A.; Hayes, P. M.; Calvin, M. *J. Am. Chem. Soc.* **1954**, 76, 4348.
- (310) Bucher, G.; Lu, C.; Sander, W. *ChemPhysChem* **2005**, 6, 2607.
- (311) Smissman, E. E.; Sorenson, J. R. J. *J. Org. Chem.* **1965**, 30, 4008.
- (312) Brown, P. R.; Edwards, J. O. *J. Org. Chem.* **1969**, 34, 3131.
- (313) Kisanuki, A.; Kimpara, Y.; Oikada, Y.; Kado, N.; Matsumoto, M.; Endo, K. *J. Polym. Sci. A Polym. Chem.* **2010**, 48, 5247.
- (314) Palui, G.; Avellini, T.; Zhan, N.; Pan, F.; Gray, D.; Alabugin, I.; Mattoussi, H. *J. Am. Chem. Soc.* **2012**, 134, 16370.
- (315) Wang, W.; Kapur, A.; Ji, X.; Safi, M.; Palui, G.; Palomo, V.; Dawson, P. E.; Mattoussi, H. *J. Am. Chem. Soc.* **2015**, 137, 5438.
- (316) Aldeek, F.; Hawkins, D.; Palomo, V.; Safi, M.; Palui, G.; Dawson, P. E.; Alabugin, I.; Mattoussi, H. *J. Am. Chem. Soc.* **2015**, 137, 2704.
- (317) Weeks, S. L.; Macco, B.; van de Sanden, M. C. M.; Agarwal, S. *Langmuir* **2012**, 28, 17295.
- (318) Jariwala, B. N.; Dewey, O. S.; Stradins, P.; Ciobanu, C. V.; Agarwal, S. *ACS Appl. Mater. Interfaces* **2011**, 3, 3033.
- (319) Socrates, G. *Infrared Characteristic Group Frequencies: Tables and Charts*, 1994.
- (320) Yu, Y.; Korgel, B. A. *Langmuir* **2015**, 31, 6532.
- (321) Bhartia, B.; Puniredd, S. R.; Jayaraman, S.; Gandhimathi, C.; Sharma, M.; Kuo, Y.-C.; Chen, C.-H.; Reddy, V. J.; Troadec, C.; Srinivasan, M. P. *ACS Appl. Mater. Interfaces* **2016**, 8, 24933.
- (322) Lai, Y.-H.; Yeh, C.-T.; Lin, Y.-H.; Hung, W.-H. *Surf. Sci.* **2002**, 519, 150.
- (323) Kachian, J. S.; Tannaci, J.; Wright, R. J.; Tilley, T. D.; Bent, S. F. *Langmuir* **2011**, 27, 179.

- (324) Ardalan, P.; Musgrave, C. B.; Bent, S. F. *Langmuir* **2009**, *25*, 2013.
- (325) Heister, K.; Zharnikov, M.; Grunze, M.; Johansson, L. S. O. *J. Phys. Chem. B* **2001**, *105*, 4058.
- (326) Bensebaa, F.; Zhou, Y.; Deslandes, Y.; Kruss, E.; Ellis, T. H. *Surf. Sci. Lett.* **1998**, *405*, L472.
- (327) Subramanian, H.; Moorthy, R.; Sibi, M. P. *Angew. Chem., Int. Ed.* **2014**, *53*, 13660.
- (328) McDonough, J. E.; Weir, J. J.; Sukcharoenphon, K.; Hoff, C. D.; Kryatova, O. P.; Rybak-Akimova, E. V.; Scott, B. L.; Kubas, G. J.; Mendiratta, A.; Cummins, C. C. *J. Am. Chem. Soc.* **2006**, *128*, 10295.
- (329) Cheng, X.; Lowe, S. B.; Ciampi, S.; Magenau, A.; Gaus, K.; Reece, P. J.; Gooding, J. J. *Langmuir* **2014**, *30*, 5209.
- (330) Yang, Z.; De los Reyes, G. B.; Titova, L. V.; Sychugov, I.; Dasog, M.; Linnros, J.; Hegmann, F. A.; Veinot, J. G. C. *ACS Photonics* **2015**, *2*, 595.
- (331) Dang, H.-S.; Roberts, B. P. *Tetrahedron Lett.* **1995**, *36*, 2875.
- (332) Haque, M. B.; Roberts, B. P. *Tetrahedron Lett.* **1996**, *37*, 9123.
- (333) Dang, H.-S.; Kim, K.-M.; P. Roberts, B. *Chem. Commun.* **1998**, 1413.
- (334) Balan, B.; Vijayakumar, C.; Tsuji, M.; Saeki, A.; Seki, S. *J. Phys. Chem. B* **2012**, *116*, 10371.
- (335) Håkansson, K.; Coorey, R. V.; Zubarev, R. A.; Talrose, V. L.; Håkansson, P. *J. Mass Spectrom.* **2000**, *35*, 337.
- (336) Najarro, M.; Davila Morris, M. E.; Staymates, M. E.; Fletcher, R.; Gillen, G. *Analyst* **2012**, *137*, 2614.
- (337) Sylvia, J. M.; Janni, J. A.; Klein, J. D.; Spencer, K. M. *Anal. Chem.* **2000**, *72*, 5834.
- (338) Luggar, R. D.; Farquharson, M. J.; Horrocks, J. A.; Lacey, R. J. *X-Ray Spectrom.* **1998**, *27*, 87.
- (339) Feng, J.; Li, Y.; Yang, M. *Sens. Actuators, B* **2010**, *145*, 438.
- (340) Fierro-Mercado, P. M.; Hernandez-Rivera, S. P. *Int. J. Spectrosc.* **2012**, *2012*, 7.
- (341) Nergiz, S. Z.; Gandra, N.; Farrell, M. E.; Tian, L.; Pellegrino, P. M.; Singamaneni, S. *J. Mater. Chem. A* **2013**, *1*, 6543.
- (342) Tu, R.; Liu, B.; Wang, Z.; Gao, D.; Wang, F.; Fang, Q.; Zhang, Z. *Anal. Chem.* **2008**, *80*, 3458.

- (343) Costa-Fernández, J. M.; Pereiro, R.; Sanz-Medel, A. *TrAC, Trends Anal. Chem.* **2006**, *25*, 207.
- (344) Zhang, K.; Zhou, H.; Mei, Q.; Wang, S.; Guan, G.; Liu, R.; Zhang, J.; Zhang, Z. *J. Am. Chem. Soc.* **2011**, *133*, 8424.
- (345) Ma, Y.; Li, H.; Peng, S.; Wang, L. *Anal. Chem.* **2012**, *84*, 8415.
- (346) Rehm, J. M.; McLendon, G. L.; Fauchet, P. M. *J. Am. Chem. Soc.* **1996**, *118*, 4490.
- (347) Garcia-Reyes, J. F.; Harper, J. D.; Salazar, G. A.; Charipar, N. A.; Ouyang, Z.; Cooks, R. G. *Anal. Chem.* **2011**, *83*, 1084.
- (348) *The Preparatory Manual of Explosives*; Legard, J., Ed.; Legard, J. : USA, 2007.
- (349) Song, J. H.; Sailor, M. J. *J. Am. Chem. Soc.* **1997**, *119*, 7381.
- (350) Scaiano, J. C.; Laferrière, M.; Galian, R. E.; Maurel, V.; Billone, P. *Phys. Status Solidi A* **2006**, *203*, 1337.
- (351) Bar, A. K.; Shanmugaraju, S.; Chi, K.-W.; Mukherjee, P. S. *Dalton Trans.* **2011**, *40*, 2257.
- (352) Liu, Y.; Ogawa, K.; Schanze, K. S. *J. Photochem. Photobiol., C* **2009**, *10*, 173.
- (353) Jin, W. J.; Fernandez-Arguelles, M. T.; Costa-Fernandez, J. M.; Pereiro, R.; Sanz-Medel, A. *Chem. Commun.* **2005**, 883.
- (354) Jin, W. J.; Costa-Fernández, J. M.; Pereiro, R.; Sanz-Medel, A. *Anal. Chim. Acta* **2004**, *522*, 1.
- (355) Shiraki, T.; Tsuchiya, Y.; Shinkai, S. *Chem. Lett.* **2010**, *39*, 156.
- (356) Toal, S. J.; Sanchez, J. C.; Dugan, R. E.; Trogler, W. C. *J. Forensic Sci.* **2007**, *52*, 79.
- (357) Shi, G. H.; Shang, Z. B.; Wang, Y.; Jin, W. J.; Zhang, T. C. *Spectrochim. Acta, Part A* **2008**, *70*, 247.
- (358) Martinez, H. P.; Grant, C. D.; Reynolds, J. G.; Trogler, W. C. *J. Mater. Chem.* **2012**, *22*, 2908.
- (359) Zakon, Y.; Lemcoff, N. G.; Marmur, A.; Zeiri, Y. *J. Phys. Chem. C* **2012**, *116*, 22815.
- (360) Neises, D.; Steglich, W. *Angew. Chem., Int. Ed.* **1978**, *17*, 522.
- (361) Feng, Y. Z.; Sun, D. W. *Crit. Rev. Food Sci. Nutr.* **2012**, *52*, 1039.
- (362) D Alessandro, A.; Zolla, L. *Food Technol. Biotechnol.* **2012**, *50*, 275.
- (363) Eom, K.-H.; Hyun, K.-H.; Lin, S.; Kim, J.-W. *Int. J. Distrib. Sens. N.* **2014**, *2014*, 9.
- (364) Vaillancourt, J.; Mouton, F.; CBC News: 2014.
- (365) Önal, A. *Food Chemistry* **2007**, *103*, 1475.

- (366) Naila, A.; Flint, S.; Fletcher, G.; Bremer, P.; Meerdink, G. *J. Food. Sci.* **2010**, *75*, R139.
- (367) Kovacs, A.; Simon-Sarkadi, L.; Ganzler, K. *J. Chromatogr., A* **1999**, *836*, 305.
- (368) Steiner, M. S.; Meier, R.; Spangler, C.; Duerkop, A.; Wolfbeis, O. *Microchim. Acta* **2009**, *167*, 259.
- (369) Erim, F. B. *TrAC, Trends Anal. Chem.* **2013**, *52*, 239.
- (370) Jorgensen, L. V.; Huss, H. H.; Dalgaard, P. *J. Agric. Food Chem.* **2001**, *49*, 2376.
- (371) Rakow, N. A.; Suslick, K. S. *Nature* **2000**, *406*, 710.
- (372) Panida Lorwongtragool, A.; Wisitsoraat, Teerakiat, Kerdcharoen *J. Nanosci. Nanotechnol.* **2011**, *11*, 10454.
- (373) Chow, C. F.; Lam, M. H.; Wong, W. Y. *Anal. Chem.* **2013**, *85*, 8246.
- (374) Sweryda-Krawiec, B.; Chandler-Henderson, R. R.; Coffey, J. L.; Rho, Y. G.; Pinizzotto, R. *F. J. Phys. Chem.* **1996**, *100*, 13776.
- (375) King, M. G.; Baragwanath, A. J.; Rosamond, M. C.; Wood, D.; Gallant, A. J. *Procedia Chem.* **2009**, *1*, 568.
- (376) Smith, B. C. *Infrared Spectral Interpretation: A Systematic Approach*, 1998.
- (377) Hu, Y.; Ma, X.; Zhang, Y.; Che, Y.; Zhao, J. *ACS Sens.* **2016**, *1*, 22.
- (378) Che, Y.; Yang, X.; Loser, S.; Zang, L. *Nano Lett.* **2008**, *8*, 2219.
- (379) Til, H. P.; Falke, H. E.; Prinsen, M. K.; Willems, M. I. *Food Chem. Toxicol.* **1997**, *35*, 337.
- (380) Choi, S. J.; Kwon, T. H.; Im, H.; Moon, D. I.; Baek, D. J.; Seol, M. L.; Duarte, J. P.; Choi, Y. K. *ACS Appl. Mater. Interfaces* **2011**, *3*, 4552.
- (381) Chen, H.; Gai, H.; Yeung, E. S. *Chem. Commun.* **2009**, 1676.
- (382) Lee, S. F.; Osborne, M. A. *J. Am. Chem. Soc.* **2007**, *129*, 8936.
- (383) Keiichi, S.; Satoshi, K.; Shinya, H.; Taeko, C.; Keiko, U.-S.; Tsukasa, T.; Yasuhiro, T.; Susumu, K. *Nanotechnology* **2007**, *18*, 465702.
- (384) Shi, X.; Tu, Y.; Liu, X.; Yeung, E. S.; Gai, H. *Phys. Chem. Chem. Phys.* **2013**, *15*, 3130.
- (385) Ma, X.; Tan, H.; Kipp, T.; Mews, A. *Nano Lett.* **2010**, *10*, 4166.
- (386) Bruhn, B.; Valenta, J.; Sangghaleh, F.; Linnros, J. *Nano Lett.* **2011**, *11*, 5574.
- (387) Lockwood, R. V., J. G. C.; Meldrum, A. *Sens. Lett.* **2013**, *11*, 1535.
- (388) Lockwood, R.; Yang, Z.; Sammynaiken, R.; Veinot, J. G. C.; Meldrum, A. *Chem. Mater.* **2014**, *26*, 5467.

- (389) Liu, S. F.; Petty, A. R.; Sazama, G. T.; Swager, T. M. *Angew. Chem., Int. Ed.* **2015**, *54*, 6554.
- (390) Steiner, M. S.; Meier, R. J.; Duerkop, A.; Wolfbeis, O. S. *Anal. Chem.* **2010**, *82*, 8402.
- (391) Harrison, D. J.; McDonald, R.; Rosenberg, L. *Organometallics* **2005**, *24*, 1398.
- (392) Lee, P. T. K.; Skjel, M. K.; Rosenberg, L. *Organometallics* **2013**, *32*, 1575.
- (393) Yao, J.; Zhang, K.; Zhu, H.; Ma, F.; Sun, M.; Yu, H.; Sun, J.; Wang, S. *Anal. Chem.* **2013**, *85*, 6461.
- (394) Regli, S.; Kelly, J. A.; Veinot, J. G. C. *Mater. Res. Soc. Symp. Proc.* **2011**, *1359*, null.
- (395) Regli, S.; Kelly, J. A.; Barnes, M. A.; Andrei, C. M.; Veinot, J. G. C. *Mater. Lett.* **2014**, *115*, 21.
- (396) Xu, S.; Lu, H.; Li, J.; Song, X.; Wang, A.; Chen, L.; Han, S. *ACS Appl. Mater. Interfaces* **2013**, *5*, 8146.
- (397) Vasapollo, G.; Del Sole, R.; Mergola, L.; Lazzoi, M. R.; Scardino, A.; Scorrano, S.; Mele, G. *Int. J. Mol. Sci.* **2011**, *12*, 5908.
- (398) Liu, H.; Fang, G.; Li, C.; Pan, M.; Liu, C.; Fan, C.; Wang, S. *J. Mater. Chem.* **2012**, *22*, 19882.
- (399) Wei, F.; Wu, Y.; Xu, G.; Gao, Y.; Yang, J.; Liu, L.; Zhou, P.; Hu, Q. *Analyst* **2014**, *139*, 5785.
- (400) Qinghong, Y.; Stephanie, L. B. *Nanotechnology* **2010**, *21*, 115502.
- (401) Wang, R.; Li, G.; Dong, Y.; Chi, Y.; Chen, G. *Anal. Chem.* **2013**, *85*, 8065.
- (402) Borsella, E.; Falconieri, M.; Botti, S.; Martelli, S.; Bignoli, F.; Costa, L.; Grandi, S.; Sangaletti, L.; Allieri, B.; Depero, L. *Mater. Sci. Eng. B* **2001**, *79*, 55.
- (403) Karlash, A. Y.; Skryshevsky, V. A.; Kuznetsov, G. V.; Kladko, V. P. *J. Alloys Compd.* **2013**, *577*, 283.
- (404) Aghajamali, M.; Iqbal, M.; Purkait, T. K.; Hadidi, L.; Sinelnikov, R.; Veinot, J. G. C. *Chem. Mater.* **2016**, *28*, 3877.